



**MASARYK UNIVERSITY**

Faculty of Science  
Department of Chemistry



and



**UNIVERSITÄT REGENSBURG**

Faculty of Chemistry and Pharmacy  
Institute of Organic Chemistry



---

**Photoactivatable Derivatives for Chemical and  
Biological Applications: Design, Synthesis and  
Mechanistic Investigation**

Ph. D. Dissertation

**Tomáš SLANINA**

**Thesis supervisors:**

prof. RNDr. Petr Klán, Ph.D.

prof. Dr. Burkhard König

**Brno 2015**

## Bibliographic entry

<b>Author:</b>	RNDr. Tomáš Slanina  Department of Chemistry, Faculty of Science, Masaryk University and Institute of Organic Chemistry, Faculty of Chemistry and Pharmacy, Universität Regensburg
<b>Title of Thesis:</b>	Photoactivatable Derivatives for Chemical and Biological Applications: Design, Synthesis and Mechanistic Investigation
<b>Ph.D. Degree Programme:</b>	Chemistry
<b>Field of Study:</b>	Organic chemistry
<b>Supervisors:</b>	prof. RNDr. Petr Klán, Ph.D. prof. Dr. Burkhard König
<b>Academic Year:</b>	2015/2016
<b>Number of Pages:</b>	108 + 69 pages of attachments
<b>Keywords:</b>	photoinduced electron transfer, boron-dipyrromethene, carbon monoxide releasing molecules, xanthene, fluorescein, acridine, eosin Y, 4-hydroxyphenacyl, heavy atom effect, intersystem crossing, transient spectroscopy, photoremovable protecting group, photocatalysis, visible light, photoactivatable molecules, aryl radicals, nitrate radical, photoreduction, reaction mechanism, regulatory small molecules, in vivo release, photochemistry, spectroscopy, quantum yield

## Bibliografický záznam

<b>Autor:</b>	RNDr. Tomáš Slanina  Ústav chemie, Přírodovědecká fakulta, Masarykova univerzita a Ústav organické chemie, Fakultät für Chemie und Pharmazie, Universität Regensburg
<b>Název práce:</b>	Fotoaktivovatelné deriváty pro chemické a biologické aplikace: návrh, syntéza a výzkum mechanismů
<b>Studijní program:</b>	Chemie
<b>Studijní obor:</b>	Organická chemie
<b>Vedoucí práce:</b>	prof. RNDr. Petr Klán, Ph.D. prof. Dr. Burkhard König
<b>Akademický rok:</b>	2015/2016
<b>Počet stran:</b>	108 + 69 stran příloh
<b>Klíčová slova:</b>	fotoindukovaný přenos elektronu, BODIPY, molekuly uvolňující oxid uhelnatý, xanthen, fluorescein, akridin, eosin Y, 4-hydroxyphenacyl, efekt těžkého atomu, mezisystémový přechod, transientní spektroskopie, fotoodstupitelná chránicí skupina, fotokatalýza, viditelné světlo, fotoaktivovatelné molekuly, aryl radikály, NO <sub>3</sub> radikál, fotoredukce, reakční mechanismus, regulační malé molekuly, in vivo uvolnění, fotochemie, spektroskopie, kvantový výtěžek





## Abstract

This thesis focuses on design, synthesis and mechanistic investigations of photoactivatable derivatives. It summarizes selected results of my Ph.D. research which have been published or submitted for publication.

In the theoretical part it summarizes basic information about selected topics relevant for the studied projects, such as photoremovable protecting groups, selected visible light absorbing chromophores, biologically relevant caged ions and small molecules, and visible light photocatalysis.

The part Results and Discussion is divided into eight chapters. The first chapter deals with a xanthene-based photoremovable protecting group (PPG). We managed to prepare the first PPG capable to release phosphates, carboxylates and halides by the action of green light ( $\lambda_{\max} \sim 520$  nm).

The second part introduces 4-hydroxyphenacyl fluoride, a caged fluoride, that can be efficiently released ( $\Phi \sim 84\%$ ) by UV-light irradiation. The mechanism of fluoride release has been studied by picosecond pump-probe spectroscopy. The released fluoride was used for etching of silicon surfaces followed by AFM.

The third project describes the first metal-free carbon monoxide-releasing molecule (CORM) activatable by visible light based on the xanthene structural motif.

The fourth chapter improves the concept of visible light absorbing CORMs by using BODIPY-based chromophores. These molecules can release CO upon irradiation by light at up to 730 nm and were successfully tested in both *in vitro* and *in vivo* biological experiments. The mechanism of the photodegradation was carefully studied.

The fifth chapter deals with a photocatalytic system for reduction of carbonyl compounds. It uses proflavine as a photocatalyst, rhodium mediator, and triethylamine as a sacrificial electron donor. The system selectively reduces aldehydes over ketones. Both electronic and steric effects are responsible for the selectivity which is kinetically controlled.

The sixth project describes a novel photocatalytic method for generation of the nitrate radical which is further used for some synthetic applications. The mechanism of generation of the nitrate radical by photooxidation of the nitrate anion has been studied in detail.

The seventh chapter discusses a new method for generation of fluorinated aryl radicals which are used in the synthesis of fluorinated biaryls as well as in late stage functionalization of some complex molecules. The transient spectroscopic study has revealed the mechanism of the aryl radical formation.

The last project focuses on the synthesis of selanyl- and tellanyl-substituted BODIPY derivatives. The quantum yield of intersystem crossing (up to 60%) has been measured by transient spectroscopy. These derivatives can be used as triplet sensitizers.

## Abstrakt

Tato disertační práce je zaměřena na návrh, syntézu a studium mechanismu fotoaktivovatelných molekul. Shrnuje vybrané projekty z mého doktorského výzkumu, které byly publikovány nebo byly podány k publikaci.

V teoretické části jsou shrnuty základní informace o vybraných tématech relevantních pro studované projekty, jako jsou například fotoodstupitelné chránicí skupiny, chromofory absorbující viditelné světlo, biologicky relevantní chráněné ionty a malé molekuly a fotokatalýza viditelným světlem.

Část Results and Discussion je rozdělena do osmi kapitol. První kapitola se zabývá fotoodstupitelnými chránicími skupinami na bázi xanthenů. Připravili jsme první fotoodstupitelnou chránicí skupinu schopnou uvolňovat fosfáty, karboxyláty a halidy pomocí zeleného světla ( $\lambda_{\max} \sim 520$  nm).

Druhá část se zabývá 4-hydroxyphenacyl fluoridem, chráněným fluoridem, který může být účinně uvolněn ( $\Phi \sim 84\%$ ) pomocí ozáření UV světlem. Mechanismus uvolnění fluoridu byl studován pomocí pikosekundové pump-probe spektroskopie. Uvolněný fluorid byl použit pro leptání povrchů na bázi křemíku, jenž byly monitorovány pomocí AFM mikroskopie.

Třetí projekt popisuje první plně organickou molekulu uvolňující oxid uhelnatý (CORM) pomocí viditelného světla, založenou na xanthenovém strukturním motivu.

Čtvrtý projekt vylepšuje koncept CORM-derivátů použitím struktur na bázi BODIPY. Tyto molekuly mohou uvolňovat CO pomocí světla o vlnové délce do 730 nm a byly úspěšně testovány *in vitro* a *in vivo* biologických experimentech. Mechanismus jejich fotochemické degradace byl pečlivě prostudován.

Pátá kapitola se zabývá fotokatalytickým systémem pro redukci karbonylových sloučenin. Tento systém používá proflavin jako fotokatalyzátor, rhodiový mediátor a triethylamin jako stechiometrický donor elektronů. Systém selektivně redukuje aldehydy v přítomnosti ketonů, kdy tato selektivita je způsobena jak elektronovými tak stericnými efekty a je řízena kineticky.

Šestý projekt popisuje novou fotokatalytickou metodu pro tvorbu radikálů  $\text{NO}_3$ , které jsou dále používány pro syntetické aplikace. Detailně byl studován mechanismus tvorby radikálu  $\text{NO}_3$  pomocí fotooxidace dusičnanu.

Sedmá kapitola popisuje novou metodu pro tvorbu fluorovaných arylových radikálů, které jsou použity pro syntézu fluorovaných biarylů a pro derivatizaci komplexních molekul. Studie pomocí transienční spektroskopie byla použita pro zjištění mechanismu tvorby aryl radikálů.

Poslední projekt je zaměřen na syntézu derivátů BODIPY obsahujících selen a tellur. Pomocí transienční spektroskopie byly změřeny kvantové výtěžky jejich mezisystémového přechodu (až 60 %). Tyto deriváty mohou být využity například pro tripletovou senzitivizaci.

## Acknowledgement

First of all, I would like to thank both of my supervisors, Petr Klán and Burkhard König, for letting me work in their research groups within my joint Ph.D. program. I was extremely fortunate to meet them for both scientific and personal reasons. They taught me a lot about contemporary science and enabled me to develop my own projects which they kindly supervised. Moreover, we started cooperation between our groups which will hopefully last after I finish my Ph.D. studies.

I am grateful to Rich Givens for a wonderful time which I could spend in his lab in Kansas. I am also obliged to Graduiertenkolleg GRK 1626 where I could meet many great scientists and where I started several cooperation projects.

I thank all members of the photochemical group from Brno and AK König from Regensburg. My special thanks belong to Peter, Marek, Lenka, Edu, Jamal, Šolo, Tombo, LuLu, Dominik, Monika, Luboš, Pavel, Niki, Janči, Lubka, Dom, Ľubica, PHorváth, Teresa, Lovely, Lucie, Tamal, Indra, Andi, Thea, Steffi, Anika, Mišo, Miško, Javier, Troppi, Malte, Melli, Chiang, Tonda, Durga, Qui, Anna, Resi, Martin, Georg, Berndt, Obstler, Nadja, Simone, Caro, Willi, Maša, Taša, Marsel, Maksim, Pepi, Andi, Namrata, Caro, Peter, Qiu, Matthias, Sanjeeva, Radek, Viktor, and Thomas. The time spent with these people was one of the most thrilling experiences ever.

I am thankful to my family for encouraging me in my studies and for their unremitting support.

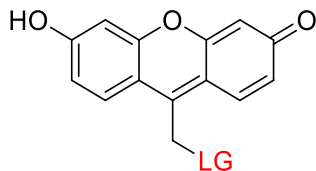
Finally, I thank Anežka for her love and for her patience during my long stays abroad.

*“Do not anticipate trouble, or worry about what may never happen. Keep in the sunlight.”*

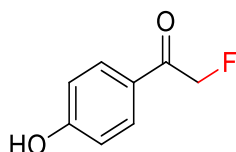
Benjamin Franklin

## Aims of the Dissertation

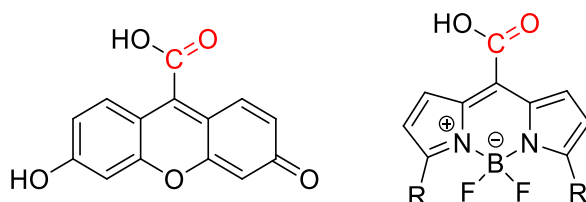
- 1) Synthesis and characterization of the new photoremovable protecting groups based on the xanthene structural motif absorbing visible light.



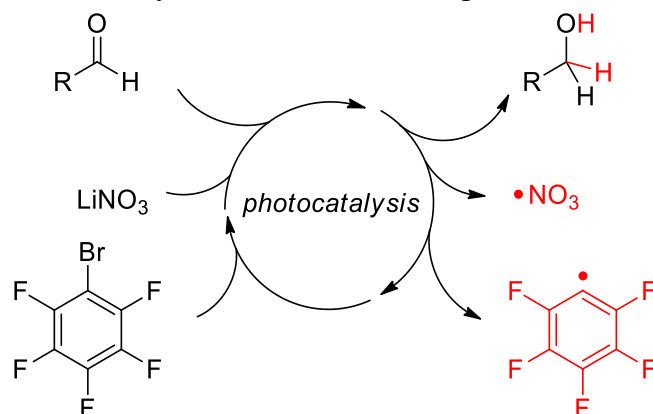
- 2) Synthesis of a caged fluoride and its application for photoinduced etching silicon surfaces.



- 3) Design, synthesis and investigation of properties of the novel photoactivatable carbon monoxide releasing molecules (photoCORMs) based on xanthene and BODIPY chromophores.



- 4) Design, optimization and detailed mechanistic investigations of various photocatalytic systems capable of reduction of the carbonyl compounds, generation of the nitrate radical, and pentafluoroarylation of aromatic compounds.



- 5) Quantification of the heavy-atom effect of chalcogen- and halogen-substituted BODIPY derivatives.

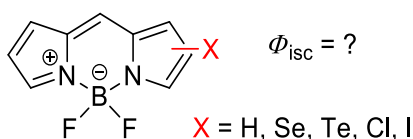


# Table of Contents

Aims of the Dissertation.....	8
Table of Contents .....	9
List of Abbreviations.....	11
1. Foreword .....	14
2. Theoretical Part .....	15
2.1. Introduction .....	15
2.1.1. Photophysical Processes .....	16
2.1.2. Photochemical Processes .....	17
2.2. Photoremovable Protecting Groups .....	20
2.2.1. Protecting Groups .....	20
2.2.2. Common Photoremovable Protecting Groups .....	21
2.2.3. 4-Hydroxyphenacyl PPG .....	24
2.2.4. Coumarinyl PPG .....	26
2.2.5. Visible Light-Absorbing PPGs .....	28
2.3. Selected Visible-Light-Absorbing Dyes .....	31
2.3.1. Xanthene Dyes .....	31
2.3.2. Acridine Dyes .....	34
2.3.3. BODIPY Dyes .....	34
2.4. Caged Ions and Small Molecules .....	37
2.4.1. Introduction.....	37
2.4.2. Fluoride Anion .....	39
2.4.3. Carbon Monoxide .....	40
2.5. Photocatalysis.....	42
2.5.1. Introduction.....	42
2.5.2. Principles of Photocatalysis .....	43
2.5.3. Common Reagents Used in Photocatalysis.....	45
3. Results and Discussion.....	47
3.1. Xanthene-Based PPG .....	47
3.1.1. Introduction.....	47
3.1.2. Synthesis .....	48
3.1.3. Photochemistry .....	50
3.1.4. Conclusion .....	51
3.1.5. Authors' Contributions .....	51
3.2. Caged Fluoride .....	51
3.2.1. Introduction.....	52
3.2.2. Synthesis .....	53
3.2.3. Photochemistry .....	53
3.2.4. Etching .....	55
3.2.5. Conclusion .....	56
3.2.6. Authors' Contributions .....	56
3.3. Xanthene-Based CORM.....	56

3.3.1.	Introduction.....	56
3.3.2.	Synthesis .....	57
3.3.3.	Photochemistry .....	57
3.3.4.	Conclusion .....	59
3.3.5.	Authors' Contributions .....	59
3.4.	BODIPY-Based CORM .....	60
3.4.1.	Introduction.....	60
3.4.2.	Synthesis and Photophysical Properties.....	61
3.4.3.	Mechanistic Studies .....	62
3.4.4.	Biological Application .....	64
3.4.5.	Conclusion .....	64
3.4.6.	Author's Contributions .....	65
3.5.	Photocatalytic Reduction of Aldehydes .....	65
3.5.1.	Introduction.....	65
3.5.2.	Synthesis .....	66
3.5.3.	Steady-State Studies and Rhodium-Based Mechanism .....	68
3.5.4.	Transient Spectroscopy and Overall Mechanism.....	71
3.5.5.	Conclusion .....	72
3.5.6.	Author's Contributions .....	73
3.6.	Photooxidation of Nitrate by Visible Light.....	73
3.6.1.	Introduction.....	73
3.6.2.	Synthetic Applications .....	74
3.6.3.	Mechanistic Studies .....	75
3.6.4.	Conclusion .....	78
3.6.5.	Authors' Contributions .....	78
3.7.	Photocatalytic Arylation by Fluorinated Aryl Bromides .....	79
3.7.1.	Introduction.....	79
3.7.2.	Synthetic Applications .....	80
3.7.3.	Mechanistic Studies .....	81
3.7.4.	Conclusion .....	84
3.7.5.	Authors' Contributions .....	85
3.8.	Heavy-Atom Effect of Selanyl- and Tellanyl-Substituted BODIPYs.....	85
3.8.1.	Introduction.....	85
3.8.2.	Photophysical properties .....	86
3.8.3.	Transient spectroscopy.....	87
3.8.4.	Conclusions.....	89
3.8.5.	Authors' Contributions .....	89
4.	Summary .....	90
5.	Literature .....	91
6.	Curriculum Vitae.....	104
7.	List of Appendices .....	108

## List of Abbreviations

A	acceptor
ATP	adenosine triphosphate
18-crown-6	1,4,7,10,13,16-hexaoxacyclooctadecane
Ac	acetyl
Acr <sup>+</sup> -Mes	9-mesityl-10-methylacridinium
AFM	atomic force microscopy
back eT	back electron transfer
Bn	benzyl
Boc	tert-butyloxycarbonyl PG
BODIPY	boron-dipyrromethene
bpy	2,2'-bipyridine
bpz	2,2'-bipyrazine
cAMP	cyclic adenosine monophosphate
CAN	cerium ammonium nitrate
Cbz	benzyloxycarbonyl
cGMP	cyclic guanosine monophosphate
COHb	carboxyhemoglobin
CORM	carbon monoxide-releasing molecule
CORM-3	ruthenium based CORM
Cp*	pentamethylcyclopentadienyl ligand
CT	charge transfer excited state
D	donor
DAC450	7-diethylaminocoumarin-4-yl PPG derivative
DACM	7-diethylaminocoumarin-4-yl PPG
DATS	diallyltrisulfide
DDQ	2,3-dichloro-5,6-dicyano-1,4-benzoquinone
DEACM	7-diethylaminocoumarin-4-yl PPG
DFT	density functional theory
DIPEA	<i>N,N</i> -Diisopropylethylamine
DMAP	4-dimethylaminopyridine
DMF	<i>N,N</i> -dimethylformamide
DMS	dimethylsulfate
DMSO	dimethylsulfoxid
DNA	deoxyribonucleic acid
DSC/TG	differential scanning calorimetry coupled with thermogravimetry
EA	electron affinity of a ground-state molecule
EA*	electron affinity of an excited molecule
EPR	electron paramagnetic resonance
eT	electron transfer
ET	energy transfer
FAD	flavin adenine dinucleotide
FADH <sub>2</sub>	reduced form of FAD

Fmoc	fluorenylmethyloxycarbonyl PG
GABA	$\gamma$ -aminobutyric acid
GTP	guanosine-5'-triphosphate
HAE	heavy atom effect
HAT	hydrogen atom transfer
Hb	hemoglobin
HepG2	hepatoblastoma type
HMO	Hückel molecular orbital method
HOMO	highest occupied molecular orbital
HRMS	high resolution mass spectroscopy
IP	ionization potential of a ground-state molecule
IP*	ionization potential of an excited molecule
IR	infrared light
isc	intersystem crossing
IUPAC	international Union of Pure and Applied Chemistry
LE	locally excited excited state
LED	light emitting diode
LFP	laser flash photolysis
LG	leaving group
LGH	conjugated acid of a leaving group
LUMO	lowest unoccupied molecular orbital
MetHb	methemoglobin
NAD <sup>+</sup>	nicotinamide adenine dinucleotide
NADH	reduced form of NAD
NADP <sup>+</sup>	nicotinamide adenine dinucleotide phosphate
NADPH	reduced form of NADP <sup>+</sup>
NMR	nuclear magnetic resonance
OLED	organic light-emitting diode
ox	oxidation
PBS	phosphate buffered saline
PDE-5	phosphodiesterase
PEG	poly(ethylene glycol)
PeT	photoinduced electron transfer
PF	proflavine
PFH <sup>+</sup>	protonated form of proflavine
PFH <sub>2</sub>	reduced form of proflavine
PGF	protecting-group-free
photoCORM	photoactive CORM
pHP	4-hydroxyphenacyl ( <i>p</i> -hydroxyphenacyl) moiety
PPG	photoremovable protecting group
red	reduction
Rh <sub>cat</sub>	[Cp*Rh <sup>III</sup> (bpy)Cl]Cl
RNA	ribonucleic acid
ROS	reactive oxygen species



SCE	standard calomel electrode
SEM	[2-(trimethylsilyl)ethoxy]methyl PPG
SH-SY5Y	neuroblastoma type
SKH1	nude mouse strain
S <sub>n</sub>	singlet (n) state
T	thermodynamic temperature
TBDPS	tert-butyldiphenylsilyl
tcOH	7-diethylaminocoumarin-4-yl PPG derivative
TEA	triethylamine
TEOA	triethanolamine
TFA	trifluoroacetic acid
THP	tetrahydropyranyl PG
TIPS	triisopropylsilyl
T <sub>n</sub>	triplet (n) state
UV	ultraviolet (light, irradiation, spectroscopy)
UVA	ultraviolet light in range 320–400 nm
vis	visible (light, irradiation, spectroscopy)
Z	benzyloxycarbonyl
ΔG <sub>0-0</sub>	HOMO-LUMO energetic difference

## 1. Foreword

This thesis is written as a compilation of the projects which have been published or submitted for publication during my Ph.D. studies. In the first part it covers the theoretical background of all discussed projects. The main photophysical and biochemical principles and the current state of the relevant literature are briefly summarized. The title: “Photoactivatable Derivatives for Chemical and Biological Applications: Design, Synthesis and Mechanistic Investigation” involves many fields of synthetic and physical organic chemistry, photochemistry, photophysics and biology. Therefore, the introductory part cannot serve as an exhaustive review but the text is written in a way that enables the reader to understand the discussed topics and clarifies our original motivation for working on the research projects.

The second part, Results and Discussion, comments on the selected published projects. The manuscripts discussed are attached in the Appendices of the dissertation. The commentary summarizes the most important results and brings them to the context of the whole Ph.D. research. The emphasis is put on parts of the projects accomplished by the author.

The individual Supporting Information texts containing experimental details, spectra and full characterization of the synthesized compounds are almost 330 pages long and, therefore, they are attached as an electronic file on a CD. They are also available online on the web pages of the corresponding publishers (The Royal Society of Chemistry and American Chemical Society).

## 2. Theoretical Part

### 2.1. Introduction

“Photochemistry is the branch of chemistry concerned with the chemical effects of light (far UV to IR).”<sup>1</sup> This rather brief definition covers immense amount of transformations which are found in many, often unexpected, fields of life. Starting with photodynamic therapy of neonatal jaundice<sup>2</sup> and ending with high-power laser engraving on marble<sup>3</sup>, photochemistry accompanies humans for their whole life.

The history of photochemistry is older than the written historical sources. The earliest written records of the use of dyestuffs and pigments in China are from 2600 B.C.<sup>4</sup> The famous tale from the history of photochemistry about photochromic materials used by the army of Alexander the Great (356 – 323 B.C.) as a tool for determination of the precise time and synchronizing the army attacks turned out to be a hoax. It was published on 5<sup>th</sup> August 1961 in an American weekly magazine *Saturday Review* as a joke of a columnist and since that it has spread into scientific publications and chemistry textbooks.<sup>5</sup> In 1669, Henning Brand prepared white phosphorus from urine which was the first material known to exhibit phosphorescence.<sup>6</sup> Fluorescein, a famous fluorescent dye, has been synthesized by Alexander von Baeyer in 1871 from phthalic anhydride and resorcinol.<sup>7</sup> Modern photochemistry that studies the interaction of molecules with light was established by pioneering works by Giacomo Ciamician at the beginning of 20<sup>th</sup> century.<sup>8</sup>

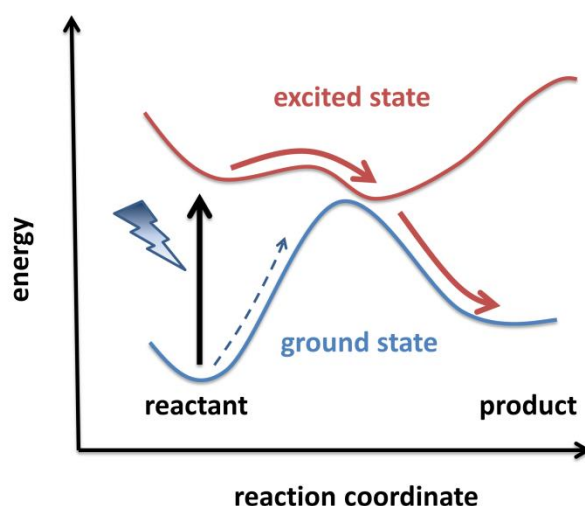


**Figure 1:** Schematic representation of the difference between ground state chemistry and chemistry induced upon excitation.

Photochemistry became so popular and ubiquitous because it enables to drive reactions which do not occur in the ground state. The ground-state (thermal) chemistry is driven by simple thermodynamics.<sup>9</sup> Figure 1 depicts a schematic representation of the difference between ground-state chemistry and photochemistry. The reactant in the ground state (blue line) does not have sufficient energy to overcome an energetic barrier towards the product (dashed arrow). Therefore, the reaction does not occur and the product is never formed under

given conditions. If the reactant absorbs a photon (blue lightning symbol), it is excited (black arrow) to the electronically excited state (red line) which is rich in energy and from which the product can be formed with a significantly lower energetic barrier (red arrows).

The thermal energy at room temperature ( $k_B T$  at 298 K) equals to 0.026 eV or 0.59 kcal mol<sup>-1</sup>. A green photon with  $\lambda = 500$  nm has energy two orders of magnitude higher: 2.48 eV (57.2 kcal mol<sup>-1</sup>). Even rising the temperature to 150 °C (423 K) increases the product of  $k_B T$  to 0.036 eV (0.83 kcal mol<sup>-1</sup>). This thus illustrates a large difference in energy delivered by heating or by absorption of light.

### 2.1.1. Photophysical Processes

The photophysical processes induced by absorption of light were summarized by Jabłoński in the state diagram.<sup>10,11</sup> The simplified version of the Jabłoński diagram is shown in Figure 2.

Most of organic molecules are diamagnetic in their ground state which means that they have even number of electrons paired in their molecular orbitals. Their multiplicity equals to 1 and we call this electronic configuration the singlet state  $S_0$ . Figure 2 depicts  $S_0$  as a thick blue line with thin blue lines which represent vibrationally excited states of the ground state singlet. The relative population of vibrational states is governed by Boltzmann distribution ( $e^{-\Delta E/kT}$ ) where  $\Delta E$  is the energetic difference between two energetic levels,  $k$  is the Boltzmann constant and  $T$  is the thermodynamic temperature. The excitation of a molecule is allowed by quantum physics only for processes that preserve the multiplicity of the system. Therefore, a ground state singlet molecule can be excited only to one of the higher excited singlet states,  $S_1$  (black vertical line, red lines, Figure 2).

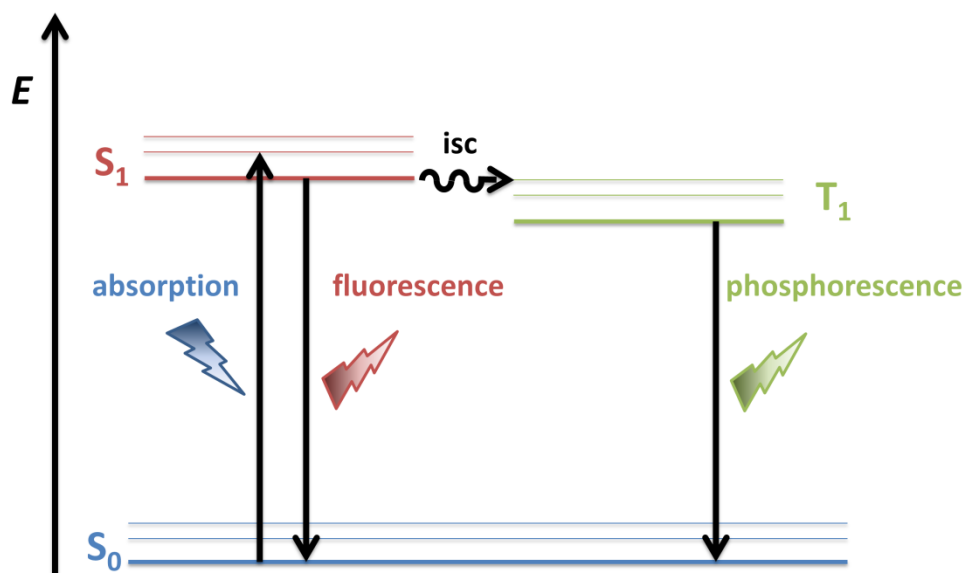


**Figure 2:** Simplified version of Jabłoński diagram, internal conversion and vibrational relaxation were omitted for clarity

The absorbed photon has to have the energy corresponding to the energy difference between these states. The photon with a lower energy is not absorbed and does not cause any photochemical transformations (Grotthuss–Draper law). A molecule can be excited to the higher excited states  $S_n$ , but in majority of cases, these states deexcite rapidly to the  $S_1$  state which is responsible for consecutive photochemical and photophysical processes (Kasha's rule).<sup>12</sup> The most common photophysical deexcitation pathways from  $S_1$  are: fluorescence (red lightning symbol) and internal conversion with vibrational relaxation to the ground state.

The excited molecule can also undergo intersystem crossing (dashed black line) from  $S_1$  to the triplet state,  $T_1$ , which has two electrons with unpaired spin and a multiplicity of 3. This process is energetically favorable due to spin correlation but is spin-forbidden. The lifetime of the triplet states is therefore usually higher than of the singlet states because they have to decay by another spin forbidden process (phosphorescence, green lightning symbol (Figure 2), or back intersystem crossing and internal conversion to the ground singlet state) in the course of deexcitation. The intersystem crossing is high for  $(n,\pi^*) \rightarrow (\pi,\pi^*)$  transitions due to its symmetry (El Sayed's rules<sup>13</sup>) and is accelerated by spin-orbit coupling in the presence of a heavy atom (inter of intramolecular heavy atom effect).

### ***2.1.2. Photochemical Processes***

All processes discussed above are of photophysical not chemical character. The electron density of a molecule changes upon excitation. The former highest occupied orbital (HOMO) loses one electron and the former lowest unoccupied molecular orbital (LUMO) accepts one electron which may change the bond order. The largest changes can be observed for bonds between atoms with high coefficients in both HOMO and LUMO. When a pair of atoms has a bonding interaction in HOMO (the same coefficient and a large orbital overlap) and a strongly antibonding interaction in LUMO (large coefficients of opposite signs and a nodal plane in between the atoms), the bond order decreases significantly upon excitation. The decreased bond order means bond prolongation and in extreme cases can lead to (homolytic) bond fission.<sup>14</sup> This mechanism applies when the bond energy is similar to the energy difference between HOMO and LUMO. Typical energies of a single bond in organic molecule correspond to the energies of photons in the UV region (4 – 5 eV, 300 – 250 nm). The photoinduced heterolytic bond cleavage often occurs when the electron density reorganized after excitation expels a leaving group<sup>15</sup> or when a stable, often gaseous, molecule is released.<sup>16</sup>

After the excitation, the symmetry of electron density is changed which also allows a molecule to react in ground-state-forbidden pericyclic reactions, isomerizations and rearrangements.<sup>17</sup>

An excited molecule simultaneously becomes a better oxidant and reductant. As it is demonstrated in Figure 3, the electron affinity (EA) of a chromophore, which demonstrates the ability of a ground state molecule to accept an electron, is the energy difference between LUMO and the continuum (electron and the ionized molecule in infinite distance from each other). The ionization potential (IP) equals to the difference between energy of HOMO and the continuum. After excitation (Figure 3, right side), the electron affinity increases by the

excitation energy ( $\Delta G_{0-0}$ ) and the ionization potential decreases by the excitation energy. This can be summarized in Equations 1 and 2:

$$EA^* = EA + \Delta G_{0-0} \quad (\text{Eq. 1})$$

$$IP^* = IP - \Delta G_{0-0} \quad (\text{Eq. 2})$$

where  $EA^*$  and  $IP^*$  are electron affinity and ionization potential in the first excited state.

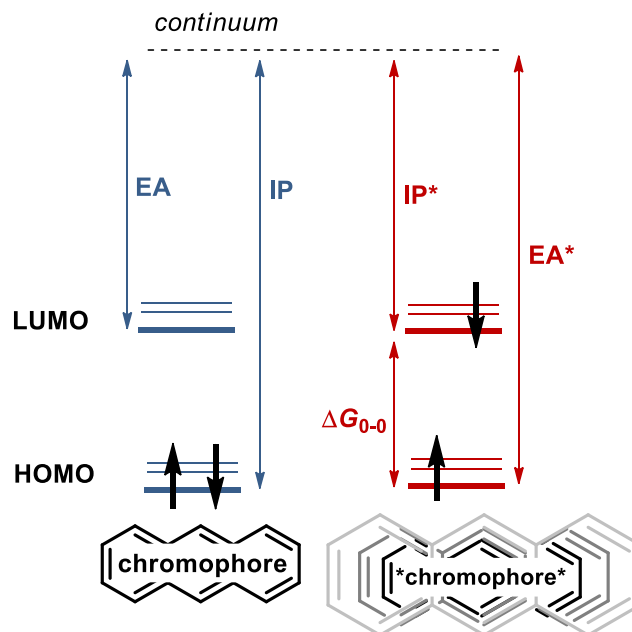


**Figure 3:** Schematic representation of the ionization potential and electron affinity of a ground-state (left) and excited-state chromophore (right)

Electron affinity and ionization potential do not consider the reorganization energy of the solvent, thus a more appropriate value, the redox potential, is often used for molecules in solutions. The equation for calculation of Gibbs energy of photoinduced electron transfer, often erroneously<sup>13</sup> called the Rehm-Weller equation<sup>18</sup> (Eq. 3), describes the thermodynamics of electron transfer between donor D and acceptor A when one of these species is in the excited state:

$$\Delta G = \Delta G(D^+/D) - \Delta G(A/A^-) - \Delta G_{0-0} - \frac{e^2}{\epsilon d} \quad (\text{Eq. 3})$$

where  $\Delta G$  is the standard Gibbs free energy of the electron transfer,  $\Delta G(D^+/D)$  is the Gibbs free energy of reduction of oxidized donor ( $D^+$ ) to neutral donor D,  $\Delta G(A/A^-)$  is the Gibbs free energy of reduction of neutral acceptor A to reduced acceptor  $A^-$ ,  $\Delta G_{0-0}$  is the HOMO – LUMO gap of either the donor or acceptor molecule, and  $\frac{e^2}{\epsilon d}$  is the Coulombic term reflecting the attraction forces in an ion pair generated upon electron transfer, where  $e$  is the elementary charge,  $\epsilon$  is the permittivity of the environment (solvent) and  $d$  is the average distance of  $D^+$  and  $A^-$  in the ion pair.

$\Delta G$  for reduction can be calculated from the corresponding reduction potential ( $\Delta E$ ) according to Equation 4:

$$\Delta G = -nF\Delta E \quad (\text{Eq. 4})$$

where  $n$  is the number of electrons participating in an electrochemical process,  $F$  is the Faraday constant.

There are two practical rules (Eq. 5 and 6) for recalculating the potentials and wavelengths into Gibbs energies:

$$\Delta G \left( \text{in } \frac{\text{kcal}}{\text{mol}} \right) = 23.06 \Delta E \text{ (in eV)} \quad (\text{Eq. 5})$$

$$\Delta G_{0-0} \left( \text{in } \frac{\text{kcal}}{\text{mol}} \right) = 28600/\lambda \text{ (in nm)} \quad (\text{Eq. 6})$$

Values for the excited-state reduction potentials of organic molecules calculated by Equation 3 are often overestimated. The equation for calculation of the Gibbs energy of photoinduced electron transfer uses  $\Delta G_{0-0}$  as the energy of the 0-0 transition from the ground state to the  $S_1$  state. However, electron transfer often occurs from the triplet state. This state has always lower energy and, therefore, the actual reduction potential of a molecule undergoing electron transfer from triplet is by  $\sim 0.2 - 0.6$  V lower than the potential predicted from the energy of  $S_1$  state.

Electron transfer between a molecule in the excited state and the donor (acceptor) in the ground state is called photoinduced electron transfer (PeT). A charge transfer complex formed immediately after PeT (Figure 4) relaxes to an ion pair which can undergo back electron transfer (back eT) resulting in the initial state. Back electron transfer is the main energy wasting pathway for many PeT processes. Most of acceptors (donors) used for PeT processes are transformed into neutral species by a follow-up reaction immediately after electron transfer occurs. This breaks down the ion pair and prevent it from back eT.

The molecule can be photoionized also in the absence of a suitable acceptor. In that case solvated electrons are formed. This process is common for UV light excitation but can occur also upon excitation by visible light.<sup>19</sup>

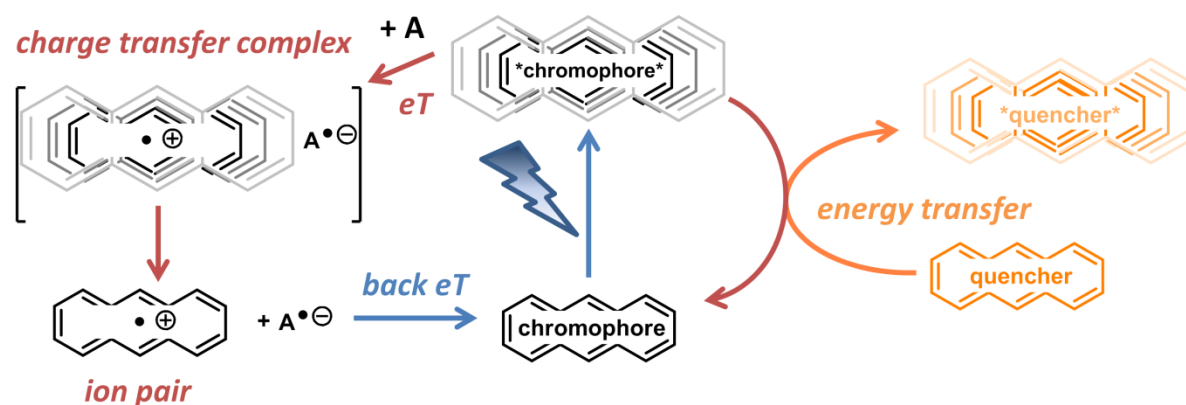


**Figure 4:** Difference between energy transfer (right side) and electron transfer to the acceptor A (left side).

Electron transfer is not the only photochemical deactivation pathway of excited molecules. The excitation energy can be transferred from the excited molecule (sensitizer) to the molecule accepting the energy (quencher). This process, energy transfer (ET, Figure 4, right side), is often accompanying electron transfer. For example, the triplet state of rose bengal is known for both eT and ET.<sup>20</sup> Energy transfer is often called sensitization and the most commonly sensitized molecule is oxygen. Diatomic molecule of oxygen is triplet in the ground state. Therefore it interacts with other triplet molecules with higher energy. Generated

singlet oxygen is a strong oxidant and is used in synthetic chemistry<sup>21</sup> as well as in photodynamic therapy.<sup>22</sup>

## 2.2. Photoremovable Protecting Groups

### 2.2.1. Protecting Groups

The concept of protecting groups (PG) is a well-known technique used in modern organic chemistry. It ensures the regio- and chemoselectivity in reaction of polyfunctional substrates. Usually, a protecting group blocks one or more functional groups and prevents them from unwanted reactions whereas the unprotected functionality is chemically transformed. The criteria for a good protecting group follow:

- the installation of a protecting group should have a high selectivity, conversion and chemical yield
- the protected functional group should be stable towards all reagents used in other synthetic transformations
- the deprotection should be easily accomplished orthogonally to that of other PGs using a selective mild reagent which does not induce any unwanted changes in the rest of the molecule (chemical reactions of other functional groups, isomerizations, polymerizations etc.)
- purification of the reaction mixture after deprotection should be simple (*e. g.*, [2-(trimethylsilyl)ethoxy]methyl (SEM) protecting group produces after deprotection volatile products which can be easily removed under reduced pressure).

The general rule for protecting groups is: the more stable protecting group tolerating many other reagents (*e. g.* –OTHP vs –OMe), the harsher reaction conditions are needed for the deprotection ( $H^+$  vs  $BBr_3$ ).<sup>23</sup>

The concept of protecting groups is essential for the synthesis of complex molecules, especially in medicinal chemistry and in total synthesis of natural products. Each protecting group used prolongs the synthetic procedure by two steps – protection and deprotection. This means that even relatively simple molecules cannot be synthesized in a useful number of synthetic steps (<15). For example, a total synthesis of (+)-Sundiversifolide by Shishido *et al.* from 2007<sup>24</sup> contains 21 synthetic steps (Figure 5), out of which 8 steps are protection and deprotection reactions.

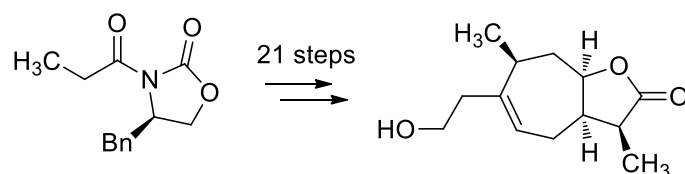


**Figure 5:** Total synthesis of (+)-Sundiversifolide by Shishido *et al.*<sup>24</sup>

Total syntheses of complex products which are protecting-group-free (PGF) are still a big challenge for synthetic chemists. A review by Baran in *Nature Chemistry*<sup>25</sup> summarizes efforts in PGF in last decade. The classical example is Robinson's PGF synthesis of tropinone published as early as in 1917 (Figure 6).<sup>26</sup>



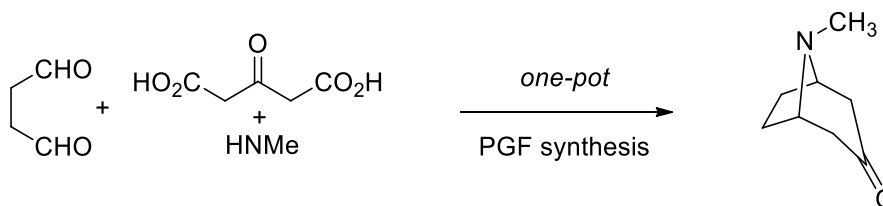


**Figure 6:** Protecting-group-free total Robinson's synthesis of tropinone

### 2.2.2. Common Photoremovable Protecting Groups

Deprotection of a protecting group always requires use of a reagent that specifically cleaves the bond between the protected functionality and the functional group. These reagents often cause unwanted transformations of the rest of the molecule. The most typical example is deprotection of other protecting groups or epimerization of stereogenic centers. In 1962, Barltrop and Schofield introduced the first "traceless" deprotection of a protecting group.<sup>27</sup> They observed the cleavage of benzyloxycarbonyl group (Cbz, Z), a commonly used protecting group for amines, by irradiation of UV light (254 nm). Their work initiated the development of photoremovable protecting groups (PPGs) and caged compounds. Photochemical protecting groups are protecting groups used for temporary blocking of functional groups in organic synthesis which are released by the action of light. Caged compounds are based on the same derivatives as PPGs, but are used for suppressing the activity of biologically relevant molecules and releasing them in cell or in tissue by light. Caged compounds help to investigate biochemical and biological processes by regulating them in a high temporal and spatial precision. The activity of an enzyme, neuron synapsis or cell metabolism can be precisely controlled by lasers focused into small volume. The criteria of a good PPG include all features relevant for protecting groups discussed above and add further<sup>28,29</sup>:

- high quantum yield of deprotection ( $\Phi_{\text{deprotection}} > 0.10$ )
- high product of  $\Phi_{\text{deprotection}}$  and molar absorption coefficient at the wavelength of irradiation  $\varepsilon$  ( $\Phi_{\text{deprotection}} \times \varepsilon = 10\text{--}10\,000$ )
- the departure of the protecting group from the substrate should occur directly from the excited state of the caging chromophore
- good aqueous solubility of both the caged substrate and photoproduct; low toxicity is required for biological studies
- photoproduct should have hypsochromically shifted absorption peak in order to neglect the internal filter effect
- photoproducts should be well defined, stable and easily separable molecules
- the photoremovable protecting group should absorb at wavelengths well above 300 nm where most of biogenic molecules (proteins, nucleic acids etc.) do not absorb
- the PPG should be released rapidly which is relevant in studies of reaction kinetics in samples such as brain tissue or cells.

Since the work of Barltrop, many chemists contributed to the field of PPGs. A review by Klán<sup>30</sup> nicely summarizes all known PPGs into a table (Figure 7).

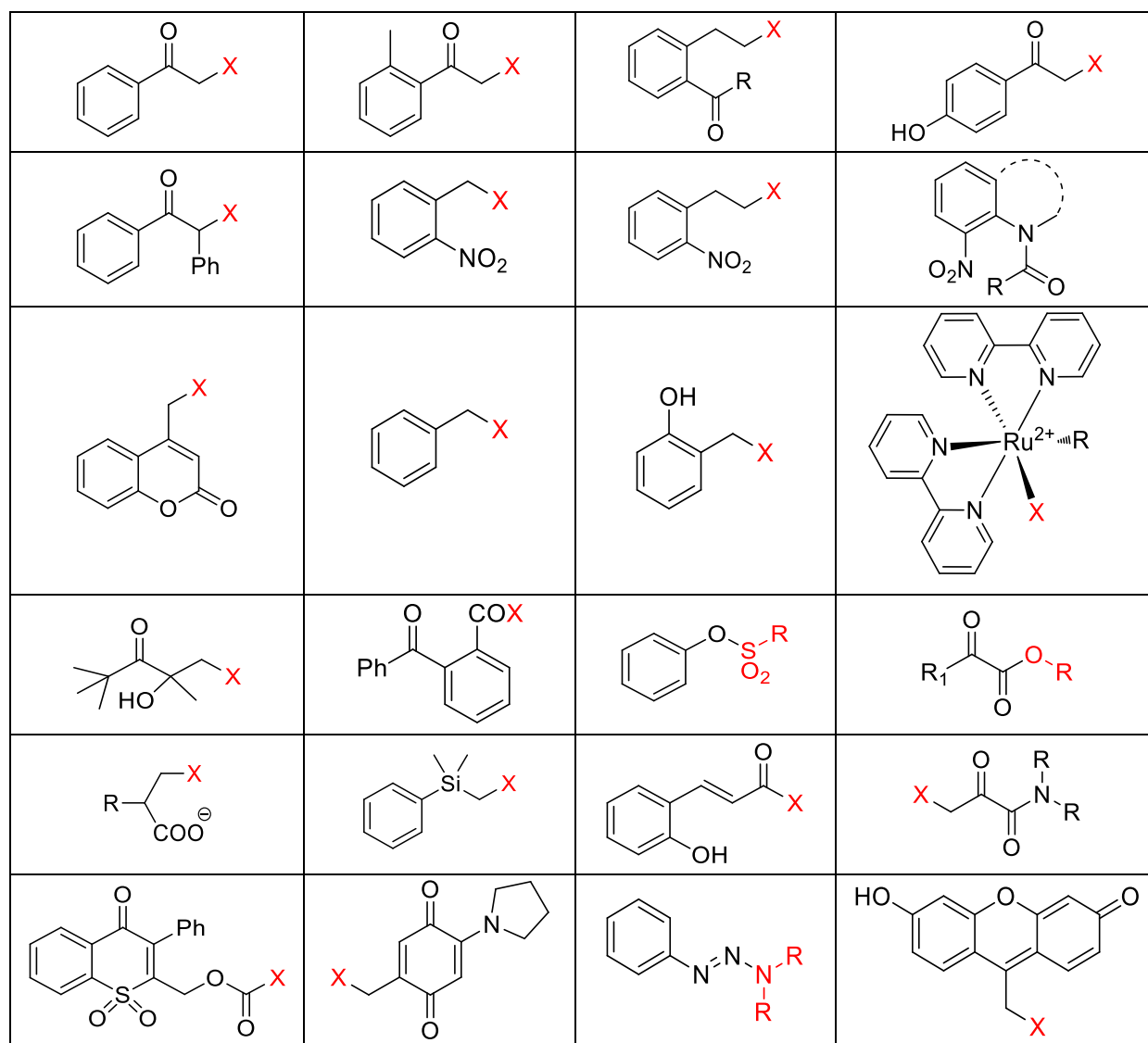


**Figure 7:** List of PPGs known in 2013, X = leaving group, taken from ref. 30.

Protecting groups can not only block the reactivity of a functional group but can also influence the reactivity of the protected molecule in a desired way. For example, the “Umpolung” strategy for aldehydes by transforming them to thioacetals (a common protecting group for carbonyls) changes the  $a^1$  synthon of a carbonyl to  $d^1$  synthon (Corey-Seebach reaction, Figure 8).<sup>31</sup> Aldehydes are electrophiles and react readily with nucleophiles. The “Umpolung” strategy makes the aldehydic carbon nucleophilic. The aldehyde reacts with 1,3-propanethiol under catalysis of a Lewis acid. The formed 1,3-dithiane is deprotonated by a strong base which generates a negative charge on the former electrophilic aldehydic carbon atom. This can react with electrophiles (alkyl/aryl halides, epoxides, carbonyls, acyl derivatives, iminiums etc.) and the subsequent deprotection (often accomplished with  $Hg^{2+}$  salt) leads to the substituted carbonyl (Figure 8).

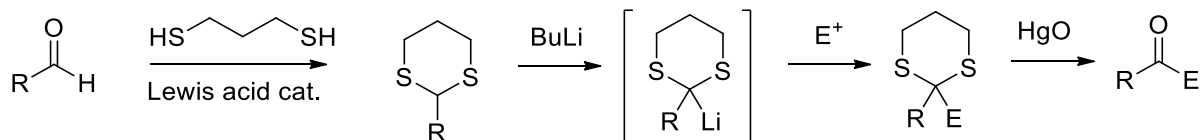


**Figure 8:** Corey-Seebach reaction, “Umpolung” of aldehyde reactivity

The photoremovable protecting group can also influence the chemical reactivity of the rest of the molecule. In 2012, we published a study on a photoremovable chiral auxiliary.<sup>32</sup> A chiral benzoin derivative is used as a photoremovable protecting group. The chirality of the PPG is transformed into the diastereoselectivity of the subsequent [4+2] Diels-Alder reaction (Figure 9). The resulting enantiomeric excess reached 96% at a quantitative conversion. After the cycloaddition, the chiral auxiliary was easily removed by irradiation at 313 nm.

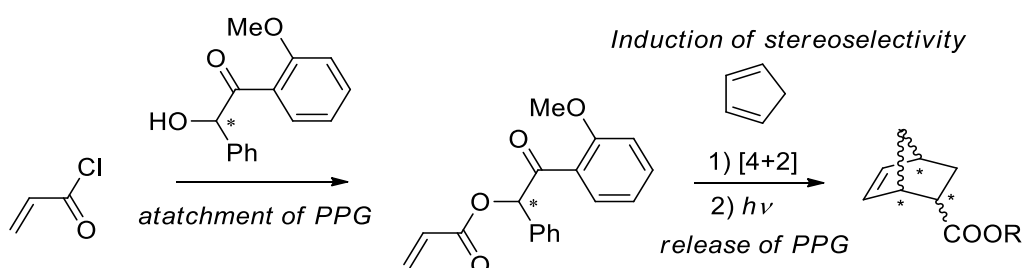


**Figure 9:** Photoremovable chiral auxiliary

As mentioned previously, different protecting groups are often deprotected by orthogonal methods. A typical example is the solid-phase-synthesis (SPS) of polypeptides.  $\text{NH}_2$  groups of amino acids are often protected by 9-fluorenylmethoxycarbonyl (Fmoc) or by *tert*-butyloxycarbonyl (Boc) protecting group. The Boc group is deprotected by Brønsted acid (trifluoroacetic acid, TFA) whereas Fmoc group by mild base (piperidine in DMF) (Figure 10).

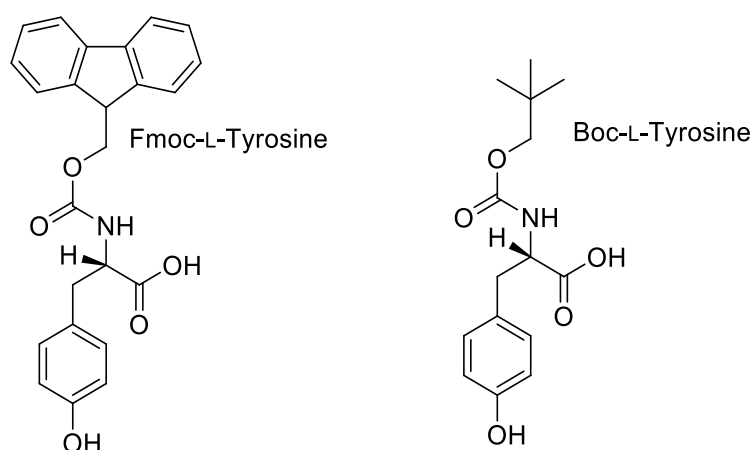


**Figure 10:** Fmoc-L-tyrosine (left) and Boc-L-tyrosine (right)

Photoremovable protecting groups can also be orthogonal. Bochet has introduced a mixed diester of pimelic acid with a 3',5'-dimethoxybenzoin group at one carboxylic functional groups and an *o*-nitrobenzyl group at the other end (Figure 11, left side).<sup>33</sup> The *o*-nitrobenzyl

PPG is cleaved at 420 nm whereas the benzoin part departs upon irradiation at 254 nm. Klán *et al.* has developed a single-chromophore orthogonal PPG which combines properties of *o*-nitrobenzyl and phenacyl PPG (Figure 11, right side).<sup>34</sup> The *o*-nitrobenzylic position cleaves preferentially and in presence of a hydrogen donor, the phenacyl group is cleaved as well. The presence (absence) of a hydrogen donor governs the release of protected substrates LG<sub>1</sub> and LG<sub>2</sub>.

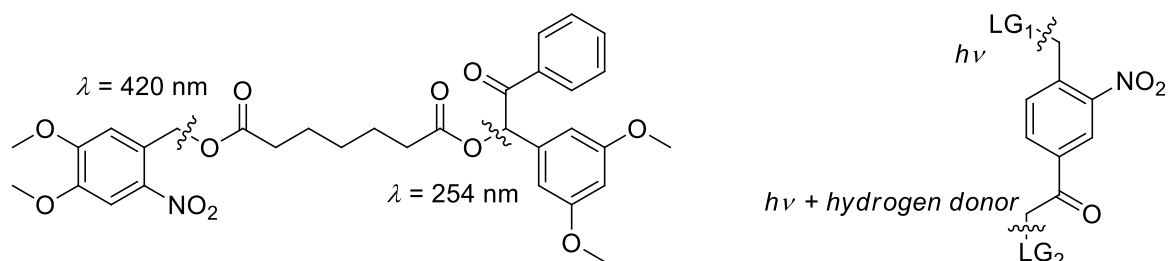


**Figure 11:** Orthogonal protecting groups introduced by Bochet (left) and Klán (right)

As shown above, photoremovable protecting groups can influence the chemistry of a protected molecule. On the other hand, protecting groups can influence the photochemistry of the protected structure. It was shown<sup>35</sup> that protecting groups can influence relative energies of excited states and can govern the course of photochemistry. Dimethoxy-substituted 2-methylphenacyl derivative is excited to the unproductive  $^3\pi,\pi^*$  excited state (Figure 12, upper part) whereas its dipivaloyl derivative goes to  $^3n,\pi^*$  which rearranges to an indanone derivative. Methoxy and pivaloyl groups in this case act as “excited-state protecting groups”.

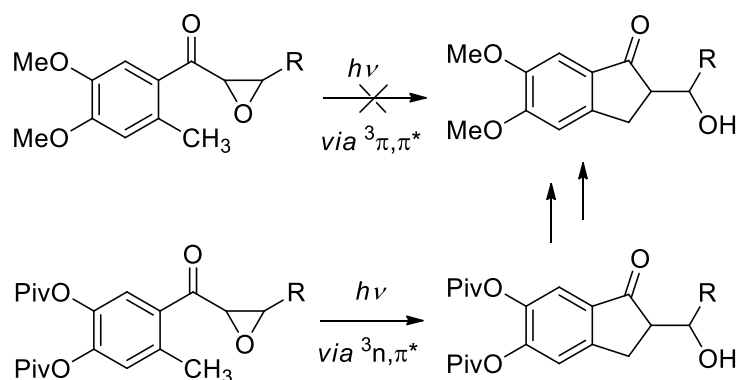


**Figure 12:** Photochemistry of 4,5-di-R-2-methylphenacyl epoxides<sup>35</sup>

### 2.2.3. 4-Hydroxyphenacyl PPG

4-Hydroxyphenacyl (*p*HP) photoremovable protecting group is one of the most commonly used PPGs. It has good water solubility, high stability at physiological pH and the quantum yield of its deprotection is high for good and mediocre leaving groups ( $\Phi_{\text{release}} \leq 1$ ). The structure has been introduced by Givens and Park.<sup>36,37</sup> It was derived from a 4-methoxyphenacyl PPG<sup>38</sup> which behaves analogous to the other members of the phenacyl protecting groups family ( $\beta$ -cleavage to form the phenacyl radical and subsequent hydrogen

abstraction leading to the corresponding acetophenone).<sup>39</sup> The 4-hydroxyphenacyl group exhibits a completely different photochemistry. The main photoproduct formed in aqueous solutions is 4-hydroxyphenylacetic acid (Figure 13, right side). The photoproduct does not absorb light of the wavelengths commonly used for deprotection of *p*HP (280 – 300 nm) and, therefore, it does not act as an internal filter. This enables to transform *p*HP with a quantitative conversion. The main drawback of the *p*HP PPG is the absorption maximum in the UVA region. Use of UVA light limits its *in vivo* applications because it can cause unwanted photochemical reactions in irradiated systems. A two-photon cleavage of *p*HP by a 532 nm laser may overcome this limitation.<sup>40</sup> Extension of the absorption of *p*HP to the edge of the visible region (~400 nm) is another possible approach which can be accomplished by installation of the methoxy groups to positions 3 and 5.<sup>41</sup>

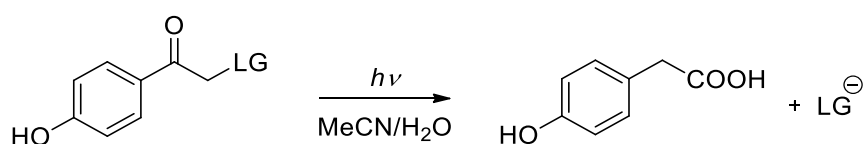


**Figure 13:** Schematic representation of photorelease of a leaving group (LG) from *p*HP-caged molecule

The 4-hydroxyphenacyl PPG has been used for protection of carboxylates,<sup>42,43</sup> phosphates,<sup>44</sup> sulfates and phenols.<sup>45</sup> Both *p*HP and its photoproduct are non-toxic and, therefore, *p*HP has been used as a cage for various biomolecules: ATP,<sup>46,47</sup> GABA,<sup>48</sup> glutamate<sup>42</sup> and oligopeptides.<sup>42,43,49</sup>

The mechanism of the deprotection of *p*HP is often called photo-Favorskii rearrangement because it resembles the Favorskii rearrangement.<sup>50</sup> Interestingly, the photochemical Favorskii rearrangement has been observed long before the *p*HP group was introduced as a PPG.<sup>51</sup> The mechanism was studied in detail, and the refined version is summarized in Figure 14.<sup>52</sup>

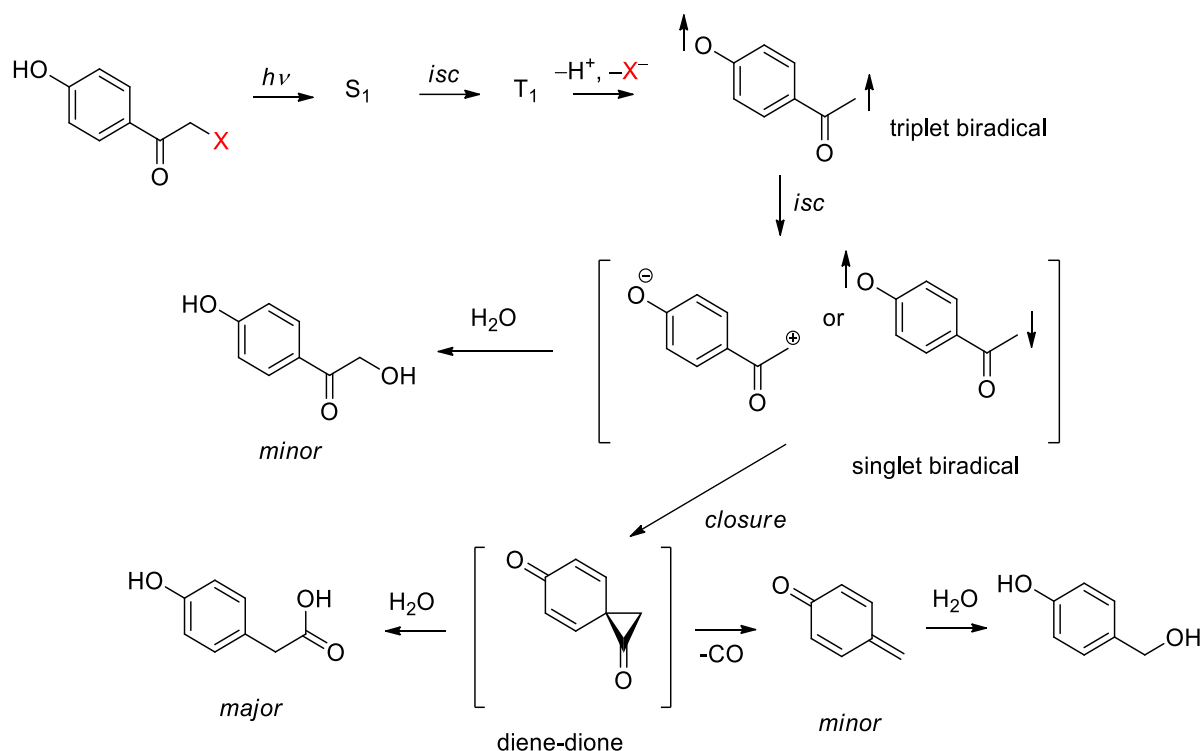


**Figure 14:** Mechanism of the deprotection of a *p*HP photoremovable protecting group.<sup>30,52</sup>

After excitation of *p*HP, a short-lived ( $\tau_S \sim 4$  ps) singlet state is formed. The triplet state ( $T_1$ ) is formed from the singlet by intersystem crossing. Also, the triplet state has a very short lifetime ( $\tau_T \sim 60$  ps) and forms triplet biradical by expelling a leaving group and hydroxyl proton (Figure 14, upper right corner). The rate of the leaving group departure depends strongly on the  $pK_a$  of the conjugated acid of the leaving group.<sup>53</sup> The release of a leaving group from the triplet state is mediated through at least two molecules of water.<sup>52,54,55</sup> The triplet biradical ( $\tau \sim 0.5$  ns) plays a pivotal role in the mechanism and its properties have been studied both experimentally and by quantum chemical calculations.<sup>56</sup> The triplet biradical undergoes an intersystem crossing to the singlet biradical (zwitterion) (Figure 14, middle row). This species is either captured by solvent (to form formally a product of hydrolysis) or cyclizes to the putative intermediate diene-dione. This spirocyclic derivative has a shorter lifetime than the triplet biradical ( $\tau < 0.5$  ns), decays faster than is formed, and therefore cannot be spectroscopically characterized. In water, it is attacked by a solvent molecule to form the photoproduct. A reaction pathway leading to the byproduct, 4-hydroxybenzyl alcohol, formed in minor amounts, includes decarbonylation and formation of the quinoid enol ( $\tau \sim 0.3$  s).

#### 2.2.4. Coumarinyl PPG

The coumarinyl PPG has been described in 1984 Givens and Matuszewski.<sup>57</sup> The (7-methoxycoumarin-4-ylmethyl) diethyl phosphate ester irradiated in methanol released free diethylphosphoric acid and formed a product of photosolvolysis, 4-methoxymethyl 7-methoxycoumarin (Figure 15). In later studies, Furuta has employed the procedure for caging

of carboxylic acids and has compared the photochemical properties of a coumarinylmethyl PPG with the known *o*-nitrobenzyl and desyl PPGs.<sup>58,59</sup>

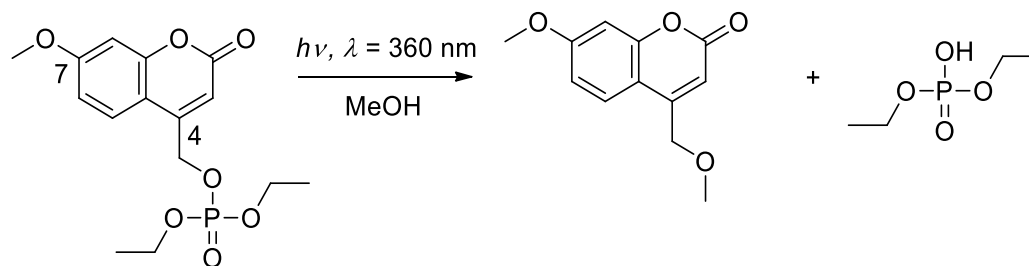


**Figure 15:** Photodeprotection of (7-Methoxycoumarin-4-yl methyl)phosphate ester

The molar absorption coefficients of the coumarinyl PPGs are high ( $\epsilon_{\max}$  typically in the range from 4 000 to 20 000  $\text{M}^{-1} \text{cm}^{-1}$ ), and their absorption maxima can be shifted to the visible region by a substitution. Commonly used coumarin derivatives have dialkylamino group in the position 7 of the coumarin moiety (7-diethylaminocoumarin-4-ylmethyl PPG, DEACM, Figure 16).<sup>30</sup> Their absorption maxima are near 400 nm which enables to use blue light for their deprotection. The two-photon cross sections of coumarinyl PPGs are usually high, and the quantum yields of deprotection are low to moderate (up to 0.25 for phosphates, 0.05 for acetate) as most of the excitation energy is lost by strong fluorescence.<sup>29,60</sup>

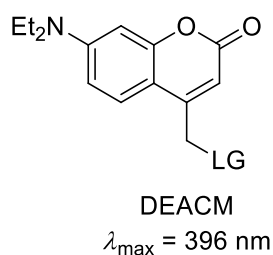


**Figure 16:** Structure of 7-diethylaminocoumarin-4-yl methyl PPG

Coumarin derivatives have been successfully used as PPGs for phosphates, carboxylates, carbonyls, alcohols, diols, amines, and sulfonates.<sup>28</sup> In biology, they have been used for caging of *cAMP*<sup>59</sup> and *mRNA*.<sup>61</sup>

The mechanism of the photodeprotection of coumarinyl PPG studied by Bendig *et al.*<sup>62-64</sup> is depicted in Figure 17. The first excited singlet state is formed after excitation of the coumarinylmethyl PPG. The leaving group is ejected from the singlet by a photo- $\text{S}_{\text{N}}1$  heterolytic bond cleavage which is most likely the rate-determining step of the photorelease ( $k_{\text{het}} \sim 10^9 \text{ s}^{-1}$ ). The formed intimate ion pair can either recombine to give the starting material (the most important energy non-emissive wasting pathway) or can be separated by nucleophilic solvent. The product of the photochemical deprotection is the product of formal solvolysis (Figure 17, bottom). The photoproduct often competes for irradiation light (internal filter effect) and, therefore, chemical yields of deprotection lower than 90% are often observed. An alternative mechanism is the homolytic bond fission forming the radical pair (Figure 17, top) which has also been suggested by observing a product of hydrogen abstraction [H] found as a minor photoproduct. The homolytic cleavage is in most cases not

significant because the recombination rate of the singlet radical pair is usually high. The reaction is facilitated in polar solvents which supports the photo-S<sub>N</sub>1 mechanism. The isotopic labeling experiments confirmed that the solvent attacks a 4-coumarinyl-methyl cation (Figure 17, middle part).

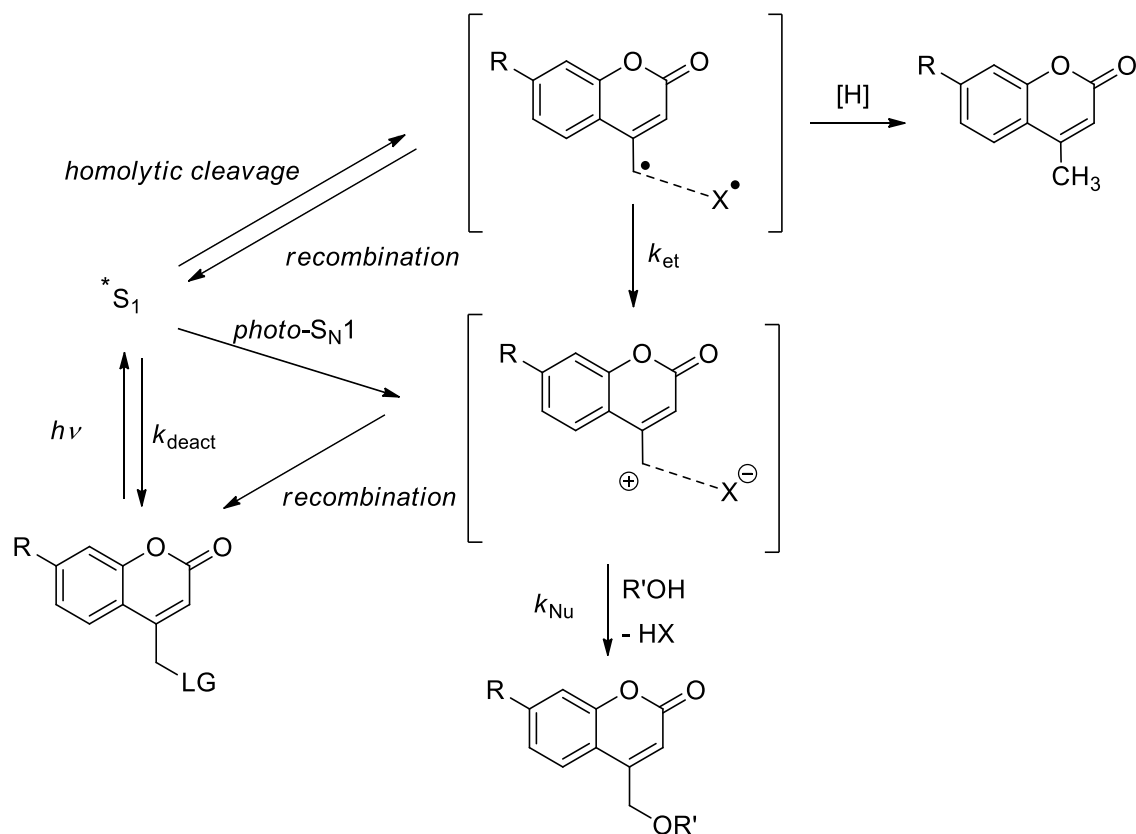


**Figure 17:** The mechanism of photodeprotection of coumarinyl PPG

### 2.2.5. Visible Light-Absorbing PPGs

The design of a visible light-absorbing PPG has always been a substantial challenge for photochemists. Classical PPGs were modified by different substituents in order to shift their absorption into the visible region, but the longest-wavelength-absorbing *p*HPs<sup>41</sup> and coumarins<sup>30</sup> absorb only up to 400 nm. Most of the known UV-absorbing PPGs have sufficient energy in the excited state (4 – 5 eV, Section 1.2) to break the chemical bond between PPG and the leaving group. The energy of visible-light photons is substantially lower (2 – 3 eV) and, therefore, other mechanisms have to be applied for the bond cleavage. The most common processes are intramolecular or intermolecular electron transfer and energy transfer.

The first attempts to design a visible-light-absorbing PPG were based on organometallic ruthenium complexes (Figure 18) used for caging of GABA.<sup>65-67</sup>



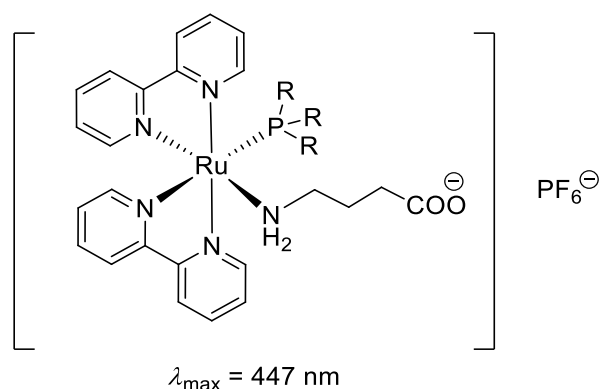


**Figure 18:** (*bis*(2,2'-Bipyridine-*N,N'*)tri-*R*-phosphine)-4-aminobutyric acid ruthenium hexafluorophosphate complex, *R* = Me, Ph

In our research group we have designed, synthesized, and characterized the first fully organic visible-light-absorbing PPG based on the xanthen chromophore (Figure 19).<sup>15</sup> The details about the synthesis, photophysical and photochemical properties are summarized in the chapter 3.1.

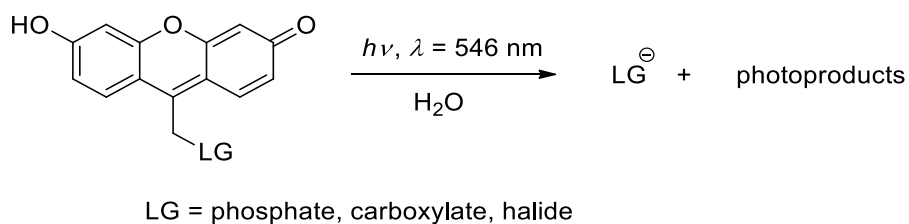


**Figure 19:** Xanthen-9-ylmethyl PPG

The introduction of xanthen-9-ylmethyl PPG in 2013 started a pursuit for PPGs based on dye chromophores. Commercial dyes have strong absorption of visible light but usually have been designed to be extremely stable towards photobleaching and other photoinduced reactions.<sup>68</sup>

First photoremovable protecting groups absorbing visible light were based on coumarins. A derivative of 7-diethylaminocoumarin-4-ylmethyl PPG, DEAC450 (Figure 20, left part), was prepared by Ellis-Davies *et al.* in 2013.<sup>69</sup> It has a strong absorption at 450 nm ( $\epsilon_{450} = 43\,000 \text{ M}^{-1} \text{ cm}^{-1}$ ) and was used to cage *c*AMP. The photodeprotection of *c*AMP occurs with exceptionally high quantum yield ( $\Phi = 0.78$ ).

The substitution of the carbonyl oxygen of a lactone functionality to sulfur leads to 7-diethylamino-4-thiocoumarinylmethyl PPG (tcOH, Figure 20, right part).<sup>70</sup> This derivative has even more red-shifted absorption ( $\lambda_{\max} = 470 \text{ nm}$ ) and has high molar absorption coefficient ( $\epsilon_{500} > 10\,000 \text{ M}^{-1} \text{ cm}^{-1}$ ) even at 500 nm. The quantum yield of leaving group release is  $\Phi \sim 5 \times 10^{-3}$ .

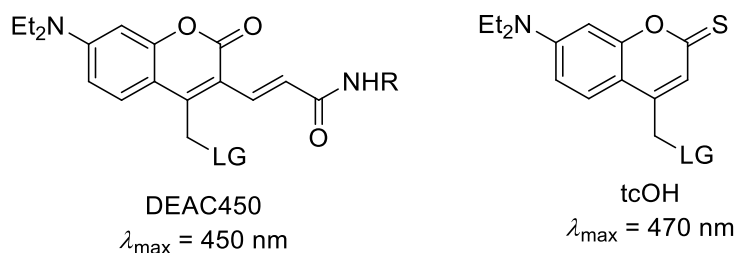


**Figure 20:** Visible-light-absorbing coumarinylmethyl PPGs

In 2014, Urano *et al.* designed a 4-aryloxyBODIPY-based PPG absorbing at 500 nm for protection of various electron-rich phenols<sup>71</sup> (Figure 21, left part). The mechanism of the deprotection includes photoinduced electron transfer from the electron rich aryl to the BODIPY moiety which is concomitantly cleaved. Histamine was caged by this methodology with substituted phenol as a linker. Further studies by Winter<sup>72</sup> and Weinstein<sup>73</sup> used *meso*-methyl BODIPY PPGs (Figure 21, right part). The absorption properties of these derivatives can be modulated by substitution and the absorption maximum reaches 550 nm. The mechanism of photodeprotection analogical to coumarinyl PPGs has been suggested by Winter. The photo-S<sub>N</sub>1 reaction heterolytically cleaves the bond between the leaving group and the BODIPY-*meso* methyl group, and the subsequent nucleophilic attack of the solvent to the *meso*-methyl cation leads to the product of photosolvolysis.

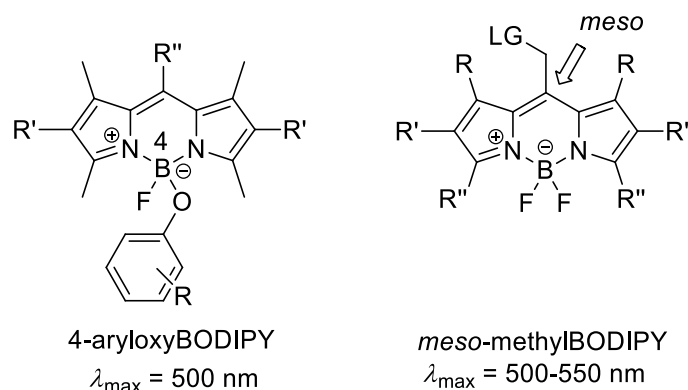


**Figure 21:** BODIPY-based photoremovable protecting groups

Very recently, the group of Schnermann has introduced a cyanine-based PPG (Figure 22) which is capable of cleavage in the near-IR region (690 nm).<sup>74</sup> The compound has been used as a photolabile linker for antibody-drug conjugates. The mechanism of the photodeprotection might be analogous to 4-aryloxyBODIPY derivatives. The excited cyanine core is reduced by photoinduced electron transfer from the amino group attached to the 4' position.

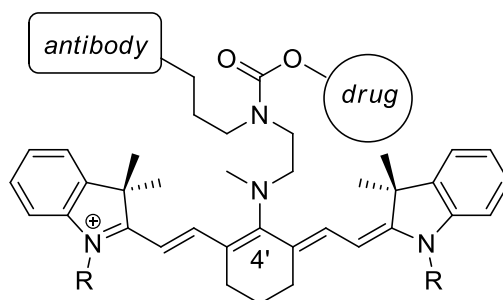


**Figure 22:** Cyanine-based PPG absorbing near-IR light

Photoremovable protecting groups have been rapidly developed over last 50 years. From the early investigations of photochemistry of “classical” protecting groups by Baltrop<sup>27</sup> to the work of Schnermann<sup>74</sup> many features have been optimized. The irradiation wavelengths have moved from deep UV to NIR, internal filter effect of photoproducts has been reduced, quantum and chemical yields of deprotection have raised. Nevertheless, there are still several issues to be solved in this field, such as unwanted singlet oxygen sensitization, phototoxicity, instability in presence of reactive oxygen species (ROS), low penetration through cell membranes, aggregation, DNA intercalation, and poor solubility.

## 2.3. Selected Visible-Light-Absorbing Dyes

### 2.3.1. Xanthene Dyes

Xanthene dyes are the most commonly used fluorescent dyes. Their application covers a broad spectrum of scientific fields, such as fluorescent microscopy,<sup>75</sup> dye lasers,<sup>76</sup> forensics,<sup>77</sup> optometry,<sup>78</sup> staining,<sup>79</sup> and dye tracing of rivers<sup>80</sup>.

Xanthene dyes are among the oldest synthetic dyes.<sup>81</sup> Fluorescein was prepared originally in 1871 by Baeyer<sup>82</sup> and since then, numerous derivatives have been synthesized. The common structural motif of all these derivatives is derived from xanthene, 10*H*-9-oxaanthracene (Figure 23). Xanthene dyes are sometimes derived from fluorine (xanthen-3-one). There are two basic families of xanthene dyes, fluorescein derivatives (with oxygen atoms attached to positions 3 and 6) and rhodamines (with nitrogen atoms attached to positions 3 and 6).

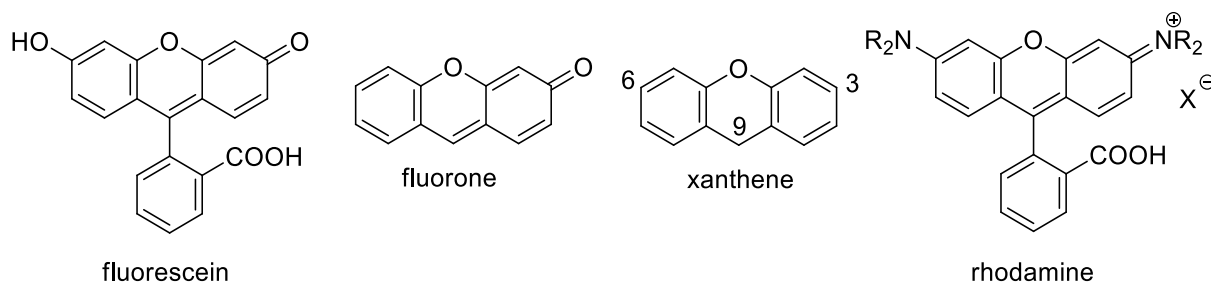


**Figure 23:** General structures of xanthene derivatives

Two subgroups of fluorescein derivatives can be distinguished. Fluorescein derivatives with substitution on the xanthene moiety (type I) and derivatives with substitution on the phenyl ring (type II) differ significantly by their photophysical properties. All type II derivatives exhibit roughly the same absorption and emission and their substitution is related to the application of the particular structure.

The substitution of type I derivatives strongly influences the position of absorption and emission maxima (LUMO localized more on the xanthene moiety is more affected than HOMO localized more on the aryl part)<sup>83</sup> and the quantum yields of fluorescence and of intersystem crossing (heavy atom effect of the substituents induces the intersystem crossing by enhanced spin orbit coupling).<sup>84</sup>

The most common type I derivatives are summarized in Figure 24. Fluorinated derivatives, Pennsylvania green and Oregon green, were developed for biological applications as fluorescent imaging agents sensitive to intracellular pH. Their different polarity enables selective staining of biomembranes.<sup>85</sup>

Brominated fluorescein is called eosin according to the ancient Greek goddess of the dawn.<sup>86</sup> Two well-spread types of eosin are both red dyes. Eosin Y (yellowish cast) and eosin B (bluish cast) differ in absorption and emission properties. While eosin Y absorbs at 525 nm and strongly emits at 543 nm ( $\Phi_{fl} = 0.2$  in aqueous solution),<sup>87</sup> eosin B absorbs at 520 nm and emits at 580 nm with a low fluorescence quantum yield ( $\Phi_{fl} = 0.045$  in aqueous solution).<sup>88</sup> Dyes of the eosin type display so called E-type delayed fluorescence. It is the process in which the first excited singlet state becomes populated by a thermally activated radiationless transition (back intersystem crossing) from the first excited triplet state. Since the population of the singlet and triplet state is in thermal equilibrium, the lifetime of delayed E-type fluorescence equals to the lifetime of phosphorescence.<sup>17</sup> Eosin is commonly used in histology for tissue staining<sup>89</sup> and in photoredox catalysis as a substitute for expensive ruthenium photocatalysts (Chapter 6.3).<sup>90</sup>

Iodine-substituted xanthene derivatives, erythrosine and rose bengal (Figure 24), exhibit only negligible fluorescence ( $\Phi_{fl} = 0.11$  for rose bengal<sup>91</sup> and  $\Phi_{fl} = 0.05$  for erythrosine<sup>92</sup>). This is caused by the heavy-atom effect of iodine atoms which facilitates the intersystem crossing to the triplet state. High yields of triplet are used for singlet oxygen production in chemistry<sup>21</sup> and biology.<sup>22</sup>

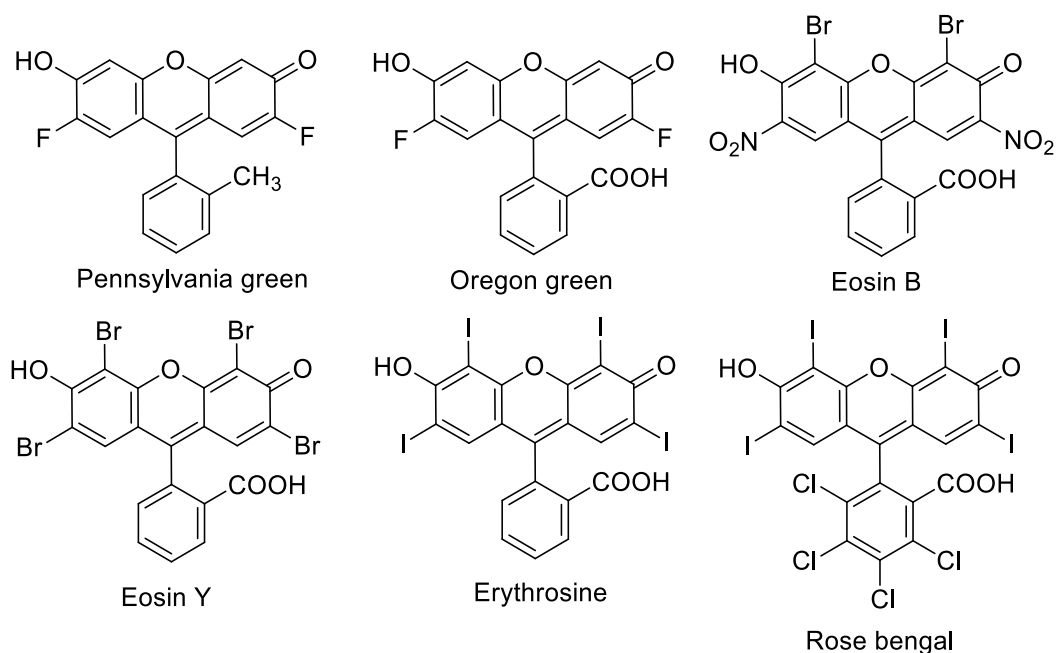


**Figure 24:** Halogen substituted xanthene dyes

Most of xanthene dyes have aryl substituent attached to the C-9 position. So far, only a limited number of compounds having a different substituent, such as cyano,<sup>93-96</sup> trifluoromethyl,<sup>95</sup> alkyl,<sup>97,98</sup> or alkenyl<sup>99</sup> groups, have been synthesized.

Our group has recently developed three types of rhodamine analogues with non-aromatic substituent in the C-9 position. The 1,3-dithian-2-yl derivatives of a 6-amino-3*H*-xanthen-3-iminium moiety (Figure 25, left side) are capable of carbon-carbon bond cleavage induced by yellow light.<sup>100</sup> The 9-phenylethynylpyronin analogues (Figure 25, middle) were used as fluorescent probes emitting in near-infrared region (705–738 nm) suitable for mitochondria in myeloma cells.<sup>101</sup> The 9-iminopyronin analogues (Figure 25, right side) were introduced as clickable fluorophores with large Stokes shift (~200 nm).<sup>102</sup>

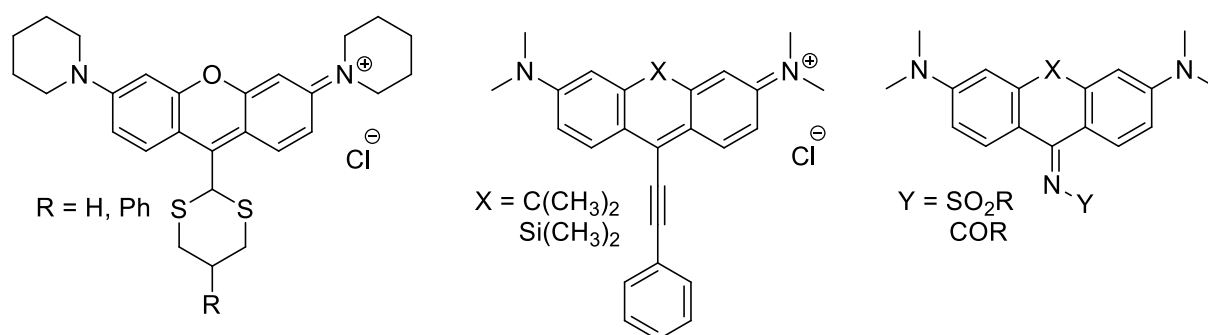


**Figure 25:** 1,3-Dithian-2-yl derivatives of a 6-amino-3*H*-xanthen-3-iminium moiety (left), 9-phenylethynylpyronin analogues (middle) and 9-iminopyronin analogues (right)

### 2.3.2. Acridine Dyes

Acridine dyes are fluorescent dyes based on the acridine, 10-azaanthracene, structure (Figure 26). Their color ranges from yellow to red and they have been used as pigments.<sup>103</sup> Industrial staining by acridine dyes has been abandoned because of their photobleaching.<sup>104</sup> Acridines are weakly basic ( $pK_a$  of proflavine conjugated acid is 9.5) and at physiological pH (pH = 7.4), the nitrogen atom in the position 10 is protonated. Acridine has been studied for its ability to intercalate DNA.<sup>105</sup> Proflavine (3,6-diaminoacridine, Figure 26) has antibacterial properties and has been used as topical antiseptics.<sup>106</sup> It intercalates DNA strongly which induces the change in the emission spectrum of proflavine. Due to this fact, proflavine was used as a model compound for studying the DNA intercalation mechanism.<sup>107</sup> It is not used as a pigment because of its mutagenicity.<sup>108</sup> Acridine yellow is used in nonlinear optics,<sup>109</sup> and acridine orange is used as a selective stain for DNA in living cells.<sup>110</sup> Other acridine dyes are often used in biology and medicine (e. g. acriflavinium chloride as antiseptic agent,<sup>111</sup> GelGreen<sup>TM</sup> as nucleic acid stain,<sup>112</sup> or amsacrine as antineoplastic agent.<sup>113</sup>

The 9-mesityl-10-methylacridinium perchlorate has been synthesized in 2004 by Fukuzumi's group.<sup>114</sup> In its excited state it is a very strong oxidant and therefore it is broadly used in photocatalysis (Chapter 6.3).

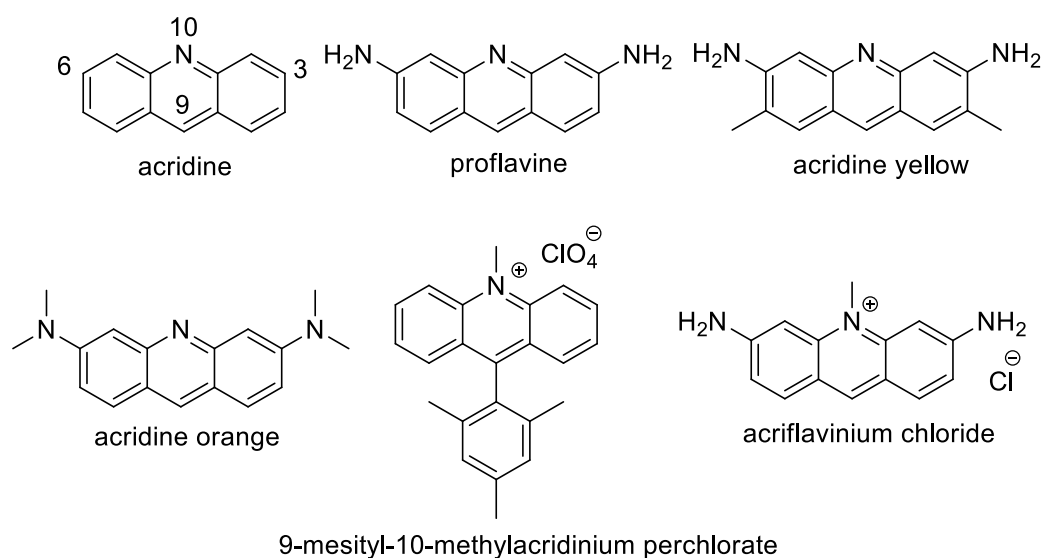


**Figure 26:** Common acridine derivatives

### 2.3.3. BODIPY Dyes

Boron-dipyrromethene (4,4-difluoro-4-bora-3a,4a-diaza-*s*-indacene, BODIPY, Figure 27) fluorescent dyes represent structural analogues of porphyrins. The first synthesis of BODIPY dyes was published by Treibs and Kreuzer in 1968.<sup>115</sup> Since the mid-1980s, BODIPYs were investigated as promising laser dyes.<sup>116</sup> BODIPY derivatives subsequently started to be used as fluorescent stains and labels in fluorescence imaging,<sup>117</sup> and as indicator dyes in sensor

applications.<sup>118</sup> In recent years, the number of publications being published on the synthesis and properties of BODIPY dyes has grown rapidly.<sup>119</sup> This fact has been related to their facile synthesis and structural versatility, and their excellent spectroscopic properties. They have been used in numerous research fields, such as photodynamic therapy<sup>120</sup>, polymer chemistry<sup>121</sup>, OLEDs<sup>122</sup> or fluorescent labeling.<sup>123</sup> The chemistry and properties of BODIPY derivatives has been a subject of many reviews.<sup>118,119,124-129</sup>

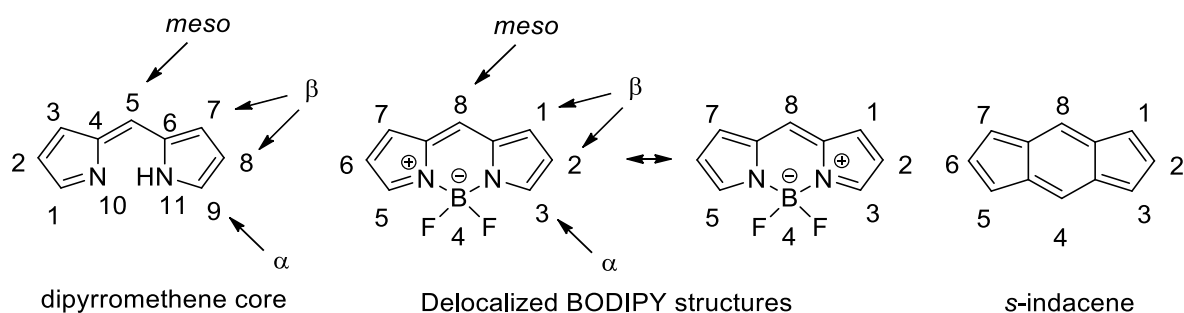


**Figure 27:** Structures and IUPAC numbering of dipyrromethene, BODIPY and *s*-indacene

BODIPY derivatives have unique photophysical properties. Their absorption and emission bands are narrow and molar absorption coefficients are high ( $\epsilon > 80\,000\text{ M}^{-1}\text{ cm}^{-1}$ ). Stokes shifts are usually very small ( $\sim 800\text{ cm}^{-1}$ ) and quantum yields of fluorescence are high ( $> 0.5$ ). Moderate redox potentials and negligible triplet-state formation result in excellent thermal and photochemical stability. Negligible sensitivity to solvent polarity and high solubility in commonly used organic solvents of different polarities are other properties useful for various applications.

The unique properties of BODIPY dyes can be attributed to extremely high rigidity of the BODIPY core. The complexation of dipyrromethene unit to boron trifluoride leads to a formation of a dipyrrometheneboron difluoride structure (Figure 27), which can be considered as being an example of a “rigidified” monomethine cyanine dye.<sup>118</sup> Cyanine dyes undergo *trans*–*cis* isomerization upon electronic excitation, which quenches their fluorescence.<sup>130</sup> BODIPY is stabilized by the bridging  $\text{BF}_2$  unit and has high oscillator strength of the transition from  $S_0$  to  $S_1$  and of the corresponding emission. It also has very low probability for vibrational relaxation processes which explains high  $\epsilon$  and  $\Phi_{\text{fl}}$ . Methyl group in the *meso* position further planarizes the BODIPY and enhances the fluorescence quantum yield. Unsymmetrically substituted BODIPY derivatives have lower oscillator strength because of the broken molecular symmetry. The potential energy surfaces of the  $S_0$  and  $S_1$  states are very similar, so narrow Gaussian-shaped absorption and emission bands are typically observed for the lowest energy transitions.<sup>128</sup>

Enormous number of BODIPY derivatives has been prepared in last 45 years. The reason for that is their very simple synthesis and derivatization. The synthesis usually starts by an acid-catalyzed condensation reaction of a properly-substituted pyrrole with an aldehyde or acyl chloride (Figure 28). The subsequent oxidation (by electron-deficient quinones, *e.g.* DDQ, fluoranil, chloranil) is required only in case of aldehyde condensation. Since dipyrromethene is usually unstable, it is subjected to a cyclization with a boron-based reagent (usually  $\text{BF}_3 \cdot \text{Et}_2\text{O}$ ) in basic media to obtain a BODIPY structure.

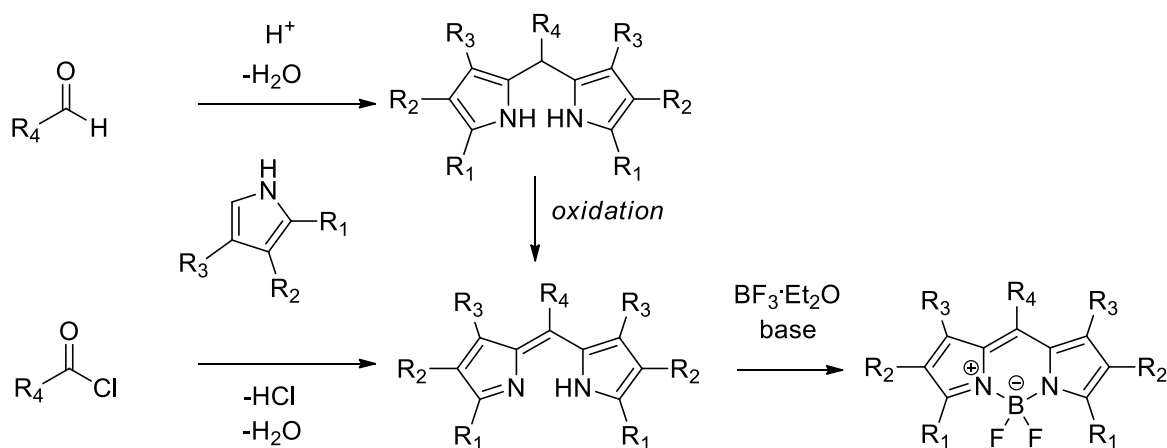


**Figure 28:** Typical synthesis of BODIPY dyes, taken from ref. 118.

Usually the starting pyrrole has methyl substituents which enhance the yield of condensation and the photostability of the resulting BODIPY derivatives. Methyl groups in the positions 1,3,5, and 7 enhance the stability of the molecule towards nucleophilic and solvolytic reactions. The methyl groups are slightly acidic and can be used for further derivatization (*e. g.* Knoevenagel condensation).<sup>118,131</sup> A substituent in the position 4 is installed in the condensation reaction (Figure 28) using a proper aldehyde or acyl chloride. The positions 2 and 6 are prone to electrophilic substitution (NIS, NBS, NCS and electrophiles),<sup>132</sup> whereas halogen atoms in the positions 3 and 5 can be displaced by a metal-catalyzed cross coupling reaction<sup>133</sup> or by nucleophilic substitution.<sup>134</sup> One or both fluorine atoms can be nucleophilically substituted by alkoxides<sup>135</sup>, aryl<sup>136</sup> or alkynyl<sup>137</sup> lithium and magnesium bromides.

Many attempts to improve desired properties of BODIPY by making their analogues have been described in last decades. The first obvious possibility for synthesis of analogues is the substitution of BF<sub>2</sub> unit to any other atom. Examples with substituted Co, Fe, Sn, Si, Pd, Cu, Ni, Zn and P (PODIPY, Figure 29) in the position 4 have been reported.<sup>138</sup> The substitution of the methylene unit in *meso* position leads to aza-BODIPY (Figure 29).<sup>139</sup> Extended BODIPY derivatives have 6-membered rings instead of pyrroles (Figure 29).<sup>140,141</sup> The ease of synthesis and derivatization enables to prepare “tailor-made” fluorescent tags which would be especially designed for particular biological application.

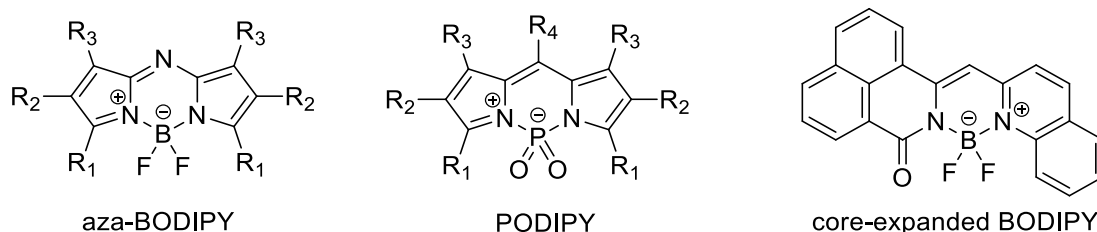


**Figure 29:** Examples of BODIPY analogues

The products of Knoevenagel condensation and cross-coupling reactions extend the absorption and emission of BODIPYs to the red and NIR part of the spectrum. A lot of NIR-



absorbing dyes have been synthesized for biological applications. Their preparation and properties were summarized by Shen *et al.* in 2014.<sup>129</sup> Some of the NIR-absorbing BODIPY derivatives with their  $\lambda_{\max}$  are shown in Figure 30.

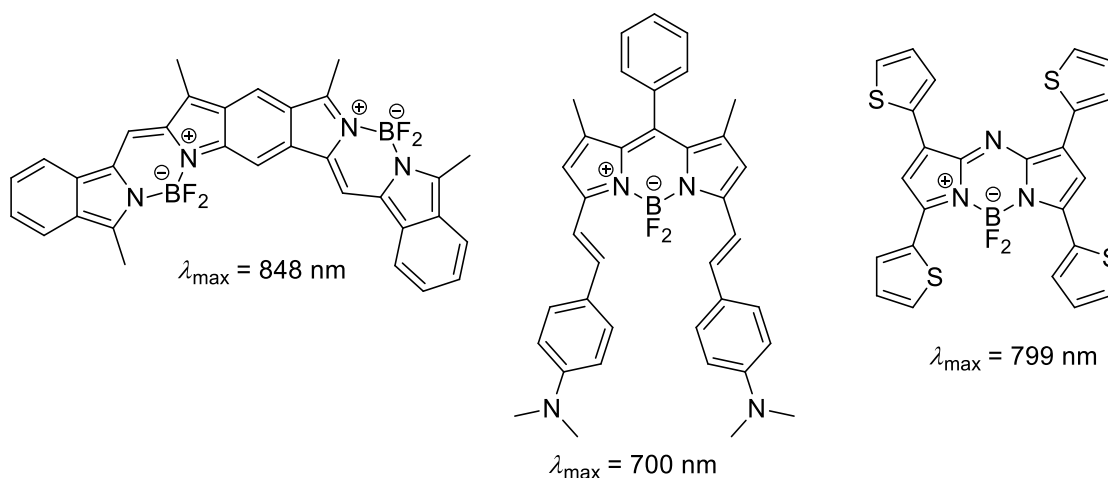


**Figure 30:** Selected NIR-absorbing BODIPYs; taken from Shen *et al.*<sup>129</sup>

We have designed a new class of BODIPY derivatives which have heavy atom attached directly to the BODIPY core and can be used as potential triplet sensitizers. Their synthesis and photophysical properties are discussed in Chapter 3.8.

## 2.4. Caged Ions and Small Molecules

### 2.4.1. Introduction

Ions play important role in the regulatory processes of organisms. The membrane potential based on the equilibrium of sodium and potassium ions governed by a  $\text{Na}^+/\text{K}^+$  pump is essential for neural function.<sup>142</sup> Ferrous ions in heme transport molecular oxygen in blood,<sup>143</sup> and manganese ions are responsible for photosynthesis.<sup>144</sup> Calcium cations regulate many biological functions by binding to proteins with carboxylic functionality in the side chain (*e. g.* glutamate residues).<sup>145</sup> This process changes the tertiary structure proteins and can cause many different effects (blood coagulation, modulation of muscle activity, apoptosis, gene expression).<sup>146-148</sup>

Recent studies revealed that small gaseous molecules have also numerous biological functions. Three known biological regulatory gases are: carbon monoxide (CO, see chapter 4.3), hydrogen sulfide ( $\text{H}_2\text{S}$ ) and nitric oxide (NO). All three gases are toxic for organisms in relatively low concentrations.  $\text{LC}_{50}$  values for rats after 4 hour exposure are following: 1784 ppm (CO), 444 ppm ( $\text{H}_2\text{S}$ ), 854 ppm (NO).<sup>149</sup> The biogenic concentrations of these gases are much lower (their concentrations are specific for given tissues).

Hydrogen sulfide ( $\text{H}_2\text{S}$ ) has vasodilatory effect in smooth muscle tissue<sup>150</sup> and acts as a neuromodulator.<sup>151</sup> It is biogenically produced from cysteine by cystathionine beta-synthase and cystathionine gamma-lyase.<sup>152,153</sup> It is recognized as a potentially cardioprotective agent

which activates the ATP-sensitive potassium channels in smooth myocytes.<sup>154</sup> One of the natural sources of biogenic H<sub>2</sub>S is allicin (Figure 31) which is responsible for the flavor and scent of garlic.<sup>155</sup> It is catabolized to hydrogen sulfide and has cardioprotective properties.<sup>150</sup> A synthetic analogue of allicin, diallyltrisulfide (DATS), is used in H<sub>2</sub>S therapy for patients with acute myocardial infarction.<sup>156</sup> H<sub>2</sub>S is mainly responsible for dilatation of small vessels, whereas NO relaxes larger vessels.<sup>157</sup>

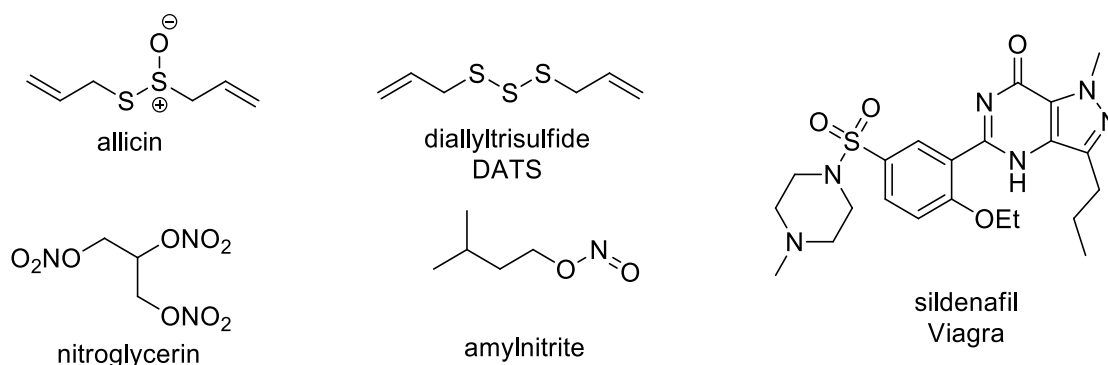


**Figure 31:** Pharmaceutical analogues of H<sub>2</sub>S and NO and the structure of sildenafil

Nitric oxide (NO) has similar biological effects as hydrogen sulfide. It is a well-known vasodilator<sup>158</sup>, redox signaling long-range neurotransmitter<sup>159</sup>, skin natural fungicide<sup>160</sup>, and regulator of cardiac contractility.<sup>161</sup> Macrophages use NO as a bactericide,<sup>162</sup> but, ironically, some bacteria use it as a cofactor for DNA-repairing enzymes.<sup>163</sup>

NO is biochemically produced from L-arginine by nitric oxide synthase (Figure 32).<sup>164</sup> Pharmaceutical analogues of NO are nitroglycerin and amyl nitrite (Figure 31) which are *in vivo* catabolically transformed to NO.<sup>165</sup> The biochemical mechanism of vasodilatory effect of NO has been studied in detail. Ferid Murad, Robert F. Furchgott, and Louis Ignarro won the Nobel Prize in Physiology and Medicine in 1998 for the discovery of signalling properties of NO.<sup>166</sup> Biogenic NO coordinates to ferrous ion in the heme-part of the enzyme (soluble) guanylate cyclase.<sup>167</sup> The enzyme gets activated and transforms guanosine triphosphate (GTP) to cyclic guanosine monophosphate (*c*GMP). *c*GMP causes vasodilation of blood vessels.<sup>168</sup> The concentration of *c*GMP is regulated by phosphodiesterase PDE-5 (Figure 32) which hydrolyzes *c*GMP to guanosine monophosphate (GMP).<sup>169</sup> In case of low activity of nitric oxide synthase or exaggerated activity of PDE-5, the concentration of *c*GMP is low and therefore a smooth muscular tissue cannot relax. This occurs in case of erectile dysfunction when the blood vessels supplying the *corpus cavernosum* are permanently contracted. Sildenafil (Viagra<sup>TM</sup>, Figure 31), a famous pharmaceutical drug for the treatment of erectile dysfunction, competitively inhibits the activity of PDE-5 and thus increases the concentration of *c*GMP.<sup>170</sup> Sildenafil is removed from body by catabolic oxidative processes by cytochrome P450 in hepatocytes.<sup>171</sup>

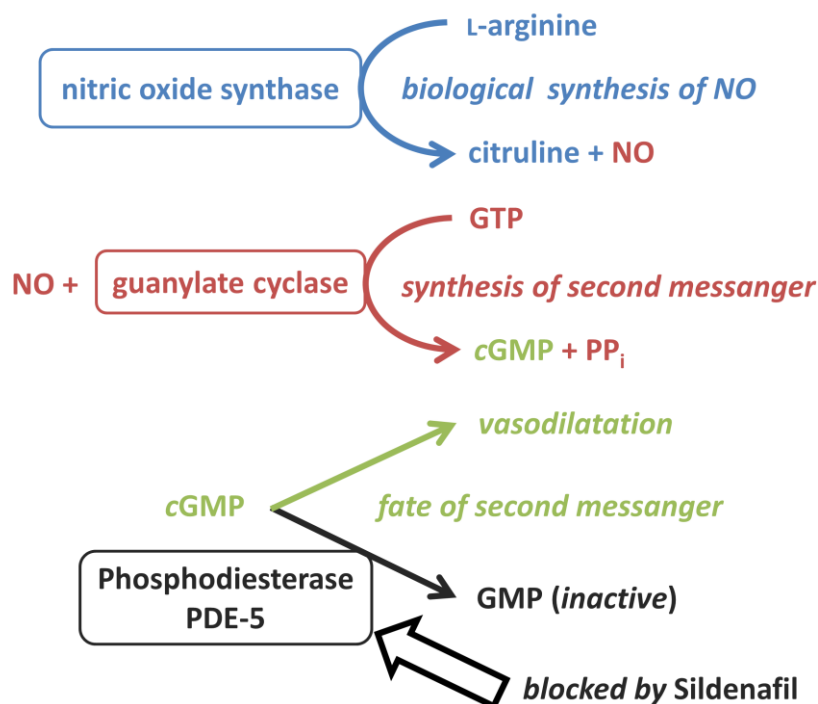


**Figure 32:** Biochemical mechanism of NO production and the regulation of vasodilatation with depiction of the effect of sildenafil, PP<sub>i</sub> = diphosphate

### 2.4.2. Fluoride Anion

Fluoride anion is a conjugate base to hydrofluoric acid. HF is a weak acid ( $pK_a = 3.2$ )<sup>172</sup> well known for its ability to etch silicon and glass surfaces.<sup>173</sup> Biogenic fluoride plays a key factor in growth of mammal hard tissues, such as teeth and bones.<sup>174</sup> Fluoride is therefore used in dental medicine applications as fluoride-releasing restorative materials.<sup>175</sup> Fluoride induces remineralization of acid-soluble hydroxyapatite by transforming it to insoluble fluoroapatite.<sup>176</sup> This mechanism protects teeth from dental caries and strengthens bones. Some countries (*e. g.* USA) have decided to artificially increase the concentration of fluoride in drinking water in order to fight with dental caries. The numbers of dental problems has indeed dropped significantly but some other health issues started to be more frequent. Especially in regions with high natural abundance of fluoride in drinking water ( $\sim 2.0 \text{ mg dm}^{-3}$ ) many patients with gastrointestinal problems have been hospitalized.<sup>177</sup> It was also found that high levels of fluoride may adversely affect neurodevelopment and intelligence of children<sup>178</sup>, can cause dental fluorosis<sup>179</sup> and that increased concentration of fluoride in human blood serum is nephrotoxic.<sup>180</sup> Despite all these facts, many countries still continue to artificially increase fluoride levels in drinking water, though to lower concentrations (up to  $0.7 \text{ mg dm}^{-3}$  which is considered by U.S. Food and Drug Administration agency to be a safe level).<sup>181</sup> Adding fluoride to toothpastes turned up to be the best and safest solution for controlled fluoride uptake. Fluoride ions from toothpaste are not swallowed and affect only dental tissue.<sup>182</sup>

Biogenic fluoride can significantly affect cell metabolism. In recent years, several investigations demonstrated that fluoride can induce oxidative stress and modulate intracellular redox homeostasis, lipid peroxidation, protein carbonyl content, as well as alter gene expression and cause apoptosis.<sup>183</sup> Recently<sup>184</sup>, fluoride has been recognized as a key component in fluoride-selective riboswitches, non-coding RNAs whose sensing domains bind small ligands and whose adjacent expression platforms contain RNA elements involved in the control of gene regulation.

We have synthesized a novel caged fluoride based on *p*HP PPG. Its synthesis and properties are summarized in the practical part of this thesis in Chapter 3.2.

### **2.4.3. Carbon Monoxide**

Carbon monoxide is a well-known toxic gas. It is dangerous because of its intrinsic high affinity for hemoglobin to form carboxyhemoglobin, which, at concentrations of 30% and above, can severely compromise oxygen delivery to tissues and consequently impair mitochondrial respiration.<sup>185</sup> It binds to hemoglobin approximately 220 times stronger than oxygen.<sup>186</sup> However, it is now evident that CO, in cellular concentrations ranging from 10 to 250 ppm, is an important tissue-protecting agent with substantial vasodilatory, anti-inflammatory, antiproliferative and anti-apoptotic effects.<sup>187-191</sup>

Verma *et al.* demonstrated that CO acts as a neurotransmitter by activation of soluble guanylate cyclase.<sup>192</sup> Similar to NO, carbon monoxide can influence the concentration of cGMP. CO is now known to influence both intra- and extra-cellular signaling.<sup>193</sup>

Endogenous CO is produced by the enzyme heme oxygenase.<sup>194</sup> Heme oxygenase induces an NADPH-dependent oxidative breakdown of heme to biliverdin, ferrous ion and carbon monoxide. Cellular stress induced by proliferation or inflammation increases the expression of heme oxygenase. This enhances the production of CO which is stored as carboxyhemoglobin. CO can then bind to other enzymes, predominantly to heme proteins, which can decrease inflammatory signaling.<sup>195</sup>

Unlike H<sub>2</sub>S or NO, no pharmaceutical agents delivering carbon monoxide are available. The direct way of CO delivery to the organism is the inhalation of air enriched with CO.<sup>196</sup> Various carbon monoxide releasing molecules (CORM) have been developed to deliver CO into the cell,<sup>197-202</sup> but none of them is used for therapeutic purposes. The most important criteria for designing CORMs are their chemical stability as well as aqueous solubility, temporal control over the CO release and low toxicity in their *in vivo* applications. CO is a stable and inert molecule (unlike NO or H<sub>2</sub>S) that reacts only with transition metals.<sup>203</sup> Thus, with a few exceptions, (boranocarbonates<sup>204</sup> or an interesting “click and release” prodrug system<sup>205</sup>), the only existing CORMs are metal-carbonyl complexes.<sup>132-136,206</sup> The most common activation of CO release from these compounds is hydrolysis in aqueous media that starts immediately upon CORM dissolution. Half-lives of CO in solution are usually low (minutes).<sup>207</sup> One of the common CORM derivatives used in many biological studies is ruthenium-based CORM-3 (Figure 33).<sup>208</sup> The release of CO *in vivo* can be monitored by head-space analysis,<sup>209</sup> determination of the concentration of carboxyhemoglobin<sup>210</sup> or by fluorescent probes.<sup>211</sup>

Light-triggered CO liberation from a photochemically active CORM (photoCORM<sup>212</sup>, Figure 33<sup>213</sup>) is an activation strategy alternative to simple hydrolysis. It allows a precise spatial and temporal control over the CO release.<sup>214</sup> Transition metal-based complexes offer a relatively good flexibility and diversity in terms of their chemical composition and release efficiencies,<sup>132,135,215</sup> however, only a few such photoCORMs, e.g. polypyridyl metallodendrimers,<sup>216</sup> Mn-complexes of azaheteroaromatic ligands<sup>217</sup> or azopyridine,<sup>218,219</sup> absorb biologically benign visible light. CO release upon irradiation with 980 nm from a Mn-based nanocarrier *via* upconversion has also been recently shown.<sup>220</sup>

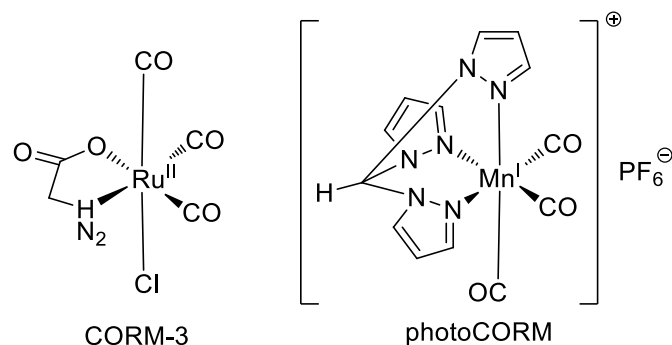


**Figure 33:** Structures of metal-carbonyl CORM-3<sup>143</sup> and photoCORM<sup>148</sup>

PhotoCORMs based on organic compounds might overcome common limitations of metalorganic CORMs (*e.g.* stability, solubility, toxicity, bioaccumulation). Several examples of organic molecules, such as cyclopropanones,<sup>221-224</sup> 1,3-cyclobutanediones,<sup>225</sup> or 1,2-dioxolane-3,5-diones,<sup>226</sup> liberate CO upon biologically adverse UV or near-UV (< 420 nm) light. Only a few purely organic photoCORMs can be activated by visible light. Liao and coworkers have developed a system based on a cyclic aromatic  $\alpha$ -diketone chromophore that liberates CO upon irradiation with light below  $\sim 500$  nm (Figure 34, left).<sup>227</sup> The molar absorption coefficients of such chromophores are however relatively low (only  $\sim 1000$  dm<sup>3</sup> mol<sup>-1</sup> cm<sup>-1</sup> at 458 nm<sup>228</sup>). We have developed a fluorescein analogue, 6-hydroxy-3-oxo-3*H*-xanthene-9-carboxylic acid (Figure 34, middle) and a BODIPY-based carboxylic acid (Figure 34, right) as fully organic visible-light absorbing photoCORMs. Their preparation and photophysical properties as well as the mechanism of CO liberation will be discussed in Chapters 3.3. and 3.4.

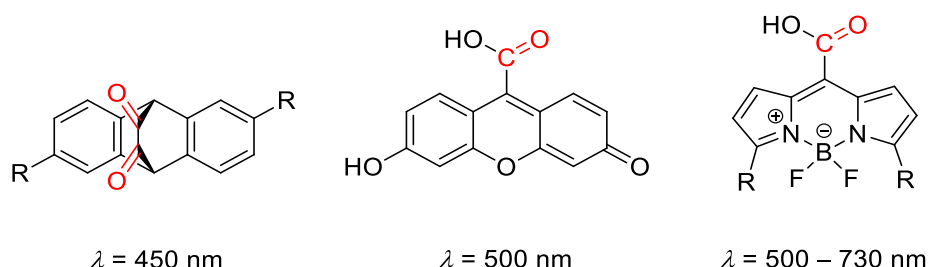


**Figure 34:** Fully organic photoCORMs based on cyclic aromatic  $\alpha$ -diketone (left), xanthene (middle) and BODIPY (right) chromophores. The irradiation wavelength needed for release of CO is shown below the structures.

## 2.5. Photocatalysis

### 2.5.1. Introduction

The previous parts have been focused on the description of photoactivatable compounds which are cleaved in a defined way upon absorption of a photon to release a leaving group. Also some chromophores as well as interesting leaving groups relevant for this thesis have been summarized. Another class of photoactivatable compounds are catalysts used in photocatalysis. Photocatalysis uses light to drive chemical redox reactions.<sup>229</sup> The molecular entity of photocatalysts does not change after excitation. Photocatalysts undergo a photoinduced electron transfer (PeT, Chapter 2.2)<sup>230</sup> with a substrate and after another electron is transferred, they are regenerated to its initial oxidation state. There are three main fields in photocatalysis: artificial photosynthesis, water splitting and synthetic photocatalysis.

Nature uses photocatalytic approach in photosynthesis. Chlorophyll (photocatalyst) and a group of redox cofactors (electron mediators) resemble many known photocatalytic systems. The direct outputs of the light-dependent reactions in a photosynthetic system are: (i) proton gradient (which drives enzyme ATP synthase that produces ATP), (ii) molecular oxygen, (iii) reduced co-factor NADPH (reduced nicotinamide adenine dinucleotide phosphate).<sup>231</sup>

In 2014, Park and coworkers introduced an example of artificial photosynthetic system that generates NADPH from  $\text{NADP}^+$  by visible light with water as an electron donor.<sup>232</sup> This a rather complicated process includes four electron transfer (eT) processes. The redox potential of each component is sufficient for reduction of the subsequent reaction partner. The excited light-harvesting photocatalyst ( $[\text{Ru}(\text{bpy})_3]^{2+}$ ) reduces a rhodium mediator ( $[\text{Cp}^*\text{Rh}(\text{bpy})(\text{H}_2\text{O})]^{2+}$ ) by a photoinduced electron transfer. The oxidized photocatalyst,  $[\text{Ru}(\text{bpy})_3]^{3+}$ , is regenerated by tetra-cobalt polyoxometalate, a water-splitting catalyst. The reduced mediator is re-oxidized by reaction with  $\text{NADP}^+$  which produces NADPH. NADPH drives a model redox enzyme, glutamate dehydrogenase, which transforms 2-ketoglutarate to L-glutamate by reductive amination.

Photocatalytic water splitting (photochemical production of gaseous oxygen and hydrogen from water by visible light) is also often called artificial photosynthesis.<sup>233</sup> Development of a long-lasting (many turnovers) photocatalytic system capable of water splitting to  $\text{O}_2$  and  $\text{H}_2$  is of a great economical interest and enormous amount of researchers are investigating this field. Despite many significant successes, mainly in water reduction of  $\text{H}_2$ ,<sup>234</sup> practically no useful system has been developed so far.<sup>235</sup> The main issue is photostability of the photocatalyst for water oxidation half-reaction. The photocatalyst is in strongly oxidizing environment which diminishes its lifetime due to photobleaching.<sup>236</sup> Due to this fact, mainly heterogenous and inorganic photocatalysts resistant towards photobleaching are used.<sup>237</sup> Organic photocatalysts can be protected from any unwanted photoreactivity by encapsulation into supramolecular hosts.<sup>238</sup> Another issue of water splitting is the separation of both half reactions (water oxidation and water reduction) by a method where electrons can flow between both systems which is required for maintaining the electroneutrality.<sup>239</sup>

Photocatalysis is also broadly used in organic synthesis and enables to perform novel synthetic transformations (C-H activation, redox reactions, coupling reactions, thermally-forbidden cycloadditions, radical reactions).<sup>240,241</sup>

### 2.5.2. Principles of Photocatalysis

The molecule of a photocatalyst upon excitation is simultaneously a stronger reductant and oxidant (Chapter 1.2). The gain in electrochemical potential for both oxidation and reduction equals to the excitation energy of the photocatalytically active excited state (Figure 3). Due to its short lifetime (ps to ns), the singlet state is often inactive in PeT processes. The triplet state (lifetime of  $\mu\text{s}$  to ms) often reacts more efficiently.<sup>242</sup> The photocatalyst can be used for both reduction and oxidation reactions. Moreover, one can distinguish systems where the photocatalyst gets reduced by PeT (reductive quenching cycle, Figure 35, left part) and systems where the excited photocatalyst gives an electron to the oxidant (oxidative quenching cycle, Figure 35, right part). In both cases the reduced (oxidized) photocatalyst is regenerated back by a ground-state electron transfer with an oxidant (reductant) (Figure 35, bottom). In principle, all four reactions can be productive and can lead to a desired product. If only one half-reaction is productive (either PeT or ground-state eT), the reaction partner in the other electron transfer process is called the sacrificial electron donor (acceptor).<sup>243,244</sup> The PeT process is limited by the lifetime of the excited state of the photocatalyst, whereas the ground-state electron transfer is governed only by the corresponding redox potentials of both reaction partners and their concentrations (pseudo-first order quenching is often considered).<sup>245</sup>

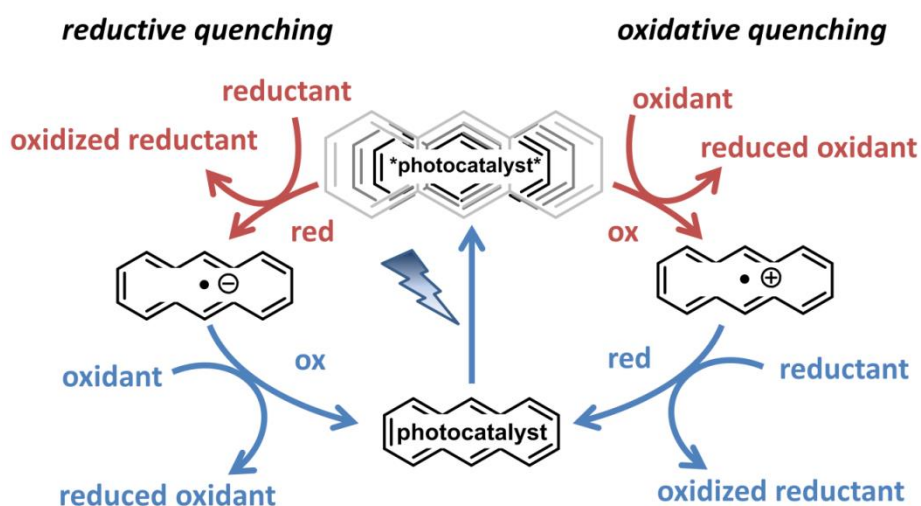


**Figure 35:** Schematic depiction of reductive (left part) and oxidative quenching cycle (right part)

An example of a reductive quenching photocatalytic system is the oxidation of benzylic alcohols by flavin published by König *et al.*<sup>246</sup> (Figure 36, top). The excited triplet state of the

flavin photocatalyst oxidizes the electron rich benzyl alcohol. The reduced flavin is re-oxidized by molecular oxygen dissolved in the solvent which produces hydrogen peroxide.

An example of an oxidative quenching photocatalytic system is the synthesis of stilbenes by reaction of aryl diazonium salts and styrenes catalyzed by eosin Y (photocatalyzed Meerwein arylation).<sup>247</sup> The excited triplet state of eosin Y reduces aryl diazonium salt which immediately decomposes to aryl radical and nitrogen. The aryl radical adds to the double bond of a styrene generating a benzylic radical. This radical is re-oxidized by reduced eosin Y which leads to a stilbene derivative.

Both mechanisms, oxidative and reductive quenching, can be active simultaneously, as it was described by Hill *et al.*<sup>248</sup>

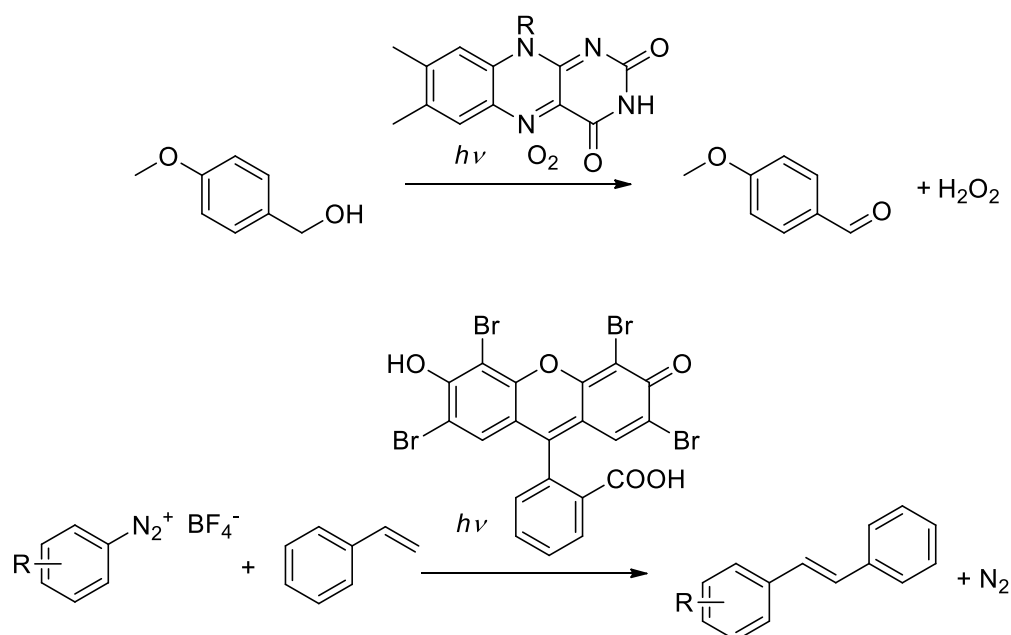


**Figure 36:** Visible-light driven oxidation of benzyl alcohols (top) and photocatalytic synthesis of stilbenes (bottom).

Two general types of photocatalytic mechanisms can be distinguished. The cyclic mechanism (type I) which does not need any sacrificial electron donor (acceptor) is depicted in the upper part of Figure 37. Both substrate and product of the reaction are in the same oxidation state. The radical<sup>1</sup> produced by PeT undergoes a subsequent reaction (rearrangement, addition, elimination, fragmentation) to form radical<sup>2</sup>. This species reacts by the ground state electron transfer with the reduced (oxidized) photocatalyst to form the product. An example of this type I mechanism is the Meerwein arylation<sup>182</sup> discussed in previously.

The electron-flow mechanism (type II, Figure 37, bottom) transforms two different substrates into two different products. The electron flows from one substrate to the other. Usually, one substrate is sacrificial. An example of this type II mechanism is the photooxidation of benzyl alcohols *al.*<sup>181</sup> (Figure 36).



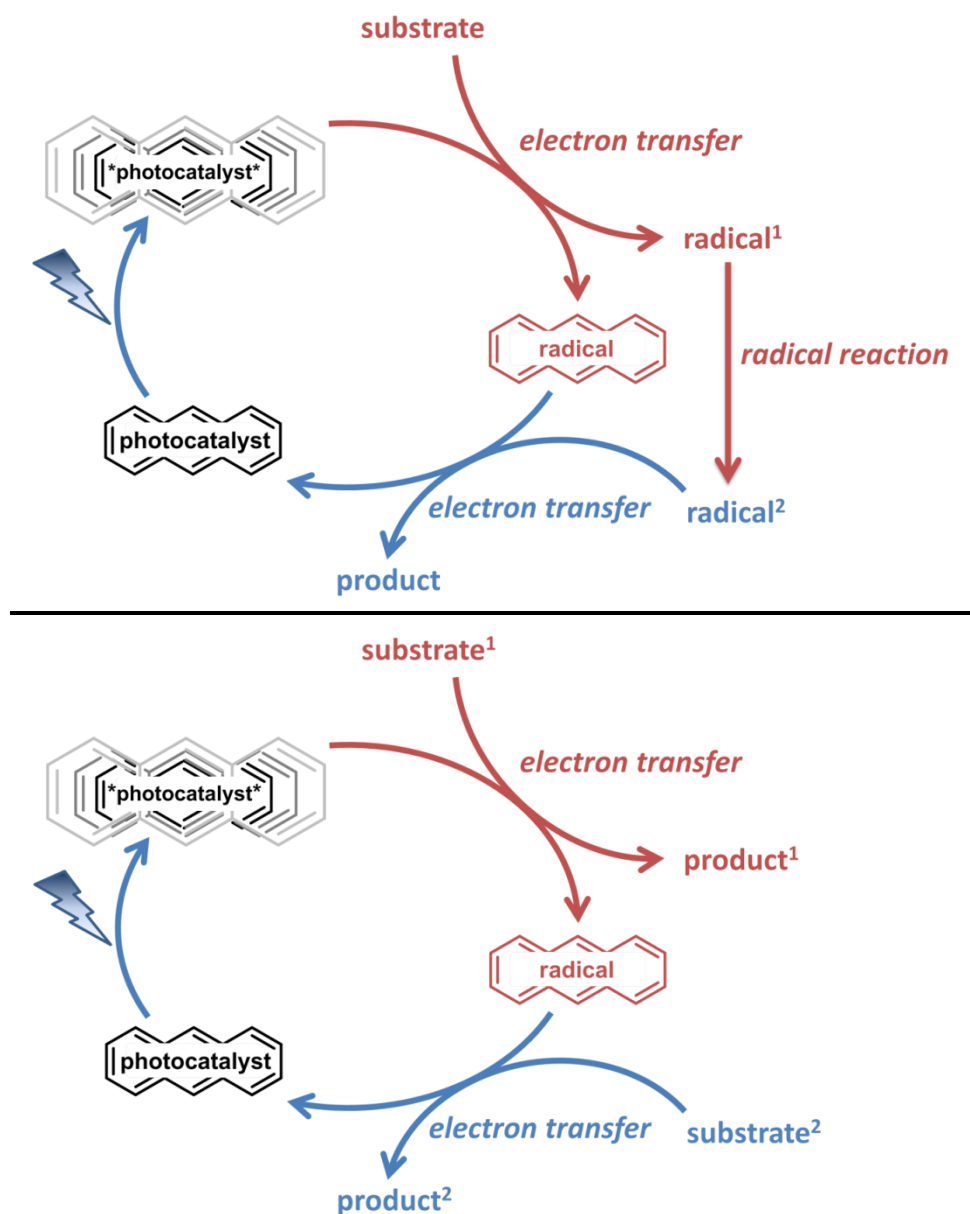


**Figure 37:** Two types of photocatalytic reaction: cyclic mechanism (type I, top), electron-flow mechanism (type II, bottom).

### 2.5.3. Common Reagents Used in Photocatalysis

This part summarizes selected electron donors and acceptors, and photocatalysts used in synthetic and mechanistic photocatalysis.

The most frequently used (sacrificial) electron donors are: organic amines (triethylamine,<sup>249</sup> triethanolamine,<sup>250</sup> EDTA,<sup>185</sup> DIPEA,<sup>251</sup> dimethylaniline<sup>252</sup>) and ascorbic acid,<sup>253</sup> electron rich benzyl alcohols<sup>254</sup> and phenols,<sup>255</sup> thiols,<sup>256</sup> and cysteine.<sup>257</sup>

Common (sacrificial) electron acceptors are: oxygen<sup>258</sup>, methyl viologen,<sup>259</sup> quinones (DDQ,<sup>260</sup> fluoranil<sup>261</sup>), sodium peroxodisulfate,<sup>262</sup> cerium ammonium nitrate (CAN),<sup>263</sup> cerium(IV) sulfate,<sup>264</sup> polysulfides,<sup>265</sup> and fullerenes.<sup>266</sup>

Inorganic visible light absorbing photocatalysts are: [Ru(bpy)<sub>3</sub>]Cl<sub>2</sub> and its derivatives,<sup>175,176,267</sup> Ru(bpz)<sub>3</sub>(PF<sub>6</sub>)<sub>2</sub> and its derivatives,<sup>268</sup> and Ir(ppy)<sub>2</sub>(dtb-bpy)<sup>+</sup> and its

derivatives.<sup>269</sup> Organic photocatalysts are following: eosin Y,<sup>182,270,271</sup> 9-mesityl-10-methylacridinium perchlorate (Fukuzumi's dye),<sup>272</sup> perylene-bisimide (PDI),<sup>273</sup> proflavine,<sup>274</sup> rose bengal,<sup>275</sup> and porphyrins.<sup>276</sup>

By a combination of reagents listed above, one can propose many different photocatalytic systems based on the ground state redox potentials of electron donors and acceptors and the excited state redox potentials of photocatalysts. The photocatalytic reactions are governed by (i) thermodynamics (and kinetics) of electron transfer (predicted by Marcus theory),<sup>277</sup> (ii) rate constants of back electron transfer, (iii) efficiency of quenching of the excited state of photocatalyst (rate constant, concentration, excited state lifetime, quenching constant), (iv) concentration of external quenchers (oxygen) and (v) solvent effects. A detailed knowledge of reaction mechanisms enables to improve existing and rationally design new photocatalytic systems.

We have designed and carefully investigated the mechanism of three new photocatalytic systems which will be discussed in Chapters 3.5. – 3.7. in the practical part.

## 3. Results and Discussion

This part consists of 8 chapters describing projects which were finished in my Ph.D. The first two projects (Chapters 3.1. and 3.2.) deal with development of new photoremovable protecting groups (PPGs). Next two projects (Chapters 3.3. and 3.4.) describe novel PPGs for release of carbon monoxide, so called carbon monoxide releasing compounds (CORMs). Chapters 3.5. – 3.7. focus on design and mechanistic studies of three photocatalytic systems driven by visible light. Finally, Chapter 3.8. concerns with new triplet sensitizers.

### 3.1. Xanthene-Based PPG

The results of this project were published in: Šebej, P.; Wintner, J.; Müller, P.; Slanina, T.; Al Anshori, J.; Antony, L. A. P.; Klán, P.; Wirz, J. *J. Org. Chem.* **2013**, *78*, 1833-1843.<sup>15</sup> The manuscript is attached in Appendix A (Pages S1-S11). The Supporting information is available at: <http://pubs.acs.org/doi/suppl/10.1021/jo301455n> and is attached as an electronic file on CD.

#### 3.1.1. Introduction

The design of a photoremovable protecting group absorbing biologically benign visible light has been a substantial challenge for decades. Chapter 2.2 in the theoretical part summarizes commonly used PPGs and presents trends and efforts in development of this field. Our approach in designing a visible light-absorbing PPG is based on coumarin-4-yl methyl moiety (Figure 38) which absorbs up to 400 nm.<sup>30</sup> Formal extension of the coumarin chromophore leads to the xanthene-based PPG (**I-1**, Figure 38). In analogy to its structural analogue, fluorescein, the proposed structure **I-1** should have high molar absorption coefficient, bright fluorescence, good solubility in aqueous media, and lowest absorption maximum close to 500 nm.<sup>81</sup>

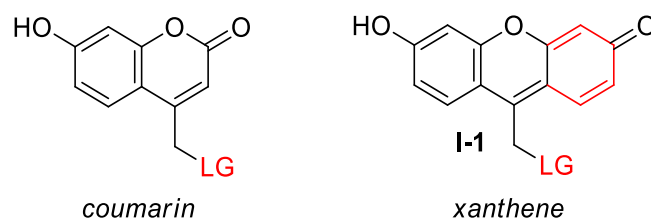


**Figure 38:** Design of a new photoremovable protecting group by extension of the coumarin chromophore (left) to xanthene (right).

The behavior of **I-1** in the excited state was predicted by calculation of its molecular orbitals (MO) by Hückel theory (predicted by software HuLiS). The calculated frontier MOs of **I-1** are shown in Figure 39. The largest change when compared the orbital coefficients in HOMO and LUMO can be noticed at the position C-9. In HOMO (Figure 39, left), the C-9

position together with the bridging oxygen atom are parts of a nodal plane and therefore have zero coefficients. On the contrary, the LUMO orbital (Figure 39, right) has a large coefficient at the position C-9. The excitation of one electron from HOMO to LUMO induces a strong charge transfer to the position C-9 which should favor the heterolytic release of an attached leaving group (LG).<sup>278</sup>

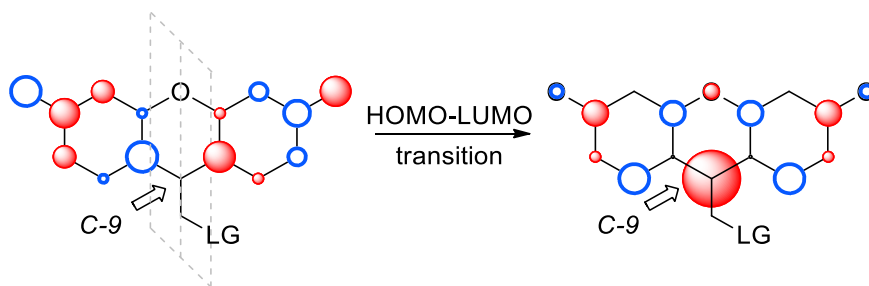


**Figure 39:** Depiction of the frontier MOs (left: HOMO, right: LUMO) of (6-hydroxy-3-oxo-3*H*-xanthen-9-yl)methyl PPG **I-1** using the Hückel MO theory (software HuLiS). The C-9 position is indicated by an arrow. The nodal plane in HOMO is depicted by gray dashed lines. The size of the circle is proportional to the orbital coefficient and its color represents the sign of the wavefunction.

### 3.1.2. Synthesis

After all theoretical calculations, we decided to synthesize the rationally-designed target molecule. **I-1** is a fluorescein derivative and its synthesis should be straightforward and analogical to the Baeyer synthesis of fluorescein from resorcinol and phthalic anhydride.<sup>7</sup> Unfortunately, all attempts for condensation of resorcinol with appropriate aliphatic anhydride lead to complex mixtures of differently colored fluorescent compounds. A detailed literature search revealed that the absolute majority of known fluorescein derivatives have aryl substituent in the position C-9. Only few derivatives with other substituents have been described and fully characterized (Chapter 2.3.1). Therefore, we designed a novel synthetic route of preparation of xanthene moiety from 2,2',4,4'-tetrahydroxybenzophenone **I-2** (Figure 40). The condensation reaction in water in an autoclave at 200°C led to very stable 3,6-dihydroxy-9*H*-xanthen-9-one **I-3**.<sup>81</sup> The carbonyl functionality in C-9 position of **I-3** was transformed, after protection of phenolic hydroxyls by dimethyl sulfate (**I-4**), by a Wittig-like reaction with trimethylaluminium into a derivative with the exocyclic double bond **I-5**.<sup>279</sup> The reactant **I-4** and the product **I-5** have a different polarity and, therefore, a mixture of benzene and toluene was used for the reaction in order to solubilize all components of the reaction mixture. The usage of other protecting groups (such as pivaloyl, TIPS, TBDPS or THP) led to unwanted partial deprotection in the reaction with trimethylaluminium.

The hydroboration-oxidation reduced the xanthene moiety into its *leuco* form and installed the hydroxyl functionality in an anti-Markovnikov fashion to give the alcohol **I-6**. The leaving group was installed to the xanthene PPG by reaction of the alcohol **I-6** with acid chloride or anhydride to give diethyl phosphate **I-7a** and acetate **I-7b**<sup>280</sup> or by Appel reaction to give

bromide **I-7c**.<sup>281</sup> The diethyl phosphate was chosen as a model for ATP and other biogenic phosphates and acetate as a model for amino acids. The deprotection of methoxy groups by  $\text{BBr}_3$  gave the 9*H*-xanthenediol derivatives **I-8a-c**. These compounds were oxidized to the final products **I-1a-c** by 2,3-dichloro-5,6-dicyano-1,4-benzoquinone (DDQ, Figure 40). This rapid oxidation resulted in precipitation of equimolar complexes **I-1a-c**•DDQ. For a long time we considered these products to be non-complexed (*i. e.* without DDQ) because DDQ complex **I-1a-c**•DDQ cannot be observed by  $^1\text{H}$  NMR as it does not contain any hydrogen atoms. Moreover, DDQ hydrolyses in solvents used for NMR analyses (DMSO,  $\text{D}_2\text{O}$ ) to a complex mixture of quinones which have very weak signals in  $^{13}\text{C}$  NMR. The complex **I-1a-c**•DDQ also dissociates after most commonly used mass spectrometry ionization techniques. Elemental analysis revealed the presence of nitrogen atoms in the sample and suggested equimolar complex **I-1a-c**•DDQ which was further characterized by direct inlet HRMS with mild ionization technique.

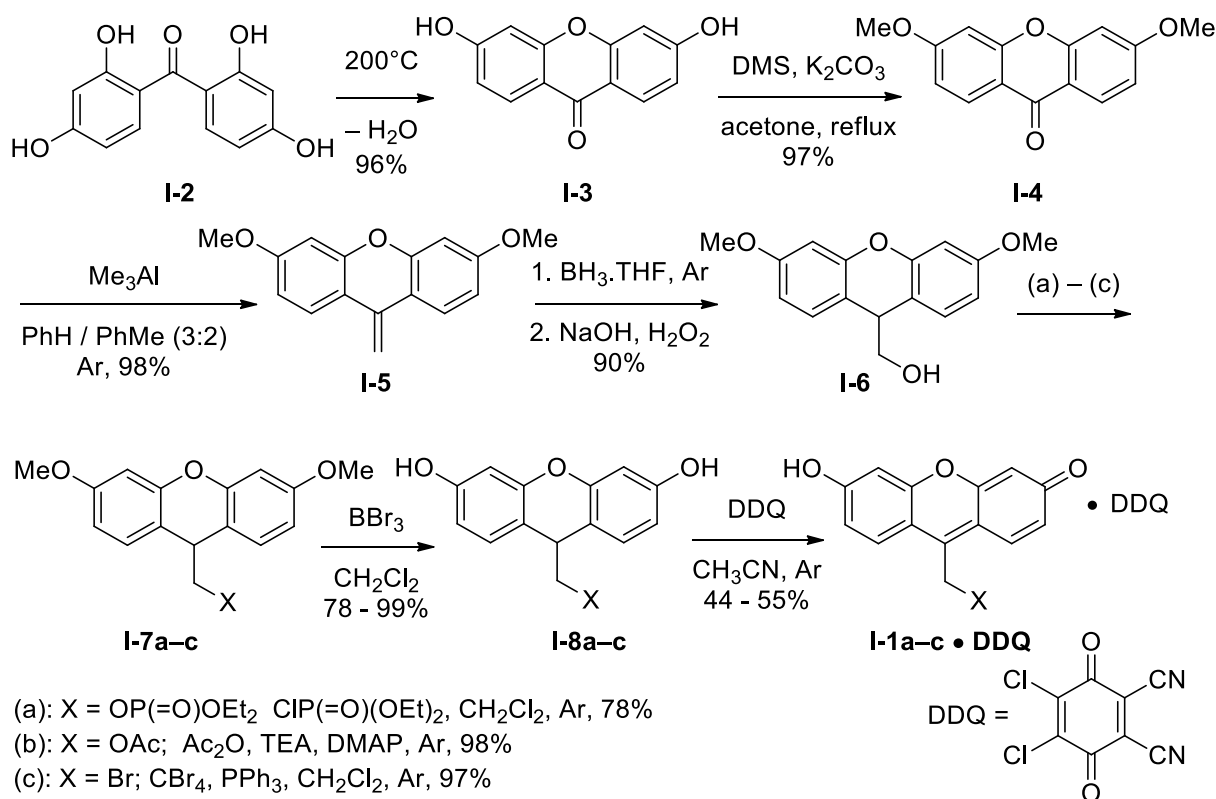


**Figure 40:** Synthesis of (6-hydroxy-3-oxo-3*H*-xanthen-9-yl)methyl derivatives **I-1a-c**

Since all our attempts of substitution of oxidation agent (fluoranil, chloranil) or removal of DDQ from the complex (lyophilization, precipitation, crystallization) failed, we attempted to change the synthetic route by excluding the hydroboration step (reduction) or by oxidizing one of precursors (**I-5** and **I-6**). Unfortunately, the starting xanthenone **I-3** (or its 3,6-dimethoxy derivative) was found as a product of most of our synthetic attempts to derivatize the xanthen moiety in *C-9* position, such as epoxidation or dihydroxylation of **I-5**, or oxidation of **I-6**.

### 3.1.3. Photochemistry

Xanthene derivatives **I-1a-c** (synthesized as complexes **I-1a-c**·DDQ) have strong absorption bands ( $\epsilon_{\max} \sim 4 \times 10^4 \text{ M}^{-1} \text{ cm}^{-1}$ ) at  $\lambda_{\max} = 519 - 528 \text{ nm}$  in analogy to fluorescein derivatives. In accordance with our expectations, all xanthene-based compounds were photoactive. The course of the irradiation of aqueous solution of **I-1a** followed by UV-vis spectrometry is shown in Figure 41. The primary photoproduct has the absorption maximum at  $\sim 500 \text{ nm}$ . This species is formed from all derivatives (**I-1a-c**) and indicates that the leaving group was released. The shape and molar absorption coefficient indicate that the primary photoproduct has also xanthene chromophore. The quantum yields of the photodegradation are ranging from  $\sim 0.3\%$  for acetate **I-1b** to  $\sim 2\%$  for bromide and phosphate **I-1c** and **I-1a**. This corresponds to the  $\text{p}K_{\text{a}}$  of the conjugated acid of the leaving group (LGH). Higher quantum yield for strong acids indicates the heterolytic bond fission from the excited state.

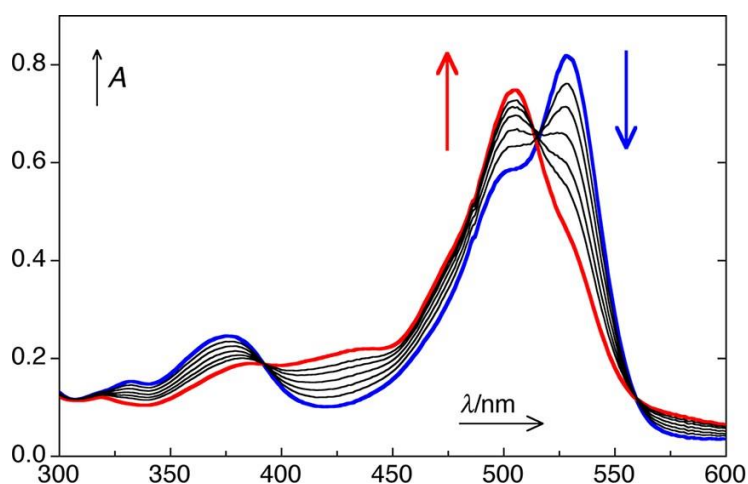


**Figure 41:** Irradiation of **I-1a** (first spectrum,  $\lambda_{\max} = 528 \text{ nm}$ , blue line,  $c \sim 2 \times 10^{-5} \text{ M}$ ) at  $\lambda = 546 \text{ nm}$  in phosphate buffer ( $I = 0.1 \text{ M}$ ,  $\text{pH} = 7.0$ ) as monitored by absorption spectroscopy. The last spectrum ( $\lambda_{\max} = 505 \text{ nm}$ , red line) was taken after 15 min of irradiation.

The photoproduct was obtained in milligram amounts by preparative irradiation and was fully characterized. Since the xanthene-based PPG have properties analogous to coumarins, we anticipated also similar photochemical behavior. Coumarins release the leaving group from the first excited singlet mainly by heterolytic bond fission and give the product of photosolvolysis (Chapter 2.2.4). To our surprise, we found that the photoproduct is not the expected (6-hydroxy-3-oxo-3*H*-xanthen-9-yl)methanol, but 6-hydroxy-3-oxo-3*H*-xanthene-9-carboxylic acid **I-9** (Figure 42). Since the presence/absence of oxygen dissolved in the reaction mixture had neither influence on the quantum yield nor the product distribution, the acid **I-9** is probably formed by rapid oxidation of the primary alcohol (solvolysis product; (6-hydroxy-3-oxo-3*H*-xanthen-9-yl)methanol) by DDQ present in the complex. The irradiation in an isotopically labeled aqueous buffer revealed that the oxygen atoms of the carboxylic functionality originate from the solvent (Figure 42).

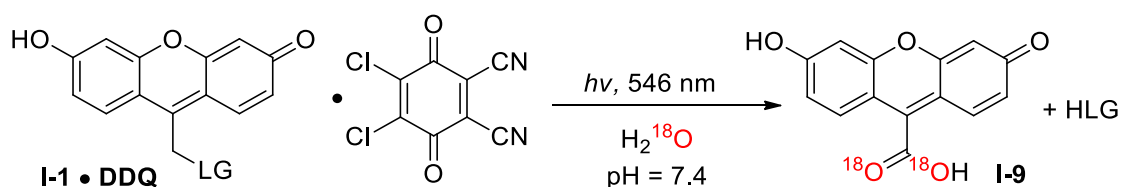


**Figure 42:** Photoinduced release of the leaving group from **I-1**•DDQ and formation of 6-hydroxy-3-oxo-3H-xanthene-9-carboxylic acid **I-9**. The incorporation of  $^{18}\text{O}$  from water is shown in red.

A detailed time-resolved fluorescence study of **I-1c** revealed that the leaving group is released from the first excited singlet with a lifetime of 0.4 ns. This observation is analogous to the mechanism of photodeprotection of coumarinyl PPG.

### 3.1.4. Conclusion

We have successfully designed and synthesized first fully organic visible-light-absorbing photoremovable protecting group based on the xanthene chromophore **I-1**. It can release phosphates, carboxylates and halides by the action of green light ( $\lambda_{\text{max}} \sim 520$  nm) with quantum yields  $\sim 2\%$ . The molecules **I-1a-c** have been isolated as complexes with DDQ which further oxidized the primary solvolysis product to the 6-hydroxy-3-oxo-3H-xanthene-9-carboxylic acid **I-9**.

This project started rapid development in field of visible-light-absorbing PPGs as described in Chapter 2.2.5.

### 3.1.5. Authors' Contributions

J.Wintner, T.S., and L.A.P.A. synthesized the compounds, T.S. and P.Š. performed mechanistic experiments (irradiation experiments,  $\text{pK}_a$  titrations, isotopic labeling). P. Š. and T.S. characterized the DDQ complex. T.S. fully characterized the photoproduct **I-9**. P. M. measured the quantum yields. J. A. A. synthesized a model compound, succinyl fluorescein and performed a photophysical study of it. J. Wirz performed quantum chemical calculations.

## 3.2. Caged Fluoride

The results of this project were published in: Slanina, T.; Šebej, P.; Heckel, A.; Givens, R. S.; Klán, P. *Org. Lett.* **2015**, *17*, 4814-4817.<sup>15</sup> The manuscript is attached in Appendix B (Pages S12-S15). The Supporting information is available at: <http://pubs.acs.org/doi/suppl/10.1021/acs.orglett.5b02374> and is attached as an electronic file on CD.

### 3.2.1. Introduction

Most of common photoremovable protecting groups are used to release “good leaving groups”, *i. e.* phosphates, sulfates, carboxylates, carbamates and bromides.<sup>30</sup> The quality of a leaving group is often assessed by the  $pK_a$  of its conjugated acid LGH (the stronger the conjugated acid, the better the leaving group). Fluoride is considered to be a moderate leaving group. Hydrogen fluoride ( $pK_a = 3.2$ ) is stronger acid than acetic acid ( $pK_a = 4.76$ ) but fluoride is worse leaving group than acetate (the C–F bond is stronger (485 kJ/mol) than the C–O bond (351 kJ/mol)).<sup>259</sup> The photoinduced release of fluoride is useful for biology (Chapter 2.4.2) as well as for material sciences (*e. g.* billion-dollar business of photochemical etching of silicon surfaces in microchip fabrication).<sup>282,283</sup> The classical protocol for etching of silicon wafers starts with covering of surface with a protecting layer or an inhibitor which is subsequently partially removed by irradiation with laser to create a mask. The etching agent (HF or  $NH_4F$ ) is then applied which etches the surface unprotected by the mask. After washing of the etching agent, the mask is chemically removed.<sup>284,285</sup> This procedure consists of 6 steps which are time-consuming and technologically demanding. The direct photorelease of an etchant (*i. e.* fluoride anion) can shorten the whole protocol to 3 steps: (i) application of deactivated etchant on the silicon surface, (ii) spatially-controlled photochemical release of the etchant and subsequent etching of the surface, and (iii) washing of the etched surface.

When we started this project, there was only one photoremovable protecting group known to release fluoride upon irradiation: 3',5'-dimethoxy desyl fluoride introduced by Wirz *et al.* (Figure 43, left) in 2007.<sup>286</sup> It suffers from all drawbacks of desyl PPG, such as low water solubility and substantial internal filter effect of the primary photoproduct, dimethoxy-2-phenylbenzofuran, which disable releasing fluoride quantitatively.

We proposed to use a well-known 4-hydroxyphenacyl protecting group for release of fluoride (**II-1**, Figure 43). 4-Hydroxyphenacyl PPG (Chapter 2.2.3) has been used for release of poor leaving groups such as phenols<sup>53</sup> and therefore seemed to be a suitable candidate for this application. Moreover, it exhibits high release quantum yields and its primary photoproduct, 4-hydroxyphenyl acetic acid, does not compete for incident light.

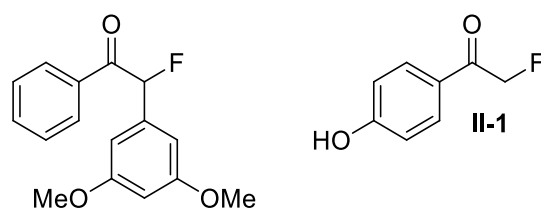


**Figure 43:** Structures of 3',5'-dimethoxydesyl fluoride (left) and 4-hydroxyphenacyl fluoride **II-1** (right)



### 3.2.2. Synthesis

We synthesized 4-hydroxyphenacyl fluoride **II-1** in a 4-step synthetic procedure in 55% overall yield (Figure 44). The hydroxyl group of the commercially available 4-hydroxyacetophenone **II-2** was protected by a benzyl protecting group to give 4-benzyloxyacetophenone **II-3**. The protection reaction was followed by bromination of the *alpha* position of the acetophenone to give **II-4**. The copper(II) bromide serves as a mild brominating agent which slowly releases bromine (by disproportionation reaction to CuBr) which reacts with the enol form of **II-3**. The bromine atom in the *alpha* position was substituted to fluoride in a halax reaction with 18-crown-6 which increases solubility of KF in acetonitrile. The 4-benzyloxyphenacyl fluoride **II-5** was treated with anhydrous trifluoroacetic acid which deprotected the benzyl protecting group. All attempts of debenzylation by classical methods using hydrogen and palladium on charcoal led to loss of fluoride.

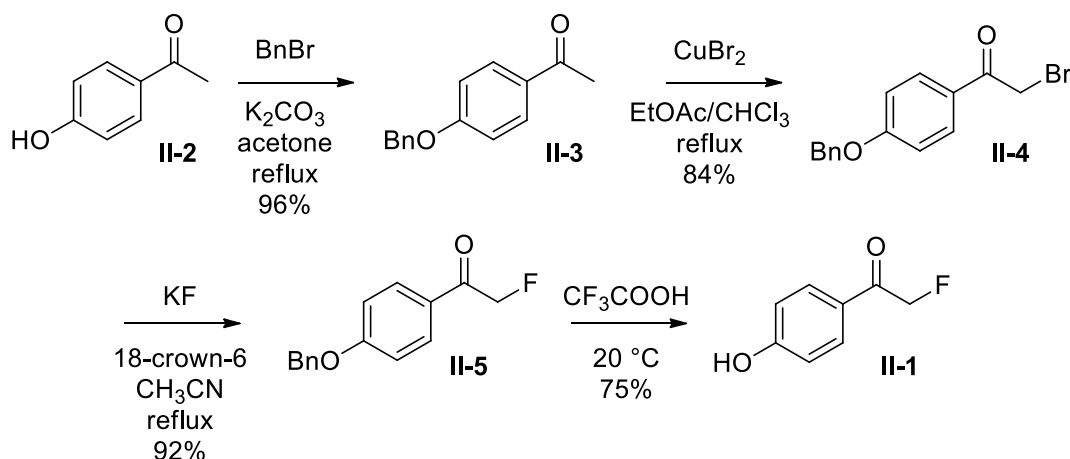


**Figure 44:** Synthesis of 4-hydroxyphenacyl fluoride **II-1**

### 3.2.3. Photochemistry

The photochemical properties of **II-1** were tested by irradiation at 313 nm in various solvent mixtures. **II-1** is photoactive only in solvent mixtures containing at least 15% (v/v) of water. This observation is in accordance with our previous knowledge of photochemistry of 4-hydroxyphenacyl PPG.<sup>287</sup> It was found that fluoride is released quantitatively and the reaction undergoes the photo-Favorskii rearrangement (Figure 14). The amount of released fluoride was quantified by <sup>19</sup>F NMR with an internal standard (NBu<sub>4</sub>PF<sub>6</sub>), and 4-hydroxyphenyl acetic acid **II-9** was found to be the sole photoproduct. The pK<sub>a</sub> of the phenolic group was found to be (7.59 ± 0.06) which means that the molecule **II-1** exists as ~1:1 mixture with its anion **II-1**<sup>-</sup> at a physiological pH (7.4). We found that the photochemistry of the neutral **II-1** measured at pH = 5.0 corresponds to the photochemistry of the anion **II-1**<sup>-</sup> measured at pH = 10.0. However, the quantum yield of the photorelease of F<sup>-</sup> measured at pH = 5.0 ( $\Phi \sim 84\%$ ) was found to be approx. 16-fold higher than that at pH =

10.0. This is in accord with a substantially lower activity of the 4-hydroxyphenacyl anion **II-1**<sup>-</sup> compared to that of the neutral form **II-1** as demonstrated by Givens *et al.*<sup>52</sup>

The mechanism of photodegradation of **II-1** was studied by means of transient pump-probe spectroscopy. The observed transient signals were assigned to corresponding species according to previous mechanistic studies of *pHP*.<sup>52</sup>

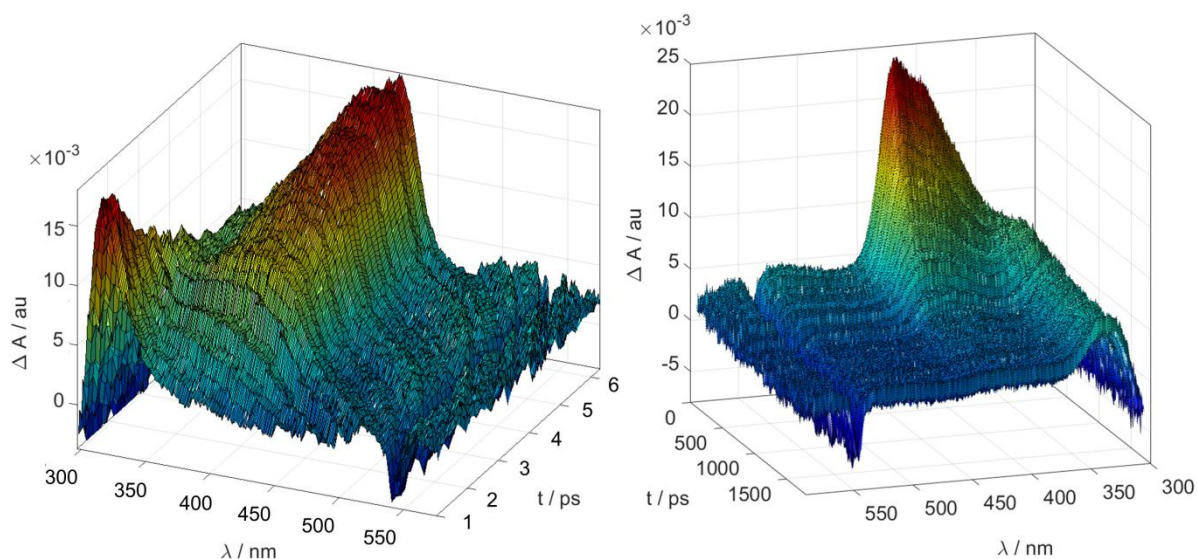


**Figure 45:** Transient spectra of **II-1** in acetate buffer (pH = 5.0,  $I = 33 \text{ mmol dm}^{-3}$ , with 40% MeCN as a co-solvent) reconstructed after a chirp correction and a global analysis in the time range from 1.0 ps to 6.3 ps in 0.15 ps steps (left) and in the time range from 0 ps to 1.7 ns in 10 ps steps (right)

The 4-hydroxyphenacyl fluoride **II-1** is excited into its lowest excited state **II-1-S<sub>1</sub>** (Figure 46) which corresponds to the transient signal with  $\lambda_{\text{max}} = 315 \text{ nm}$  (Figure 45, left part, initial spectrum). This species has a very short lifetime of  $\sim 2.5 \text{ ps}$  and it undergoes fast intersystem crossing to the triplet state. The triplet state **II-1-T<sub>1</sub>** has higher molar absorption coefficient and maximum at  $\lambda_{\text{max}} = 405 \text{ nm}$  (Figure 45, left part: end spectrum; right part: initial spectrum). The triplet decay is shown in Figure 45, right part. The triplet state **II-1-T<sub>1</sub>** decays with the rate constant of  $k_{\text{dec}} = (2.3 \pm 0.2) \times 10^9 \text{ s}^{-1}$  to the triplet biradical **II-6** (Figure 46). The biradical has a weak absorption, and its spectrum was obtained by global analysis method. The end spectrum at 1.7 ns after excitation (Figure 45, right part) with the absorption maximum at 330 nm corresponds to the anion **II-8**. This unusual species is formed by the nucleophilic attack of water molecule to the unstable intermediate **II-7** which has shorter lifetime than the triplet biradical **II-6** and cannot be therefore observed spectroscopically. The phenolate **II-8** is deprotonated at the position with weaker basicity than its carboxylic functionality and therefore its proton is shifted by general acid-base catalysis from the carboxylic moiety to the phenolate to create **II-9**. The rate of this protomeric equilibrium (in order of  $\mu\text{s}$ ) depends on the concentration of buffer used.

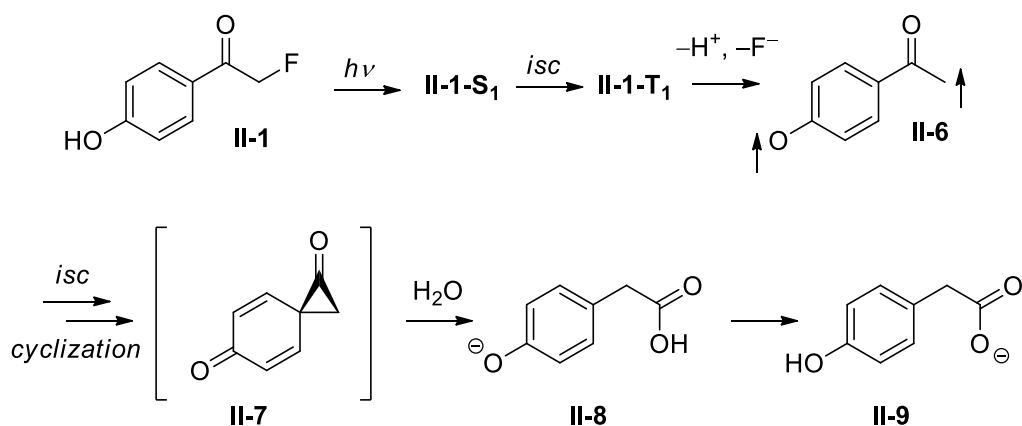


**Figure 46:** Mechanism of the photodeprotection of 4-hydroxyphenacyl fluoride **II-1**

### 3.2.4. Etching

We studied the photoinduced release of fluoride from **II-1** for its applicability for etching of silicon surfaces. We tested two materials, mica (silicate with sheet structure commonly used in AFM), and monocrystalline silicon wafer. The surface roughness of examined solid samples was monitored by tapping-mode atomic force microscopy (AFM). The surface of both materials before etching exhibited roughness below 400 pm (Figure 47, left). The surface of a sample with a drop of a solution of **II-1** in aqueous acetonitrile kept in dark had the same roughness as the untreated surface. This indicates that no etching occurs in the dark. After irradiation and subsequent fluoride release the surface was etched to distinct flat dents of ~2 nm depth (Figure 47, right). Both shape and size of the etched objects correspond to the structure of a sample which was etched by solution of KF of the same concentration as **II-1**. A similar type of etching was published for mica<sup>288-290</sup> and silicon.<sup>291</sup>

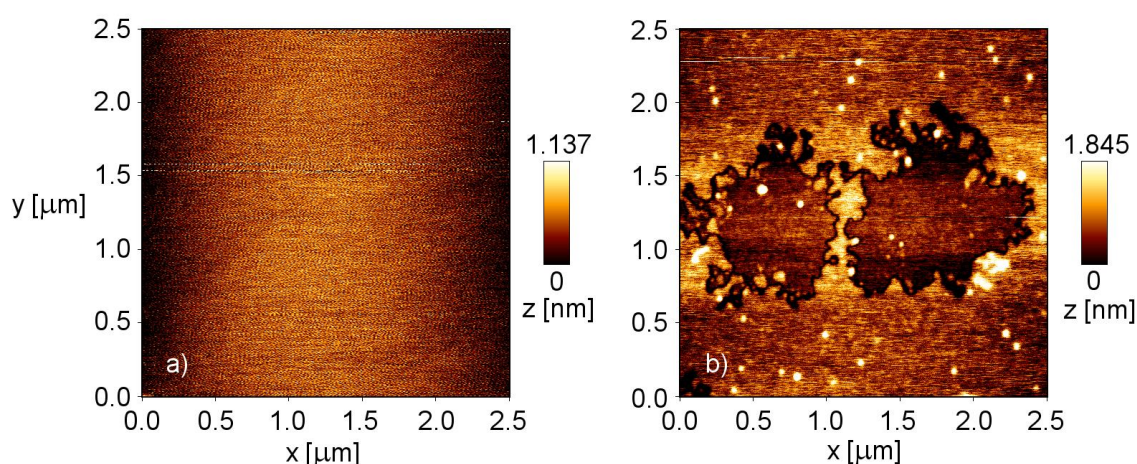


**Figure 47:** Representative AFM images ( $2.5 \times 2.5 \mu\text{m}$ ) of a fresh and untreated mica surface (left), and a mica surface treated with **II-1** ( $c = 22 \text{ mmol dm}^{-3}$ , in a 7:3 (v/v) mixture of  $\text{CH}_3\text{CN}$  and aqueous acetate buffer ( $c = 0.1 \text{ mol dm}^{-3}$ ,  $\text{pH} = 5$ )) irradiated with LEDs ( $\lambda_{\text{em}} = 281 \pm 6 \text{ nm}$ ) for 2 h and then left in the dark for 14 h (right).

### 3.2.5. Conclusion

We have successfully synthesized 4-hydroxyphenacyl fluoride **II-1** which quantitatively and efficiently ( $\Phi \sim 84\%$ ) releases the fluoride ion upon UV-irradiation in aqueous media. The mechanism of the photorelease corresponds to that of other *p*HP derivatives (the photo-Favorskii rearrangement). Modification of surfaces by photoinduced etching of mica and silicon followed by AFM has been demonstrated.

### 3.2.6. Authors' Contributions

T.S. and P.Š. synthesized the compounds, T.S. and P.Š. performed irradiation experiments. T.S. measured quantum yields, quantified chemical yields, accomplished  $pK_a$  titrations and pump-probe measurements. P. Š. performed the etching experiments.

## 3.3. Xanthene-Based CORM

The results of this project were published in: Antony, L. A. P.; Slanina, T.; Šebej, P.; Šolomek, T.; Klán, P. *Org. Lett.* **2013**, *15*, 4552-4555.<sup>292</sup> The manuscript is attached in Appendix C (Pages S16-S19). The Supporting information is available at: <http://pubs.acs.org/doi/suppl/10.1021/ol4021089> and is attached as an electronic file on CD.

### 3.3.1. Introduction

In our research of xanthene-based photoremovable protecting groups (Chapter 3.1.), we found that the product of photochemical degradation of xanthenylmethyl PPGs **I-1**, 6-hydroxy-3-oxo-3*H*-xanthene-9-carboxylic acid (**III-1**, Figure 48), is also photochemically active. Its photochemical degradation was approximately two orders of magnitude slower than the release of a leaving group from **I-1** and, therefore, we did not pay much attention this process. Nevertheless we analyzed the reaction mixture after exhaustive irradiation of **III-1** and found that the only product is 3,6-dihydroxy-9*H*-xanthen-9-one **III-2** (Figure 48). The structure of the product invoked our interest in this reaction. The carboxylic group of **III-1** got cleaved and the carbon at the position *C-9* is oxidized to ketone. Therefore, we wanted to reveal the mechanism of this transformation and find out possible applications of this process.

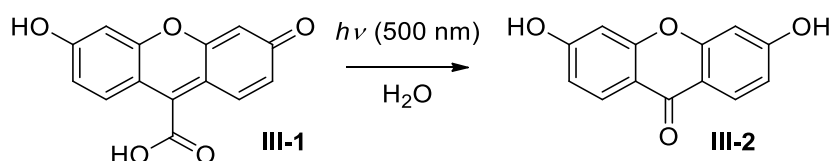


**Figure 48:** Photodegradation of 6-hydroxy-3-oxo-3*H*-xanthene-9-carboxylic acid **III-1** to 3,6-dihydroxy-9*H*-xanthen-9-one **III-2**

### 3.3.2. Synthesis

First of all, we needed a reliable synthetic method for preparation of **III-1** in at least multi-milligram amounts. The first batches of **III-1** were prepared by irradiation of solutions of **I-1a•DDQ** in NMR tubes according to our previous research<sup>15</sup> (Figure 49 and Chapter 3.1.) and the isolated amounts of the target acid were in the range of 1–2 mg.

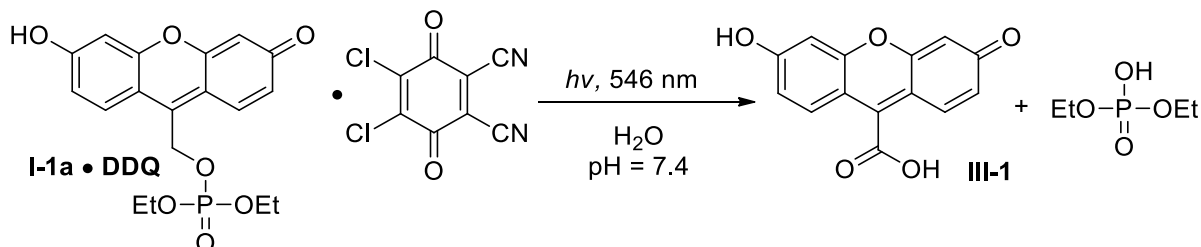


**Figure 49:** Photochemical synthesis of **III-1** from complex **I-1a•DDQ**

We decided to synthesize the acid **III-1** by an alternative chemical method. We tested the oxidation of 9-methyl xanthenes, hydrolysis and subsequent oxidation of **I-1a•DDQ** and **I-1b•DDQ**, acid- or base-catalyzed hydrolysis of 9-cyanoxanthene and acidic hydrolysis of  $-\text{CX}_3$  derivative ( $\text{X} = \text{F}, \text{Cl}$ ) (Figure 50). Unfortunately, all attempts either did not yield any product and starting material was isolated, or led to xanthenone **III-2**.

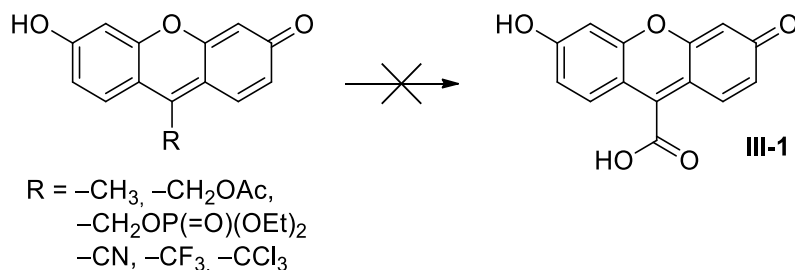


**Figure 50:** Attempted syntheses of **III-1**

After a year of unsuccessful experiments, we decided to return back to the photochemical preparation of the xanthene carboxylic acid **III-1**. We managed to scale up the synthesis by irradiating a solution of **I-1a•DDQ** in a large Petri-dish with a 400 W broad-band halogen lamp. With this method we produced **III-1** in amounts of tens of milligrams (up to ~100 mg in one batch) and in high purity.

### 3.3.3. Photochemistry

The xanthene carboxylic acid **III-1** can exist in four acid-base forms (dianion, anion, neutral and cation). The respective  $\text{pK}_{\text{a}}$ s of acid-base equilibria were found by spectrophotometric titration ( $\text{pK}_{\text{a},1} = 2.96$ ;  $\text{pK}_{\text{a},2} = 5.08$ ;  $\text{pK}_{\text{a},3} = 6.39$ ). At physiological pH (7.4), > 90% of dianion is present in the solution. The quantum yield of the photodegradation is pH dependent which indicates that different acid-base forms have different reactivity. At  $\text{pH} = 2.5$  the acid precipitates and the quantum yield could not be determined. At  $\text{pH} = 4.5$

(neutral form of **III-1** prevails) almost no photochemistry was observed. The highest quantum yield ( $\sim 4 \times 10^{-3}$ ) was measured at pH = 5.7 where the anion form of **III-1** dominates. The complex analysis of the quantum yields measured at different pH and the distribution of the respective acid-base forms of **III-1** revealed that the monoanion is about one order of magnitude more reactive than the dianion (the other forms are non-active).

The photodegradation of **III-1** to **III-2** involves a formal loss of one carbon atom in the molecule. The most common mechanism of the cleavage of carboxylic group is decarboxylation (loss of  $\text{CO}_2$ ).<sup>293</sup> We therefore suggested a bimolecular mechanism of photoinduced decarboxylation and subsequent photo-oxidation of the formed 6-hydroxy-3-oxo-3*H*-xanthenone to **III-2**. The second part of this mechanism has been described before on similar substrates in presence of oxygen as an oxidant.<sup>294</sup> Moreover, the thermal decomposition of **III-1** gives carbon dioxide which was proved by DSC/TG analysis with coupled IR detector.

The photoinduced decarboxylation/photo-oxidation mechanism was ruled out by the fact that the reaction quantum yield was independent on oxygen presence/absence in the reaction system (no oxidant present for possible photo-oxidation) and by isotope scrambling experiments. We prepared  $^{18}\text{O}$ -labeled **III-1** according to our previously published procedure<sup>15</sup> (Chapter 3.1., Figure 42). The irradiation of labeled acid in  $^{16}\text{O}$ -based aqueous buffer did not lead in any incorporation of  $^{16}\text{O}$  into the structure of the xanthenone **II-2** (Figure 51). Also the experiment with the non-labeled **III-1** in  $^{18}\text{O}$ -based aqueous buffer did not show any isotope scrambling. This suggests an intramolecular mechanism through an  $\alpha$ -lactone **III-3**.  $\alpha$ -Lactones are short-lived intermediates known to release CO by decarbonylation.<sup>295-297</sup> The expected product of the photodegradation of **III-1** was therefore carbon monoxide if the intramolecular mechanism is valid.

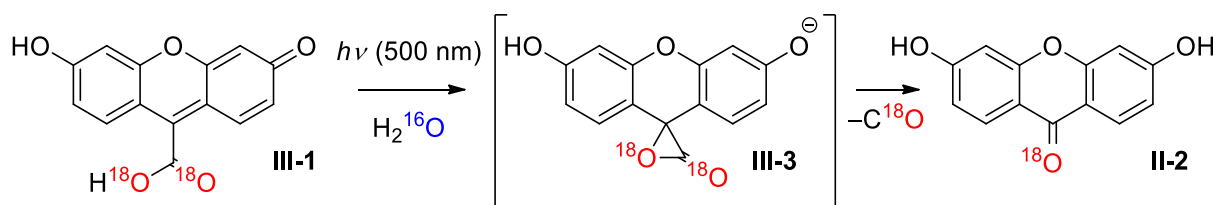


**Figure 51:** Mechanism of the CO release from isotopically labeled **III-1** in  $\text{H}_2^{16}\text{O}$ -based buffer with the depiction of the putative intermediate **III-3**.

We attempted many tests to determine/exclude the presence of carbon monoxide in the reaction mixture after irradiation of **III-1**. The initial experiments with head-space mass spectrometry did not detect any CO. Also experiments with gas-phase IR were unsuccessful due to low concentrations of released CO. Finally, we tried to detect the released carbon monoxide by biomimetic trapping with hemoglobin (Hb). Hemoglobin is known to form a strong complex with CO by creating carboxyhemoglobin (COHb). The characteristic change of absorption spectrum of Hb to COHb is used in physiology for determination of CO in blood.<sup>298</sup> We prepared the solution of Hb from commercially available methemoglobin (MetHb) isolated from bovine blood by reduction with sodium dithionite according to a known procedure.<sup>299</sup> Hemoglobin ( $\lambda_{\text{max}} = 405 \text{ nm}$ , Figure 52) mixed with **III-1** was



quantitatively transformed to COHb ( $\lambda_{\text{max}} = 419 \text{ nm}$ ) after irradiation at  $\sim 500 \text{ nm}$ . This clearly indicates that carbon monoxide is released by photodegradation of **III-1** to **III-2**.

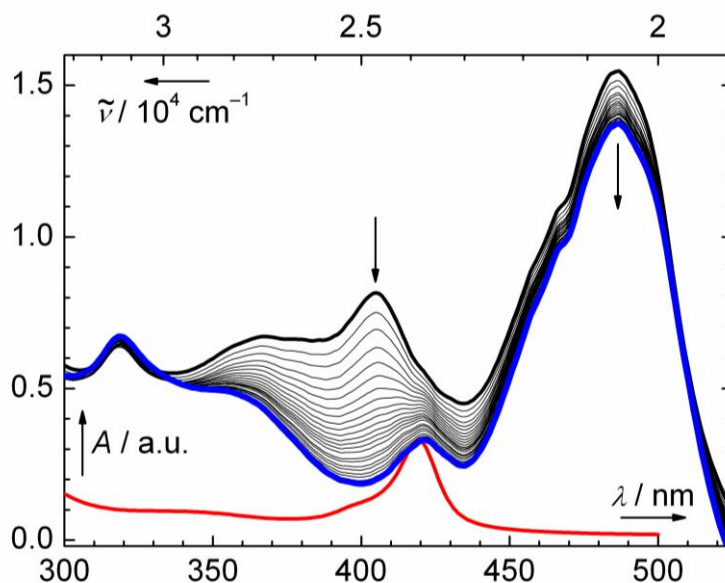


**Figure 52:** Absorption spectra (black lines) measured following irradiation of **III-1** ( $c \sim 1.3 \times 10^{-4} \text{ M}$ ; the total irradiation time was 4.6 h) in the presence of MetHb ( $c \sim 2.3 \times 10^{-5} \text{ M}$ ) and  $\text{Na}_2\text{S}_2\text{O}_4$  ( $c = 2.5 \times 10^{-5} \text{ M}$ ) in 0.1 M aq phosphate buffer at pH = 7.4 purged with  $\text{N}_2$  at  $503 \pm 15 \text{ nm}$ . The initial (black bold line) and final (blue bold line) spectra are highlighted. Pure COHb formed from Hb and CO dissolved in water (red line) is shown for comparison.

After we have proven the photoinduced release of carbon monoxide from **III-1**, we looked for some applications of this process. Carbon monoxide is known to be toxic for humans at high concentrations but it was found recently that it has many beneficial effects (Chapter 2.4.3.). Since the delivery of carbon monoxide by direct inhalation to body is rather complex, a family of compounds called carbon monoxide releasing molecules (CORMs) has been developed. We suggested the xanthene carboxylic acid **III-1** as a novel metal-free CORM.

### 3.3.4. Conclusion

We have introduced **III-1** as the first metal-free CORM activatable by visible light that allows precise spatio-temporal control over the release of carbon monoxide. Its favorable spectroscopic properties, negligible toxicity, good aqueous solubility, and transformation to a noninterfering non-toxic photoproduct make it a promising molecule for biological and medicinal applications.

### 3.3.5. Authors' Contributions

L.A.P.A and T.S. synthesized the compounds, T.S. and P.Š. performed irradiation experiments and  $pK_a$  titrations. P. Š. accomplished isotope labeling experiments. T.S.

measured quantum yields, quantified chemical yields and determined the released carbon monoxide by biomimetic trapping. T. Š. performed quantum chemical calculations.

### 3.4. BODIPY-Based CORM

The results of this project were submitted for publication. The submitted manuscript is attached in Appendix D (Pages S20-S30). The Supporting information is attached as an electronic file on CD.

#### 3.4.1. Introduction

After we introduced the 6-hydroxy-3-oxo-3*H*-xanthene-9-carboxylic acid **III-1** as the first metal-free CORM activatable by visible light (Chapter 3.3.), we decided to design a second generation of fully organic CORMs that could be easily synthesized and would absorb light of a wavelength in the tissue-transparent window (650–950 nm).<sup>300</sup> Both of these factors would help to establish this system in practical biological and medicinal research.

In order to rationally design an alternative chromophore with photoreactivity similar to **III-1**, we searched for the system with frontier molecular orbitals with similar nodal properties and symmetry.<sup>301</sup> Using Hückel molecular orbital calculations (HMO), we screened the frontier molecular orbitals (MOs) of several well-known chromophores which have strong absorption in the visible region, and we identified that the boron-dipyrromethene (BODIPY) molecule has a similar antisymmetric highest occupied MO (HOMO) compared to that of **III-1** (Figure 53). HMO predicts an increase in electronic density on the *C-9* (*meso*) position upon excitation for both systems. Therefore, we deduced that *meso*-carboxy BODIPY derivatives are promising photoCORM candidates. Moreover, BODIPY derivatives are well-known for their distinctive and easily tunable absorption and emission properties.<sup>302-304</sup>

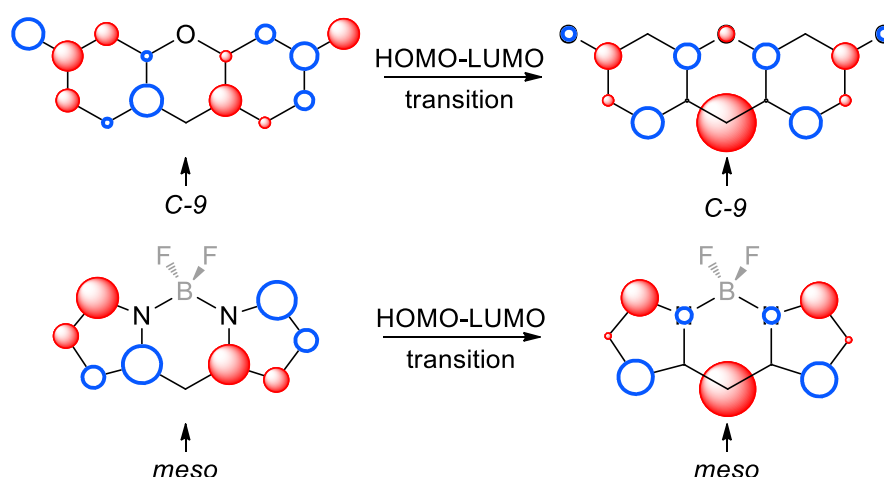


**Figure 53:** A comparison of the frontier MOs (left: HOMO, right: LUMO) of 6-hydroxy-3-oxo-3*H*-xanthene (top) and BODIPY (bottom) chromophores using the Hückel MO theory. The *C-9* (*meso*) positions are indicated by an arrow. The BF<sub>2</sub> group of BODIPY (in grey) was not explicitly considered in the Hückel calculation.



### 3.4.2. Synthesis and Photophysical Properties

To test our hypothesis, we synthesized three model compounds **IV-1** to **IV-3** (Figure 54). The compound **IV-1** was prepared as a simple model structure by a simple two-step procedure. The condensation of benzyl chlorooxalate and 2-methylpyrrole<sup>305</sup> produces a benzyl ester of **IV-1** and subsequent debenzylation by hydrogenolysis leads to the target compound in overall 82% yield. We further prepared the compound **IV-2** which has extended chromophore by two styryl groups. This feature shifts the absorption maximum to the red part of the visible spectrum. The compound **IV-2** was prepared from **4a** by condensation with the corresponding PEG-substituted benzaldehyde in the presence of piperidine in glacial acetic acid and subsequent hydrogenation on Pd/C in 56% overall yield. The PEG substituents were used to increase the solubility in water. The heavy-atom substituted BODIPY analogue, compound **IV-3** was synthesized by direct electrophilic iodination of **IV-1** by ICl in 68% yield.

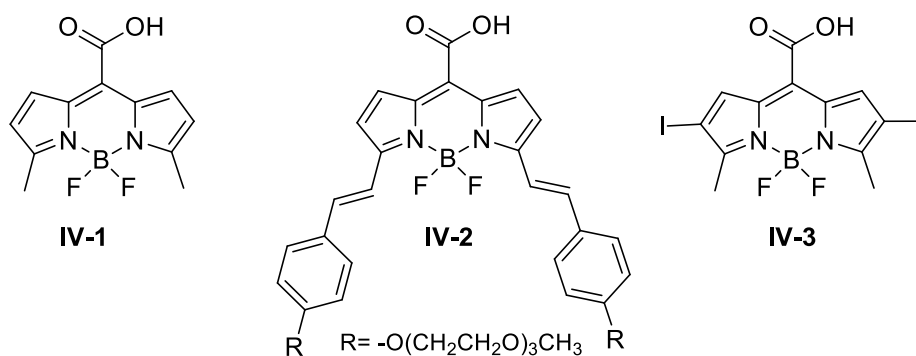


**Figure 54:** Structures of synthesized BODIPY derivatives **IV-1** to **IV-3**

Absorption and emission spectra of aqueous solutions of **IV-1** and **IV-2** are shown in Figure 55. The unsubstituted BODIPY acid **IV-1** shows a major band with  $\lambda_{\max} = 502$  nm and exhibits a bright fluorescence with a quantum yield  $\Phi_f$  of 67%. The absorption and emission resemble the photophysical properties of xanthene-based CORM **III-1**. The quantum yield of fluorescence is higher than **III-1** ( $\Phi_f \sim 40\%$ ) which corresponds to a lower fraction of non-radiative decay processes for a BODIPY derivative. The compound **IV-2** has the absorption maximum bathochromically shifted by  $\sim 150$  nm compared to that of **IV-1** to  $\lambda_{\max} = 652$  nm with a tail absorption up to  $\sim 750$  nm; Figure 55. The presence of two styryl groups in **IV-2** are probably responsible for its lower fluorescence quantum yield ( $\Phi_f = 12\%$ ) as compared to that of **IV-1** due to enhanced radiationless decay of the singlet excited state.<sup>306,307</sup> The absorption properties of **IV-3** are similar to **IV-1**. The absorption maximum is bathochromically shifted by  $\sim 40$  nm to 540 nm and the fluorescence quantum yield dropped significantly to 2%. This was expected as the presence of two iodine atoms enhances the intersystem crossing which diminishes the fluorescence quantum yield.<sup>308</sup>

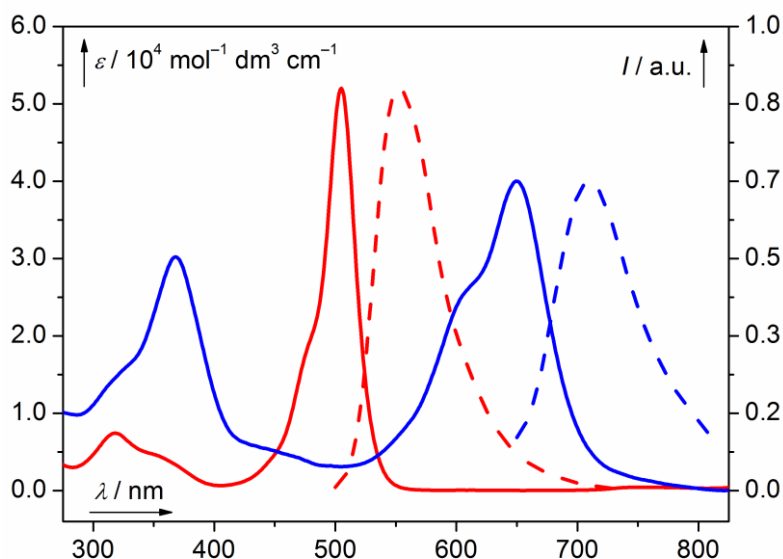


**Figure 55:** Absorption (solid lines) and normalized emission (dashed lines) spectra of **IV-1** (red) and **IV-2** (blue) ( $c = 1 \times 10^{-5} \text{ mol dm}^{-3}$ ; phosphate buffered saline pH = 7.4;  $I = 0.15 \text{ mol dm}^{-3}$ ).

### 3.4.3. Mechanistic Studies

All three derivatives **IV-1** to **IV-3** are photoactive. The compound **IV-1** underwent a complete decomposition upon irradiation at  $\sim 500 \text{ nm}$  with quantum yields of  $(2.7 \pm 0.4) \times 10^{-4}$  and  $(1.1 \pm 0.1) \times 10^{-4}$  in degassed and aerated buffered solutions (pH = 7.4), respectively. The benzyl ester of **IV-1** was found to be stable upon irradiation. This indicates that the free carboxylic group is needed for efficient photodegradation of studied BODIPY derivatives. We found by head-space gas chromatographic analysis of irradiated solutions that CO is released almost quantitatively from **IV-1** (87%). Only UV-light absorbing photoproducts were formed in the solution upon exhaustive irradiation. 2-Methylpyrrol and 2H-pyrrole-4-carbaldehyde were found by HRMS analysis of exhaustively irradiated reaction mixture.

Irradiation of **IV-2** in an aqueous solution (PBS, pH = 7.4) released CO not only upon excitation at the major absorption band maxima (368 and 652 nm) but also at the absorption tail in the near-infrared region (732 nm). The quantum yield of photorelease of CO was approx. one order of magnitude lower ( $\sim 1.2 \times 10^{-5}$ ) than that of **IV-1** which is probably caused by higher fraction of non-radiative decay pathways induced by flexible PEG chains.

The influence of oxygen on the photolysis quantum yield of **IV-1** ( $\Phi_{\text{decomp}}$  is lower by a factor of 2 in an aerated sample) suggested that its excited triplet state is involved in the CO release. The formation of a triplet state in **IV-1** is apparently not efficient due to fluorescence ( $\Phi_{\text{f}} = 67\%$ ) and perhaps other radiationless processes, and this may also partially explain the rather low decomposition quantum yields. Despite the fact that the quantum yield of photolysis of **IV-3** is high ( $\sim 1 \times 10^{-2}$ ) compared to other derivatives, the total chemical yield of released CO is low ( $\sim 3\%$ ). This indicates that the excited triplet of **IV-3** undergoes a photoreaction that does not lead to CO production.

To characterize the triplet state, we measured nanosecond transient spectroscopy of derivatives **IV-1** and **IV-3**. The triplet state of **IV-1** has a very weak signal due to its low quantum efficiency of formation and sophisticated methods for data accumulation had to be used to measure its transient spectrum. The triplet state of **IV-1** possesses absorption maxima at 430 and 640 nm and has a lifetime of  $\sim(5 \pm 1) \mu\text{s}$  in an aerated solution.

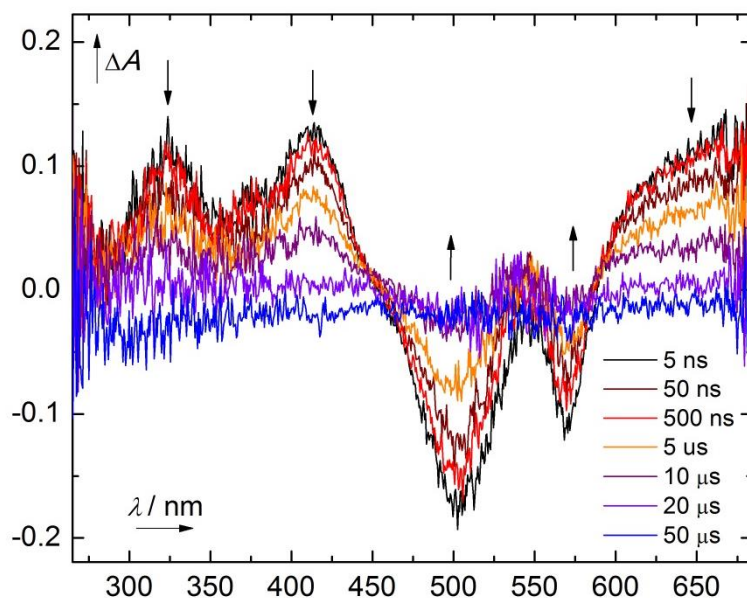


**Figure 56:** The transient absorption spectrum of **IV-3** ( $c \sim 5.0 \times 10^{-5} \text{ M}$ ; phosphate buffered saline; pH = 7.4; non-degassed); excited by a 532 nm laser pulse measured after 5 ns – 50  $\mu\text{s}$  after excitation

The compound **IV-3** has much higher population of triplet (which corresponds to the diminished fluorescence quantum yield discussed above). The transient triplet-triplet absorption spectrum of **IV-3** possesses three absorption maxima at 325, 415 and 660 nm (Figure 56) which exhibit the same decay kinetics. Triplet-state absorption bands in the region of 410–450 nm have already been reported for analogous brominated BODIPY derivatives.<sup>308</sup>

The final evidence that a triplet state is involved in the mechanism of CO release was provided by irradiation of **IV-1** in a degassed aqueous solution containing CsCl (1 M aqueous solution; an analogous NaCl-containing sample was used as a reference) as a heavy-atom effect mediator<sup>309</sup>. The quantum yield of photodegradation and CO production increased by a factor of 1.6 in the presence of  $\text{Cs}^+$  ions due to enhancement of the intersystem crossing, whereas the fluorescence quantum yield decreased from 67% to 53%.

Based on our findings, we proposed the mechanism of photolysis of BODIPY-based CORMs (Figure 57). The model chromophore **IV-4** (the methyl groups of **IV-1** were omitted due to limited number of atoms suitable for sophisticated quantum chemical calculations) undergoes an inter system crossing to the triplet state upon excitation. Our DFT calculations suggest that a photoinduced intramolecular electron transfer (PeT) takes place between the carboxylate and the BODIPY system in the triplet excited state to form a triplet diradical **IV-5**. The thermodynamics of the electron transfer has been calculated from the ground state redox potentials of BODIPY reduction and carboxylate oxidation determined by cyclic

voltammetry and from the triplet energy of excited BODIPYs estimated from its phosphorescence spectra.<sup>310</sup> The diradical **IV-5** closes to the  $\alpha$ -lactone **IV-6** and releases carbon monoxide. The unstable primary photoproduct with hydroxyl in the *meso*-position is hydrolyzed to a mixture of products.

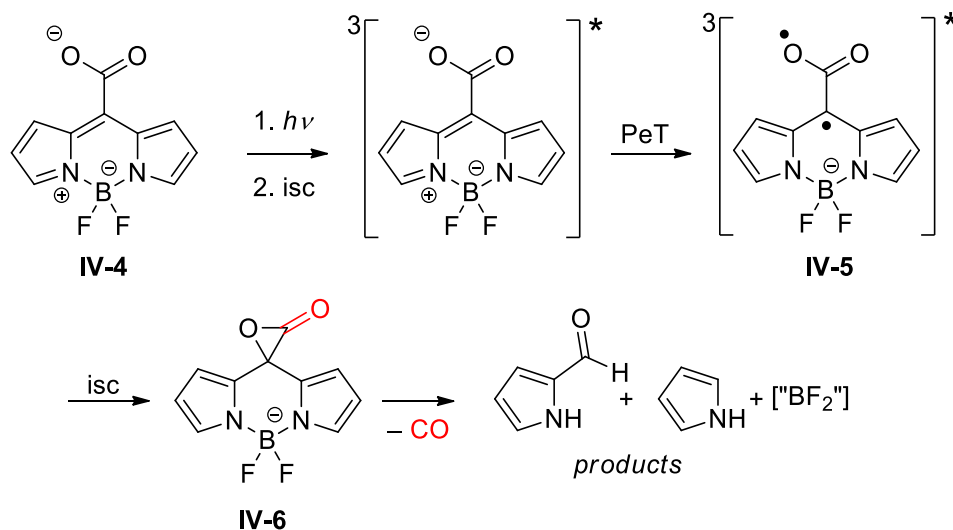


**Figure 57:** Proposed mechanism of photoinduced release of carbon monoxide from a BODIPY-based CORM.

### 3.4.4. Biological Application

We tested the toxicity of **IV-1** and **IV-2** and their photoproducts in *in vitro* experiments on hepatoblastoma HepG2 and/or neuroblastoma SH-SY5Y cell lines. No toxicity was found up to the concentrations of 100  $\mu\text{mol l}^{-1}$ . Encouraged by these results, we tested the photoinduced release of CO *in vitro* in samples of blood and *in vivo* with a nude SKH1 mouse strain. We observed a significant rise of the COHb concentration in blood samples as well as in blood and tissue (hepatic and kidney tissue) of live animals upon application of **IV-2** and irradiation with polychromatic white light. No rise has been observed in the control samples and groups of animals (no CORM added and/or no irradiation).

### 3.4.5. Conclusion

We managed to improve our xanthene-based CORM **III-1** and introduced a novel structural type of CORMs based on *meso*-substituted BODIPY. The synthesis of these derivatives is simple and high-yielding and they can be activated by visible-to-NIR (up to 730 nm) light. We investigated the ability of **IV-1** and **IV-2** to efficiently release CO in a fully controllable way, and demonstrated their performance in both *in vitro* and *in vivo* experimental settings. We performed a detailed mechanistic study of the photodegradation of derivatives **IV-1** to **IV-3**. Based on our steady-state and transient absorption spectroscopy experiments and quantum chemical calculations, we proposed a mechanism of the CO release. The decarbonylation occurs through photoinduced electron transfer from the triplet state of BODIPY and subsequent formation of the  $\alpha$ -lactone **IV-6**.

### 3.4.6. Author's Contributions

E.P. synthesized the compounds, E.P. and T.S. measured steady-state spectroscopy (absorption, emission and excitation spectra) and performed irradiation experiments. T.S. measured the quantum yields, voltammetry and transient spectroscopy data. L. M. accomplished the biological experiments and head-space gas chromatography measurements. T. Š. did the quantum chemical calculations.

## 3.5. Photocatalytic Reduction of Aldehydes

The results of this project were published in: Ghosh, T.; Slanina, T.; König, B. *Chem. Sci.* **2015**, *6*, 2027-2034.<sup>311</sup> The manuscript is attached in Appendix E (Pages S31-S38).

The Supporting information is available at:

<http://www.rsc.org/suppdata/sc/c4/c4sc03709j/c4sc03709j1.pdf> and is attached as an electronic file on CD.

### 3.5.1. Introduction

In 2012, Park and Nam have introduced<sup>312</sup> a photocatalytic system using proflavine (**V-1**, PF, 3,6-diaminoacridine) as photocatalyst and [Cp\*Rh<sup>III</sup>(bpy)Cl]Cl (**V-2**, Rh<sub>cat</sub>) as a mediator for the regeneration of NADH from NAD<sup>+</sup> produced by enzymatic synthesis of L-glutamate demonstrating an artificial photosynthetic approach. The schematic mechanism of this process is depicted in Figure 58. Proflavine gets reduced by photoinduced electron transfer (PeT) from sacrificial electron donor, triethanolamine (TEOA). Reduced proflavine is re-oxidized back by rhodium mediator **V-2** which generates rhodium hydride, [Cp\*Rh<sup>III</sup>(bpy)H]Cl (**V-3**, Rh(III)–H). **V-3** regioselectively reduces NAD<sup>+</sup> (or FAD) to NADH + H<sup>+</sup> (or FADH<sub>2</sub>). This reduced co-factor drives the transformation of 2-oxoglutarate to L-glutamate accomplished by the enzyme L-glutamate dehydrogenase.

We wanted to modify this system for synthetic purposes, especially for photocatalytic reductions of synthetically useful substrates. This method would use visible light and a cheap and safe organic amine for reduction reactions usually accomplished with sensitive, dangerous and expensive reagents such as hydrides.

Proflavine (**V-1**) is a well-known acridine dye studied in detail for its ability to bind with DNA.<sup>313</sup> It has also been used as a promising molecule for the photogeneration of hydrogen.<sup>314</sup> Rhodium catalyst **V-2** has been first described by Youinou and Ziessel in 1989.<sup>315</sup> Since then it has frequently been used as a hydride transferring agent for cofactor regeneration.<sup>316</sup> Unlike other hydrides, it exhibits an outstanding regioselectivity in the reduction of NAD<sup>+</sup>.<sup>317</sup> It has also been used for the chemical reduction of both aldehydes and ketones by hydride transfer from formic acid.<sup>318,319</sup>

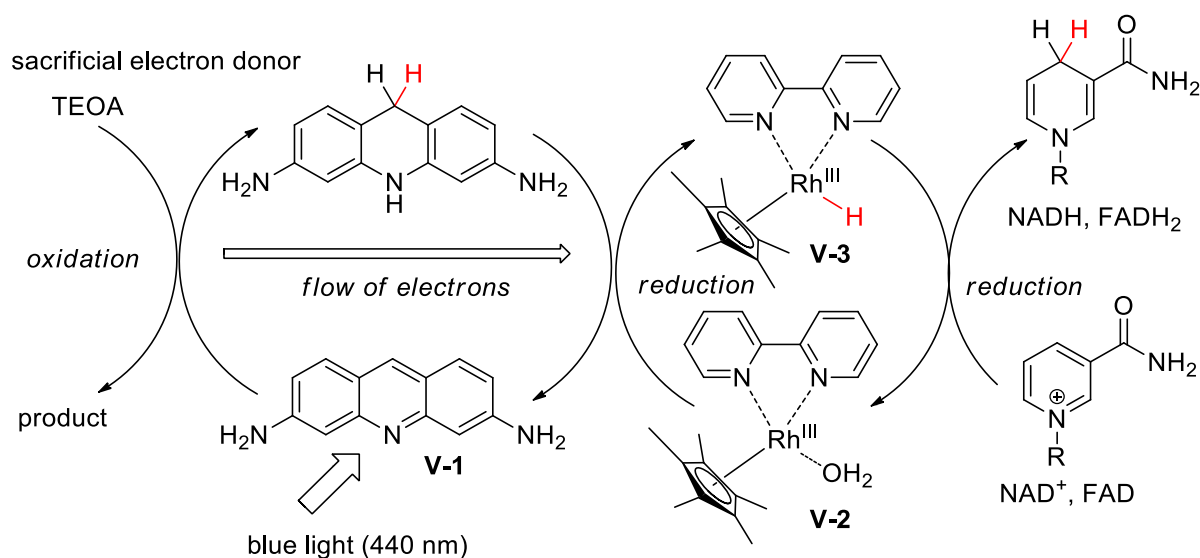


**Figure 58:** Mechanism of cofactor regeneration introduced by Park and Nam.<sup>312</sup>

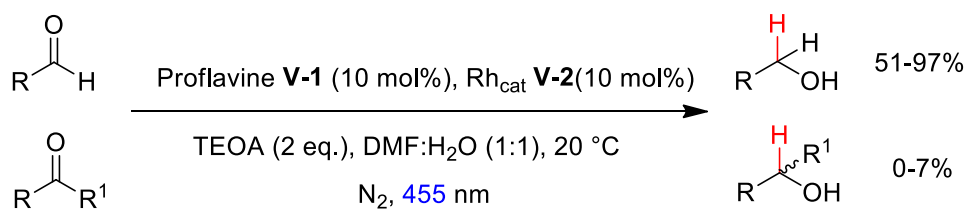
### 3.5.2. Synthesis

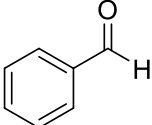
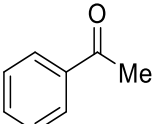
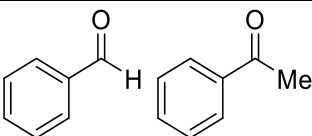
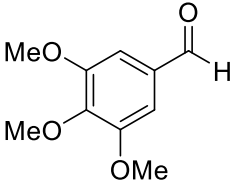
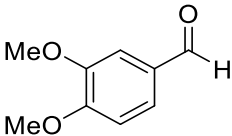
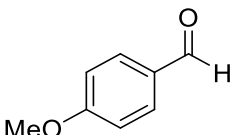
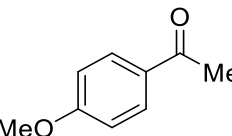
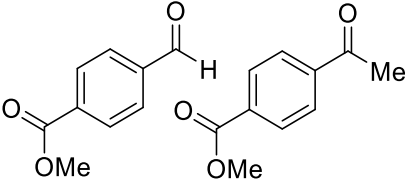
We tested our photocatalytic system for reduction of carbonyl compounds (Figure 58, carbonyl as a substrate instead of NAD<sup>+</sup>). The initial trials revealed that benzaldehyde can be efficiently reduced to benzyl alcohol and therefore it was used as a model substrate for optimization of the reaction conditions. The yields of benzyl alcohol were highest in case of 10 mol % of both V-1 and V-2. Both MeCN and DMF could be used as solvents but DMF was preferred since the aliphatic substrates dissolve better in it. However, all reactions in anhydrous organic solvents did not yield a significant amount of product as water is required as a proton source for generation of Rh(III)–H V-3.<sup>320</sup> We therefore used a mixture of DMF/H<sub>2</sub>O (1:1, v/v) as a solvent for all reactions. Moreover, all components (sacrificial electron donor, photocatalyst, mediator, and water-containing solvent) and features (degassed system, blue light) of the system had to be present unless the reaction did not occur as found by control experiments. The non-degassed reaction yielded only 30% of the product which indicates that the presence of oxygen does not shut the reaction down; it only slows it by the factor of ~3.

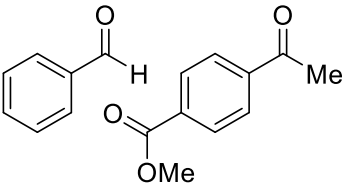
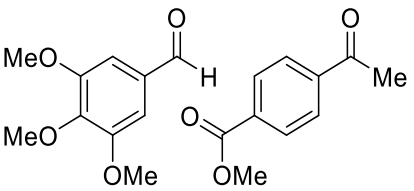
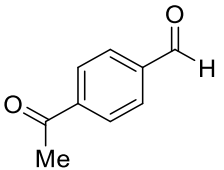
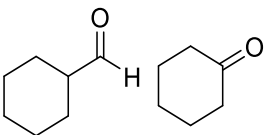
Various aromatic and aliphatic aldehydes and ketones were tested as substrates in the catalytic system (Table 1). The optimized reaction conditions were used for all substrates (Table 1, upper part). The reaction rate could be accelerated by a factor of 5, without affecting the selectivity (Table 1, entries 1–3) using a flow reactor, which uses more intense light source. Excellent yields were obtained for neutral, electron rich and electron poor aldehydes, whereas the corresponding ketones remained unreacted. Using an activated ketone as one reactant, we performed the reduction reactions varying the other reactant from electron-poor to electron-neutral to electron-rich aldehyde with notable selectivity (Table 1, entry 8-10). The selectivity was observed not only for a mixture of aldehyde and ketone, but also for a bifunctional molecule (Table 1, entry 11). Somewhat lower yield in entry 11 is caused by a

side reaction leading to a pinacol-type product. In entry 12 a lower yield was obtained, because of decomposition of the substrate, which is not related to the photoreaction.

**Table 1:** Substrate scope for photocatalytic reduction of carbonyl compounds



Entry	Substrate(s)	Reaction type	Time/h	Yield(s)
1		batch	15	97
		flow	3.5	91
2		batch	15	7
		flow	3.5	4
3		batch	15	95 (4)*
		flow	3.5	82 (<1)*
4		batch	25	95
5		batch	25	83
6		batch	32	84
7		batch	32	3
8		batch	18	76 (2)*

9		batch	16	91 (2)*
10		batch	25	93 (4)*
11		batch	16	51 (<1)**
12		batch	42	56 (3)*

\*Yields of ketone reductions; \*\*Yield of doubly reduced product

The rate of the reduction is partially dependent on the electron density of the aldehyde functionality. That indicates that the hydride transfer from Rh(III)–H **V-3** to the carbonyl compound is the rate-determining step. Generally, the photoreduction is slower for electron-rich aldehydes, but no clear trend was observed. Ketones are almost unreacted, which is mainly caused by steric effects. Rhodium catalyst **V-2** is sufficiently crowded to create selectivity even between similar substrates, which was demonstrated on various  $\text{NAD}^+$  model compounds.<sup>317</sup>

### 3.5.3. Steady-State Studies and Rhodium-Based Mechanism

We investigated the mechanism of the photocatalytic reduction system in detail. The interaction of **V-1** with TEOA and **V-2** has been studied by steady state. Titration of protonated PFH<sup>+</sup> ( $\text{p}K_{\text{a}} = 9.5^{317}$ ) solution (aq.,  $c = 5.0 \times 10^{-6}$  M) with TEOA or TEA resulted in a decrease in fluorescence intensity as observed by Basu *et al* (Figure 59, upper part).<sup>321</sup> They suggest that TEA is quenching the singlet excited state of **V-1** by PeT which is in contradiction with the well-established PeT from proflavine triplet. The absorption spectra indicate the formation of a free base - PF by a simple acidobasic equilibrium, which was also supported by the UV and fluorescence pH titrations. We did not observe the formation of PFH<sup>+</sup>...TEA ground-state complex as proposed by Basu *et al*.<sup>321</sup>



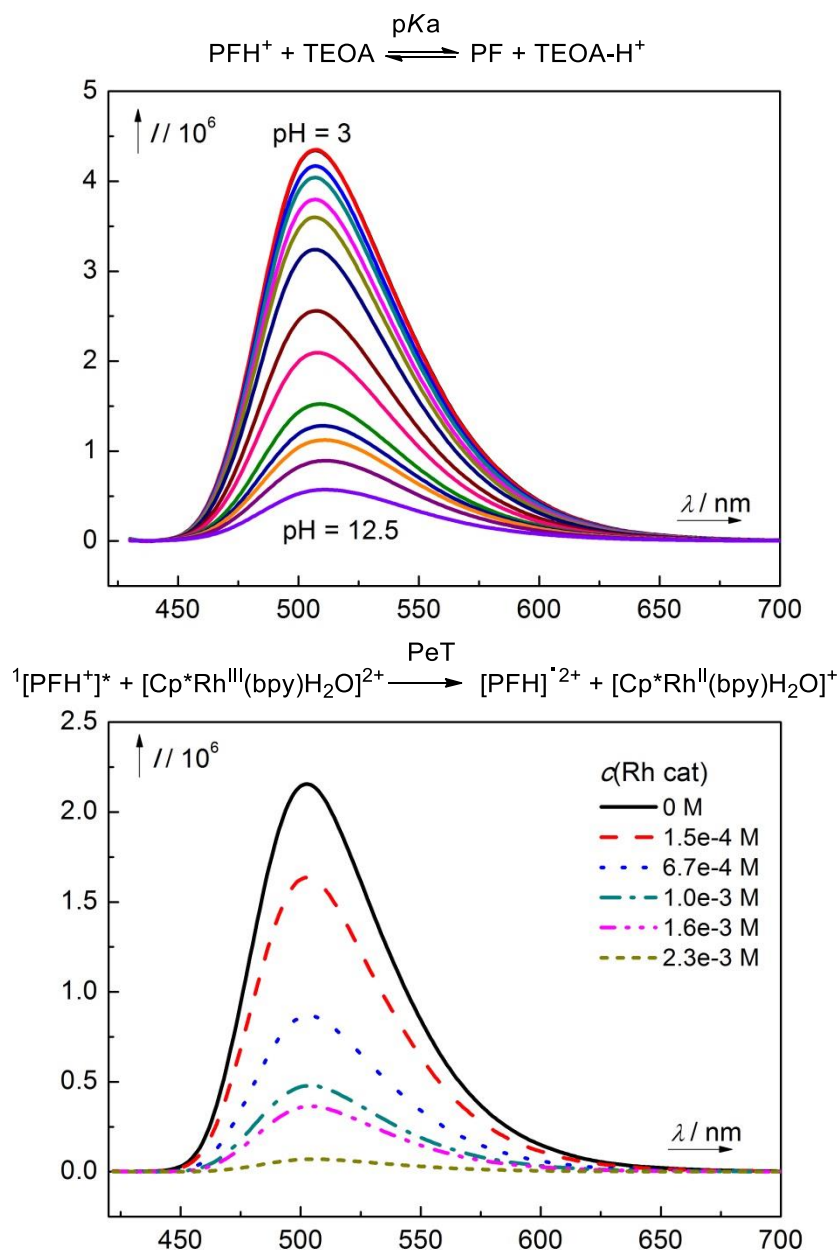


**Figure 59:** Fluorescence quenching of proflavine with TEOA (upper part) and with **V-2** (lower part).

Fluorescence quenching of proflavine with **V-2** is shown in Figure 59, lower part. Unlike TEOA, the Rh catalyst does not interact with PF in the ground state and the quenching is observed due to photooxidation of proflavine from the singlet excited state  ${}^1[\text{PFH}^+]$ .

Based on the literature data and our experimental results we suggest the mechanism of the rhodium catalytic cycle depicted in the Figure 60. The aqueous solution of **V-2** contains  $[\text{Cp}^*\text{Rh}^{\text{III}}(\text{bpy})\text{H}_2\text{O}]\text{Cl}_2$  **V-4**, formed after the ligand exchange of  $\text{Cl}^-$  to  $\text{H}_2\text{O}$ . This process is important for the catalytic activity making the central metal ion more accessible.<sup>322</sup> In the next step, the rhodium aqua-complex is reduced. In principle, two different mechanisms are possible: the one electron reduction<sup>320</sup> or a hydride transfer from a suitable hydrogen donor (*e.g.*  $\text{HCOO}^-$ )<sup>322</sup> have both been described in detail.

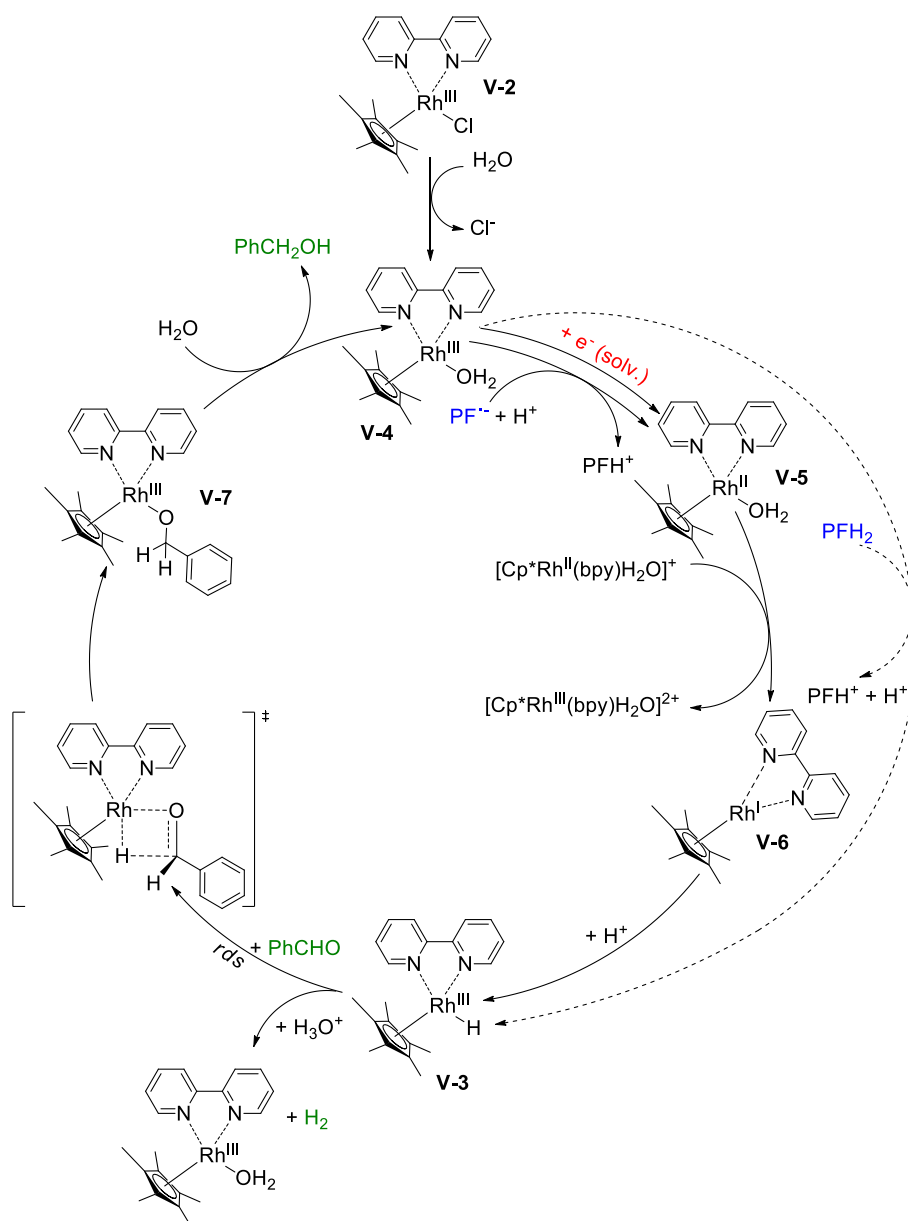


**Figure 60:** Proposed rhodium catalytic cycle, rds = rate determining step

The first mechanism applies for PFH<sup>•</sup> generated by PET from <sup>3</sup>[PFH<sup>+</sup>]<sup>\*</sup> and TEOA and subsequent deprotonation ( $pK_a(\text{PFH}\cdot) = 4.5$ )<sup>323</sup>. The d<sup>7</sup> complex [Cp\*Rh<sup>II</sup>(bpy)H<sub>2</sub>O]<sup>+</sup>, **V-5**, created after the one electron reduction is not stable and disproportionates fast to a rhodium(I) complex **V-6**. This d<sup>8</sup> complex, [Cp\*Rh<sup>I</sup>(bpy)], is then protonated by a protic solvent to give Rh(III)–H, **V-3**.

In case of a possible direct hydride transfer between [Cp\*Rh<sup>III</sup>(bpy)H<sub>2</sub>O]Cl<sub>2</sub> and PFH<sub>2</sub>, **V-3** is formed directly. **V-3** can either reduce the corresponding carbonyl (productive reaction) or can be protonated again to produce dihydrogen regenerating the catalyst. This step is responsible for the kinetic selectivity of the reduction of aldehydes over ketones. In case of hydride reduction the carbonyl group is reduced to an alkoxy ligand **V-7**, which is easily hydrolyzed<sup>318</sup> giving the corresponding alcohol.

### 3.5.4. Transient Spectroscopy and Overall Mechanism

We further investigated the mechanism by means of transient absorption and emission spectroscopy. We managed to develop a method suitable for detailed investigation of any photocatalytic mechanism. Most photocatalytic systems use three components – photocatalyst, substrate and an electron donor/acceptor (or electron mediator). Our method enables to determine whether reductive or oxidative quenching cycle occurs and which reaction step plays the key role in the whole system.

The method consists of measurement of ground state spectroscopy, time-resolved fluorescence and transient spectroscopy (transient spectra and kinetics) of four solutions: (i) solution of photocatalyst, (ii) solution of photocatalyst with the electron donor/acceptor, (iii) solution of photocatalyst with substrate, (iv) solution of photocatalyst with substrate and electron donor/acceptor. The conditions (concentrations, equivalency) should be as close as possible to the investigated system.

Our method can clearly detect the operating excited state of the photocatalyst (singlet or triplet) and can distinguish between reductive and oxidative quenching by observation of the transient radical species formed upon PeT. It can also determine the order of consecutive redox reactions together with the rate constants of quenching. We applied this method for determination of mechanism of photocatalytic systems described in Chapters 3.5. and 3.7.

An example of this method used to study the mechanism of photocatalytic reduction is shown below.

(i) The solution of PF ( $c = 2.2 \times 10^{-4}$  M) in DMF/water mixture exhibited a strong fluorescence negative peak directly after the excitation flash. After  $\sim 50$  ns, when the fluorescence decays (the fluorescence lifetime was reported to be  $\sim 5$  ns)<sup>324</sup> three peaks were observed at 550, 610 and 670 nm, respectively. This was assigned to the  $^3[\text{PFH}^+]$ . The lifetime of the PF triplet was approx. 2  $\mu\text{s}$  in aerated solution. The triplet spectrum and lifetime corresponds to the previously published data.<sup>325</sup>

(ii) The solution of PF and  $\text{Rh}_{\text{cat}}$  ( $c_{\text{Rh}} = 2.0 \times 10^{-4}$  M) showed partially quenched fluorescence and the intensity of the PF triplet peak was significantly lowered. This finding indicates that  $\text{Rh}_{\text{cat}}$  partially quenches the excited singlet state, which also leads to a diminished triplet yield.

(iii) The transient spectra of the solution of PF and TEOA ( $c_{\text{TEOA}} = 25.8 \times 10^{-3}$  M) exhibited a new peak with an absorption maximum at  $\sim 530$  nm and with a lifetime of approx. 8  $\mu\text{s}$  in aerated solution. The observed peak was oxygen-sensitive and corresponds to the proflavine radical  $\text{PF}\cdot^-$ ,<sup>325</sup> which confirms the PeT from TEOA to  $^3[\text{PFH}^+]$ .

(iv) The transient spectrum of the solution of PF, TEOA and  $\text{Rh}_{\text{cat}}$  exhibited the absorption peak of  $\text{PF}\cdot^-$ . The intensity of the peak was lower than in the case of  $\text{PFH}^+$  and TEOA solution and its lifetime shortened to  $\sim 3$   $\mu\text{s}$  caused by the electron transfer from the  $\text{PF}\cdot^-$  to  $\text{Rh}_{\text{cat}}$ .

Based on our mechanistic experiments and literature reports we propose the overall catalytic mechanism depicted in Figure 61 with two mechanistic pathways. The main pathway operates in degassed samples (Figure 61, right blue part). After absorption of a blue photon  $\text{PFH}^+$  is excited to the first excited singlet state. Fluorescence (prompt and delayed) is a significant deactivation pathway with an overall quantum yield of 39%.<sup>326</sup> Intersystem

crossing (isc) gives the triplet state which accepts an electron from TEOA. The radical PFH $\cdot$  is deprotonated to the radical anion PF $\cdot^-$ , which is then oxidized by Rh $_{\text{cat}}$  back to PFH $^+$ . In the absence of the metal complex the radical anion dimerizes to “LeucoPF” or disproportionates to PFH $_2$ .<sup>327</sup> The reduced Rh $_{\text{cat}}$  reacts according to the catalytic cycle depicted in Figure 60.

Another, oxygen-insensitive, mechanism is dominant in non-degassed solutions. As oxygen can efficiently quench both  $^3[\text{PFH}^+]^*$  and PF $\cdot^-$ , the product cannot be formed in this case through the triplet reductive pathway (Figure 61, right side). PF is known for its photoionization from  $^1[\text{PFH}^+]^*$  after excitation (Figure 61, left red part).<sup>324</sup> The photoionization produces solvated electrons<sup>325</sup> which react either with PFH $^+$  to form PF $\cdot^-$  or with Rh $_{\text{cat}}$  to form Rh(II) species **V-5**.<sup>327</sup> The oxidized PF radical cation [PF $\cdot^+$ ] $^+$  is then reduced back by TEOA present in the system. These two parallel mechanisms (oxidative and reductive quenching operating simultaneously) have been recently found in an iridium-based photocatalytic system.<sup>328</sup>

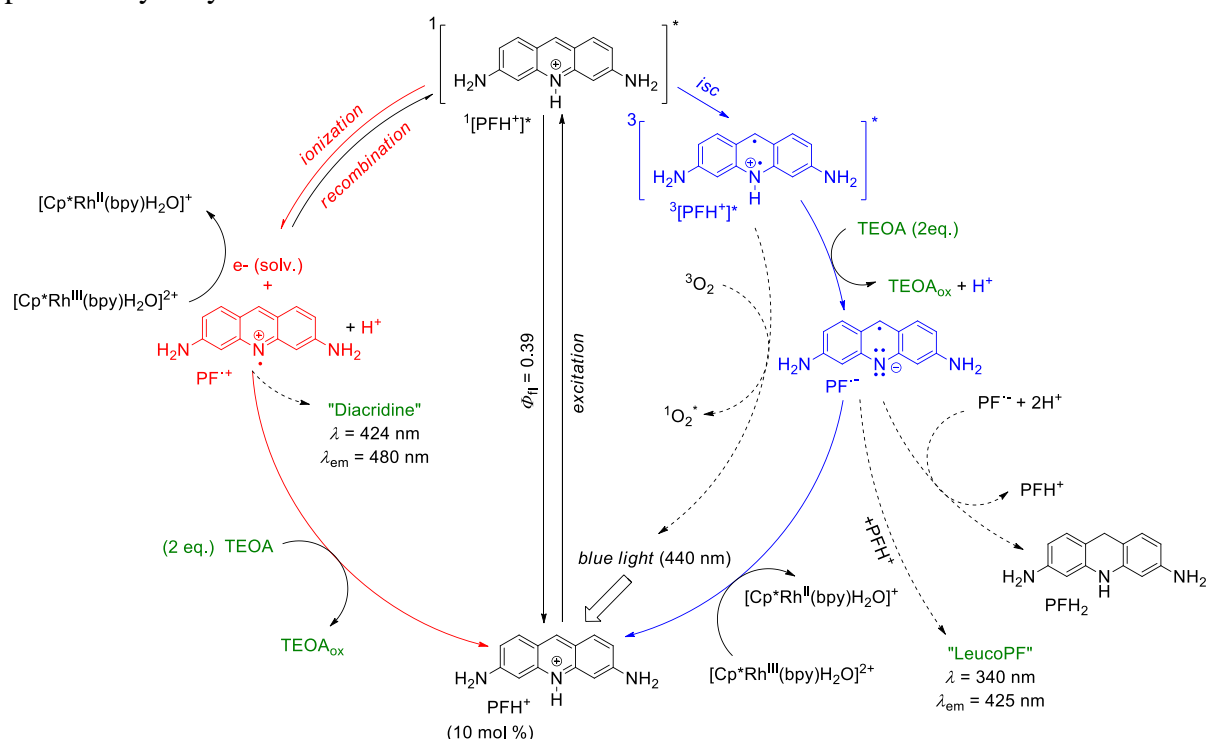


**Figure 61:** Proposed proflavine catalytic cycle.

### 3.5.5. Conclusion

We have achieved selective photocatalytic reduction of aldehydes over ketones with a broad substrate scope employing *in situ* generated Rh(III)–H **V-3** as the reduction reagent. Unlike in the case of formate based aqueous buffer system, the Rh(III)–H is formed slowly in the reaction medium and is therefore able to kinetically distinguish between aldehydes and ketones. The photoreduction proceeds both *via* photoinduced electron transfer from triethylamine to proflavine triplet and by subsequent reduction of Rh $_{\text{cat}}$ .

### 3.5.6. Author's Contributions

T.G. and T.S. investigated the substrate scope. T.G. optimized the reaction conditions. T.S. synthesized standards for GC calibration. T.S. performed the steady-state and transient spectroscopy measurements and other mechanistic studies.

## 3.6. Photooxidation of Nitrate by Visible Light

The results of this project were published in: Hering, T.; Slanina, T.; Hancock, A.; Wille, U.; König, B. *Chem. Commun.* **2015**, *51*, 6568-6571.<sup>329</sup> The manuscript is attached in Appendix F (Pages S39-S42).

The Supporting information is available at: <http://www.rsc.org/suppdata/c5/cc/c5cc01580d/c5cc01580d1.pdf> and is attached in electronic version on CD.

### 3.6.1. Introduction

The nitrate radical ( $\text{NO}_3^\cdot$ , **VI-1**) is the most important nocturnal free radical oxidant in the troposphere.<sup>330</sup> In the gas phase  $\text{NO}_3^\cdot$  oxidizes a broad scope of volatile organic species.<sup>331,332</sup> It is a highly reactive and chemically versatile O-centered radical<sup>333</sup> with an oxidation potential of +2.00 V (vs. SCE in MeCN).<sup>334</sup> It exhibits several modes of reactivity, such as electron transfer (eT),<sup>335,336</sup> addition to  $\pi$  systems<sup>330,337</sup> and hydrogen abstraction (hydrogen atom transfer, HAT).<sup>334,338,339</sup> Overall, the reactivity of  $\text{NO}_3^\cdot$  with organic molecules can be seen in between that of hydroxyl radicals ( $\text{OH}^\cdot$ ) and sulfate radical anions ( $\text{SO}_4^{\cdot-}$ ).<sup>340</sup> Despite its high chemical versatility, only limited synthetic applications of  $\text{NO}_3^\cdot$  are available so far. Shono *et al.* reported the addition of electrochemically generated  $\text{NO}_3^\cdot$  to alkenes.<sup>337</sup> The reaction of  $\text{NO}_3^\cdot$  with alkyne ethers leads to tetrasubstituted tetrahydrofurans.<sup>341,342</sup>

One reason for the limited use of  $\text{NO}_3^\cdot$  as a reagent in organic transformations is its rather difficult accessibility. Common methods for  $\text{NO}_3^\cdot$  generation on preparative scale in solution are the reaction of nitrogen dioxide and ozone,<sup>330,343</sup> electrooxidation of nitrate anions<sup>337</sup> or the photolysis of  $(\text{NH}_4)_2\text{Ce}(\text{NO}_3)_6$  (CAN) with UV light ( $\lambda_{\text{irr}} = 350 \text{ nm}$ )<sup>340,344</sup> However, the use of toxic gases, high electrode potentials,<sup>334</sup> or UV irradiation are so far limiting the applications and lead to undesired side reactions.

We therefore investigated the possibility of generation of **VI-1** by a photocatalytic method using a highly oxidizing photocatalyst, 9-mesityl-10-methylacridinium perchlorate ( $\text{Acr}^+$ -Mes, **VI-2** Figure 62), blue light and oxygen as a terminal oxidant. Acetonitrile turned out to be the most suitable organic solvent since the lithium nitrate dissolves reasonably well in it.

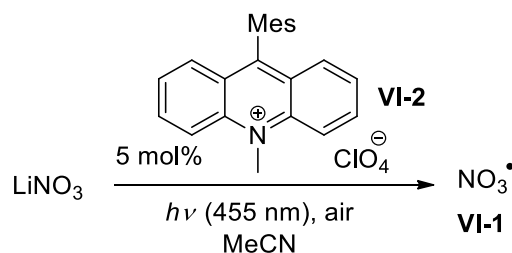


**Figure 62:** Photocatalytic system for generation of nitrate radical **VI-1**.

### 3.6.2. Synthetic Applications

We selected the well-studied reaction of  $\text{NO}_3^\bullet$  with diphenylacetylene (**VI-3**, Figure 63) yielding benzil (**VI-6**) and benzophenone (**VI-9**) to chemically prove the ability of the photocatalytic system to generate nitrate radical. Under photocatalytic conditions using 5 mol% of  $\text{Acr}^+\text{-Mes}$  (**VI-2**), 0.25 mmol of alkyne **VI-3** and 2 eq. of  $\text{LiNO}_3$ , diketone **VI-6** (~30% yield) and ketone **VI-9** (~20%) were obtained after 2 h of irradiation with blue light ( $\lambda = 455 \text{ nm}$ ) with yields comparable to previous methods.<sup>345</sup> When oxygen was replaced by ammonium persulfate as the electron acceptor in a degassed system, the yield and product ratio were not changed significantly. This shows that potential interfering reactions by singlet oxygen could be excluded. In the absence of light or catalyst no reaction occurred. However, small amounts (~13%) of diketone **VI-6** were formed in the direct reaction of **VI-3** with the excited catalyst in the absence of nitrate ions. This indicates the direct oxidation of diphenylacetylene by acridinium photocatalyst **VI-2**.

The mechanism of the  $\text{NO}_3^\bullet$ -induced oxidation of diphenylacetylene has been studied by quantum chemical computations.<sup>345</sup> The oxidation starts with addition of nitrate radical to the triple bond of **VI-3** which forms a vinyl radical adduct **VI-4** (Figure 63). While diketone **VI-6** results from a 5-endo cyclization of the radical adduct to **VI-5**, followed by loss of  $\text{NO}^\bullet$ , the key-step in the formation of benzophenone (**VI-9**) is  $\gamma$ -fragmentation with elimination of  $\text{NO}_2^\bullet$ , and subsequent Wolff-rearrangement of the carbene intermediate **VI-7** to ketene **VI-8** followed by oxidative decarboxylation.

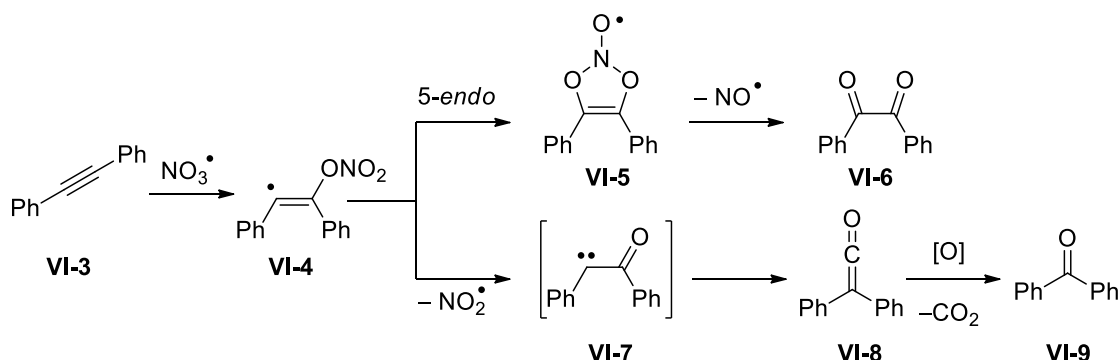


**Figure 63:** Proposed mechanism for the oxidation of aromatic alkynes by nitrate radical.

Apart from addition to  $\pi$  systems,  $\text{NO}_3^\bullet$  is known for its ability to abstract hydrogen atoms,<sup>334,338,339</sup> which we explored in the catalytic oxidation of non-activated alcohols. In this reaction,  $\text{NO}_3^\bullet$  acts as a redox mediator, which is regenerated during the catalytic cycle,

according to the mechanism in Figure 64. Initial HAT from the alcohol carbon atom in **VI-10** by  $\text{NO}_3^{\cdot}$ <sup>346</sup> leads to the regeneration of  $\text{NO}_3^-$  in form of nitric acid and formation of radical **VI-11**. The radical is subsequently oxidized by either another equivalent of  $\text{NO}_3^{\cdot}$  or by oxygen to give the cationic intermediate **VI-12**, which deprotonates to yield ketone **VI-13**. This mechanism is supported by findings of Donaldson and Styler who reported the enhanced gas phase oxidation of propanol under UV irradiation using  $\text{TiO}_2$  co-embedded with  $\text{KNO}_3$ . The finding was explained by formation of  $\text{NO}_3^{\cdot}$  and its ability to abstract hydrogen atoms from the alcohol carbon atom.<sup>347</sup> This method enabled to oxidize alcohols to ketones in moderate yields (40 – 50%).

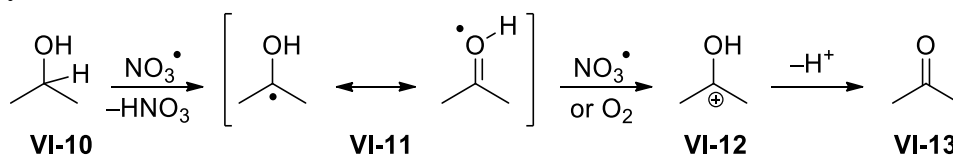


**Figure 64:** General mechanism of the nitrate mediated alcohol oxidation *via* initial hydrogen abstraction followed by oxidation and loss of a proton.

### 3.6.3. Mechanistic Studies

Since the results of the synthetic part were suggesting *in situ* generation of nitrate radical **VI-1**, we wanted to elucidate the mechanism of its formation. Unfortunately, our first attempts for direct detection of **VI-1** by electron paramagnetic resonance (EPR) coupled with online irradiation were unsuccessful. Moreover, the absorption spectrum of **VI-1** could not be detected by nanosecond transient spectroscopy of the photocatalytic system. The control experiment with the photolysis of  $\text{CAN}^{340,344}$  detected  $\text{NO}_3^{\cdot}$  but in the measurements of the whole photocatalytic systems the acridinium catalyst **VI-2** always interfered with the used analytical technique (EPR or transient spectroscopy).

The long-lived triplet state of **VI-2** with a microsecond lifetime is generally discussed as the reactive state in most oxidative photocatalytic reactions.<sup>348,349</sup> The exact nature of this state is controversial and could be both a charge-transfer ( $\text{CT}^{\text{T}}$ , Figure 68) state with an oxidation potential of +1.88 V vs. SCE, as reported by Fukuzumi<sup>348</sup> or a locally excited triplet state,  $\text{LE}^{\text{T}}$ , with an oxidation potential of +1.45 V vs. SCE as reported by Verhoeven,<sup>349</sup> However, neither would have the oxidative capacity to oxidize  $\text{NO}_3^-$ . We detected the triplet state of **VI-2** by nanosecond transient spectroscopy (Figure 65). Its characteristic absorption spectrum with maximum absorption at 490 nm is at short times after excitation (10 ns, Figure 65, black line) superimposed by the fluorescence of **VI-2** (the differential of transient signal at 10 ns (black line) and at 30 ns (blue line) after excitation is shown in Figure 65 as a red line; it reasonably corresponds with the fluorescence spectrum of **VI-2** (orange line)). The triplet is quenched by oxygen as demonstrated by the difference in signal intensity of transient spectra at 150 ns after excitation in degassed (navy blue line) and aerated solution of **VI-2** (magenta line). The presence of nitrate did not influence the lifetime of triplet which corresponds to the insufficient redox potentials of  $\text{CT}^{\text{T}}$  and  $\text{LE}^{\text{T}}$  for oxidation of  $\text{LiNO}_3$ .

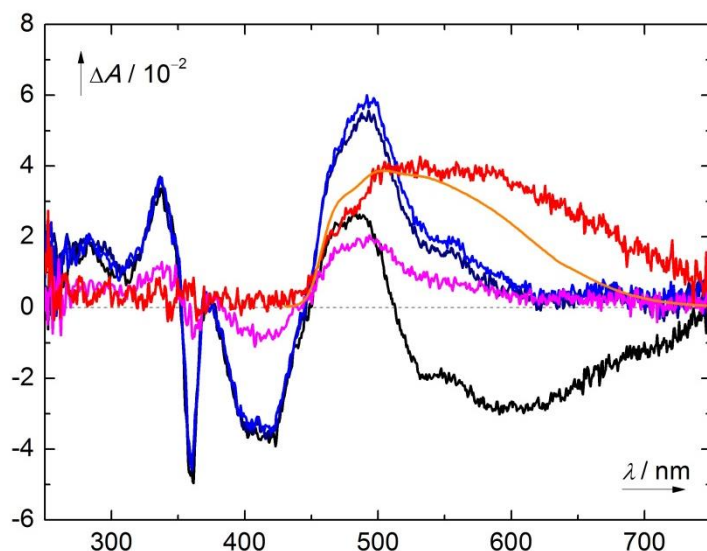


**Figure 65:** Transient spectra of **VI-2** in MeCN excited at 355 nm at different times after excitation (black: 10 ns; blue: 30 ns; navy blue: 150 ns, degassed; magenta: 150 ns, aerated), differential spectrum (transient spectrum at 30 ns – transient spectrum at 10 ns; red line) and normalized fluorescence spectrum (orange line)

Recent detailed mechanistic investigations by the group of Nicewicz revealed that for substrates with oxidation potentials exceeding +1.88 V (vs. SCE), a reaction should occur out of the short-lived excited singlet state (mainly the charge transfer singlet  $CT^S$ ), which has an estimated oxidation potential of 2.08 V.<sup>350</sup> Since both singlet states (charge transfer singlet  $CT^S$  and locally excited singlet  $LE^S$ , Figure 68) are fluorescent ( $\Phi_{fl} \sim 8\%$ ), whereas the triplet states do not emit,<sup>350</sup> we performed fluorescence quenching experiments to explore the nature of the reactive state involved in  $NO_3^-$  oxidation. A quenching of the fluorescence by  $LiNO_3$  clearly confirms that oxidation of  $NO_3^-$  occurs from the singlet excited state of **VI-2** (Figure 66).

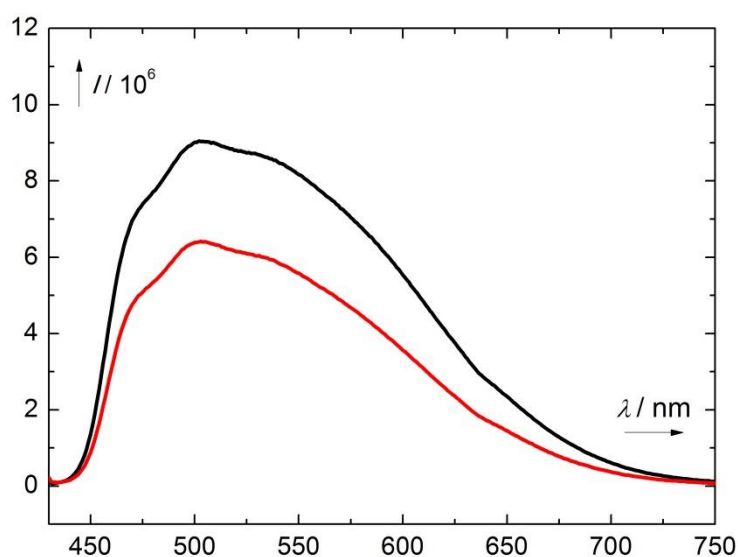


**Figure 66:** Fluorescence spectra of **VI-2** in MeCN ( $\lambda_{exc} = 412$  nm) in absence (black line) and in presence of  $LiNO_3$  (saturated solution in MeCN, red line)



In order to have a solid proof of the electron transfer between  $\text{NO}_3^-$  and **VI-2**, we monitored the generation of reduced catalyst **VI-14** (Figure 67) in the presence of  $\text{LiNO}_3$  upon continuous irradiation of a 5  $\mu\text{M}$  solution of **VI-2** in MeCN with 455 nm light under anaerobic conditions. The differential absorption spectrum shows the appearance of **VI-14** with a maximum at 520 nm (blue line, Figure 67) after irradiation for 120 s. The spectrum exactly matches the transient spectroscopy results published others.<sup>114,350</sup>

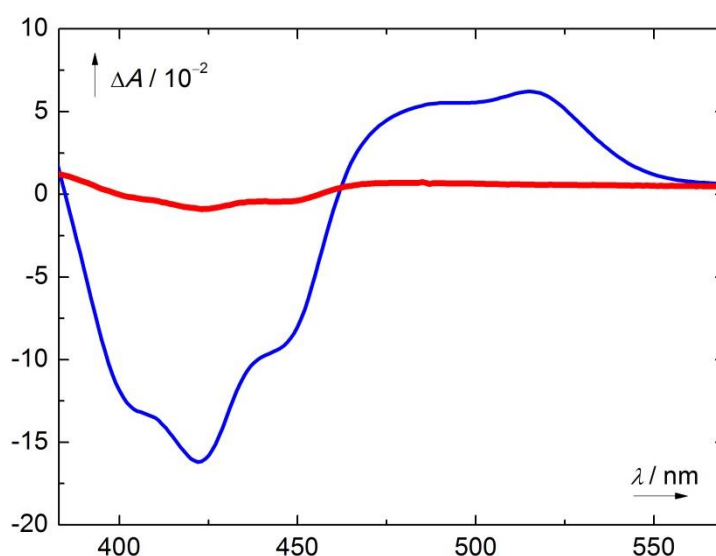


**Figure 67:** Differential absorption spectra (blank was taken on a solution before irradiation) of degassed solution of **VI-2** and  $\text{LiNO}_3$  in MeCN irradiated by 455 nm for 120 s (blue line) and after aeration (red line).

This observation suggests a direct oxidation of  $\text{NO}_3^-$  by the excited catalyst thus demonstrating that  $\text{NO}_3^-$  can act as an electron donor to the excited catalyst. The radical **VI-14** is stable under argon, however, the signal vanishes completely after aeration of the reaction mixture due to reoxidation of **VI-14** to the ground state catalyst **VI-2** by oxygen (Figure 67, red line).<sup>351</sup> The negative signal at  $\lambda < 460$  nm in the differential absorption spectrum (blue line, ground state bleach) is caused mainly by the decrease of the ground state absorption of **VI-2** as a result of **VI-14** formation and partial photobleaching of **VI-2** (after aeration the ground state absorption of **VI-2** cannot be fully recovered; Figure 67, red line).

The overall reaction mechanism is summarized in Figure 68. The electron transfer from  $\text{NO}_3^-$  occurs from the short-lived singlet state of **VI-2** ( $\text{LE}^{\text{S}}$  or  $\text{CT}^{\text{S}}$ ) with sufficient oxidative capacity to generate the reduced catalyst **VI-14** and  $\text{NO}_3^{\cdot-}$  (**VI-1**). The longer-lived transient triplet species ( $\text{CT}^{\text{T}}$  or  $\text{LE}^{\text{T}}$ ) are not reactive towards  $\text{NO}_3^-$ . The reduced catalyst **VI-14** is regenerated by oxygen producing a superoxide anion.

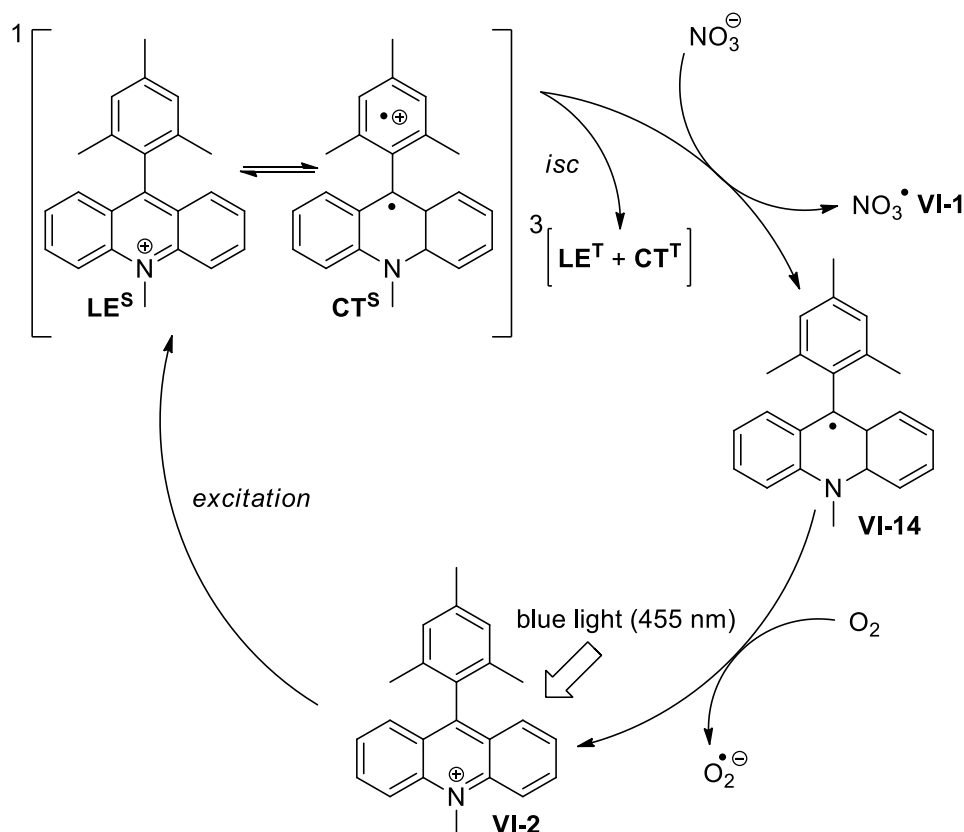


**Figure 68:** Overall mechanism of generation of NO<sub>3</sub><sup>•</sup> mediated by visible light.

### 3.6.4. Conclusion

We described a new and simple access to highly reactive nitrate radicals using visible light photocatalysis with an acridinium dye **VI-2** as the photoredox catalyst. This method avoids the use of toxic compounds, or high electrochemical potentials and is, to our best knowledge, the first method yielding NO<sub>3</sub><sup>•</sup> in a catalytic process using visible light. By carefully designed differential absorption spectroscopic experiments, we verified the formation of nitrate radicals by observation of the reduced catalyst **VI-14** and we showed that the mechanism is proceeding *via* the singlet excited state of the catalyst. By investigating the addition to aromatic alkynes, a previously well-studied model reaction of NO<sub>3</sub><sup>•</sup>, we showed that the photocatalytic procedure is as efficient as the previously employed methods.

### 3.6.5. Authors' Contributions

T.H. synthesized the compounds, optimized reaction conditions and isolated the products. T.S. accomplished quenching experiments, steady-state differential spectra and irradiation experiments. A.H. measured transient spectroscopy.

### 3.7. Photocatalytic Arylation by Fluorinated Aryl Bromides

The results of this project were submitted for publication. The submitted manuscript is attached in Appendix G (Pages S43-S50). The Supporting information is attached in electronic version on CD.

#### 3.7.1. Introduction

Aryl radicals (**VII-1**, Figure 69) play an important role as intermediates of many photocatalytic reactions. They are so versatile as they can be used in C–H arylation reactions leading to products which would normally require usage of transition metal catalysts, such as palladium<sup>352,353</sup> or copper,<sup>354</sup> and often the use of organometallic starting materials, such as boronic acids,<sup>355-357</sup> borate salts,<sup>358,359</sup> benzoates,<sup>360,361</sup> copper species,<sup>362</sup> or stannanes<sup>363</sup>.

There are several methods known for generation of aryl radicals (Figure 69). The method of generation of aryl radicals from diazonium salts (*route A*) was developed by our group for Meerwein arylations<sup>247</sup> and was further used for reactions with  $\sigma$ -donors<sup>364</sup>.

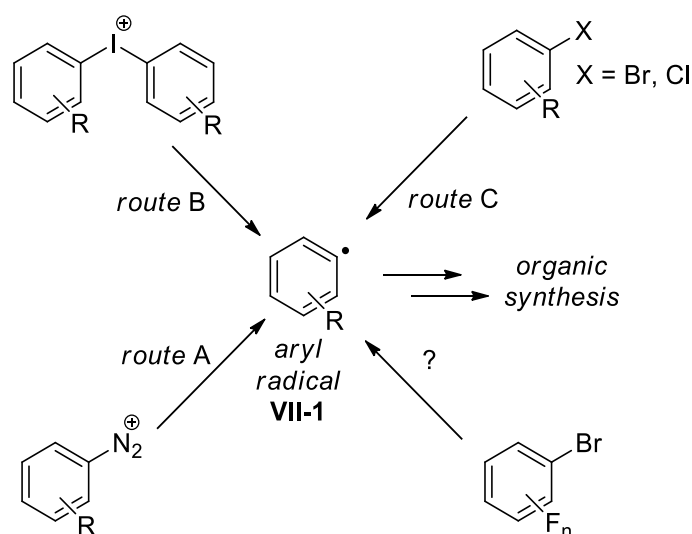


**Figure 69:** Methods for photocatalytic generation of aryl radicals.

Diaryl iodonium salts have similar redox potential as diazonium salts ( $\sim 0$  V vs SCE) and were also used as precursors for **VII-1** (*route B*).<sup>365</sup> In 2014, our group has developed a method for generation of aryl radicals by consecutive visible light-induced electron transfer processes using perylene bisimide as a photocatalyst (*route C*).<sup>273</sup> Two photons are needed to reach a sufficient redox potential to reduce aryl bromide and some aryl chlorides which limits the quantum efficiency of the process.

We wanted to use polyfluorinated bromoarenes as sources of **VII-1** (*route D*) which should have redox potential sufficiently low for photoinduced reduction by a common organic photocatalyst such as eosin Y.

### 3.7.2. Synthetic Applications

To test our hypothesis, we used a photocatalytic reaction system containing a mixture of 1-bromo-2,3,4,5,6-pentafluorobenzene (**VII-2**, Figure 70), benzene, eosin Y (**VII-3**) and triethylamine and irradiated it with green LED light under nitrogen atmosphere. After optimization of the reaction conditions (equivalency of all components, the optimized conditions are shown in Figure 70) we achieved satisfactory yield of 63% of biphenyl derivative **VII-4** (Ar = Ph, Figure 70) with two equivalents of the electron donor in acetonitrile as solvent. The use of other solvents, like DMSO and DMF, and different electron donors, such as DIPEA, decreased the product yield. Control experiments without base, catalyst or light, confirmed that all components are necessary for product formation. In non-degassed reaction mixtures the yield of product decreased drastically (6%), most likely due to the competing quenching of the eosin excited triplet state by molecular oxygen.<sup>366</sup>

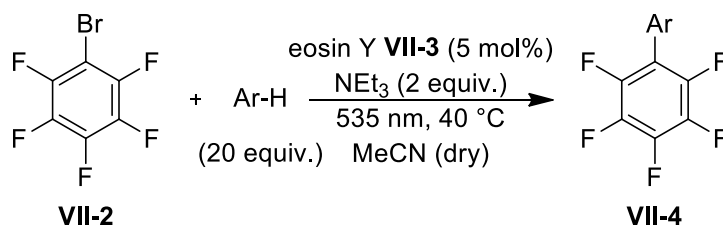


**Figure 70:** Model C–H arylation reaction with optimized conditions.

The reaction scope was extended by using various fluorinated bromoarenes and together with arenes used in excess (20 eq). Electron donating or electron withdrawing substituents are generally well tolerated. Surprisingly, the pentafluorophenyl radical **VII-1** is also able to ipso-substitute arene methoxy groups as illustrated by compound **3q**. Reports of methoxy groups as leaving groups in radical reactions are rare in the literature.<sup>367-370</sup> This approach was used for derivatization of a complex non-protected natural product, brucine **VII-5**, to demonstrate the functional group tolerance and the use in late stage functionalization (Figure 71). The methoxy group in position *C-II* is substituted by **VII-1**.

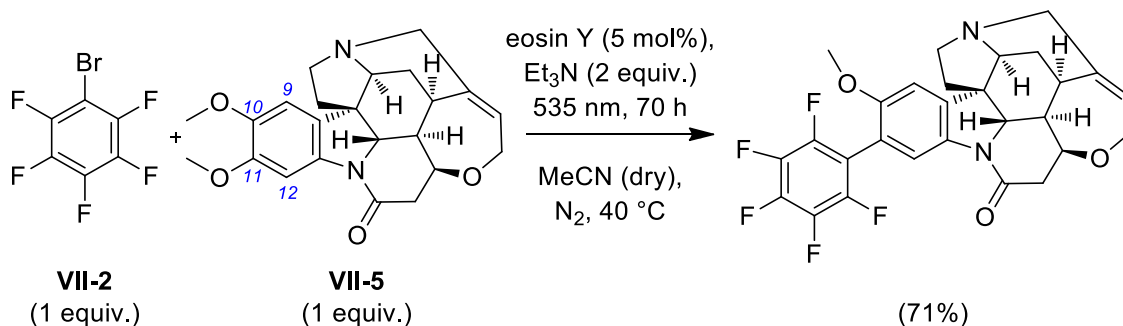


**Figure 71:** Aromatic functionalization of brucine (**VII-5**)

### 3.7.3. Mechanistic Studies

The mechanistic studies were accomplished using a model reaction with bromoarene **VII-2**, eosin Y (**VII-3**, triethylammonium salt) as a photocatalyst and triethylamine (TEA) as a sacrificial electron donor and a base. Eosin Y is a xanthene dye with ambivalent reactivity as a photocatalyst. It was used in oxidative quenching cycles as a photoreductant of diazonium salts<sup>371</sup> as well as for the photoinduced reduction of nitrobenzenes, where eosin enters the reductive quenching cycle with a suitable sacrificial electron donor.<sup>372</sup> Based on the known photoreactivity of eosin Y, two plausible mechanisms for the here described photocatalytic reaction of fluorinated aryl bromides **VII-2** can be proposed (Figure 72).

The reductive quenching cycle (Figure 72, upper part) involves a photoinduced electron transfer from TEA to the excited eosin Y and subsequent re-oxidation of the generated radical **VII-6** by bromopentafluorobenzene **VII-2**. The reduced fluorinated arene cleaves the C<sub>Ar</sub>-Br bond yielding the pentafluorophenyl radical **VII-1**, which reacts to the product.<sup>373</sup> The oxidative quenching cycle is based on photoinduced electron transfer from excited eosin Y to bromopentafluorobenzene. In both cases hydrobromic acid is produced, which is neutralized by one equivalent of TEA present in the reaction mixture. Another equivalent of TEA is needed for the efficient quenching of the triplet excited state of eosin Y and also partially as a base for deprotonation of the lactone isomer of eosin Y used for the reactions. The photocatalytically active forms of eosin Y are the anion and dianion.<sup>270</sup>

The mechanism of the photocatalytic reaction was elucidated by steady-state (UV-vis, fluorimetry) and transient spectroscopy (nanosecond pump-probe spectroscopy) and electrochemical measurements.

The thermodynamics of electron transfer calculated from ground state redox potential of **VII-2** (determined by cyclic voltammetry) and excited state redox potentials of **VII-3**<sup>270</sup> excluded the oxidative quenching mechanism through oxidized eosin Y **VII-7** (Figure 72, bottom). It also predicted a low quantum yield for the studied system since the re-oxidation of **VII-6** by **VII-2** is slightly endothermic. The endothermic reaction equilibrium is shifted towards the products by the subsequent irreversible fission of the bromide anion from the fluorinated arene.<sup>373</sup>

The fluorescence experiments did not find any quenching of fluorescence of **VII-3** by either TEA or **VII-2**. This indicates that the excited state of **VII-3** involved in the photocatalytic cycle is the triplet state.

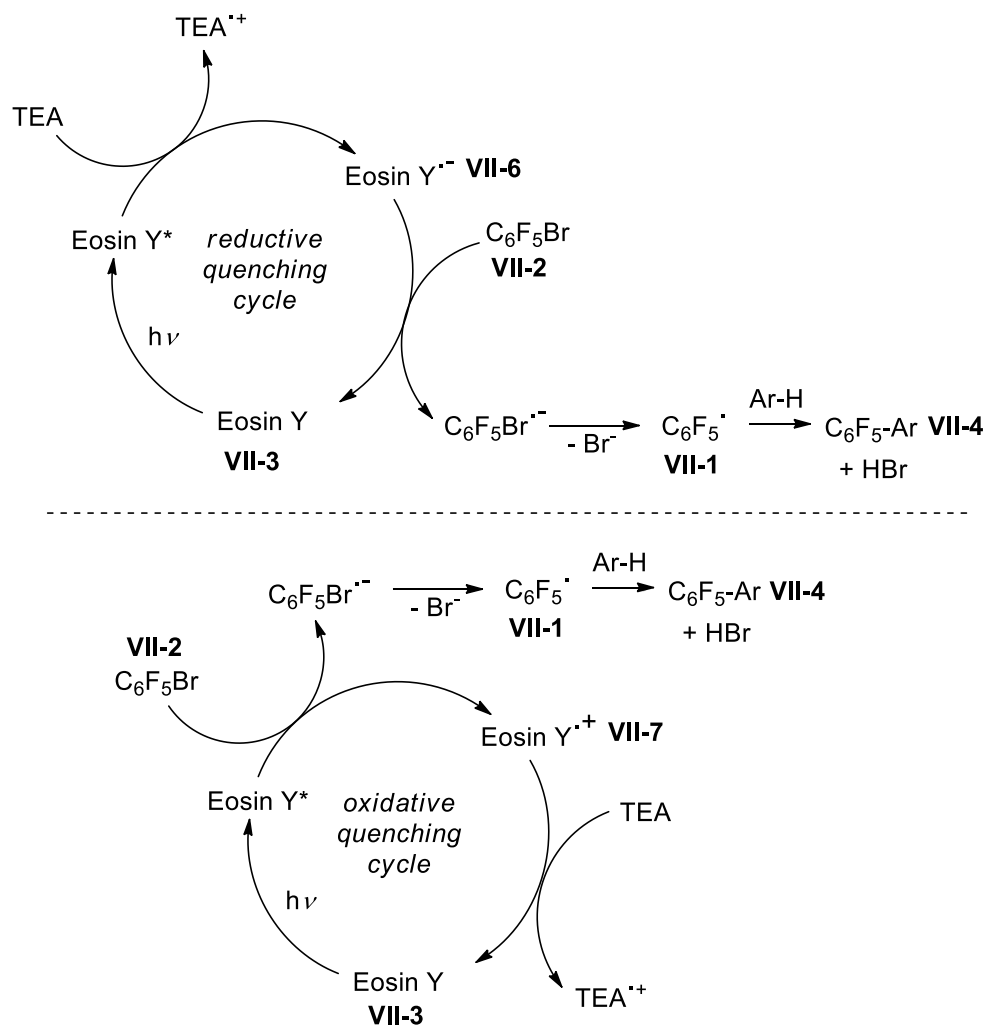


**Figure 72:** Two proposed catalytic reaction cycles: reductive (top) and oxidative (bottom) quenching of **VII-3**.

We further studied the reaction mechanism by nanosecond transient spectroscopy. We used our method for determination of quenching of excited photocatalyst which was introduced in Chapter 3.5.4. The transient spectra of a solution of **VII-3** revealed both excited states of eosin Y. Immediately after excitation the singlet absorption peak ( $\lambda_S = 440$  nm), ground state bleach ( $\lambda_{GS} = 550$  nm) and fluorescence ( $\lambda_{FI} = 645$  nm) can be observed. The singlet state spectrum corresponds to the literature data.<sup>374</sup> Ground state bleach and fluorescence signal correspond to the absorption and emission spectra of eosin Y. The singlet decays with  $\tau_S = 6$  ns, which corresponds to the measured fluorescence lifetime. After the intersystem crossing, the triplet of **VII-3** is formed with its characteristic absorption peak at 580 nm corresponding to published data.<sup>375</sup> The triplet lifetime of eosin Y in non-degassed acetonitrile is  $\tau_T = 320$  ns. The triplet is quenched by oxygen present in the system as well as triplet-triplet interactions, but the bimolecular processes do not play an important role and the decay can be fitted with a mono-exponential function.

The transient spectra and the respective kinetic decays of transients (singlet a triplet of eosin Y) did of solution of **VII-3** and **VII-2** corresponded to those of free eosin Y which indicates that there is no interaction between eosin Y and bromopentafluorobenzene.

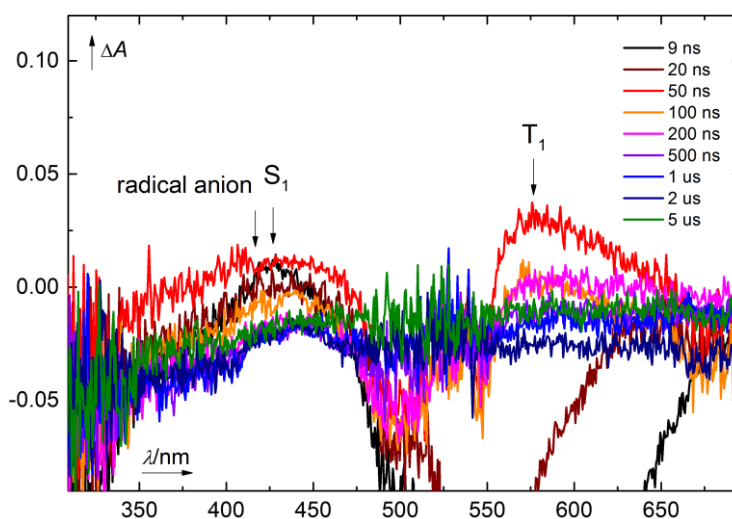


**Figure 73:** Transient absorption spectra of **VII-3** ( $10^{-4}$  M in acetonitrile, non-degassed, excitation wavelength 532 nm) and TEA ( $10^{-2}$  M) at different times after excitation

The transient spectra of a solution of **VII-3** and triethylamine contain all features of previous spectra (ground state bleach at 550 nm, fluorescence at 645 nm, singlet at 440 nm and triplet at 580 nm; Figure 73). The triplet lifetime of EY under these conditions is  $\tau_T = 280$  ns, which is lower than in solution of pure eosin Y indicating the quenching of the triplet state by TEA. Moreover, a new transient appears at 405 nm, which is assigned to the radical anion **VII-6** according to literature data.<sup>372</sup> The lifetime of the radical anion is 500 ns in non-degassed solution and is quenched mainly by re-oxidation by oxygen.

Since the absorption spectra of singlet and radical anion of eosin Y overlap, we performed kinetic analysis of the transient absorption at 435 nm of solutions of **VII-3** + TEA (Figure 74, top) and **VII-3** + **VII-2** (Figure 74, bottom). In the upper part, the fast decay corresponds to the singlet state and in the lower part the singlet is observed together with the radical anion (slow decay).

The solution of all three components, eosin Y, bromopentafluorobenzene and TEA exhibited transient spectra analogical to the solution of eosin Y and TEA. Only the lifetime of **VII-6** shortened from 500 ns to 250 ns. The results of the laser flash experiments are summarized in Table 2. The lifetimes clearly indicate that the triplet state is reductively quenched by TEA to create **VII-6**, which further transfers an electron to pentafluorobromobenzene.

Based on our detailed mechanistic study we can conclude that the reductive quenching mechanism is operating as depicted in Figure 72, upper part.

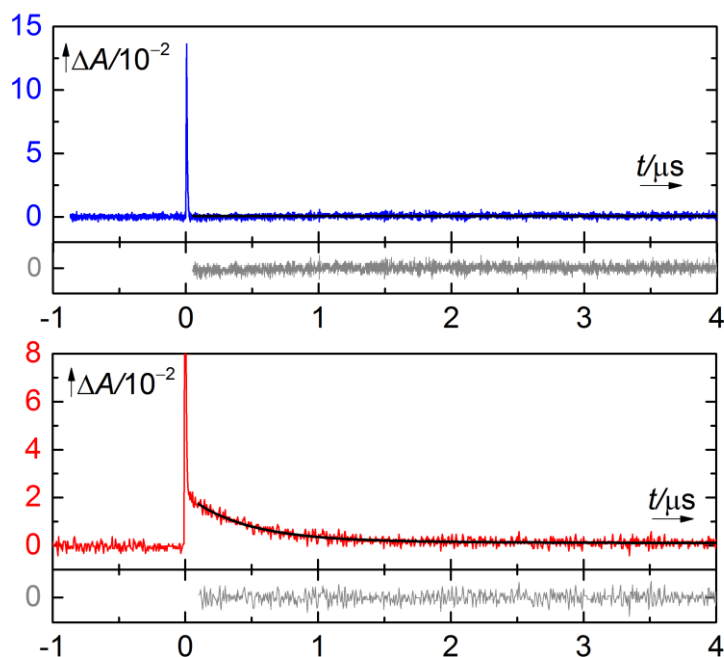


**Figure 74:** Decay traces of solutions of **VII-3** + **VII-2** (top, blue) and **VII-3** + TEA (bottom, red) ( $10^{-4}$  M eosin Y and  $10^{-2}$  M TEA/**VII-2**) at 435 nm and the corresponding fits (black) and residuals (gray) after mono-exponential fit. The decay of the singlet (fast decay, both spectra) and of the radical anion **VII-6** (slow decay, bottom) can be observed.

**Table 2:** Transient species of eosin Y **VII-3** and its lifetimes in non-degassed MeCN under various conditions; n. o. = not observed.

transient		singlet	fluorescence	triplet	<b>VII-6</b>
$\lambda$ [nm]		440	645	580	405
$\tau$ [ns]	<b>VII-3</b>	6	6	320	n. o.
	<b>VII-3</b> + <b>VII-2</b>	6	6	320	n. o.
	<b>VII-3</b> +TEA	6	6	280	500
	<b>VII-3</b> + <b>VII-2</b> + TEA	6	6	280	250

### 3.7.4. Conclusion

We have developed a new method for photocatalytic generation of fluorinated aryl radicals and we have used it in the synthesis of fluorinated biaryls as well as in late stage functionalization of brucine. We found that the photocatalytic reaction system operates through reductive quenching mechanism where eosin Y **VII-3** is photoreduced by TEA *via* its triplet state by green light irradiation. The corresponding radical anion **VII-6** is then re-oxidized by bromopentafluorobenzene **VII-2** or bromotetrafluoro arenes. The radical anion of the halogenated arene fragmentates to give the corresponding fluorinated aryl radical **VII-1** and a bromine anion.



### **3.7.5. Authors' Contributions**

C.J.Y. accomplished preliminary experiments and tested the model reactions. A.M. investigated the substrate scope, optimized the reaction conditions and synthesized the standards. A.M. expanded the project with late-stage derivatization of brucine. T.S. studied the mechanism by means of transient and steady-state spectroscopy and thermodynamic calculations.

## **3.8. Heavy-Atom Effect of Selanyl- and Tellanyl-Substituted BODIPYs**

The results of this project were submitted for publication. The submitted manuscript is attached in Appendix H (Pages S51-S69). The Supporting information is attached as an electronic file on CD.

### **3.8.1. Introduction**

4,4-Difluoro-4-bora-3a,4a-diaza-*s*-indacene (BODIPY, Chapter 2.3.3.) derivatives have found extensive applications as fluorescent dyes and biological probes due to their robust and easily tunable photophysical properties.<sup>302-304,376-380</sup> BODIPY chromophores typically exhibit sharp absorption peaks, high molar absorption coefficient and very high quantum yields of fluorescence. The intersystem crossing (isc) quantum yield ( $\Phi_{ISC}$ ) of most derivatives of BODIPYs is negligible.

Molecules with high population of triplet state have broad applications as triplet photosensitizers in photocatalysis, photovoltaics, photodynamic therapy (singlet oxygen generation), or triplet-triplet annihilation upconversion.<sup>381</sup> Since BODIPYs are excellent chromophores, many attempts have been undertaken to increase their intersystem crossing quantum yield. Nagano and his collaborators were first to prepare a 2,6-diiodo BODIPY derivative.<sup>382</sup> The presence of the iodine atoms enhances intersystem crossing due to a strong spin-orbit coupling between singlet and triplet states (heavy atom effect).<sup>383,384</sup> High photoinduced cytotoxicity of this compound initiated intensive research in the field of heavy-atom substituted BODIPY derivatives. Various bromo and iodo analogues with different substituents<sup>378</sup> as well as those bearing alternative ISC promoters, such as heavy metal containing units, were designed and studied.<sup>379,385,386</sup> Heavy atom-free BODIPY dimers represent an alternative solution in the design of triplet sensitizers.<sup>387-391</sup> Structural variations of this type as well as extension of the BODIPY  $\pi$ -system by styryl or thiophene substituents shifts the absorption band maxima bathochromically to the spectral region called the phototherapeutic (tissue-transparent) window (650–950 nm).<sup>300</sup>

Recently, Vosch and coworkers found that the presence of heavy chalcogen atoms (Se, Te) dramatically reduces the fluorescence due to efficient intersystem crossing.<sup>392</sup> We decided to design several selenium- and tellurium-containing BODIPY derivatives as potential triplet sensitizers and compare their quantum yields of isc with halogen-substituted BODIPYs.

### 3.8.2. Photophysical properties

We have synthesized a series of 7 BODIPY derivatives (**VIII-1–7**, Figure 75) according to known procedures of derivatization of BODIPY chromophore.<sup>392,393</sup>

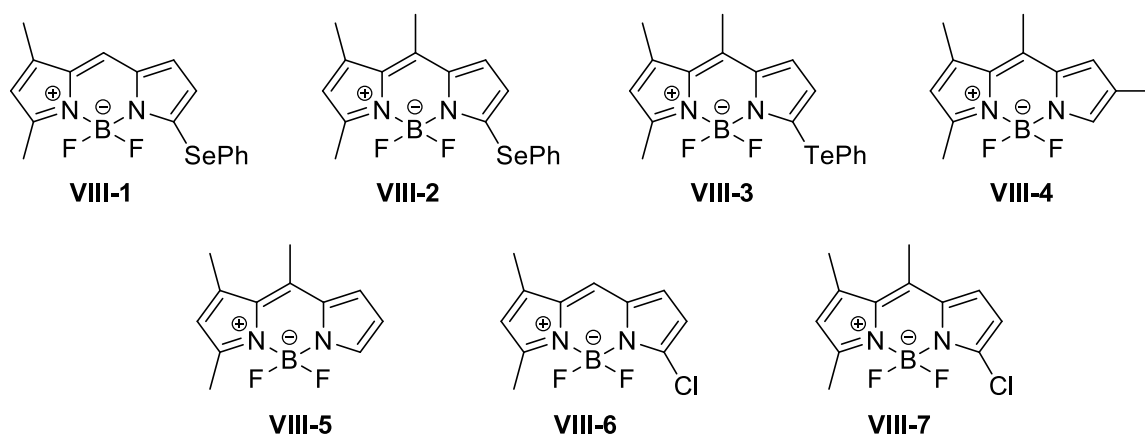


**Figure 75:** Structures of studied BODIPY derivatives **VIII-1–7**

The absorption properties of the BODIPY derivatives **VIII-1–7** in acetonitrile are summarized in Table 3. The absorption spectra possess characteristic features of the basic BODIPY chromophore.<sup>394</sup> The maximum absorption band has the absorption ( $\lambda_{\max}$ ) in the region of 482–540 nm. A sharp peak and its shoulder in the absorption spectra is a manifestation of the allowed  $S_0 \rightarrow S_1$  transition of the delocalized  $\pi$ -conjugated system. Smaller molar absorption coefficients ( $35\text{--}55 \times 10^3 \text{ mol}^{-1} \text{ dm}^3 \text{ cm}^{-1}$ ) than those of unsubstituted symmetrical BODIPY derivatives ( $80\text{--}120 \times 10^3 \text{ mol}^{-1} \text{ dm}^3 \text{ cm}^{-1}$ )<sup>380</sup> are probably caused by an asymmetric substitution pattern, leading to charge separation between the pyrrole rings.<sup>395</sup> A second, less pronounced band observed in the region of 225–400 nm is attributed to the  $S_0 \rightarrow S_2$  transition. The absorption bands are bathochromically shifted for the derivatives **VIII-1–3** compared to those of **VIII-4–7**. A bathochromic shift observed is clearly a consequence of an increasing electron-donating ability of the substituent. The relatively small Stokes shifts (13–45 nm) observed in all derivatives are related to the rigidity of the BODIPY system.

The compounds **VIII-5–7** exhibit bright fluorescence, whereas the heavy atom (I, Se, Te) containing derivatives **VIII-1–4** are only weakly fluorescent at room temperature. The bathochromic shifts caused by the heavy atoms is also apparent in emission spectra of **VIII-1–3**. The fluorescence lifetimes,  $\tau_f$ , of **VIII-1**, **VIII-2** and **VIII-4** were shorter than those of the BODIPY derivatives **VIII-5–7**. We were unable to determine  $\tau_f$  of **VIII-3** because the compound photochemically degraded during the fluorescence measurement, and a new signal of a photoproduct overlapped that of **VIII-3**. The derivatives **VIII-2** and **VIII-3** were photochemically degraded to the H-derivative **VIII-5**. The effect of heavy atoms (Se, Te, I) on the fluorescence quantum yield clearly indicates the enhancement of the intersystem crossing.

**Table 3:** Absorption photophysical properties of **VIII-1–7** in acetonitrile

compound	$\lambda_{\max}/\text{nm}$	$\varepsilon_{\max}/\text{mol}^{-1} \text{ dm}^3 \text{ cm}^{-1}$	$\lambda_f/\text{nm}^a$	$\Phi_f/\%^b$	$\tau_f/\text{ns}^c$
<b>VIII-1</b>	538	52000	551	$6.3 \pm 0.4$	$0.53 \pm 0.01$
<b>VIII-2</b>	527	38200	545	$20 \pm 1$	$1.23 \pm 0.01$
<b>VIII-3</b>	540	36600	585	$0.09 \pm 0.03$	n. d. <sup>e</sup>
<b>VIII-4</b>	493	35400	521	$4.8 \pm 0.2$	$0.34 \pm 0.01$
<b>VIII-5</b>	483	37100	496	$92 \pm 3$	$5.98 \pm 0.01$
<b>VIII-6</b>	497	51640	507	$74^d$	$5.46 \pm 0.01$
<b>VIII-7</b>	488	37840	501	$73^d$	$5.60 \pm 0.01$

<sup>a</sup> **VIII-1–4** and **VIII-7**:  $\lambda_{\text{exc}} = \lambda_{\text{max}}$ ; **VIII-5**:  $\lambda_{\text{exc}} = 452 \text{ nm}$ ; **VIII-6**:  $\lambda_{\text{exc}} = 460 \text{ nm}$ . <sup>b</sup> The standard deviations were calculated from 5 independent measurements. <sup>c</sup> The standard deviations were calculated from 3 independent measurements. <sup>d</sup> From the ref.<sup>396</sup> <sup>e</sup> n. d. = not determined.

### 3.8.3. Transient spectroscopy

We investigated the properties of the excited states of BODIPY derivatives by nanosecond transient spectroscopy. Derivatives **VIII-1–4** exhibited strong absorption after 8 ns after excitation pulse. The representative transient absorption spectrum of **VIII-1** in non-degassed acetonitrile at different times after excitation (8 ns – 1  $\mu\text{s}$ ) is shown in Figure 76. Absorption maxima at 420 and  $\sim 650 \text{ nm}$  as well as a ground state bleach at 535 nm, resembling its absorption spectrum, were observed. The decay or rise of the signals at the corresponding wavelengths followed the same monoexponential kinetics, and we attribute the signal to the lowest triplet state of **VIII-1**. Similar transient absorption of the triplet state of BODIPY derivatives has been reported before.<sup>308,392</sup> The decay of the triplet state signals of **VIII-1** in both aerated and degassed acetonitrile solutions gave the triplet lifetimes of  $\tau_T = 0.24$  and 7.3  $\mu\text{s}$ , respectively (Table 4).

The transient spectral characteristics of triplet states of **VIII-1–4** (absorption maxima, lifetimes and molar absorption coefficients) are shown in Table 4. Compound **VIII-1** has the highest molar absorption coefficient at  $\lambda_{\text{max}}$  in both the triplet-triplet and  $S_0 \rightarrow S_1$  absorption spectra. The triplet lifetimes are similar for all four derivatives and quenching by oxygen can be clearly observed.

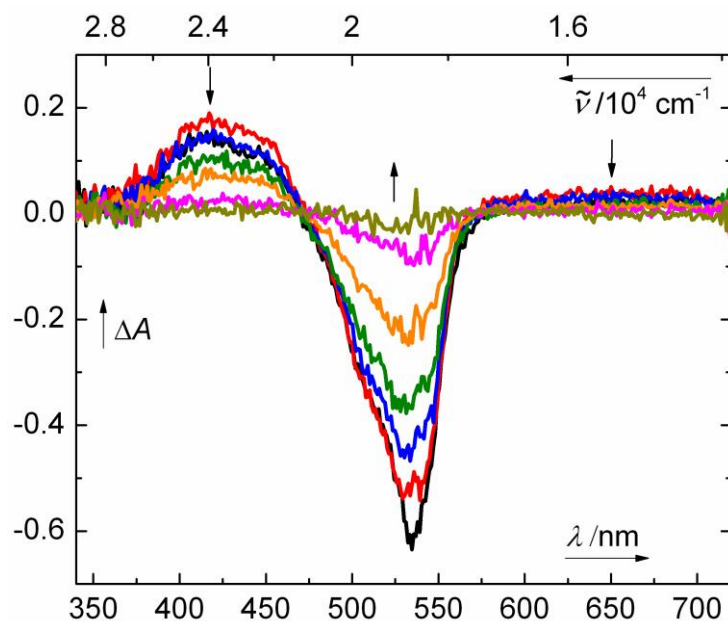


**Figure 76:** Transient spectra ( $\lambda_{\text{exc}} = 532 \text{ nm}$ ) of **VIII-1** in non-degassed acetonitrile ( $c = 1.10 \times 10^{-5} \text{ mol dm}^{-3}$ ) obtained 8 ns–1  $\mu\text{s}$  after excitation.

In order to quantify the amount of the triplet state formed after excitation of **VIII-1-4**, we developed a method for determination of quantum yield of intersystem crossing by nanosecond transient spectroscopy. Many studies on heavy-atom substituted BODIPYs attempted to determine the quantum yield of triplet formation by different methods. The most common is the use of the Ermolayev's rule ( $\Phi_{\text{ISC}} = 1 - \Phi_{\text{fl}}$ ).<sup>397</sup> This approach assumes that there are no other non-radiative pathways deactivating the excited singlet state and therefore it usually over-estimates the actual value of  $\Phi_{\text{ISC}}$ . The more precise method is determining the quantum yield of singlet oxygen formation,  $\Phi_{\Delta}$ . This value can be measured directly by luminescence<sup>398</sup> of singlet oxygen or by chemical trapping method.<sup>399</sup> In 2013, Yang and Zhang introduced a method of  $\Phi_{\text{ISC}}$  measurement based on transient spectroscopy.<sup>400</sup> However, it uses only one wavelength to determine the quantum yield of intersystem crossing. This can be strongly influenced by noise of the spectrum. We therefore used our method where the intersystem crossing quantum yields are determined from the relative ratios of the areas (determined by integration) of the absorption spectrum and the ground state bleach bands in the transient spectrum. The results are summarized in Table 4.

The results in Table 4 show that heavy atom-substituted BODIPY derivatives **VIII-1-4** undergo efficient intersystem crossing ( $\Phi_{\text{ISC}} \sim 0.4 - 0.6$ ). The tellanyl derivative **VIII-3** exhibits the largest heavy atom effect but is photochemically unstable. The selanyl derivative **VIII-2** has a good triplet quantum yield ( $\sim 44\%$ ) and is about three orders of magnitude more photostable than **VIII-4** and  $\sim 13$  fold more photostable than iodo-derivative **VIII-4**. It makes it a promising candidate for photodynamic therapy and triplet sensitizing applications.

**Table 4:** Transient absorption data for **VIII-1–4**.

compd <sup>a</sup>	$\lambda_{\text{exc}}/\text{nm}^b$	cond <sup>c</sup>	$k_d^T/\text{s}^{-1}^d$	$\Phi_{\text{ISC}}^e$	$\lambda_{\text{max}}^T{}^f$	$\epsilon_{\text{max}}^T/\text{mol}^{-1} \text{ dm}^3 \text{ cm}^{-1}{}^g$
<b>VIII-1</b>	532	deg	$(1.4 \pm 0.1) \times 10^5$	$0.40 \pm 0.02$	418	$16400 \pm 1700$
		air	$(4.2 \pm 0.2) \times 10^6$			
<b>VIII-2</b>		deg	$(1.4 \pm 0.1) \times 10^5$	$0.44 \pm 0.02$	435	$6500 \pm 500$
		air	$(4.3 \pm 0.1) \times 10^6$			
<b>VIII-3</b>		deg	$(1.2 \pm 0.1) \times 10^5$	$0.59 \pm 0.02$	437	$9900 \pm 800$
		air	$(4.2 \pm 0.2) \times 10^6$			
<b>VIII-4</b>	355	deg	$(1.4 \pm 0.1) \times 10^5$	$0.54 \pm 0.03$	417	$11800 \pm 1300$
		air	$(4.4 \pm 0.1) \times 10^6$			

<sup>a</sup> Solutions in acetonitrile: **VIII-1–3**:  $c = \sim 1.5 \times 10^{-5} \text{ mol dm}^{-3}$ ; **VIII-4**:  $c = \sim 4.5 \times 10^{-5} \text{ mol dm}^{-3}$ . <sup>b</sup> Laser pulses of  $\leq 170 \text{ ps}$ ;  $E_{\text{pulse}} = 240 \text{ mJ}$  at  $\lambda_{\text{exc}} = 532 \text{ nm}$  or  $E_{\text{pulse}} = 160 \text{ mJ}$  at  $\lambda_{\text{exc}} = 355 \text{ nm}$ . <sup>c</sup> deg: degassed; air: aerated. <sup>d</sup> Rate constants of triplet decay; a monoexponential fit based on 6 measurements. <sup>e</sup> Quantum yields of intersystem crossing (determined by a previously published method<sup>401</sup>), averaged from  $\geq 6$  measurements. <sup>f</sup> The maximum of triplet–triplet absorption and <sup>g</sup> its molar absorption coefficient (the standard deviation was calculated from  $\geq 6$  independent measurements).

### 3.8.4. Conclusions

We have designed and synthesized three new monosubstituted 3-phenylselanyl and 3-phenyltellanyl BODIPY derivatives **VIII-1–3** and compared their spectroscopic properties to iodine and chlorine-atom containing analogues as well as an unsubstituted BODIPY derivative **VIII-4–7**. The fluorescence quantum yields were found to decrease, whereas the intersystem crossing quantum yields ( $\Phi_{\text{ISC}}$ ), determined by transient spectroscopy, increase in the order of the H→Cl→Se/I→Te substitution. The maximum  $\Phi_{\text{ISC}}$ , found for the 3-phenyltellanyl derivative **VIII-3**, was 59%. The compound **VIII-2** has a sufficient photostability and quantum yield of intersystem crossing for applications as a triplet sensitizer.

### 3.8.5. Authors' Contributions

J.A.A. and E.P. synthesized the compounds. J.A.A. measured steady-state absorption spectroscopy and fluorescence spectra, quantum yields and lifetimes. T. S. measured transient spectroscopy and developed a method for determination of quantum yields of intersystem crossing.

## 4. Summary

In my Ph.D. studies, I investigated various photoactivatable derivatives. This term describes molecules that exhibit useful photochemical properties. This interaction can be extremely diverse, such as controllable release of leaving groups upon irradiation (Chapters 3.1. – 3.4.), photoinduced electron transfer for generation of reactive molecules in photocatalysis (Chapters 3.5. – 3.7.), or formation of the triplet state enhanced by heavy atom effect in prospective triplet sensitizers (Chapter 3.8.). In most cases (except Chapter 3.2.), I focused on the systems absorbing visible light. This has generally two motivations: (i) biologically benign visible light is preferred for activation of molecules in medicine and biology (Chapters 3.1. – 3.4. and 3.8.); (ii) solar irradiation can be used as an energy source to produce chemically valuable compounds by photocatalysis (Chapters 3.5. – 3.7.).

I was fortunate to be able take part in all stages of the research projects: design, synthesis, investigation of photophysical properties and reactivity, study the reaction mechanism and subsequent improvement of the systems. However, all projects were accomplished in a research team and I am grateful to all my collaborators for fruitful cooperation. All collaborations have always motivated me to become involved in other fields of science, such as biology or physics. I have learned numerous laboratory and instrumental techniques within my Ph.D. studies. I started as an organic chemist with an average knowledge of photochemical techniques. In last almost four years I have learned to handle various absorption and emission spectroscopy techniques (both steady-state and transient), electrochemistry, and other useful methods for determination the reaction mechanisms. The knowledge of designing experiments which would determine a desired feature of a complex mechanism turned out to be the most useful skill I have gained.

## 5. Literature

- (1) Verhoeven, J. W. *Pure Appl. Chem.* **1996**, 68.
- (2) Maisels, M. J.; McDonagh, A. F. *New England J. Med.* **2008**, 358, 920-928.
- (3) Li, L. *Opt. Laser Eng.* **2000**, 34, 231-253.
- (4) Kuhad, R. C., and Ajay Singh. *Biotechnology for Environmental Management and Resource Recovery*; Springer: New Delhi 2013.
- (5) <http://donaitkin.com/not-everyone-knows-this/> *Not Everyone Knows This* **2015**.
- (6) Weeks, M. E. *J. Chem. Educ.* **1933**, 10, 302.
- (7) David H. Volman, G. S. H., Douglas C. Neckers *Advances in Photochemistry*; Wiley-Interscience: New York, 1971; Vol. 18.
- (8) Ciamician, G.; Silber, P. *Ber. Dtsch. Chem. Ges.* **1902**, 35, 1992-2000.
- (9) Atkins, P. W., and Julio De. Paula *Physical Chemistry*; W. H. Freeman, New York (N.Y.), 2010.
- (10) Jablonski, A. *Z. Phys.* **1935**, 94, 38-46.
- (11) Frackowiak, D. *J. Photochem. Photobiol. B* **1988**, 2, 399.
- (12) Kasha, M. *Discuss. Faraday Soc.* **1950**, 9, 14.
- (13) Braslavsky, S. E. *Pure Appl. Chem.* **2007**, 79.
- (14) Fleming, I. *Molecular Orbitals and Organic Chemical Reactions*; Wiley: Chichester, 2009.
- (15) Šebej, P.; Wintner, J.; Müller, P.; Slanina, T.; Al Anshori, J.; Antony, L. A. P.; Klán, P.; Wirz, J. *J. Org. Chem.* **2013**, 78, 1833-1843.
- (16) Hari, D. P.; Schroll, P.; König, B. *J. Am. Chem. Soc.* **2012**, 134, 2958-2961.
- (17) Klán, P. W., J. *Photochemistry of Organic Compounds: From Concepts to Practice*; Wiley: Chichester, West Sussex, U.K., 2009.
- (18) Rehm, D. W., A. H. *Ber. Bunsen-Ges. Phys. Chem.* **1969**, 73, 834-839.
- (19) Naik, D. B.; Schnabel, W. *Chem. Phys. Lett.* **1999**, 315, 416-420.
- (20) Shimizu, O.; Watanabe, J.; Naito, S.; Shibata, Y. *J. Phys. Chem. A* **2006**, 110, 1735-1739.
- (21) Montagnon, T.; Tofi, M.; Vassilikogiannakis, G. *Acc. Chem. Res.* **2008**, 41, 1001-1011.
- (22) Niedre, M.; Patterson, M. S.; Wilson, B. C. *Photochem. Photobiol.* **2002**, 75, 382-391.
- (23) Green, T. W. W., P. G. M. *Protective Groups in Organic Synthesis*; Wiley-Interscience: New York, 1999.
- (24) Yokoe, H.; Sasaki, H.; Yoshimura, T.; Shindo, M.; Yoshida, M.; Shishido, K. *Org. Lett.* **2007**, 9, 969-971.
- (25) Young, I. S.; Baran, P. S. *Nat. Chem.* **2009**, 1, 193-205.
- (26) Robinson, R. *J. Chem. Soc. Transactions* **1917**, 111, 762.
- (27) Bartrop, J. A.; Schofield, P. *Tetrahedron Lett.* **1962**, 3, 697-699.
- (28) Yousef, A. L., J.; Conrad, P.; Givens, R. *CRC Handbook of Organic Photochemistry and Photobiology*; 2nd edition ed.; CRC Press, 2003.
- (29) Pelliccioli, A. P.; Wirz, J. *Photochem. Photobiol. Sci.* **2002**, 1, 441-458.
- (30) Klán, P.; Šolomek, T.; Bochet, C. G.; Blanc, A.; Givens, R.; Rubina, M.; Popik, V.; Kostikov, A.; Wirz, J. *Chem. Rev.* **2013**, 113, 119-191.
- (31) Smith, A. B.; Xian, M. *J. Am. Chem. Soc.* **2006**, 128, 66-67.
- (32) Kammath, V. B.; Šebej, P.; Slanina, T.; Kříž, Z.; Klán, P. *Photochem. Photobiol. Sci.* **2012**, 11, 500-507.
- (33) Bochet, C. G. *Angew. Chem. Int. Ed.* **2001**, 40, 2071-2073.

- (34) Kammari, L.; Šolomek, T.; Ngoy, B. P.; Heger, D.; Klán, P. *J. Am. Chem. Soc.* **2010**, *132*, 11431-11433.
- (35) Štacko, P.; Šolomek, T.; Klán, P. *Org. Lett.* **2011**, *13*, 6556-6559.
- (36) Givens, R. S.; Park, C.-H. *Tetrahedron Lett.* **1996**, *37*, 6259-6262.
- (37) Park, C.-H.; Givens, R. S. *J. Am. Chem. Soc.* **1997**, *119*, 2453-2463.
- (38) Sheehan, J. C.; Umezawa, K. *J. Org. Chem.* **1973**, *38*, 3771-3774.
- (39) Banerjee, A.; Falvey, D. E. *J. Am. Chem. Soc.* **1998**, *120*, 2965-2966.
- (40) Pickens, C. J.; Gee, K. R. *Tetrahedron Lett.* **2011**, *52*, 4989-4991.
- (41) Conrad, P. G.; Givens, R. S.; Weber, J. F. W.; Kandler, K. *Org. Lett.* **2000**, *2*, 1545-1547.
- (42) Givens, R. S.; Jung, A.; Park, C. H.; Weber, J.; Bartlett, W. *J. Am. Chem. Soc.* **1997**, *119*, 8369-8370.
- (43) Givens, R. S.; Weber, J. F. W.; Conrad, P. G.; Orosz, G.; Donahue, S. L.; Thayer, S. A. *J. Am. Chem. Soc.* **2000**, *122*, 2687-2697.
- (44) Conrad, P. G.; Givens, R. S.; Hellrung, B.; Rajesh, C. S.; Ramseier, M.; Wirz, J. *J. Am. Chem. Soc.* **2000**, *122*, 9346-9347.
- (45) Givens, R. S. Unpublished results, 2006.
- (46) Givens, R. S.; Park, C. H. *Tetrahedron Lett.* **1996**, *37*, 6259-6262.
- (47) Geibel, S.; Barth, A.; Amslinger, S.; Jung, A. H.; Burzik, C.; Clarke, R. J.; Givens, R. S.; Fendler, K. *Biophys. J.* **2000**, *79*, 1346-1357.
- (48) Givens, R. S.; Stensrud, K.; Conrad, P. G.; Yousef, A. L.; Perera, C.; Senadheera, S. N.; Heger, D.; Wirz, J. *Can. J. Chem.* **2011**, *89*, 364-384.
- (49) Zou, K. Y.; Miller, W. T.; Givens, R. S.; Bayley, H. *Angew. Chem. Int. Ed.* **2001**, *40*, 3049-3051.
- (50) Favorskii, A. E. *J. Prakt. Chem.* **1894**, *51*, 559.
- (51) Anderson, J. C.; Reese, C. B. *Tetrahedron Lett.* **1962**, *3*, 1-4.
- (52) Givens, R. S.; Heger, D.; Hellrung, B.; Kamdzhilov, Y.; Mac, M.; Conrad, P. G.; Cope, E.; Lee, J. I.; Mata-Segreda, J. F.; Schowen, R. L.; Wirz, J. *J. Am. Chem. Soc.* **2008**, *130*, 3307-3309.
- (53) Givens, R. S.; Rubina, M.; Wirz, J. *Photochem. Photobiol. Sci.* **2012**, *11*, 472.
- (54) Stensrud, K.; Noh, J.; Kandler, K.; Wirz, J.; Heger, D.; Givens, R. S. *J. Org. Chem.* **2009**, *74*, 5219-5227.
- (55) Cao, Q.; Guan, X. G.; George, M. W.; Phillips, D. L.; Ma, C. S.; Kwok, W. M.; Li, M. D.; Du, Y.; Sun, X. Z.; Xue, J. D. *Faraday Discuss.* **2010**, *145*, 171-183.
- (56) Šolomek, T.; Heger, D.; Ngoy, B. P.; Givens, R. S.; Klán, P. *J. Am. Chem. Soc.* **2013**, *135*, 15209-15215.
- (57) Givens, R. S.; Matuszewski, B. *J. Am. Chem. Soc.* **1984**, *106*, 6860-6861.
- (58) Furuta, T.; Torigai, H.; Osawa, T.; Iwamura, M. *Chem. Lett.* **1993**, 1179-1182.
- (59) Furuta, T.; Torigai, H.; Sugimoto, M.; Iwamura, M. *J. Org. Chem.* **1995**, *60*, 3953-3956.
- (60) *Dynamic Studies in Biology: Phototriggers, Photoswitches and Caged Biomolecules*; John Wiley & Sons, 2006.
- (61) Ando, H.; Furuta, T.; Tsien, R. Y.; Okamoto, H. *Nat. Genet.* **2001**, *28*, 317-325.
- (62) Schade, B.; Hagen, V.; Schmidt, R.; Herbrich, R.; Krause, E.; Eckardt, T.; Bendig, J. *J. Org. Chem.* **1999**, *64*, 9109-9117.
- (63) Eckardt, T.; Hagen, V.; Schade, B.; Schmidt, R.; Schweitzer, C.; Bendig, J. *J. Org. Chem.* **2002**, *67*, 703-710.
- (64) Hagen, V.; Frings, S.; Wiesner, B.; Helm, S.; Kaupp, U. B.; Bendig, J. *ChemBioChem* **2003**, *4*, 434-442.



- (65) Zayat, L.; Noval, M. G.; Campi, J.; Calero, C. I.; Calvo, D. J.; Etchenique, R. *ChemBioChem* **2007**, *8*, 2035-2038.
- (66) Rial Verde, E. M. *Front. Neur. Circuits* **2008**, *2*.
- (67) Filevich, O.; Etchenique, R. *Photochem. Photobiol. Sci.* **2013**, *12*, 1565.
- (68) Egerton, G. S.; Morgan, A. G. *J. Soc. Dyers Colour.* **2008**, *86*, 242-249.
- (69) Olson, J. P.; Banghart, M. R.; Sabatini, B. L.; Ellis-Davies, G. C. R. *J. Am. Chem. Soc.* **2013**, *135*, 15948-15954.
- (70) Fournier, L.; Gauron, C.; Xu, L.; Aujard, I.; Le Saux, T.; Gagey-Eilstein, N.; Maurin, S.; Dubruille, S.; Baudin, J.-B.; Bensimon, D.; Volovitch, M.; Vrizz, S.; Jullien, L. *ACS Chem. Biol.* **2013**, *8*, 1528-1536.
- (71) Umeda, N.; Takahashi, H.; Kamiya, M.; Ueno, T.; Komatsu, T.; Terai, T.; Hanaoka, K.; Nagano, T.; Urano, Y. *ACS Chem. Biol.* **2014**, *9*, 2242-2246.
- (72) Goswami, P. P.; Syed, A.; Beck, C. L.; Albright, T. R.; Mahoney, K. M.; Unash, R.; Smith, E. A.; Winter, A. H. *J. Am. Chem. Soc.* **2015**, *137*, 3783-3786.
- (73) Rubinstein, N.; Liu, P.; Miller, E. W.; Weinstain, R. *Chem. Commun.* **2015**, *51*, 6369-6372.
- (74) Nani, R. R.; Gorke, A. P.; Nagaya, T.; Kobayashi, H.; Schnermann, M. J. *Angew. Chem. Int. Ed.* **2015**, *54*, 13635-13638.
- (75) Song, L.; Hennink, E. J.; Young, I. T.; Tanke, H. J. *Biophys. J.* **1995**, *68*, 2588-2600.
- (76) Snavely, B. B. *Proceedings of the IEEE* **1969**, *57*, 1374-1390.
- (77) Vandewoestyne, M.; Lepez, T.; Van Hoofstat, D.; Deforce, D. *J. Forensic Sci.* **2015**, *60*, 707-711.
- (78) Ward, K. W. *Optometry Vision Sci.* **2008**, *85*, 8-16.
- (79) Jones, K. H.; Senft, J. A. *J. Histochem. Cytochem.* **1985**, *33*, 77-79.
- (80) Nienow, P.; Sharp, M.; Willis, I. *Earth Surf. Proc. Land.* **1998**, *23*, 825-843.
- (81) Shi, J.; Zhang, X.; Neckers, D. C. *J. Org. Chem.* **1992**, *57*, 4418-4421.
- (82) von Baeyer, A. *Chem. Ber.* **1871**, *5*, 255.
- (83) Urano, Y.; Kamiya, M.; Kanda, K.; Ueno, T.; Hirose, K.; Nagano, T. *J. Am. Chem. Soc.* **2005**, *127*, 4888-4894.
- (84) Joshi, N. B.; Gangola, P.; Pant, D. D. *J. Lumin.* **1979**, *21*, 111-118.
- (85) Mottram, L. F.; Boonyarattanakalin, S.; Kovel, R. E.; Peterson, B. R. *Org. Lett.* **2006**, *8*, 581-584.
- (86) <http://www.collinsdictionary.com/dictionary/english>
- (87) Penzkofer, A.; Beidoun, A.; Daiber, M. *J. Lumin.* **1992**, *51*, 297-314.
- (88) Fita, P.; Fedoseeva, M.; Vauthey, E. *J. Phys. Chem. A* **2011**, *115*, 2465-2470.
- (89) Fischer, A. H.; Jacobson, K. A.; Rose, J.; Zeller, R. *Cold Spring Harbor Prot.* **2008**, *2008*, 4986.
- (90) Hari, D. P.; König, B. *Chem. Commun.* **2014**, *50*, 6688-6699.
- (91) Seybold, P. G.; Gouterman, M.; Callis, J. *Photochem. Photobiol.* **1969**, *9*, 229-242.
- (92) Soinikov, Y. A.; Ketsle, G. A.; Levshin, L. V. *J. Appl. Spectrosc.* **1979**, *30*, 309-314.
- (93) Dela Cruz, J. L.; Blanchard, G. J. *J. Phys. Chem. A* **2002**, *106*, 10718-10724.
- (94) Klimtchuk, E.; Rodgers, M. A. J.; Neckers, D. C. *J. Phys. Chem.* **1992**, *96*, 9817-9820.
- (95) Müller, R.; Zander, C.; Sauer, M.; Deimel, M.; Ko, D. S.; Siebert, S.; Arden-Jacob, J.; Deltau, G.; Marx, N. J.; Drexhage, K. H.; Wolfrum, J. *Chem. Phys. Lett.* **1996**, *262*, 716-722.
- (96) Timpe, H.-J.; Kronfeld, K.-P.; Mahlow, R. *Z. Chem.* **2010**, *30*, 55-56.

- (97) Amat-Guerri, F.; Martin, M. E.; Martinez-Utrilla, R.; Pascual, C. *J. Chem. Res., Synop.* **1988**, 1411.
- (98) Casalnuovo, A. L.; Calabrese, J. C. *J. Am. Chem. Soc.* **1990**, *112*, 4324-4330.
- (99) Turk, S.; Kovač, A.; Boniface, A.; Bostock, J. M.; Chopra, I.; Blanot, D.; Gobec, S. *Biorg. Med. Chem.* **2009**, *17*, 1884-1889.
- (100) Štacko, P.; Šebej, P.; Veetil, A. T.; Klán, P. *Org. Lett.* **2012**, *14*, 4918-4921.
- (101) Pastierik, T.; Šebej, P.; Medalová, J.; Štacko, P.; Klán, P. *J. Org. Chem.* **2014**, *79*, 3374-3382.
- (102) Horváth, P.; Šebej, P.; Šolomek, T.; Klán, P. *J. Org. Chem.* **2015**, *80*, 1299-1311.
- (103) Albert, A.; Bird, C. L. *J. Soc. Dyers Colour.* **2008**, *59*, 74-76.
- (104) Ferguson, J.; Mau, A. W. H. *Aust. J. Chem.* **1973**, *26*, 1617.
- (105) Lerman, L. S. *Proc. Nat. Acad. Sci. U.S.A.* **1963**, *49*, 94-102.
- (106) Browning, C. H.; Gulbransen, R.; Thornton, L. H. D. *Br. Med. J.* **1917**, *2*, 70-75.
- (107) Li, H. J.; Crothers, D. M. *J. Mol. Biol.* **1969**, *39*, 461-477.
- (108) Speck, W. T.; Rosenkranz, H. S. *Mutat. Res.-Genet. Tox.* **1980**, *77*, 37-43.
- (109) He, K. X.; Bryant, W.; Venkateswarlu, P. *Appl. Phys. Lett.* **1991**, *59*, 1935.
- (110) McMaster, G. K.; Carmichael, G. G. *Proc. Nat. Acad. Sci.* **1977**, *74*, 4835-4838.
- (111) Can, H.; Karakus, G.; Tuzcu, N. *Polym. Bull.* **2014**, *71*, 2903-2921.
- (112) Valdés, A.; García-Cañas, V.; Cifuentes, A. *Electrophoresis* **2013**, *34*, 1555-1562.
- (113) Hornedo, J.; Van Echo, D. A. *Pharmacotherapy* **1985**, *5*, 78-90.
- (114) Fukuzumi, S.; Kotani, H.; Ohkubo, K.; Ogo, S.; Tkachenko, N. V.; Lemmetyinen, H. *J. Am. Chem. Soc.* **2004**, *126*, 1600-1601.
- (115) Treibs, A.; Kreuzer, F.-H. *Liebigs Ann. Chem.* **1968**, *718*, 208-223.
- (116) Guggenheimer, S. C.; Boyer, J. H.; Thangaraj, K.; Shah, M.; Soong, M.-L.; Paviopoulos, T. G. *Appl. Opt.* **1993**, *32*, 3942.
- (117) Rao, J.; Dragulescu-Andrasi, A.; Yao, H. *Curr. Opin. Biotechnol.* **2007**, *18*, 17-25.
- (118) Lu, H.; Zhang, S.; Liu, H.; Wang, Y.; Shen, Z.; Liu, C.; You, X. *J. Phys. Chem. A* **2009**, *113*, 14081-14086.
- (119) Ulrich, G.; Ziessel, R.; Harriman, A. *Angew. Chem. Int. Ed.* **2008**, *47*, 1184-1201.
- (120) Kamkaew, A.; Lim, S. H.; Lee, H. B.; Kiew, L. V.; Chung, L. Y.; Burgess, K. *Chem. Soc. Rev.* **2013**, *42*, 77-88.
- (121) Kim, B.; Ma, B.; Donuru, V. R.; Liu, H.; Fréchet, J. M. J. *Chem. Commun.* **2010**, *46*, 4148.
- (122) Liu, C.-L.; Chen, Y.; Shelar, D. P.; Li, C.; Cheng, G.; Fu, W.-F. *J. Mat. Chem. C* **2014**, *2*, 5471.
- (123) Gonçalves, M. S. T. *Chem. Rev.* **2009**, *109*, 190-212.
- (124) Loudet, A.; Burgess, K. *Chem. Rev.* **2007**, *107*, 4891-4932.
- (125) Boens, N.; Leen, V.; Dehaen, W. *Chem. Soc. Rev.* **2012**, *41*, 1130-1172.
- (126) Ziessel, R.; Ulrich, G.; Harriman, A. *New J. Chem.* **2007**, *31*, 496.
- (127) Awuah, S. G.; You, Y. *RSC Advances* **2012**, *2*, 11169.
- (128) Nepomnyashchii, A. B.; Bard, A. J. *Acc. Chem. Res.* **2012**, *45*, 1844-1853.
- (129) Lu, H.; Mack, J.; Yang, Y.; Shen, Z. *Chem. Soc. Rev.* **2014**, *43*, 4778.
- (130) Karolin, J.; Johansson, L. B. A.; Strandberg, L.; Ny, T. *J. Am. Chem. Soc.* **1994**, *116*, 7801-7806.

- (131) Saki, N.; Dinc, T.; Akkaya, E. U. *Tetrahedron* **2006**, *62*, 2721-2725.
- (132) Boyer, J. H.; Haag, A. M.; Sathyamoorthi, G.; Soong, M.-L.; Thangaraj, K.; Pavlopoulos, T. G. *Heteroat. Chem* **1993**, *4*, 39-49.
- (133) Rohand, T.; Qin, W.; Boens, N.; Dehaen, W. *Eur. J. Org. Chem.* **2006**, *2006*, 4658-4663.
- (134) Rohand, T.; Baruah, M.; Qin, W.; Boens, N.; Dehaen, W. *Chem. Commun.* **2006**, 266-268.
- (135) Kim, H.; Burghart, A.; Welch, M. B.; Reibenspies, J.; Burgess, K. *Chem. Commun.* **1999**, 1889-1890.
- (136) Goze, C.; Ulrich, G.; Mallon, L. J.; Allen, B. D.; Harriman, A.; Ziessel, R. J. *Am. Chem. Soc.* **2006**, *128*, 10231-10239.
- (137) Goze, C.; Ulrich, G.; Ziessel, R. *Org. Lett.* **2006**, *8*, 4445-4448.
- (138) Jiang, X.-D.; Zhao, J.; Xi, D.; Yu, H.; Guan, J.; Li, S.; Sun, C.-L.; Xiao, L.-J. *Chem. Eur. J.* **2015**, *21*, 6079-6082.
- (139) Kamkaew, A.; Burgess, K. *Chem. Commun.* **2015**, *51*, 10664-10667.
- (140) Feng, J.; Wang, D.; Wang, S.; Zhang, L.; Li, X. *Dyes Pigments* **2011**, *89*, 23-28.
- (141) Liu, H.; Lu, H.; Zhou, Z.; Shimizu, S.; Li, Z.; Kobayashi, N.; Shen, Z. *Chem. Commun.* **2015**, *51*, 1713-1716.
- (142) Grisar, T. *Ann. Neurol.* **1984**, *16*, S128-S134.
- (143) Pauling, L.; Coryell, C. D. *Proc. Nat. Acad. Sci. U.S.A.* **1936**, *22*, 210-216.
- (144) Debus, R. J. *BBA-Bioenergetics* **1992**, *1102*, 269-352.
- (145) Smith, M. J.; Koch, G. L. *EMBO J.* **1989**, *8*, 3581-3586.
- (146) Schmidt, C. L. A.; Greenberg, D. M. *Physiol. Rev.* **1935**, *15*, 297-434.
- (147) Orrenius, S.; Zhivotovsky, B.; Nicotera, P. *Nat. Rev. Mol. Cell Biol.* **2003**, *4*, 552-565.
- (148) Ghosh, A.; Ginty, D. D.; Bading, H.; Greenberg, M. E. *J. Neurobiol.* **1994**, *25*, 294-303.
- (149) <http://www.cdc.gov/niosh/idlh/intridl4.html> NIOSH Database.
- (150) Lefer, D. J. *Proc. Nat. Acad. Sci.* **2007**, *104*, 17907-17908.
- (151) Kimura, H. *Mol Neurobiol* **2002**, *26*, 13-19.
- (152) Szabo, C.; Coletta, C.; Chao, C.; Modis, K.; Szczesny, B.; Papapetropoulos, A.; Hellmich, M. R. *Proc. Nat. Acad. Sci.* **2013**, *110*, 12474-12479.
- (153) Wang, K.; Ahmad, S.; Cai, M.; Rennie, J.; Fujisawa, T.; Crispi, F.; Baily, J.; Miller, M. R.; Cudmore, M.; Hadoke, P. W. F.; Wang, R.; Gratacos, E.; Buhimschi, I. A.; Buhimschi, C. S.; Ahmed, A. *Circulation* **2013**, *127*, 2514-2522.
- (154) Gade, A. R.; Kang, M.; Akbarali, H. I. *Mol. Pharmacol.* **2012**, *83*, 294-306.
- (155) Ankri, S.; Mirelman, D. *Microbes Infect.* **1999**, *1*, 125-129.
- (156) Predmore, B. L.; Lefer, D. J.; Gojon, G. *Antioxid. Redox Sign.* **2012**, *17*, 119-140.
- (157) Wang, R. *Physiol. Rev.* **2012**, *92*, 791-896.
- (158) Van Hove, C. E.; Van der Donckt, C.; Herman, A. G.; Bult, H.; Franssen, P. *Br. J. Pharmacol.* **2009**, *158*, 920-930.
- (159) Kuriyama, K.; Ohkuma, S. *Jpn. J. Pharmacol.* **1995**, *69*, 1-8.
- (160) Suschek, C. V.; Opländer, C.; van Faassen, E. E. *Nitric Oxide* **2010**, *22*, 120-135.
- (161) Paulus, W. J.; Frantz, S.; Kelly, R. A. *Circulation* **2001**, *104*, 2260-2262.
- (162) MacMicking, J.; Xie, Q.-w.; Nathan, C. *Annu. Rev. Immunol.* **1997**, *15*, 323-350.

- (163) Reece, S. Y.; Woodward, J. J.; Marletta, M. A. *Biochemistry* **2009**, *48*, 5483-5491.
- (164) Riveros-Moreno, V.; Beddell, C.; Moncada, S. *Eur. J. Biochem.* **1993**, *215*, 801-808.
- (165) Sanders, D. B.; Kelley, T.; Larson, D. *Perfusion* **2000**, *15*, 97-104.
- (166) [http://www.nobelprize.org/nobel\\_prizes/medicine/laureates/1998/](http://www.nobelprize.org/nobel_prizes/medicine/laureates/1998/).
- (167) Feelisch, M.; Noack, E. A. *Eur. J. Pharmacol.* **1987**, *139*, 19-30.
- (168) Murad, F. *J. Clin. Invest.* **1986**, *78*, 1-5.
- (169) Lugnier, C. *Pharmacol. Ther.* **2006**, *109*, 366-398.
- (170) Corbin, J. D. *Int. J. Impot. Res.* **2004**, *16*, S4-S7.
- (171) Dresser, G. K.; Spence, J. D.; Bailey, D. G. *Clin. Pharmacokinet.* **2000**, *38*, 41-57.
- (172) M., S. *Principles of General Chemistry*; McGraw-Hill Science/Engineering/Math, 2009.
- (173) Kolasinski, K. W. *PCCP* **2003**, *5*, 1270-1278.
- (174) Ozsvath, D. L. *Rev. Environ. Sci. Biotech.* **2008**, *8*, 59-79.
- (175) Wiegand, A.; Buchalla, W.; Attin, T. *Dent. Mater.* **2007**, *23*, 343-362.
- (176) Featherstone, J. D. B. *Aust. Dent. J.* **2008**, *53*, 286-291.
- (177) Meenakshi; Maheshwari, R. C. *J. Hazard. Mater.* **2006**, *137*, 456-463.
- (178) Tang, Q.-q.; Du, J.; Ma, H.-h.; Jiang, S.-j.; Zhou, X.-j. *Biol. Trace Elem. Res.* **2008**, *126*, 115-120.
- (179) Grobler, S. R.; Louw, A. J.; Van W. Kotze, T. J. *Int. J. Paediatr. Dent.* **2001**, *11*, 372-379.
- (180) Usuda, K.; Kono, K.; Dote, T.; Nishiura, K.; Miyata, K.; Nishiura, H.; Shimahara, M.; Sugimoto, K. *Arch. Toxicol.* **1997**, *72*, 104-109.
- (181) <http://www.fda.gov/Food/GuidanceRegulation/GuidanceDocumentsRegulatoryInformation/BottledWaterCarbonatedSoftDrinks/ucm444373.htm>.
- (182) Bartlett, D. W.; Smith, B. G.; Wilson, R. F. *Br. Dent. J.* **1994**, *176*, 346-348.
- (183) Barbier, O.; Arreola-Mendoza, L.; Del Razo, L. M. *Chem. Biol. Interact.* **2010**, *188*, 319-333.
- (184) Ren, A.; Rajashankar, K. R.; Patel, D. J. *Nature* **2012**.
- (185) Chance, B.; Erecinska, M.; Wagner, M. *Ann. N.Y. Acad. Sci.* **1970**, *174*, 193-204.
- (186) Joels, N.; Pugh, L. G. C. E. *J. Physiol.* **1958**, *142*, 63-77.
- (187) Motterlini, R.; Otterbein, L. E. *Nat. Rev. Drug Discov.* **2010**, *9*, 728-743.
- (188) Romão, C. C.; Blättler, W. A.; Seixas, J. D.; Bernardes, G. J. L. *Chem. Soc. Rev.* **2012**, *41*, 3571.
- (189) García-Gallego, S.; Bernardes, G. J. L. *Angew. Chem. Int. Ed.* **2014**, *53*, 9712-9721.
- (190) Zuckerbraun, B. S.; McCloskey, C. A.; Gallo, D.; Liu, F.; Ifedigbo, E.; Otterbein, L. E.; Billiar, T. R. *Shock* **2005**, *23*, 527-532.
- (191) Vitek, L.; Gbelcová, H.; Muchová, L.; Váňová, K.; Zelenka, J.; Koníčková, R.; Šuk, J.; Zadinova, M.; Knejzlík, Z.; Ahmad, S.; Fujisawa, T.; Ahmed, A.; Ruml, T. *Digest. Liver Dis.* **2014**, *46*, 369-375.
- (192) Verma, A.; Hirsch, D.; Glatt, C.; Ronnett, G.; Snyder, S. *Science* **1993**, *259*, 381-384.
- (193) Otterbein, L. E.; Soares, M. P.; Yamashita, K.; Bach, F. H. *Trends Immunol.* **2003**, *24*, 449-455.

- (194) Tenhunen, R.; Marver, H. S.; Schmid, R. *Proc. Nat. Acad. Sci. U.S.A.* **1968**, *61*, 748-755.
- (195) Piantadosi, C. A. *Free Radical Biol. Med.* **2008**, *45*, 562-569.
- (196) Andersen, M. E.; Clewell, H. J.; Gargas, M. L.; MacNaughton, M. G.; Reitz, R. H.; Nolan, R. J.; McKenna, M. J. *Toxicol. Appl. Pharmacol.* **1991**, *108*, 14-27.
- (197) Schatzschneider, U. *Br. J. Pharmacol.* **2015**, *172*, 1638-1650.
- (198) Heinemann, S. H.; Hoshi, T.; Westerhausen, M.; Schiller, A. *Chem. Commun.* **2014**, *50*, 3644-3660.
- (199) Romao, C. C.; Blattler, W. A.; Seixas, J. D.; Bernardes, G. J. L. *Chem. Soc. Rev.* **2012**, *41*, 3571-3583.
- (200) Schatzschneider, U. *Eur. J. Inorg. Chem.* **2010**, 1451-1467.
- (201) Mann, B. E. *Organometallics* **2012**, *31*, 5728-5735.
- (202) Motterlini, R.; Mann, B. E.; Foresti, R. *Expert Opin. Inv. Dr.* **2005**, *14*, 1305-1318.
- (203) Boczkowski, J.; Poderoso, J. J.; Motterlini, R. *Trends Biochem. Sci* **2006**, *31*, 614-621.
- (204) Motterlini, R.; Sawle, P.; Hammad, J.; Bains, S.; Alberto, R.; Foresti, R.; Green, C. J. *FASEB J.* **2005**, *19*, 284-286.
- (205) Wang, D. Z.; Viennois, E.; Ji, K.; Damera, K.; Draganov, A.; Zheng, Y. Q.; Dai, C. F.; Merlin, D.; Wang, B. H. *Chem. Commun.* **2014**, *50*, 15890-15893.
- (206) Garcia-Gallego, S.; Bernardes, G. J. L. *Angew. Chem. Int. Ed.* **2014**, *53*, 9712-9721.
- (207) Muchová, L.; Jašprová, J.; Slanina, T.; Šebej, P.; Klán, P.; Vitek, L. *Nitric Oxide* **2015**, *47*, S35.
- (208) Foresti, R.; Hammad, J.; Clark, J. E.; Johnson, T. R.; Mann, B. E.; Friebe, A.; Green, C. J.; Motterlini, R. *Br. J. Pharmacol.* **2004**, *142*, 453-460.
- (209) Sakata, M.; Haga, M. *J. Toxicol. Sci.* **1980**, *5*, 35-43.
- (210) van Kampen, E. J.; Klouwen, H. *Recl. Trav. Chim. Pays-Bas* **2010**, *73*, 119-128.
- (211) Yuan, L.; Lin, W.; Tan, L.; Zheng, K.; Huang, W. *Angew. Chem. Int. Ed.* **2013**, *52*, 1628-1630.
- (212) Rimmer, R. D.; Richter, H.; Ford, P. C. *Inorg. Chem.* **2010**, *49*, 1180-1185.
- (213) Berends, H.-M.; Kurz, P. *Inorg. Chim. Acta* **2012**, *380*, 141-147.
- (214) Klan, P.; Solomek, T.; Bochet, C. G.; Blanc, A.; Givens, R.; Rubina, M.; Popik, V.; Kostikov, A.; Wirz, J. *Chem. Rev.* **2013**, *113*, 119-191.
- (215) Schatzschneider, U. *Inorg. Chim. Acta* **2011**, *374*, 19-23.
- (216) Govender, P.; Pai, S.; Schatzschneider, U.; Smith, G. S. *Inorg. Chem.* **2013**, *52*, 5470-5478.
- (217) Gonzalez, M. A.; Carrington, S. J.; Fry, N. L.; Martinez, J. L.; Mascharak, P. K. *Inorg. Chem.* **2012**, *51*, 11930-11940.
- (218) Carrington, S. J.; Chakraborty, I.; Mascharak, P. K. *Chem. Commun.* **2013**, *49*, 11254-11256.
- (219) Chakraborty, I.; Carrington, S. J.; Mascharak, P. K. *Acc. Chem. Res.* **2014**, *47*, 2603-2611.
- (220) Pierri, A. E.; Huang, P. J.; Garcia, J. V.; Stanfill, J. G.; Chui, M.; Wu, G.; Zheng, N.; Ford, P. C. *Chem. Commun.* **2015**, *51*, 2072-2075.
- (221) Kuzmanich, G.; Gard, M. N.; Garcia-Garibay, M. A. *J. Am. Chem. Soc.* **2009**, *131*, 11606-11614.
- (222) Poloukhine, A.; Popik, V. V. *J. Org. Chem.* **2003**, *68*, 7833-7840.
- (223) Poloukhine, A.; Popik, V. V. *J. Phys. Chem. A* **2006**, *110*, 1749-1757.

- (224) Poloukhine, A. A.; Mbua, N. E.; Wolfert, M. A.; Boons, G.-J.; Popik, V. V. *J. Am. Chem. Soc.* **2009**, *131*, 15769-15776.
- (225) Kuzmanich, G.; Garcia-Garibay, M. A. *J. Phys. Org. Chem.* **2011**, *24*, 883-888.
- (226) Chapman, O. L.; Wojtkowski, P. W.; Adam, W.; Rodriguez, O.; Rucktaeschel, R. *J. Am. Chem. Soc.* **1972**, *94*, 1365-1367.
- (227) Peng, P.; Wang, C. M.; Shi, Z.; Johns, V. K.; Ma, L. Y.; Oyer, J.; Copik, A.; Igarashi, R.; Liao, Y. *Org. Biomol. Chem.* **2013**, *11*, 6671-6674.
- (228) Birnbaum, H.; Cookson, R. C.; Lewin, N. *J. Chem. Soc.* **1961**, 1224-&.
- (229) Balzani, V.; Scandola, F. In *Energy Resources Through Photochemistry and Catalysis*; Grätzel, M., Ed.; Academic Press: 1983, p 1-48.
- (230) Fox, M. A. *Photochem. Photobiol.* **1990**, *52*, 617-627.
- (231) Raven, P. H.; Evert, R. F.; Eichhorn, S. E. *Biology of plants*; Macmillan, 2005.
- (232) Ryu, J.; Nam, D. H.; Lee, S. H.; Park, C. B. *Chem. Eur. J.* **2014**, *20*, 12020-12025.
- (233) Bard, A. J.; Fox, M. A. *Acc. Chem. Res.* **1995**, *28*, 141-145.
- (234) Wang, X.; Maeda, K.; Thomas, A.; Takanabe, K.; Xin, G.; Carlsson, J. M.; Domen, K.; Antonietti, M. *Nat. Mater.* **2008**, *8*, 76-80.
- (235) Moniz, S. J. A.; Shevlin, S. A.; Martin, D. J.; Guo, Z.-X.; Tang, J. *Energ. Environ. Sci.* **2015**, *8*, 731-759.
- (236) Orlandi, M.; Argazzi, R.; Sartorel, A.; Carraro, M.; Scorrano, G.; Bonchio, M.; Scandola, F. *Chem. Commun.* **2010**, *46*, 3152.
- (237) Kudo, A.; Miseki, Y. *Chem. Soc. Rev.* **2009**, *38*, 253-278.
- (238) Duan, L.; Tong, L.; Xu, Y.; Sun, L. *Energ. Environ. Sci.* **2011**, *4*, 3296.
- (239) Mani, K. N. *J. Membr. Sci.* **1991**, *58*, 117-138.
- (240) Narayanam, J. M. R.; Stephenson, C. R. J. *Chem. Soc. Rev.* **2011**, *40*, 102-113.
- (241) Prier, C. K.; Rankic, D. A.; MacMillan, D. W. C. *Chem. Rev.* **2013**, *113*, 5322-5363.
- (242) Wasielewski, M. R. *Chem. Rev.* **1992**, *92*, 435-461.
- (243) Castillo, N. C.; Ding, L.; Heel, A.; Graule, T.; Pulgarin, C. *J. Photochem. Photobiol. A* **2010**, *216*, 221-227.
- (244) Islam, S. D. M.; Konishi, T.; Fujitsuka, M.; Ito, O.; Nakamura, Y.; Usui, Y. *Photochem. Photobiol.* **2007**, *71*, 675-680.
- (245) Fox, M. A.; Cardona, R.; Gaillard, E. *J. Am. Chem. Soc.* **1987**, *109*, 6347-6354.
- (246) Megerle, U.; Wenninger, M.; Kutta, R.-J.; Lechner, R.; König, B.; Dick, B.; Riedle, E. *PCCP* **2011**, *13*, 8869.
- (247) Hari, D. P.; König, B. *Angew. Chem. Int. Ed.* **2013**, *52*, 4734-4743.
- (248) Lv, H.; Guo, W.; Wu, K.; Chen, Z.; Bacsá, J.; Musaev, D. G.; Geletii, Y. V.; Lauinger, S. M.; Lian, T.; Hill, C. L. *J. Am. Chem. Soc.* **2014**.
- (249) Somasundaram, S.; Ramannairchenthamarakshan, C.; Detacconi, N.; Rajeshwar, K. *Int. J. Hydrogen Energy* **2007**, *32*, 4661-4669.
- (250) Du, P.; Schneider, J.; Jarosz, P.; Eisenberg, R. *J. Am. Chem. Soc.* **2006**, *128*, 7726-7727.
- (251) Pitre, S. P.; McTiernan, C. D.; Ismaili, H.; Scaiano, J. C. *J. Am. Chem. Soc.* **2013**, *135*, 13286-13289.
- (252) Lei, P.; Hedlund, M.; Lomoth, R.; Rensmo, H.; Johansson, O.; Hammarström, L. *J. Am. Chem. Soc.* **2008**, *130*, 26-27.
- (253) Zhao, W.-W.; Ma, Z.-Y.; Yan, D.-Y.; Xu, J.-J.; Chen, H.-Y. *Anal. Chem.* **2012**, *84*, 10518-10521.
- (254) Zhang, M.; Chen, C.; Ma, W.; Zhao, J. *Angew. Chem.* **2008**, *120*, 9876-9879.
- (255) Ding, Z.; Lu, G. Q.; Greenfield, P. F. *J. Phys. Chem. B* **2000**, *104*, 4815-4820.

- (256) Iliev, V.; Alexiev, V.; Bilyarska, L. *J. Mol. Catal. A: Chem.* **1999**, *137*, 15-22.
- (257) Lachheb, H.; Dappozze, F.; Houas, A.; Guillard, C. *J. Photochem. Photobiol. A* **2012**, *246*, 1-7.
- (258) Wöhrle, D.; Suvorova, O.; Gerdes, R.; Bartels, O.; Lapok, L.; Baziakina, N.; Makarov, S.; Slodek, A. *J. Porphyrins Phthalocyanines* **2004**, *08*, 1020-1041.
- (259) Ward, M. D.; White, J. R.; Bard, A. J. *J. Am. Chem. Soc.* **1983**, *105*, 27-31.
- (260) Walsh, K.; Sneddon, H. F.; Moody, C. J. *Org. Lett.* **2014**, *16*, 5224-5227.
- (261) Robertson, P. K. J.; Eggins, B. R. *The Analyst* **1994**, *119*, 827.
- (262) Frame, F. A.; Townsend, T. K.; Chamousis, R. L.; Sabio, E. M.; Dittrich, T.; Browning, N. D.; Osterloh, F. E. *J. Am. Chem. Soc.* **2011**, *133*, 7264-7267.
- (263) Najafpour, M. M.; Sedigh, D. J.; Pashaei, B.; Nayeri, S. *New J. Chem.* **2013**, *37*, 2448.
- (264) Bamwenda, G. R.; Uesigi, T.; Abe, Y.; Sayama, K.; Arakawa, H. *Appl. Catal., A* **2001**, *205*, 117-128.
- (265) Milczarek, G.; Kasuya, A.; Tohji, K.; Arai, T.; Ito, T. *Sol. Energy Mater. Sol. Cells* **2005**, *86*, 43-52.
- (266) Zhang, N.; Zhang, Y.; Yang, M.-Q.; Tang, Z.-R.; Xu, Y.-J. *J. Catal.* **2013**, *299*, 210-221.
- (267) Teplý, F. *Collect. Czech. Chem. Commun.* **2011**, *76*, 859-917.
- (268) Crutchley, R. J.; Lever, A. B. P. *J. Am. Chem. Soc.* **1980**, *102*, 7128-7129.
- (269) Yoon, T. P.; Ischay, M. A.; Du, J. *Nat. Chem.* **2010**, *2*, 527-532.
- (270) Majek, M.; Filace, F.; Wangelin, A. J. v. *Beilstein J. Org. Chem.* **2014**, *10*, 981-989.
- (271) Hari, D. P.; König, B. *Org. Lett.* **2011**, *13*, 3852-3855.
- (272) Kotani, H.; Ohkubo, K.; Fukuzumi, S. *J. Am. Chem. Soc.* **2004**, *126*, 15999-16006.
- (273) Ghosh, I.; Ghosh, T.; Bardagi, J. I.; König, B. *Science* **2014**, *346*, 725-728.
- (274) Korn, S.; Tausch, M. W. *J. Chem. Educ.* **2001**, *78*, 1238.
- (275) Zhang, P.; Wang, M.; Dong, J.; Li, X.; Wang, F.; Wu, L.; Sun, L. *J. Phys. Chem. C* **2010**, *114*, 15868-15874.
- (276) Fateeva, A.; Chater, P. A.; Ireland, C. P.; Tahir, A. A.; Khimyak, Y. Z.; Wiper, P. V.; Darwent, J. R.; Rosseinsky, M. J. *Angew. Chem.* **2012**, *124*, 7558-7562.
- (277) Marcus, R. A. *Rev. Mod. Phys.* **1993**, *65*, 599-610.
- (278) Zimmerman, H. E.; Sandel, V. R. *J. Am. Chem. Soc.* **1963**, *85*, 915-922.
- (279) Alberola, A.; Andrés, C.; Ortega, A. G.; Pedrosa, R.; Vicente, M. *J. Heterocycl. Chem.* **1986**, *23*, 1781-1783.
- (280) Höfle, G.; Steglich, W.; Vorbrüggen, H. *Angew. Chem. Int. Ed. Engl.* **1978**, *17*, 569-583.
- (281) Ohno, M.; Miyamoto, M.; Hoshi, K.; Takeda, T.; Yamada, N.; Ohtake, A. *J. Med. Chem.* **2005**, *48*, 5279-5294.
- (282) Nakagawa, T.; Tanaka, T.; Niwa, D.; Osaka, T.; Takeyama, H.; Matsunaga, T. *J. Biotechnol.* **2005**, *116*, 105-111.
- (283) Tsai, Y.-C.; Jen, H.-P.; Lin, K.-W.; Hsieh, Y.-Z. *J. Chromatogr. A* **2006**, *1111*, 267-271.
- (284) French, R. H.; Tran, H. V. *Annu. Rev. Mater. Res.* **2009**, *39*, 93-126.
- (285) Moon, S.; Kim, J. *J. Photochem. Photobiol. C* **2008**.
- (286) Boudebous, H.; Košmrlj, B.; Šket, B.; Wirz, J. *J. Phys. Chem. A* **2007**, *111*, 2811-2813.
- (287) Sebej, P.; Lim, B. H.; Park, B. S.; Givens, R. S.; Klan, P. *Org. Lett.* **2011**, *13*, 644-647.

- (288) Patel, A. R.; Tolansky, S. *Proc. R. Soc. A* **1957**, *243*, 33-40.
- (289) Rufe, E. *Science* **1999**, *285*, 874-876.
- (290) Nagahara, L. A. *J. Vac. Sci. Technol. B* **1994**, *12*, 1694.
- (291) Miyake, S.; Wang, M.; Kim, J. *J. Nanotechnol.* **2014**, *2014*, 1-19.
- (292) Antony, L. A. P.; Slanina, T.; Šebej, P.; Šolomek, T.; Klán, P. *Org. Lett.* **2013**, *15*, 4552-4555.
- (293) Goossen, L. J.; Manjolinho, F.; Khan, B. A.; Rodríguez, N. *J. Org. Chem.* **2009**, *74*, 2620-2623.
- (294) Hassoon, S.; Neckers, D. C. *J. Phys. Chem.* **1995**, *99*, 9416-9424.
- (295) L'Abbé, G. *Angew. Chem. Int. Ed. Engl.* **1980**, *19*, 276-289.
- (296) Coe, P. L.; Sellars, A.; Tatlow, J. C.; Whittaker, G.; Fielding, H. C. *J. Chem. Soc., Chem. Commun.* **1982**, 362.
- (297) Adam, W.; Liu, J.-C.; Rodriguez, O. *J. Org. Chem.* **1973**, *38*, 2269-2270.
- (298) Widdop, B. *Ann. Clin. Biochem.* **2002**, *39*, 378-391.
- (299) Rodkey, F. L. H., T. A.; Pitts, L. L.; Robertson, R. F. *Clin. Chem.* **1979**, *25*, 1388-1393.
- (300) König, K. *J. Microsc.* **2000**, *200*, 83-104.
- (301) Similar nodal properties of frontier MOs is a necessary but not sufficient condition for predicting the same type of a photoreaction of two, seemingly unrelated chromophores.
- (302) Boens, N.; Leen, V.; Dehaen, W. *Chem. Soc. Rev.* **2012**, *41*, 1130-1172.
- (303) Bessette, A.; Hanan, G. S. *Chem. Soc. Rev.* **2014**, *43*, 3342-3405.
- (304) Lu, H.; Mack, J.; Yang, Y. C.; Shen, Z. *Chem. Soc. Rev.* **2014**, *43*, 4778-4823.
- (305) Lo, M. M. C.; Fu, G. C. *J. Am. Chem. Soc.* **2002**, *124*, 4572-4573.
- (306) Ortiz, M. J.; Garcia-Moreno, I.; Agarrabeitia, A. R.; Duran-Sampedro, G.; Costela, A.; Sastre, R.; Arbeloa, F. L.; Prieto, J. B.; Arbeloa, I. L. *Phys. Chem. Chem. Phys.* **2010**, *12*, 7804-7811.
- (307) Costela, A.; Garcia-Moreno, I.; Pintado-Sierra, M.; Amat-Guerri, F.; Liras, M.; Sastre, R.; Arbeloa, F. L.; Prieto, J. B.; Arbeloa, I. L. *J. Photochem. Photobiol. A* **2008**, *198*, 192-199.
- (308) Zhang, X. F.; Yang, X. D. *J. Chem. Phys. B* **2013**, *117*, 5533-5539.
- (309) Saito, F.; Tobita, S.; Shizuka, H. *J. Chem. Soc., Faraday Trans.* **1996**, *92*, 4177-4185.
- (310) Zhang, X. F.; Yang, X. D.; Niu, K.; Geng, H. *J. Photochem. Photobiol. A* **2014**, *285*, 16-20.
- (311) Ghosh, T.; Slanina, T.; König, B. *Chem. Sci.* **2015**, *6*, 2027-2034.
- (312) Nam, D. H.; Park, C. B. *ChemBioChem* **2012**, *13*, 1278-1282.
- (313) Armstrong, R. W.; Panzer, N. M. *J. Am. Chem. Soc.* **1972**, *94*, 7650-7653.
- (314) Krasna, A. I. *Photochem. Photobiol.* **1979**, *29*, 267-276.
- (315) Youinou, M. T.; Ziessel, R. *J. Organomet. Chem.* **1989**, *363*, 197-208.
- (316) Hollmann, F.; Schmid, A.; Steckhan, E. *Angew. Chem., Int. Ed.* **2001**, *40*, 169-171.
- (317) Lo, H. C.; Buriez, O.; Kerr, J. B.; Fish, R. H. *Angew. Chem., Int. Ed.* **1999**, *38*, 1429-1432.
- (318) Leiva, C.; Lo, H. C.; Fish, R. H. *J. Organomet. Chem.* **2010**, *695*, 145-150.
- (319) Himeda, Y.; Onozawa-Komatsuzaki, N.; Sugihara, H.; Arakawa, H.; Kasuga, K. *J. Mol. Catal. A: Chem.* **2003**, *195*, 95-100.
- (320) Kölle, U.; Grätzel, M. *Angew. Chem., Int. Ed. Engl.* **1987**, *99*, 572-574.
- (321) Chakraborty, B.; Basu, S. *Chem. Phys. Lett.* **2009**, *477*, 382-387.



- (322) Lo, H. C.; Leiva, C.; Buriez, O.; Kerr, J. B.; Olmstead, M. M.; Fish, R. H. *Inorg. Chem.* **2001**, *40*, 6705-6716.
- (323) Kalyanasundaram, K.; Grätzel, M. *J. Chem. Soc., Chem. Commun.* **1979**, 1137.
- (324) Pileni, M. P.; Grätzel, M. *J. Phys. Chem.* **1980**, *84*, 2402-2406.
- (325) Kalyanasundaram, K.; Dung, D. *J. Phys. Chem.* **1980**, *84*, 2551-2556.
- (326) Parker, C. A.; Joyce, T. A. *Photochem. Photobiol.* **1973**, *18*, 467-474.
- (327) Solar, S.; Solar, W.; Getoff, N. *Z. Naturforsch.* **1982**, *37a*, 1077-1082.
- (328) Lv, H.; Guo, W.; Wu, K.; Chen, Z.; Bacsa, J.; Musaev, D. G.; Geletii, Y. V.; Lauinger, S. M.; Lian, T.; Hill, C. L. *J. Am. Chem. Soc.* **2014**, *136*, 14015-14018.
- (329) Hering, T.; Slanina, T.; Hancock, A.; Wille, U.; König, B. *Chem. Commun.* **2015**, *51*, 6568-6571.
- (330) Wayne, R. P.; Barnes, I.; Biggs, P.; Burrows, J. P.; Canosa-Mas, C. E.; Hjorth, J.; Le Bras, G.; Moortgat, G. K.; Perner, D.; Poulet, G.; Restelli, G.; Sidebottom, H. *Atmos. Environ., Part A* **1991**, *25*, 1-203.
- (331) Rousse, D.; George, C. *PCCP* **2004**, *6*, 3408.
- (332) Pérez-Casany, M. P.; Nebot-Gil, I.; Sánchez-Marín, J.; Tomás-Vert, F.; Martínez-Ataz, E.; Cabañas-Galán, B.; Aranda-Rubio, A. *J. Org. Chem.* **1998**, *63*, 6978-6983.
- (333) Ito, O.; Akiho, S.; Iino, M. *J. Phys. Chem.* **1989**, *93*, 4079-4083.
- (334) Baciocchi, E.; Giacco, T. D.; Murgia, S. M.; Sebastiani, G. V. *J. Chem. Soc., Chem. Commun.* **1987**, 1246.
- (335) Suzuki, H.; Mori, T. *J. Chem. Soc. Perk. Trans. 2* **1996**, 677.
- (336) Baciocchi, E.; Del Giacco, I.; Rol, C.; Sebastiani, G. V. *Tetrahedron Lett.* **1985**, *26*, 541-544.
- (337) Shono, T.; Chuankamnerdkarn, M.; Maekawa, H.; Ishifune, M.; Kashimura, S. *Synthesis* **1994**, *1994*, 895-897.
- (338) Fokin, Andrey A.; Peleshanko, Sergey A.; Gunchenko, Pavel A.; Gusev, Dmitriy V.; Schreiner, Peter R. *Eur. J. Org. Chem.* **2000**, *2000*, 3357-3362.
- (339) Mella, M.; Freccero, M.; Soldi, T.; Fasani, E.; Albini, A. *J. Org. Chem.* **1996**, *61*, 1413-1422.
- (340) Wille, U. *Chem. Eur. J.* **2002**, *8*, 340-347.
- (341) Wille, U.; Lietzau, L. *Tetrahedron* **1999**, *55*, 11465-11474.
- (342) Wille, U.; Lietzau, L. *Tetrahedron* **1999**, *55*, 10119-10134.
- (343) Gamon, L. F.; White, J. M.; Wille, U. *Org. Biomol. Chem.* **2014**, *12*, 8280-8287.
- (344) Sigmund, D. C. E.; Wille, U. *Chem. Commun.* **2008**, 2121.
- (345) Wille, U.; Andropof, J. *Aust. J. Chem.* **2007**, *60*, 420.
- (346) Langer, S.; Ljungström, E. *J. Chem. Soc., Faraday Trans.* **1995**, *91*, 405.
- (347) Styler, S. A.; Donaldson, D. J. *Environ. Sci. Technol.* **2011**, *45*, 10004-10012.
- (348) Fukuzumi, S.; Ohkubo, K.; Suenobu, T. *Acc. Chem. Res.* **2014**, *47*, 1455-1464.
- (349) Benniston, A. C.; Harriman, A.; Li, P.; Rostron, J. P.; van Ramesdonk, H. J.; Groeneveld, M. M.; Zhang, H.; Verhoeven, J. W. *J. Am. Chem. Soc.* **2005**, *127*, 16054-16064.
- (350) Romero, N. A.; Nicewicz, D. A. *J. Am. Chem. Soc.* **2014**, *136*, 17024-17035.
- (351) Ohkubo, K.; Mizushima, K.; Fukuzumi, S. *Res. Chem. Intermed.* **2012**, *39*, 205-220.
- (352) Smith, R. C.; Bodner, C. R.; Earl, M. J.; Sears, N. C.; Hill, N. E.; Bishop, L. M.; Sizemore, N.; Hehemann, D. T.; Bohn, J. J.; Protasiewicz, J. D. *J. Organomet. Chem.* **2005**, *690*, 477-481.
- (353) Zhao, H.; Wei, Y.; Xu, J.; Kan, J.; Su, W.; Hong, M. *J. Org. Chem.* **2011**, *76*, 882-893.
- (354) Xiao, J.-C.; Ye, C.; Shreeve, J. n. M. *Org. Lett.* **2005**, *7*, 1963-1965.

- (355) Korenaga, T.; Kosaki, T.; Fukumura, R.; Ema, T.; Sakai, T. *Org. Lett.* **2005**, *7*, 4915-4917.
- (356) Wei, Y.; Kan, J.; Wang, M.; Su, W.; Hong, M. *Org. Lett.* **2009**, *11*, 3346-3349.
- (357) Kinzel, T.; Zhang, Y.; Buchwald, S. L. *J. Am. Chem. Soc.* **2010**, *132*, 14073-14075.
- (358) Frohn, H. J.; Adonin, N. Y.; Bardin, V. V.; Starichenko, V. F. *Tetrahedron Lett.* **2002**, *43*, 8111-8114.
- (359) Frohn, H.-J.; Adonin, N. Y.; Bardin, V. V.; Starichenko, V. F. *J. Fluorine Chem.* **2002**, *117*, 115-120.
- (360) Shang, R.; Fu, Y.; Wang, Y.; Xu, Q.; Yu, H.-Z.; Liu, L. *Angew. Chem. Int. Ed.* **2009**, *48*, 9350-9354.
- (361) Shang, R.; Xu, Q.; Jiang, Y.-Y.; Wang, Y.; Liu, L. *Org. Lett.* **2010**, *12*, 1000-1003.
- (362) DePasquale, R. J.; Tamborski, C. *J. Org. Chem.* **1969**, *34*, 1736-1740.
- (363) Coe, P. L.; Pearl, G. M. *J. Organomet. Chem.* **1971**, *31*, 55-57.
- (364) Majek, M.; Jacobi von Wangelin, A. *Angew. Chem. Int. Ed.* **2015**, *54*, 2270-2274.
- (365) Baralle, A.; Fensterbank, L.; Goddard, J.-P.; Ollivier, C. *Chem. Eur. J.* **2013**, *19*, 10809-10813.
- (366) Redmond, R. W.; Gamlin, J. N. *Photochem. Photobiol.* **1999**, *70*, 391-475.
- (367) Aihara, K.; Urano, Y.; Higuchi, T.; Hirobe, M. *J. Chem. Soc., Perkin Trans. 2* **1993**, 2165-2170.
- (368) Rosa, A. M.; Lobo, A. M.; Branco, P. S.; Sundaresan, P. *Tetrahedron* **1997**, *53*, 285-298.
- (369) Zhang, W.; Pugh, G. *Tetrahedron Lett.* **2001**, *42*, 5613-5615.
- (370) Ohno, H.; Wakayama, R.; Maeda, S.-i.; Iwasaki, H.; Okumura, M.; Iwata, C.; Mikamiyama, H.; Tanaka, T. *J. Org. Chem.* **2003**, *68*, 5909-5916.
- (371) Hari, D. P.; König, B. *Chem. Commun.* **2014**, *50*, 6688.
- (372) Yang, X.-J.; Chen, B.; Zheng, L.-Q.; Wu, L.-Z.; Tung, C.-H. *Green Chem.* **2014**, *16*, 1082-1086.
- (373) Costentin, C.; Robert, M.; Savéant, J.-M. *J. Am. Chem. Soc.* **2004**, *126*, 16051-16057.
- (374) Penzkofer, A.; Beidoun, A.; Speiser, S. *Chem. Phys.* **1993**, *170*, 139-148.
- (375) Liu, Q.; Li, Y.-N.; Zhang, H.-H.; Chen, B.; Tung, C.-H.; Wu, L.-Z. *Chem. Eur. J.* **2012**, *18*, 620-627.
- (376) Benniston, A. C.; Copley, G. *Phys. Chem. Chem. Phys.* **2009**, *11*, 4124-4131.
- (377) Benstead, M.; Mehl, G. H.; Boyle, R. W. *Tetrahedron* **2011**, *67*, 3573-3601.
- (378) Kamkaew, A.; Lim, S. H.; Lee, H. B.; Kiew, L. V.; Chung, L. Y.; Burgess, K. *Chem. Soc. Rev.* **2013**, *42*, 77-88.
- (379) Loudet, A.; Burgess, K. *Chem. Rev.* **2007**, *107*, 4891-4932.
- (380) Ulrich, G.; Ziesel, R.; Harriman, A. *Angew. Chem. Int. Ed.* **2008**, *47*, 1184-1201.
- (381) Zhao, J. Z.; Wu, W. H.; Sun, J. F.; Guo, S. *Chem. Soc. Rev.* **2013**, *42*, 5323-5351.
- (382) Yogo, T.; Urano, Y.; Ishitsuka, Y.; Maniwa, F.; Nagano, T. *J. Am. Chem. Soc.* **2005**, *127*, 12162-12163.
- (383) Klan, P.; Wirz, J. *Photochemistry of organic compounds: From concepts to practice*; 1<sup>st</sup> ed.; John Wiley & Sons Ltd.: Chichester, 2009.
- (384) Solovyov, K. N.; Borisevich, E. A. *Phys. Usp.* **2005**, *48*, 231-253.

- (385) Galletta, M.; Campagna, S.; Quesada, M.; Ulrich, G.; Ziessel, R. *Chem. Commun.* **2005**, 4222-4224.
- (386) Rachford, A. A.; Ziessel, R.; Bura, T.; Retailleau, P.; Castellano, F. N. *Inorg. Chem.* **2010**, *49*, 3730-3736.
- (387) Wu, W. H.; Guo, H. M.; Wu, W. T.; Ji, S. M.; Zhao, J. Z. *J. Org. Chem.* **2011**, *76*, 7056-7064.
- (388) Cakmak, Y.; Kolemen, S.; Duman, S.; Dede, Y.; Dolen, Y.; Kilic, B.; Kostereli, Z.; Yildirim, L. T.; Dogan, A. L.; Guc, D.; Akkaya, E. U. *Angew. Chem. Int. Ed.* **2011**, *50*, 11937-11941.
- (389) Duman, S.; Cakmak, Y.; Kolemen, S.; Akkaya, E. U.; Dede, Y. *J. Org. Chem.* **2012**, *77*, 4516-4527.
- (390) Broring, M.; Kruger, R.; Link, S.; Kleeberg, C.; Kohler, S.; Xie, X.; Ventura, B.; Flamigni, L. *Chem. Eur. J.* **2008**, *14*, 2976-2983.
- (391) Ventura, B.; Marconi, G.; Broring, M.; Krugerb, R.; Flamigni, L. *New J. Chem.* **2009**, *33*, 428-438.
- (392) Fron, E.; Coutino-Gonzalez, E.; Pandey, L.; Sliwa, M.; Van der Auweraer, M.; De Schryver, F. C.; Thomas, J.; Dong, Z. Y.; Leen, V.; Smet, M.; Dehaen, W.; Vosch, T. *New J. Chem.* **2009**, *33*, 1490-1496.
- (393) Leen, V.; Braeken, E.; Luckermans, K.; Jackers, C.; Van der Auweraer, M.; Boens, N.; Dehaen, W. *Chem. Commun.* **2009**, 4515-4517.
- (394) Rohand, T.; Qin, W. W.; Boens, N.; Dehaen, W. *Eur. J. Org. Chem.* **2006**, 4658-4663.
- (395) Ortiz, M. J.; Agarrabeitia, A. R.; Duran-Sampedro, G.; Prieto, J. B.; Lopez, T. A.; Massad, W. A.; Montejano, H. A.; Garcia, N. A.; Arbeloa, I. L. *Tetrahedron* **2012**, *68*, 1153-1162.
- (396) Leen, V.; Leemans, T.; Boens, N.; Dehaen, W. *Eur. J. Org. Chem.* **2011**, *2011*, 4386-4396.
- (397) Mironov, L. Y.; Sveshnikova, E. B.; Ermolaev, V. L. *Opt. Spectrosc.* **2014**, *117*, 896-907.
- (398) Kořinek, M.; Dědic, R.; Svoboda, A.; Hála, J. *J. Fluoresc.* **2004**, *14*, 71-74.
- (399) Lagorio, M. G.; Dicalio, L. E.; San Román, E. A.; Braslavsky, S. E. *J. Photochem. Photobiol. B* **1989**, *3*, 615-624.
- (400) Zhang, X.-F.; Yang, X. *J. Phys. Chem. B* **2013**, *117*, 5533-5539.
- (401) Bonneau, R.; Carmichael, I.; Hug, G. L. *Pure Appl. Chem.* **1991**, *63*, 290-299.

## 6. Curriculum Vitae

---

### Personal information

Name: Tomáš Slanina  
Academic title: RNDr. (*Doctor rerum naturalium*)  
Date of birth: 25<sup>th</sup> August 1988  
Address: Mackovec 458/27  
Lelekovice 664 31  
Czech Republic  
Telephone: +420723576911  
Email: Slanina.Tomas@seznam.cz

---

### Education

1994 – 1999 Primary school, Lelekovice  
1999 – 2007 Secondary school, Brno – Řečkovice  
2007 – 2010 Masaryk University Brno, Faculty of Science, Chemistry  
2010 bachelor degree, Bc., *summa cum laude*  
2010 – 2012 Masaryk University Brno, Faculty of Science, Organic Chemistry  
2012 master degree, Mgr., *summa cum laude*  
2012 – 2015 joint Ph.D. program:  
Universität Regensburg, Fakultät Chemie und Pharmazie, Organic  
Chemistry  
Masarykova univerzita Brno, Přírodovědecká fakulta, Organická  
chemie  
2014 Charles University in Prague, Faculty of Science, Rigorous exam  
2014 RNDr. degree

---

### Employment

2013 (9 months) research specialist, Research Centre for Toxic Compounds in the  
Environment (RECETOX), Faculty of Science, Masaryk  
University, Brno  
2014 – 2015 (9 months) Spin-off Technology Development, stage Proof of Concept at  
the Masaryk University, Brno  
2015 – research specialist, Research Centre for Toxic Compounds in the  
Environment (RECETOX), Faculty of Science, Masaryk  
University, Brno

---

## Publications

1. Balachandran Kammath V., Šebej P., Slanina T., Kříž Z., Klán P. Photoremovable Chiral Auxiliary. *Photochem. Photobiol. Sci.* **2012**, 11, 500-507.
2. Šebej P., Wintner J., Müller P., Slanina, T., Al Anshori J., Lovely Angel P. A., Klán P., Wirz J. Fluorescein Analogues as Photoremovable Protecting Groups Absorbing at ~520 nm. *J. Org. Chem.* **2013**, 78, 1833–1843.
3. Lovely Angel P. A\*, Slanina T.\*, Šebej P., Šolomek T., Klán P. Fluorescein Analogue Xanthene-9-Carboxylic Acid: A Transition-Metal Free CO Releasing Molecule Activated by Green Light. *Org. Lett.* **2013**, 15, 4552–4555.
4. Ghosh, T.\*; Slanina, T.\*; König, B. Visible light photocatalytic reduction of aldehydes by Rh(III)–H: a detailed mechanistic study. *Chem. Sci.* **2015**, 6, 2027-2034.
5. Hering, T.; Slanina, T.; Hancock, A.; Wille, U.; König, B. Visible light photooxidation of nitrate: the dawn of a nocturnal radical. *Chem. Commun.* **2015**, 51, 6568-6571.
6. Muchová L.; Jašprová J.; Slanina T.; Šebej P.; Klán P.; Vitek L. Xanthene-9-carboxylic acid: A photo-activatable transition-metal-free carbon monoxide-releasing molecule with extraordinary long half-life. *Nitric Oxide-Biol. Chem.* **2015**, 47, S35.
7. Slanina T.; Šebej P.; Heckel A.; Givens R. S.; Klán P. Caged Fluoride: Photochemistry and Applications of 4-Hydroxyphenacyl Fluoride. *Org. Lett.* **2015**, 17, 4814.
  
8. Palao E.\*; Slanina T.\*; Muchová L.; Šolomek T.; Vitek L.; Klán P. Transition-Metal-Free CO-Releasing BODIPY Derivatives Activatable by Visible to NIR Light as Promising Bioactive Molecules. **2015**, *submitted*
9. Meyer A. U.; Slanina T.; Yao C. J.; König B. Metal-Free C–H Arylation with Fluorinated Aryl Bromides by Visible Light Photoredox Catalysis. **2015**, *submitted*
10. Al Anshori J.; Slanina T.; Palao E.; Klán P. On the Efficiency of Intersystem Crossing of Heavy-Atom-Substituted BODIPY Derivatives. **2015**, *submitted*

\* = joint first authorship; \*\* = corresponding author

---

## Scholarships and Awards

2003 – 2007	Chemistry and Biology Olympiad, regional and national round
2007	InterSoB – multidisciplinary competition
2006 – 2010	<b>Program for Talented Students, JCMM</b>
2007 – 2012	scholarship for excellent study results
2010 – 2012	research scholarship
2011 – 2012	mobility scholarship – Erasmus program
2011	Department of Chemistry Award
2012	<b>Dean's Award</b>
2012	scholarship for outstanding study results
2012 – 2015	Doctoral Students Scholarship
2012 – 2015	Scholarship for Creativity in Research

2013	Department of Chemistry Award
2013 – 2014	<b>GRK 1626 Chemical Photocatalysis Graduate School Scholarship</b> (16 months)
2014 –	GRK 1626 Chemical Photocatalysis Graduate School associated member
2015	<b>Dean's Award</b>
2015	first place <b>Jean Marie Lehn Ph.D. Chemistry Prize</b>

---

#### Conferences and Fellowships

2005	High School Research Project at FNUSA in Brno (SOČ)
2009	J. Heyrovsky Institute of Physical Chemistry, Academy of Sciences of the Czech Republic, Prague
2009	Czech School of Chromatography, Olomouc
2009-2010 (4 months)	fellowship, Synthron, s. r. o., Blansko
2011	Institute of Macromolecular Chemistry, Academy of Sciences of the Czech Republic, Prague
2011 (2 months)	fellowship, Teva Czech Industries, s.r.o., Opava
2011	Graduate School of Photochemistry, Fraueninsel
2011 – 2012 (6 months)	fellowship Univesität Regensburg, Regensburg, Erasmus program
2012	Graduate School of Photochemistry, Regensburg
2012	ACS National Meeting, Philadelphia, PA, USA
2012 (3 months)	research stay University of Kansas, Lawrence, KS, USA
2012	The Edward E. Smissman Memorial Lectures
2012	ACS Midwest Regional Meeting, Omaha, NE, USA
2013	Czech School of Spectroscopy, Brno
2013	Co-Author of Correspondence Seminar ViBuCh
2013	ESOR 2013, Prague
2013 – 2014 (16 months)	fellowship Univesität Regensburg, Regensburg, Ph.D. student
2013	Graduate School of Photochemistry, Regensburg
2013	INDIGO Research Conference and Intensive Course, Regensburg
2014	Graduate School of Photochemistry, Kostenz, Germany
2014	Analytica 2014, München, Germany
2014	research visit Ludwig-Maximilians-Universität, München, Germany
2014	Graduate School of Photochemistry, Regensburg
2014 – 2015	research visits IOCB, Prague; VFN + LF UK Prague
2015	Graduate School of Photochemistry, Regensburg
2015	DocDays 2015, Graz
2015	XV. Workshop of Physical Chemists and Electrochemists
2015	IX. Summer Electrochemical School, tutor
2015	research visit Universität Regensburg
2015	Graduate School of Photochemistry, München
2015	ESOR 2015, Kiel

2015  
2015

Graduate School of Photochemistry, Kostenz  
Liblice Conference, Olomouc

---

#### Posters and Lectures

- Balachandran Kammath, V., Šebej P., Slanina T., Klán P. Benzoin as a photoremovable chiral auxiliary. *238<sup>th</sup> American Chemical Society National Meeting & Exposition*. Washington, USA, **2009** (poster)
- Balachandran Kammath, V., Šebej P., Slanina T., Klán P. Asymmetric Diels-Alder reaction using benzoin as a photoremovable chiral auxiliary. *240<sup>th</sup> American Chemical Society National Meeting & Exposition*. Boston, USA, **2010** (poster)
- Slanina T., Wintner J., Šebej P., Al Anshori J., Lovely Angel P. A., Müller P., Wirz J., Klán P. New Photoremovable Protecting Group Absorbing Over 500 nm. *244<sup>th</sup> American Chemical Society National Meeting & Exposition*. Philadelphia, USA, **2012** (poster)
- Slanina T., Rubina M., Bolton S. D., Šebej P., Givens R. S. p-Hydroxyphenacyl Photoremovable Protecting Group with Trialkylammonium Probe. *47<sup>th</sup> ACS Midwest Regional Meeting*. Omaha, USA, **2012** (poster)
- Slanina T., Šebej P., Lovely Angel P. A., Wintner J., Müller P., Al Anshori J., Wirz J., Klán P. Xanthene-9-carboxylic Acid: Caged Carbon Monoxide Released by Green Light. *ESOR 2013*. Prague, Czech Republic, **2013** (poster)
- Ghosh T., Slanina T., König B. Photochemical slow in situ generation of Rh(III) hydride leading to chemoselectivity of aldehydes over non-activated ketones. *24<sup>th</sup> Lecture Conference on Photochemistry*. Cologne, Germany, **2014** (poster)
- Slanina T.; Oberschmid T. Electrofluorimetry – a useful tool for investigation of photocatalytic mechanisms. *DocDays 2015*. Graz, Austria, **2015** (poster)
- Slanina T. Spectroelectrochemistry and electrofluorimetry of biologically relevant fluorescent dyes. *XV. Workshop of Physical Chemists and Electrochemists*. Brno, Czech Republic, **2015 (invited lecture)**
- Slanina T.; Palao E.; Muchová L.; Jašprová J.; Šebej P.; Vitek L.; Klán P. Visible Light Photoactivated Metal-Free Carbon Monoxide-Releasing Molecules (photoCORM) Suitable for Bioapplications. *ESOR 2015*. Kiel, Germany, **2015** (lecture)
- Slanina T. Electrofluorimetry – a Useful Tool for Investigation of Organic Radicals. *Liblice 2015.*, Olomouc, **2015** (lecture)

## 7. List of Appendices

Appendix A: Šebej, P.; Wintner, J.; Müller, P.; Slanina, T.; Al Anshori, J.; Antony, L. A. P.; Klán, P.; Wirz, J. <i>J. Org. Chem.</i> <b>2013</b> , 78, 1833-1843.....	S1
Appendix B: Slanina, T.; Šebej, P.; Heckel, A.; Givens, R. S.; Klán, P. <i>Org. Lett.</i> <b>2015</b> , 17, 4814-4817.....	S12
Appendix C: Antony, L. A. P.; Slanina, T.; Šebej, P.; Šolomek, T.; Klán, P. <i>Org. Lett.</i> <b>2013</b> , 15, 4552-4555.....	S16
Appendix D: BODIPY-based CORM, submitted manuscript.....	S20
Appendix E: Ghosh, T.; Slanina, T.; König, B. <i>Chem. Sci.</i> <b>2015</b> , 6, 2027-2034.....	S31
Appendix F: Hering, T.; Slanina, T.; Hancock, A.; Wille, U.; König, B. <i>Chem. Commun.</i> <b>2015</b> , 51, 6568-6571.....	S39
Appendix G: Photocatalytic arylation by fluorinated aryl bromides, submitted manuscript.....	S43
Appendix H: Heavy-atom effect on selanyl- and tellanyl-substituted BODIPYs, submitted manuscript.....	S51



## Fluorescein Analogues as Photoremovable Protecting Groups Absorbing at ~520 nm

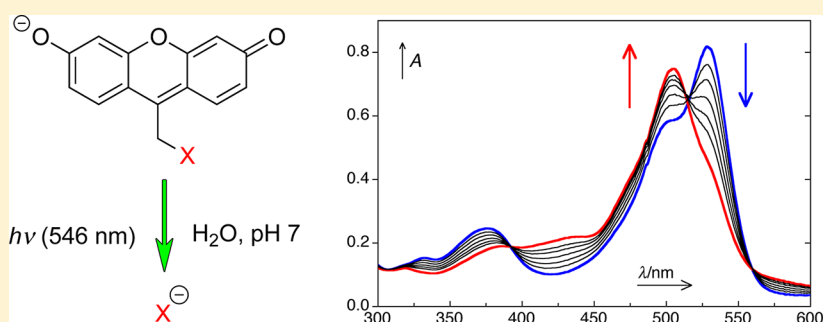
Peter Šebej,<sup>†,‡</sup> Jürgen Wintner,<sup>§</sup> Pavel Müller,<sup>§</sup> Tomáš Slanina,<sup>†</sup> Jamaludin Al Anshori,<sup>†</sup> Lovely Angel Panamparambil Antony,<sup>†</sup> Petr Klán,<sup>\*,†,‡</sup> and Jakob Wirz<sup>\*,§</sup>

<sup>†</sup>Department of Chemistry, Faculty of Science, Masaryk University, Kamenice 5, 625 00, Brno, Czech Republic

<sup>‡</sup>Research Centre for Toxic Compounds in the Environment, Faculty of Science, Masaryk University, Kamenice 3, 625 00 Brno, Czech Republic

<sup>§</sup>Department of Chemistry, University of Basel, Klingelbergstrasse 80, CH-4056 Basel, Switzerland

### Supporting Information



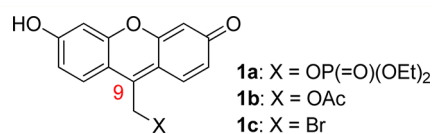
**ABSTRACT:** A new photoremovable protecting group, (6-hydroxy-3-oxo-3*H*-xanthen-9-yl)methyl (**1**), with a molar absorption coefficient  $\epsilon$  of  $\sim 4 \times 10^4 \text{ m}^{-1} \text{ cm}^{-1}$  at  $\sim 520 \text{ nm}$  for the release of carboxylates or phosphates is reported. Three derivatives of **1** (diethyl phosphate, acetate, and bromide) were isolated as complexes with DDQ and shown to release the ligands with quantum yields  $\leq 2.4\%$  in aqueous solution.

Photoremovable protecting groups (PPGs) are increasingly used as versatile tools allowing for the temporally and spatially controlled release of various bioagents in order to study the kinetics of chemical processes in living cells.<sup>1,2</sup> Attractive features of coumarin-derived PPGs are their strong absorption extending to the visible range and appearance rate constants of the free substrates that are on the order of  $10^9 \text{ s}^{-1}$  following excitation with a short light pulse.<sup>3</sup>

In an effort to extend the wavelength range of coumarin PPGs we undertook to synthesize and study the (6-hydroxy-3-oxo-3*H*-xanthen-9-yl)methyl derivatives **1a–c**. Encouraging MO calculations had indicated that strong charge transfer to the C9 position is associated with electronic excitation of the xanthenyl chromophore to the first excited singlet state, which should favor the heterolytic release of an attached leaving group.<sup>4,5</sup> Most xanthenes derivatives such as fluorescein are substituted with an aromatic ring at position C9. So far, only a limited number of compounds having a different substituent, such as cyano,<sup>6–9</sup> trifluoromethyl,<sup>8</sup> alkyl,<sup>10,11</sup> or alkenyl<sup>12</sup> groups, have been synthesized and their structure properly elucidated.

## RESULTS AND DISCUSSION

**Synthesis.** 3,6-Dihydroxy-9*H*-xanthen-9-one (**3**) was prepared from 2,2',4,4'-tetrahydroxybenzophenone **2** by cyclizing

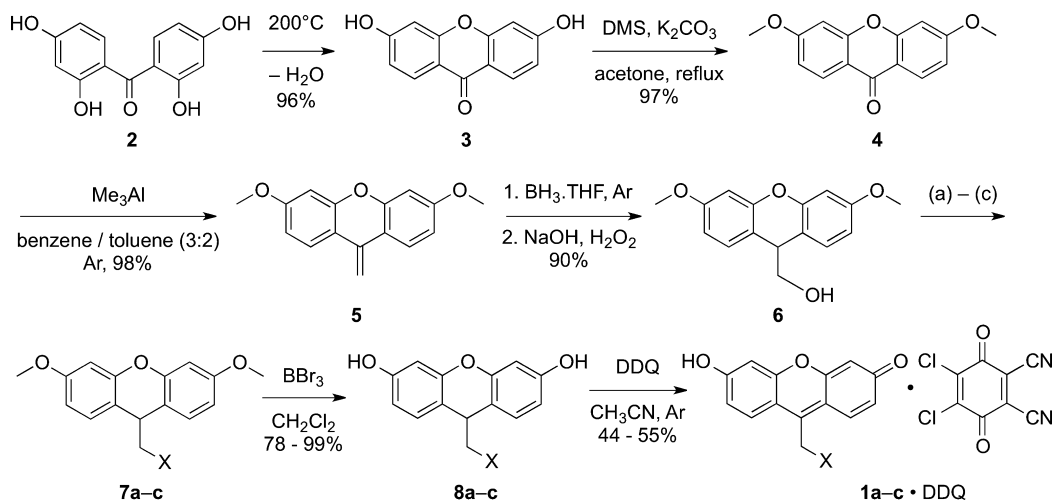


condensation in water in an autoclave at 200 °C according to a known procedure (Scheme 1).<sup>13</sup> The two hydroxy groups of **3** were protected using dimethyl sulfate to give **4**, which was subsequently treated with trimethylaluminum in a Wittig-like fashion<sup>14</sup> to give 3,6-dimethoxy-9-methylene-9*H*-xanthenone (**5**). Hydroboration resulted in formation of the corresponding primary alcohol **6** in 90% yield, which served as a common precursor for the preparation of the synthetic intermediates phosphate **7a**, acetate **7b**,<sup>15</sup> and bromide **7c**.<sup>16</sup> Deprotection of the methoxy groups<sup>17</sup> in **7a–c** using 13 equiv of boron tribromide gave the 9*H*-xanthen-3,6-diol derivatives **8a–c** in 78–99% yield. 2,3-Dichloro-5,6-dicyano-1,4-benzoquinone (DDQ) was then used to oxidize these compounds in dry acetonitrile.<sup>18</sup> However, instead of the anticipated (6-hydroxy-3-oxo-3*H*-xanthen-9-yl)methyl derivatives **1a–c**, 1:1 complexes with DDQ (**1a–c**-DDQ) precipitated as fine red powders from

**Special Issue:** Howard Zimmerman Memorial Issue

**Received:** July 17, 2012

**Published:** July 24, 2012

Scheme 1. Synthesis of Complexes **1a-c**·DDQ<sup>a</sup>

<sup>a</sup>Reagents and conditions: (a) X = OP(=O)(OEt)<sub>2</sub>; CIP(=O)(OEt)<sub>2</sub>, CH<sub>2</sub>Cl<sub>2</sub>, Ar, 78%; (b) X = OAc: Ac<sub>2</sub>O, TEA, DMAP, Ar, 98%; (c) X = Br: CBr<sub>4</sub>, PPh<sub>3</sub>, CH<sub>2</sub>Cl<sub>2</sub>, Ar, 97%. DMS = dimethyl sulfate.

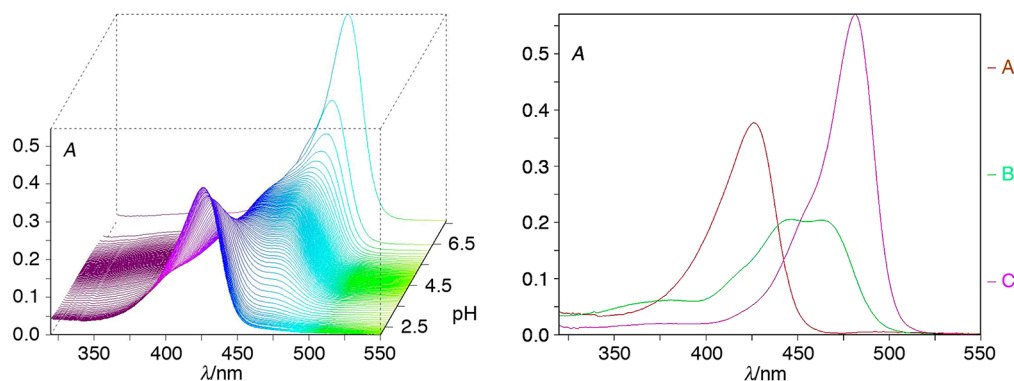


**Figure 1.** Spectrophotometric titration of 6-hydroxy-9-methyl-3H-xanthene-3-one **11**. Left: Plot of the absorption spectra at pH values ranging from 2 to 7. Right: Species spectra (A, cation **11**<sup>+</sup>; B, neutral **11**; C, anion **11**<sup>-</sup>) resulting from global analysis.

the solution in 44–55% yield (calculated with respect to the molecular weight of the complex; a 1.25-molar excess of DDQ was used for the reaction). Their chemical composition was determined by a combination of complementary analytical methods described below. The overall optimized chemical yield of **1a-c**·DDQ was 20–25% over 7 steps.

Charge-transfer (CT) complexes are known to be formed between DDQ and many electron donors<sup>19</sup> such as durene,<sup>20</sup> perylene, pyrene,<sup>21</sup> phenanthroline, and aromatic amines.<sup>22</sup> The reduction potential of DDQ ( $E[A/A^{\cdot-}] = +0.51$  V in CH<sub>3</sub>CN vs SCE)<sup>19</sup> is higher than that of tetracyanoethylene (+0.24 V in CH<sub>3</sub>CN vs SCE).<sup>23</sup> On the other hand, xanthene dyes, such as fluorescein ( $E[D^{\cdot+}/D] = -1.22$  V for fluorescein in acetonitrile vs SCE)<sup>24</sup> are good electron donors. Thus the formation of the CT complexes **1a-c**·DDQ is in line with previous experience.

Several other reagents to oxidize compounds **8** were tested. For example, 2,3,5,6-tetrafluoro-1,4-benzoquinone (fluoranil)<sup>25</sup> was used in a stoichiometric amount under various preparative conditions; however, **8a** was found to be inert to the oxidation. In a different unsuccessful synthetic approach, we attempted to carry out epoxidation<sup>26</sup> of the C=C bond in **5**, the product of which could have subsequently been hydrolyzed and converted to the target molecules **1**.

**Identification of the Complexes 1·DDQ.** Elemental analyses showed that the isolated products are equimolar

complexes of compounds **1** and DDQ. For all three products both direct inlet and HPLC–HRMS analyses provided clearly the molecular ions of **1a-c**·DDQ with isotope patterns typical for the presence of two chlorine atoms (Supplementary Figures S14, S22, and S30–31). Moreover, characteristic vibrations of the cyano group were observed in the IR spectra (Supplementary Figure S21).

The solubility of **1a**·DDQ is very low in all common organic solvents, except for DMSO and DMF. All attempts to isolate the free compounds **1a-c** were unsuccessful. The components of the complexes **1a-c**·DDQ could not be separated chromatographically. We were also unable to crystallize the compounds from DMSO or DMF to produce crystals suitable for X-ray analysis.

To determine whether the formation of CT complexes of **1** with DDQ is a general behavior of 6-hydroxy-3H-xanthene-3-one derivatives, we studied the interactions of DDQ with succinylfluorescein **9**, synthesized according to a known procedure (Experimental Section, Scheme 4),<sup>10</sup> with its methyl ester **10** and with the parent compound 6-hydroxy-9-methyl-3H-xanthene-3-one **11** (Experimental Section, Scheme 5). DDQ was not used in the synthesis of these compounds.

DDQ is only moderately stable in methanol;<sup>27</sup> its half-life was estimated to be ~4 h by UV spectroscopy. The formation of the complexes **9–10**·DDQ in methanol solutions of **9–10**

containing equimolar amounts of DDQ was observed by direct inlet and LC–HRMS, which clearly showed the molecular ions of the complexes and the corresponding isotope patterns typical for the presence of 2 chlorine atoms (Supplementary Figures S43 and S44), as in the case of **1a**–c–DDQ. However, in dilute (30  $\mu\text{M}$ ) solutions of **9**–**11** with up to 100-fold excess of DDQ, absorption and fluorescence spectroscopy did not provide any evidence for complex formation.

The complexes **1a**–c–DDQ dissolved relatively well (up to  $\sim 10$  mM) in 0.1 M aqueous buffer solutions (pH 7–8) or water. DDQ is known to decompose rapidly in water.<sup>19</sup> It reacts within seconds forming 2,3-dichloro-5-cyano-6-hydroxy-1,4-benzoquinone (**12**) and HCN. We conclude that compounds **1a**–c are no longer associated with DDQ when the solid complexes **1a**–c–DDQ are dissolved in aqueous solvents. Slow decomposition of **1a**–c occurred in phosphate buffer (pH 7,  $I = 0.1$  M) in the dark at room temperature with a half-life of 7 days in 30 mM solution.

Strong bands at  $\lambda_{\text{max}} \sim 528$  (**1a**), 522 (**1b**), and 519 nm (**1c**), typical for xantheno dyes,<sup>28</sup> were found in their absorption spectra in aqueous phosphate buffer, pH = 7 ( $\epsilon_{\text{max}} \sim 4 \times 10^4$   $\text{m}^{-1} \text{cm}^{-1}$ ; Supplementary Figures S13, S20, and S29). The bathochromic shifts of the first absorption band associated with the electronegative substituents on 9-methyl indicated that excitation to the first singlet state is accompanied by charge transfer to carbon 9, as expected.

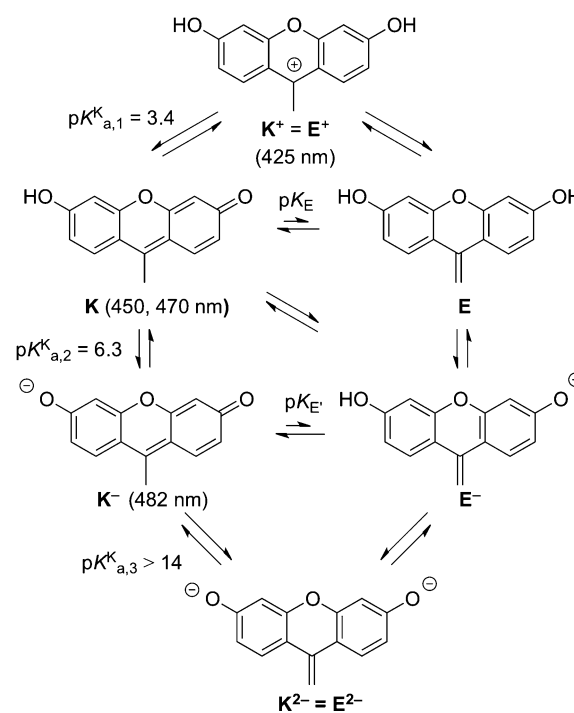
**Titration.** To determine the acidity constants of the 6-hydroxy-3*H*-xanthen-3-one chromophore we first used the parent compound 6-hydroxy-9-methyl-3*H*-xanthen-3-one **11**. A series of spectra was measured by addition of 0.1 M HCl to a solution of **11** in 0.1 M aqueous sodium acetate (Figure 1). The acidity constants resulting from a global analysis of the spectra and fitting with a titration model allowing for two acidity constants are  $\text{p}K_{\text{a,c},1} = 3.44 \pm 0.11$  and  $\text{p}K_{\text{a,c},2} = 6.31 \pm 0.03$  (standard deviations obtained by three independent titration runs,  $I = 0.1$  M,  $25 \pm 0.3$  °C). Similar measurements with the bromide **1c** gave  $\text{p}K_{\text{a},1} = 2.9 \pm 0.1$  and  $\text{p}K_{\text{a},2} = 6.1 \pm 0.1$ .

Succinylfluorescein **9** exists in the form of several tautomers that undergo slow equilibration at 20 °C.<sup>10,29</sup> Similarly, two tautomeric forms of neutral **11** and its anion may participate in the protomeric equilibria, the keto form **K** and the enol form **E** (Scheme 2). However, the characteristic absorption spectra of **11** in the visible range (Figure 1) indicate that the keto forms of the neutral species and the anion, **K** and **K<sup>-</sup>**, predominate in aqueous solutions up to pH 13. In the hydrogen-bond acceptor solvent DMSO, **11** is converted largely to the enol form (Figures S40 and S41; Supporting Information). Following injection of a concentrated DMSO solution into water, the reketonization reaction could be monitored by the rising absorption in the visible range. The ketonization rate constants were slowest in neutral solutions pH 6–9,  $k_{\text{rise}} \approx 1 \times 10^{-2} \text{ s}^{-1}$ , and increased linearly with pH as it was decreased below 5 (acid catalysis) or increased above 10 (base catalysis).

A  $\sim 20\%$  increase in the absorbance of **11** at 482 nm was observed upon addition of 1 M HCl to a solution of **11** in 1 M aqueous KOH. Therefore, the third acidity constant of **11** is probably not far greater than 14. At pH 7, the compound **11** is mostly in the anionic form **K<sup>-</sup>** (83%); therefore the compounds **1a**–c carrying an electronegative substituent at the exocyclic carbon will be almost exclusively anionic at pH 7.

**Calculations.** Density functional theory (DFT) calculations were done with the Gaussian package of programs<sup>30</sup> to calculate the energy difference between the keto and enol forms

**Scheme 2.** Protonation and Tautomerization Equilibria of **11**<sup>a</sup>



<sup>a</sup>**K** and **E** are the keto and enol forms, respectively.

**K** and **E** of **11** (see Scheme 2). Geometries were fully optimized at the B3LYP level of theory with the 6-31+g(d) basis set and the PCM solvation model for water; vibrational frequencies were calculated. The free energy differences were found to be  $\Delta_{\text{K} \rightarrow \text{E}}G(298 \text{ K}) = 26.0 \text{ kJ mol}^{-1}$  and  $\Delta_{\text{K}^- \rightarrow \text{E}^-}G(298 \text{ K}) = 54.8 \text{ kJ mol}^{-1}$ , corresponding to enolization constants  $\text{p}K_{\text{E}} = 4.6$  and  $\text{p}K_{\text{E}'} = 9.4$  for the neutral and anionic forms, respectively.

The same calculations were done for the acetate derivative **1b**. The acetate substituent favored the enol forms to give  $\text{p}K_{\text{E}} = -0.06$  and  $\text{p}K_{\text{E}'} = 6.3$  for the neutral and anionic forms, respectively.

**Photochemistry.** Solutions of **1a** (10  $\mu\text{M}$ ) in aqueous phosphate buffers (0.1 M, pH = 7.0–7.4) were irradiated with green light isolated from a high-pressure mercury arc ( $\lambda = 546$  nm). The course of the reaction was followed by UV–vis spectroscopy (Figure 2 and Supplementary Figure S45). The absorption maximum of **1a** at  $\lambda \sim 528$  nm was replaced by a new maximum at  $\lambda \sim 500$  nm during irradiation indicating the formation of a new product. Similar changes in the absorption spectra were observed when either **1b** or **1c** were irradiated in phosphate buffer solutions (Supplementary Figures S48 and S49, respectively). The <sup>1</sup>H NMR and <sup>31</sup>P NMR spectral changes upon irradiation of **1a** are presented in Supplementary Figures S46 and S47. The primary photoproduct(s) are not stable and the absorption spectra change upon standing in the dark for hours.

The leaving group (*O,O*-diethyl phosphate) was released in high chemical yield upon irradiation of **1a** (>90%, as detected by both <sup>1</sup>H and <sup>13</sup>C NMR; Supplementary Figures S46, S51, and S52). In addition, two photoproducts, 3,6-dihydroxy-9*H*-xanthen-9-one (**3**) and 6-hydroxy-3-oxo-3*H*-xanthen-9-carboxylic acid (**13**), were identified (Scheme 3). Their chemical yields varied with the solvent used. Following irradiation of

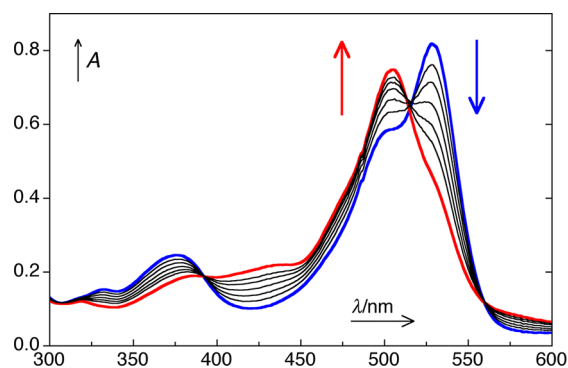
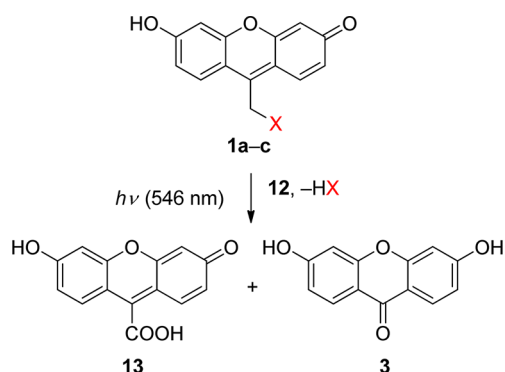


**Figure 2.** Irradiation of **1a** (first spectrum,  $\lambda_{\max} = 528$  nm, blue) at  $\lambda = 546$  nm in phosphate buffer (0.1 M, pH = 7.0) as monitored by absorption spectroscopy. The last spectrum ( $\lambda_{\max} = 505$  nm, red) was taken after 15 min of irradiation.

### Scheme 3. Photochemistry of **1a–c**



water/methanol (1:1, v/v) solutions, the xanthone **3** was isolated in 70% yield, whereas **13** was not detected. In aqueous phosphate buffer solutions of **1a** (10  $\mu$ M), **13** formed as the major photoproduct. In a more concentrated solution (10 mM), 40% of the starting material precipitated during irradiation. The product **13** was then obtained in 50% yield (calculated on the basis of the starting material consumed) by precipitation upon acidification of the remaining filtered solution using aq  $\text{CF}_3\text{COOH}$ , whereas only a small amount of **3** (<5%) was detected in the reaction mixture.

The same photoproducts were formed by irradiation of degassed solutions of **1a**. The hydrolysis product of DDQ, compound **12**, that is formed by dissolving the solid complexes **1a–c**-DDQ in water presumably serves to oxidize the expected primary product 6-hydroxy-9-hydroxymethyl-3H-xanthen-3-one to **13** either photochemically or in the dark. Careful removal of air oxygen did not affect the course of the reaction and no other oxidation agents were present.

The absorption maxima of the pure (isolated) acid **13** in a phosphate buffer and in methanol are  $\lambda_{\max} = 489$  and 492 nm, respectively; its structural characterization is provided in the Supporting Information. Formation of **13** by condensation of resorcinol and chloral hydrate in sulfuric acid has been claimed in the literature;<sup>31</sup> we have reproduced that procedure, but the red product so obtained was found to be a complex mixture. The absorption spectra of the irradiated buffer solutions of **1b** and **1c** clearly show that the acid **13** was also formed as the major photoproduct (Supplementary Figures S48 and S49).

The quantum yields of photorelease from the compounds **1a–c** are listed in Table 1. Degassing did not affect the observed UV changes nor the quantum yields.

**Table 1. Quantum Yields of Disappearance ( $\Phi_{\text{disapp}}$ ) for **1a–c** in Aqueous Solutions**

compound	$\Phi_{\text{disapp}}^a$ (%)
<b>1a</b>	$1.7 \pm 0.3$
<b>1b</b>	$0.27 \pm 0.08$
<b>1c</b>	$2.4 \pm 0.2$

<sup>a</sup>Quantum yields of disappearance were obtained spectrophotometrically (Figure 2) by irradiation of the compounds in aq phosphate buffer solutions (pH = 7.0,  $I = 0.1$  M) with light pulses from a NOPA at  $\lambda = 538 \pm 7$  nm. *meso*-Diphenylhelianthrene was used as an actinometer.<sup>32</sup> Each value represents an average of at least five measurements; standard deviations of the means are given.

**Fluorescence.** The fluorescence spectra of **11** in aqueous solution are similar to those of fluorescein.<sup>33</sup> A series of fluorescence spectra was measured by adding 0.1 M aqueous HCl to a solution of **11** in 0.1 M phosphate buffer, pH 7. Global analysis of the spectra recorded in the range pH 2–7 indicated two spectral components, which are attributed to the emission spectra of the anion **11<sup>-</sup>** and of the neutral compound (Figure 3). Remarkably, the emission band of the neutral ( $\lambda_{\max}$

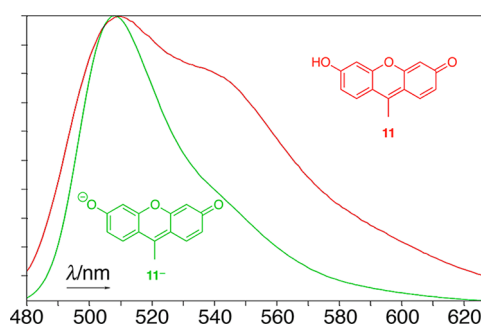


**Figure 3.** Fluorescence emission spectra (uncorrected, normalized) of **11** and its anion **11<sup>-</sup>** in aqueous solution.

= 510 nm, strong shoulder at 540 nm) extends to longer wavelength than that of the anion ( $\lambda_{\max} = 507$  nm, weak shoulder at 540 nm).

Fitting of a titration function to these data gave an apparent acidity constant  $\text{p}K_{a,2}^* = 5.4 \pm 0.1$  for the ionization of  $S_1(\mathbf{11})$ . However, the equilibrium  $\mathbf{11}^* \rightarrow \mathbf{11}^{-*} + \text{H}^+$  is presumably not fully established during the excited state lifetime. The fluorescence decay of  $\mathbf{11}^*/\mathbf{11}^{-*}$  obeyed a single exponential rate law with a lifetime of  $\tau = 3.5 \pm 0.2$  ns at all wavelengths and pH values from 3–11.

The fluorescence decay of the bromide **1c** was measured with freshly prepared solutions in 0.1 M aqueous phosphate buffer, pH 7. With an ordinary (nonflow) cuvette the observed fluorescence emission ( $\lambda_{\max} = 530$  nm and a shoulder at 570 nm) obeyed a single exponential rate law ( $\tau = 3.6 \pm 0.1$  ns). The signal increased in intensity with continued irradiation, but its lifetime and spectrum remained the same. We therefore suspected that the observed signal must largely be due to the photoproduct. We then used a flow cell to reduce dual irradiation of the sample. Now the decay obeyed a biexponential rate law with lifetimes  $\tau_1 = 0.38 \pm 0.03$  ns (amplitude 23%) and  $\tau_2 = 3.6 \pm 0.1$  ns (77%) (Figure 4).



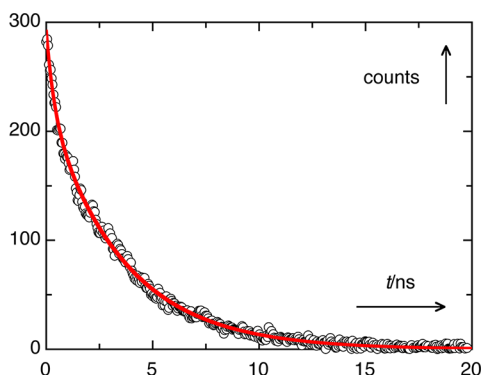


Figure 4. Fluorescence decay of **1c** in aq phosphate, pH 7.

Assuming that the weak component decaying faster can be attributed to the bromide **1c** and the slower decay to its photoproduct, this indicates that the release of bromide from **1c** occurs with a lifetime of 0.4 ns.

## CONCLUSION

The (6-hydroxy-3-oxo-3*H*-xanthen-9-yl)methyl complexes **1a–c**–DDQ have been synthesized in 7 steps with an overall chemical yield of 20–25%. In aqueous solutions, nonassociated **1a–c** were shown to release diethyl phosphate, acetate, and bromide, respectively, upon irradiation at over 500 nm. Compounds **1a–c** are among the rare examples of visible-light-triggered caged systems. The 9-methylxanthenone chromophore thus holds promise as a photoremovable protecting group for use with the second harmonic of Nd:YAG lasers.

## EXPERIMENTAL SECTION

**Materials and Methods.** The reagents and solvents of the highest purity available were used as purchased or were purified/dried when necessary. Acetone, acetonitrile, dichloromethane, and tetrahydrofuran were dried by standard procedures and kept over high-temperature-dried 3 Å molecular sieve (8–12 mesh) under dry N<sub>2</sub>; they were freshly distilled for each experiment. Synthetic steps were performed under ambient atmosphere unless stated otherwise. All glassware was flame-dried prior to use when water- and/or air-sensitive reagents were used. Oxygen was removed from solutions by three freeze–pump–thaw cycles or bubbling with inert gas (N<sub>2</sub> or Ar) for at least 15 min. All column chromatography purification procedures were performed with silica.

NMR spectra were recorded on 300, 400, 500, or 600 MHz spectrometers in acetonitrile-*d*<sub>3</sub>, chloroform-*d*, dichloromethane-*d*<sub>2</sub>, dimethylsulfoxide-*d*<sub>6</sub>, methanol-*d*<sub>4</sub>, trifluoroacetic acid-*d*, water-*d*<sub>2</sub>, or their mixtures. The signals in <sup>1</sup>H and <sup>13</sup>C NMR were referenced to the residual peak of a (major) solvent except for H<sub>2</sub>O, and those of the <sup>31</sup>P NMR were unreferenced. The deuterated solvents (except for CF<sub>3</sub>COOD and D<sub>2</sub>O) were kept over high-temperature-dried 3 Å molecular sieve (8–12 mesh) under dry N<sub>2</sub>. Mass spectra were recorded on a GC-coupled (30 m DB-XLB column) spectrometer in a positive mode with EI or FAB. MALDI-MS analyses were performed using an automatic spectrometer with *p*-nitroaniline as a matrix. UV spectra were obtained with matched 1.0 cm quartz cells. IR spectra were obtained on an FT spectrometer. Fluorescence emission spectra (uncorrected) were recorded on a Spex Fluorolog spectrophotometer 111C equipped with a 150-W xenon arc for excitation and an R928 photomultiplier. Excitation spectra were corrected with a built-in Rhodamine-6G quantum counter. Fluorescence lifetime measurements were done by excitation with subpicosecond pulses at 515 nm from a Clark-MXR Ti:Sa laser CPA 2001 coupled to a non-colinear optical parametric amplifier (NOPA). The fluorescence spectra and decays were measured with a Hamamatsu C5680 streak camera operated with 20-ps time windows. Exact masses were performed using a triple

quadrupole electrospray ionization mass spectrometer in positive or negative modes. Melting points were obtained in open-end-capillary tubes using a noncalibrated digital melting point apparatus or a non-calibrated Kofler's hot stage melting point apparatus. Elemental analyses were performed on an automatic analyzer. Lyophilization was performed at 5 Pa and –110 °C. The solution pH values were determined using a glass electrode calibrated with certified buffer solutions at pH = 4, 7, or 10. A 40-W medium pressure mercury arc equipped with the corresponding band-pass or cutoff filters was used for irradiation.

**Quantum Yield Measurements.** The quantum yield measurements were performed using a Ti:Sa laser coupled to a non-colinear optical parametric amplifier (NOPA) producing light at  $\lambda = 538 \pm 7$  nm (bandwidth at half height). The number of photons entering the sample cell was  $\sim 4.8 \times 10^{-9}$  einstein s<sup>-1</sup> (the quantum flux was determined precisely before and after each measurement, and the average of the two measurements was used for the quantum yield calculation). The absorbance  $A(\lambda_{\max})$  of all sample solutions was kept below 2.0. The course of the photoreactions was followed spectrophotometrically (UV–vis absorption). *meso*-Diphenylhelianthrene (*mDPH*) was used as an actinometer. *mDPH* is known to undergo a uniform and well-described<sup>32</sup> self-sensitized photooxidation reaction in a solution of air-saturated toluene to form the corresponding endoperoxide. All measurements were done at ambient temperature. Each sample was measured at least five times and quantum yields were obtained with less than 15% standard deviation.

**3,6-Dihydroxy-9*H*-xanthen-9-one (3).** A stirred suspension of 2,2',4,4'-tetrahydroxybenzophenone (**2**, 4.00 g, 16.3 mmol) in distilled water (24 mL) was heated in an autoclave at 200 °C for 6 h. The mixture was cooled to 20 °C, and 3,6-dihydroxy-9*H*-xanthen-9-one was obtained as a cluster of needles. It was filtered off, washed with hot distilled water (3 × 10 mL), and dried under reduced pressure to give a pure title product. Yield: 3.55 g (96%). Light orange needles. Mp: 330 °C (decomp) (lit. 320 °C;<sup>34</sup> 347 °C<sup>35</sup>). <sup>1</sup>H NMR (400 MHz, DMSO-*d*<sub>6</sub>):  $\delta$  (ppm) 6.82 (d, 2H,  $J = 2.0$  Hz), 6.86 (dd, 2H,  $J_1 = 8.7$  Hz,  $J_2 = 2.1$  Hz), 7.98 (d, 2H,  $J = 8.7$  Hz), 10.82 (s, 2H, –OH). <sup>13</sup>C NMR (100.5 MHz, DMSO-*d*<sub>6</sub>):  $\delta$  (ppm) 102.0, 113.5, 113.9, 127.6, 157.3, 163.2, 173.8. MS (ESI<sup>+</sup>; CH<sub>3</sub>OH + 2% NH<sub>3</sub>,  $\gamma \sim 0.1$  mg cm<sup>-3</sup>):  $m/z = 227.2$  (M – H<sup>+</sup>, 100), 228.25 (M<sup>+</sup>, 12.8). FTIR (cm<sup>-1</sup>): 3382, 3095, 1629, 1611, 1575, 1454, 1393, 1352, 1324, 1291, 1273, 1254, 1245, 1243, 1169, 1115, 1104, 986, 847, 831, 790, 693, 665, 635. UV–vis (C<sub>2</sub>H<sub>5</sub>OH,  $c 1.46 \times 10^{-6}$  mol dm<sup>-3</sup>):  $\lambda_{\max}/\text{nm}$  ( $\epsilon/\text{M}^{-1} \text{cm}^{-1}$ ) = 209 (29000), 239 (42500), 267 (11400), 280 (8050), 312 (24400), 321 (23600). Anal. Calcd for C<sub>13</sub>H<sub>8</sub>O<sub>4</sub>: C, 68.42; H, 3.53; O, 28.04. Found: C, 67.81; H, 3.70; O, 28.49. This compound has also been characterized elsewhere.<sup>13,36,37</sup>

**3,6-Dimethoxy-9*H*-xanthen-9-one (4).** A mixture of anhydrous potassium carbonate (3.30 g, 23.9 mmol) in acetone (75 mL) was added to a stirred suspension of 3,6-dihydroxy-9*H*-xanthen-9-one (**3**, 840 mg, 3.68 mmol). Dimethyl sulfate (6.3 mL, 66.4 mmol) was then added dropwise in 20 min. The resulting solution was stirred for 30 min at 20 °C and then refluxed for 20 h. After cooling to 0 °C, aqueous ammonia ( $c 0.5$  mol L<sup>-1</sup>, 15 mL) was added dropwise, and the reaction mixture was stirred for an additional 1 h at 20 °C. A white precipitate, obtained by addition of water (100 mL) to the mixture, was filtered off, washed with distilled water (3 × 10 mL), and dried under reduced pressure to give pure **4**. Yield: 914 mg (97%). White solid. Mp: 184.5–186.0 °C (lit. 187–188 °C).<sup>38,39</sup> <sup>1</sup>H NMR (500 MHz, CD<sub>2</sub>Cl<sub>2</sub>):  $\delta$  (ppm) 3.90 (s, 6H), 6.84 (dd, 2H,  $J_1 = 2.4$  Hz,  $J_2 = 1.0$  Hz), 6.90 (ddd, 2H,  $J_1 = 8.8$  Hz,  $J_2 = 2.4$  Hz,  $J_3 = 0.7$  Hz), 8.13 (d, 2H,  $J = 8.8$  Hz). <sup>13</sup>C NMR (126 MHz, CD<sub>2</sub>Cl<sub>2</sub>):  $\delta$  (ppm) 56.2, 100.5, 113.1, 116.1,

128.1, 158.3, 165.0, 175.3. MS (ESI<sup>+</sup>; CH<sub>3</sub>OH/H<sub>2</sub>O, 1:1 (v/v) + NH<sub>4</sub>OAc (5 mM),  $\gamma \sim 0.1 \text{ mg cm}^{-3}$ ):  $m/z = 257.1$  (M + H<sup>+</sup>, 100), 258.1 (M + 2 H<sup>+</sup>, 16.2). MS (EI; 70 eV, 150 °C):  $m/z = 256.1$  (M). FTIR (cm<sup>-1</sup>): 1612, 1501, 1428, 1357, 1302, 1257, 1211, 1157, 1099, 1018, 979, 925, 825, 763, 663. UV-vis (C<sub>2</sub>H<sub>5</sub>OH,  $c 1.27 \times 10^{-5} \text{ mol dm}^{-3}$ ):  $\lambda_{\text{max}}/\text{nm}$  ( $\epsilon/\text{M}^{-1} \text{ cm}^{-1}$ ) = 209 (26700), 240 (43000), 266 (11000), 307 (22700). Anal. Calcd for C<sub>15</sub>H<sub>12</sub>O<sub>4</sub>: C, 70.31; H, 4.72; O, 24.97. Found: C, 70.18; H, 4.75; O, 25.07. This compound has also been characterized elsewhere.<sup>38,39</sup>

**3,6-Dimethoxy-9-methylene-9H-xanthene (5).** Trimethylaluminium (1.1 mL, 2.2 mmol, 2 M solution in toluene) was added dropwise to a stirred suspension of 3,6-dimethoxy-9H-xanthen-9-one (**4**, 500 mg, 1.95 mmol) in a mixture of dry benzene (15 mL) and dry toluene (10 mL) under argon atmosphere at 25 °C to give a yellow mixture. It became homogeneous after warming to 50 °C. After cooling to 25 °C, trimethylaluminium (2.2 mL, 4.4 mmol, 2 M solution in toluene) was slowly added (caution: methane as a side product is released). The reaction mixture was then heated to 65 °C for 90 min, cooled to 0 °C, and ice (20 g) and aq HCl (0.1 M, 3 mL) were cautiously added (methane is released). The mixture was extracted with CH<sub>2</sub>Cl<sub>2</sub> (3 × 15 mL), the combined organic layers were dried with Na<sub>2</sub>SO<sub>4</sub>, and the solvent was removed under reduced pressure to give the title product. Yield: 485 mg (98%). Yellow solid. Mp: 144.5–145.8 °C (lit. 146–147 °C<sup>40</sup>). <sup>1</sup>H NMR (400 MHz, CD<sub>2</sub>Cl<sub>2</sub>):  $\delta$  (ppm) 3.83 (s, 6H), 5.29 (s, 2H), 6.62 (d, 2H,  $J = 2.6 \text{ Hz}$ ), 6.72 (dd, 2H,  $J_1 = 8.8 \text{ Hz}$ ,  $J_2 = 2.6 \text{ Hz}$ ), 7.66 (d, 2H,  $J = 8.8 \text{ Hz}$ ). <sup>1</sup>H NMR (400 MHz, DMSO-*d*<sub>6</sub>):  $\delta$  (ppm) 3.80 (s, 6H), 5.39 (s, 2H), 6.72 (d, 2H,  $J = 2.6 \text{ Hz}$ ), 6.78 (dd, 2H,  $J_1 = 8.8 \text{ Hz}$ ,  $J_2 = 2.6 \text{ Hz}$ ), 7.78 (d, 2H,  $J = 8.9 \text{ Hz}$ ). <sup>13</sup>C NMR (100.5 MHz, DMSO-*d*<sub>6</sub>):  $\delta$  (ppm) 55.4, 97.2, 100.8, 111.3, 113.3, 125.2, 130.5, 150.7, 160.4. MS (EI; 70 eV, 150 °C):  $m/z = 254.1$  (M). FTIR (cm<sup>-1</sup>): 1625, 1619, 1599, 1567, 1467, 1462, 1440, 1425, 1386, 1330, 1265, 1247, 1207, 1171, 1160, 1109, 1098, 1078, 1028, 983, 946, 925, 838, 818, 783, 636. UV-vis (C<sub>2</sub>H<sub>5</sub>OH,  $c 8.71 \times 10^{-6} \text{ mol dm}^{-3}$ ):  $\lambda_{\text{max}}/\text{nm}$  ( $\epsilon/\text{M}^{-1} \text{ cm}^{-1}$ ) = 220 (27700), 231 (32600), 273 (3200). Anal. Calcd for C<sub>16</sub>H<sub>14</sub>O<sub>3</sub>: C, 75.57; H, 5.55; O, 18.88. Found: C, 75.55; H, 5.59; O, 18.86. This compound has also been characterized elsewhere.<sup>40,41</sup> Note: **5**, both in the solid state or dissolved in polar solvents, is oxidized rapidly to a mixture of green products; therefore it should be stored in dark under N<sub>2</sub> atmosphere. If necessary, it can be easily purified by recrystallization from *n*-hexane.

**(3,6-Dimethoxy-9H-xanthen-9-yl)methanol (6).** BH<sub>3</sub>·THF (1.0 M in THF, 3.5 mL, 3.5 mmol) was added to a stirred solution of **5** (200 mg, 0.79 mmol) in dry THF (25 mL) over a period of 20 min at 0 °C. The reaction mixture was stirred for 4 h at 20 °C and cooled to 0 °C, and then water (2 mL, 10% solution in THF), aq NaOH (3.0 M, 2.5 mL, 7.50 mmol), and aq hydrogen peroxide (30%, 2.7 mL, 26.4 mmol) were cautiously added. The resulting mixture was stirred for 1.5 h at 20 °C, then poured into water (50 mL), and neutralized with aq HCl (1 M, ~8 mL) to pH = 7, and the organic material was extracted with diethyl ether (3 × 20 mL). The combined organic layers were washed with brine (50 mL), dried with Na<sub>2</sub>SO<sub>4</sub>, and filtered, and the solvent was removed under reduced pressure to give the title product. No further purification was necessary. Yield: 193 mg (90%). Pale yellow solid. Mp: 83.9–85.0 °C. <sup>1</sup>H NMR (600 MHz, DMSO-*d*<sub>6</sub>):  $\delta$  (ppm) 3.43 (t, 2H,  $J = 5.7 \text{ Hz}$ ), 3.75 (s, 6H), 3.86 (t, 1H,  $J = 6.1 \text{ Hz}$ ), 4.81 (t, 1H,  $J = 5.3 \text{ Hz}$ , -OH), 6.63 (d, 2H,  $J = 2.5$

Hz), 6.68 (dd, 2H,  $J_1 = 8.4 \text{ Hz}$ ,  $J_2 = 2.6 \text{ Hz}$ ), 7.23 (d, 2H,  $J = 8.5 \text{ Hz}$ ) (Supplementary Figure S1). <sup>13</sup>C NMR (126 MHz, DMSO-*d*<sub>6</sub>):  $\delta$  (ppm) 39.7, 55.2, 68.2, 100.8, 109.4, 114.9, 130.2, 152.0, 158.8 (Supplementary Figure S2). MS: (ESI<sup>+</sup>; CH<sub>3</sub>OH/H<sub>2</sub>O, 1:1 (v/v) + 5 mM NH<sub>4</sub>OAc,  $\gamma \sim 0.1 \text{ mg cm}^{-3}$ ):  $m/z = 255.1$  (M - OH<sup>-</sup>, 32.4), 272.1 (M, 3.1), 273.0 (M + H<sup>+</sup>, 100), 289.7 (M + NH<sub>4</sub><sup>+</sup>, 3.9), 561.5 (M<sub>2</sub> + NH<sub>4</sub><sup>+</sup>, 33.4). FTIR (cm<sup>-1</sup>): 3299, 3053, 2941, 2921, 2875, 2831, 1633, 1614, 1574, 1500, 1462, 1435, 1425, 1325, 1276, 1259, 1205, 1184, 1161, 1149, 1097, 1053, 1034, 1022, 983, 976, 925, 824, 815, 638, 617. UV-vis (C<sub>2</sub>H<sub>5</sub>OH,  $c 1.19 \times 10^{-5} \text{ mol dm}^{-3}$ ):  $\lambda_{\text{max}}/\text{nm}$  ( $\epsilon/\text{M}^{-1} \text{ cm}^{-1}$ ) = 212 (46400), 278 (300). Anal. Calcd for C<sub>16</sub>H<sub>16</sub>O<sub>4</sub>: C, 70.58; H, 5.92; O, 23.50. Found: C, 70.63; H, 6.06; O, 23.31.

**Diethyl-(6-hydroxy-3-oxo-3H-xanthen-9-yl) Methyl Phosphate-DDQ Complex (1a-DDQ).** (3,6-Dimethoxy-9H-xanthen-9-yl)methyl Diethyl Phosphate (**7a**). Diethyl chlorophosphate (0.11 mL, 0.75 mmol) in dry dichloromethane (20 mL) was added to a solution containing **6** (170 mg, 0.625 mmol) and 4-dimethylaminopyridine (91 mg, 0.75 mmol). The resulting solution was stirred at 20 °C under argon atmosphere for 24 h, and water (20 mL) was added. The reaction mixture was extracted with ethyl acetate (3 × 20 mL); the combined organic layers were washed with brine (50 mL), dried over anhydrous Na<sub>2</sub>SO<sub>4</sub>, and filtered; and the solvent was removed under reduced pressure. The remaining yellow oil was purified by column chromatography (*n*-hexane/ethyl acetate, 60:40, v/v) to give the pure title product. Yield: 199 mg (78%). Slightly yellow oil. <sup>1</sup>H NMR (400 MHz, DMSO-*d*<sub>6</sub>):  $\delta$  (ppm) 1.07 (dt, 6H,  $J_1 = 7.1 \text{ Hz}$ ,  $J_2 = 0.8 \text{ Hz}$ ), 3.72 (m, 4H), 3.76 (s, 6H), 4.02 (t, 2H,  $J = 4.9 \text{ Hz}$ ), 4.24 (dt, 1H,  $J_1 = 4.5 \text{ Hz}$ ,  $J_2 = 1.5 \text{ Hz}$ ), 6.67 (d, 2H,  $J = 2.5 \text{ Hz}$ ), 6.73 (dd, 2H,  $J_1 = 8.5 \text{ Hz}$ ,  $J_2 = 2.6 \text{ Hz}$ ), 7.30 (d, 2H,  $J = 8.6 \text{ Hz}$ ). <sup>1</sup>H NMR (600 MHz, CD<sub>2</sub>Cl<sub>2</sub>):  $\delta$  (ppm) 1.19 (dt, 6H,  $J_1 = 7.1 \text{ Hz}$ ,  $J_2 = 0.9 \text{ Hz}$ ), 3.80 (s, 6H), 3.87 (m, 4H), 4.01 (t, 2H,  $J = 5.9 \text{ Hz}$ ), 4.18 (t, 1H,  $J = 5.9 \text{ Hz}$ ), 6.64 (d, 2H,  $J = 2.5 \text{ Hz}$ ), 6.68 (dd, 2H,  $J_1 = 8.4 \text{ Hz}$ ,  $J_2 = 2.6 \text{ Hz}$ ), 7.21 (d, 2H,  $J = 8.4 \text{ Hz}$ ) (Supplementary Figure S3). <sup>13</sup>C NMR (126 MHz, CD<sub>2</sub>Cl<sub>2</sub>):  $\delta$  (ppm) 16.2, 38.7, 55.8, 64.0, 72.6, 101.7, 110.3, 113.6, 130.5, 153.5, 160.5 (Supplementary Figure S4). <sup>31</sup>P NMR (162 MHz):  $\delta$  (ppm) -1.47. MS (FAB):  $m/z = 406.1$  (M<sup>2-</sup>, 0.74), 407.1 (M<sup>-</sup>, 4.66), 408.1 (M, 1.34), 409.1 (M + H<sup>+</sup>, 3.85), 410.1 (M + 2H<sup>+</sup>, 1.0). MALDI-MS (positive mode):  $m/z = 406.978$ , 407.977, 408.979. FTIR (cm<sup>-1</sup>): 2980, 2940, 2906, 2836, 2360, 2332, 1733, 1634, 1614, 1599, 1574, 1500, 1464, 1437, 1427, 1394, 1369, 1326, 1258 (P=O), 1202, 1196, 1162 (P-O-C), 1121, 1101, 1014 (P-O-C), 971 (P-O-C), 891, 830, 800, 733. UV-vis (CHCl<sub>3</sub>):  $\lambda_{\text{max}}/\text{nm}$  (relative intensities) = 241 (100), 278 (62). Anal. Calcd for C<sub>20</sub>H<sub>25</sub>O<sub>7</sub>P: C, 58.82; H, 6.17. Found: C, 58.90; H, 6.25.

**(3,6-Dihydroxy-9H-xanthen-9-yl)methyl Diethyl Phosphate (8a).** Boron tribromide (1 M in dichloromethane, 9.56 mL, 9.56 mmol) was added dropwise to a solution of (3,6-dimethoxy-9H-xanthen-9-yl)methyl diethyl phosphate (**7a**, 300 mg, 0.735 mmol) in dry CH<sub>2</sub>Cl<sub>2</sub> (30 mL) under nitrogen atmosphere at -78 °C. The reaction mixture was stirred and left to warm to -10 °C in 24 h. Water (30 mL) was then added, and the mixture was extracted with ethyl acetate (3 × 20 mL). The combined organic layers were washed with brine (50 mL) and dried over MgSO<sub>4</sub>, and the solvent was removed under reduced pressure. The resulting solid was dried under reduced pressure to give the pure title product. Yield: 276 mg (99%). Beige powder. Mp: 135 °C (decomp). <sup>1</sup>H NMR (400 MHz, DMSO-*d*<sub>6</sub>):  $\delta$  (ppm) 1.09 (t, 6H,  $J = 7.1 \text{ Hz}$ ), 3.74 (m, 4H), 3.94 (t, 2H,  $J = 5.2 \text{ Hz}$ ), 4.12 (t, 1H,  $J = 4.3 \text{ Hz}$ ), 6.45 (d,

2H,  $J = 2.2$  Hz), 6.53 (dd, 2H,  $J_1 = 8.3$  Hz,  $J_2 = 2.2$  Hz), 7.15 (d, 2H,  $J = 8.4$  Hz), 9.56 (s, 2H, -OH) (Supplementary Figure S5).  $^{13}\text{C}$  NMR (126 MHz, DMSO- $d_6$ ):  $\delta$  (ppm) 15.70, 15.76, 37.1, 62.87, 62.93, 72.2, 102.3, 110.8, 111.3, 129.8, 152.3, 157.3 (Supplementary Figure S6).  $^{31}\text{P}$  NMR (162 MHz):  $\delta$  (ppm) -4.77. MS (ESI $^+$ ; CH<sub>3</sub>OH/H<sub>2</sub>O, 1:1 (v/v) + 5 mM NH<sub>4</sub>OAc,  $\gamma \sim 0.1$  mg cm $^{-3}$ ):  $m/z = 380.7$  (M $^+$ ), 381.7 (M + H $^+$ ). FTIR (cm $^{-1}$ ): 3296, 2960, 2925, 2873, 2853, 2357, 2332, 1736, 1612, 1589, 1502, 1487, 1458, 1365, 1309, 1285, 1262, 1227 (P=O), 1208, 1198, 1174, 1147, 1098, 1069, 1032 (P-O-C), 984 (P-O-C), 859, 851, 820, 801, 778, 668, 651. UV-vis (CH<sub>3</sub>OH,  $c$  1.20  $\times 10^{-5}$  mol dm $^{-3}$ ):  $\lambda_{\text{max}}/\text{nm}$  ( $\epsilon/\text{M}^{-1}$  cm $^{-1}$ ) = 211 (34700), 279 (4200). Anal. Calcd for C<sub>18</sub>H<sub>21</sub>O<sub>7</sub>P: C, 56.84; H, 5.57. Found: C, 56.90; H, 5.77.

**Diethyl (6-Hydroxy-3-oxo-3H-xanthen-9-yl)methyl Phosphate-DDQ Complex (1a-DDQ).** 2,3-Dichloro-5,6-dicyano-1,4-benzoquinone (DDQ, 23 mg, 0.1 mmol) was added to a solution of (3,6-dihydroxy-9H-xanthen-9-yl)methyl diethyl phosphate (8a, 31 mg, 0.08 mmol) in dry acetonitrile (2 mL) at 20 °C, and the mixture was stirred at this temperature for 20 min. The resulting red precipitate was filtered off, washed with acetonitrile (20 mL), and dried under reduced pressure to give the pure title complex. Yield: 25 mg (50%). Orange powder. Mp 170 °C (decomp).  $^1\text{H}$  NMR (600 MHz, DMSO- $d_6$ ):  $\delta$  (ppm) 1.04 (t, 3H,  $J = 7.0$  Hz), 1.17 (t, 3H,  $J = 7.0$  Hz), 3.74 (m, 2H), 3.94 (m, 2H), 5.89 (d, 1H,  $J = 7.1$  Hz), 6.47 (dd, 2H,  $J_1 = 3.8$  Hz,  $J_2 = 2.4$  Hz), 6.63 (dt, 2H,  $J_1 = 8.7$  Hz,  $J_2 = 2.2$  Hz), 7.53 (d, 1H,  $J = 8.6$  Hz), 7.57 (d, 1H,  $J = 8.6$  Hz), 9.66 (s, 2H, -OH) (Supplementary Figure S7). The peak at 5.89 (d, 1H,  $J = 7.1$  Hz) is split to a doublet by the  $^{31}\text{P}$  atom, which was proved by a phosphorus decoupled  $^1\text{H}[^{31}\text{P}]$  NMR.  $^1\text{H}$  NMR (300 MHz, phosphate buffer in D<sub>2</sub>O, pH = 7.4,  $I = 0.1$  M):  $\delta$  (ppm) 0.99 (t, 3H,  $J = 6.9$  Hz), 1.07 (t, 3H,  $J = 6.9$  Hz), 3.79–3.94 (m, 4H), 6.55 (s, 2H), 6.90 (d, 2H,  $J = 9.2$  Hz), 7.14 (d, 1H,  $J = 5.4$  Hz), 7.84–8.85 (2  $\times$  bs, 2H) (Supplementary Figure S10).  $^{13}\text{C}$  NMR (126 MHz, DMSO- $d_6$ ):  $\delta$  (ppm) 15.4, 15.5, 15.6, 15.7, 63.6, 68.1, 68.2, 101.3, 101.5, 103.1, 103.2, 110.3, 110.6, 111.9, 112.7, 114.2, 128.7, 129.4, 134.0, 151.6, 151.8, 158.1 (Supplementary Figure S8) (the weak C<sub>q</sub> signals from DDQ were not observed; the compound probably decomposes in DMSO).  $^{13}\text{C}$  NMR (500 MHz, phosphate buffer in D<sub>2</sub>O, pH = 7.4,  $I = 0.1$  M):  $\delta$  (ppm) 15.1, 15.2, 66.4, 96.9, 98.6, 114.9, 117.2, 132.3, 133.6, 139.5, 143.1, 158.7, 166.2 (Supplementary Figure S11).  $^{31}\text{P}$  NMR (162 MHz, DMSO- $d_6$ ):  $\delta$  (ppm) -2.92 (q,  $J = 6.4$  Hz) (Supplementary Figure S9). FTIR (cm $^{-1}$ ): 3151, 2712, 2586, 2367, 2336, 1722 (C=O), 1599, 1561, 1552, 1480, 1463, 1424, 1413, 1384, 1361, 1323, 1266, 1240 (P=O), 1152, 1125, 1090, 1039 (P-O-C), 992, 954 (P-O-C), 925, 863, 793, 641. UV-vis (aq phosphate buffer, pH = 7.0,  $I = 0.1$  M):  $\lambda_{\text{max}}/\text{nm}$  ( $\epsilon/\text{M}^{-1}$  cm $^{-1}$ ) = 214 (37300), 245 (46600), 332 (6500), 528 (39100) (Supplementary Figure S13). HRMS (TOF ES $^+$ ): calcd for C<sub>26</sub>H<sub>20</sub>Cl<sub>2</sub>N<sub>2</sub>O<sub>9</sub>P (M + H $^+$ ): 605.0283 (C<sub>26</sub>H<sub>19</sub><sup>35</sup>Cl<sup>35</sup>ClN<sub>2</sub>O<sub>9</sub>P + H $^+$ ), 607.0254 (C<sub>26</sub>H<sub>19</sub><sup>35</sup>Cl<sup>37</sup>ClN<sub>2</sub>O<sub>9</sub>P + H $^+$ ). Found: 605.0283, 607.0272 (Supplementary Figure S14). Anal. Calcd for C<sub>26</sub>H<sub>19</sub>Cl<sub>2</sub>N<sub>2</sub>O<sub>9</sub>P: C, 51.59; H, 3.16; N, 4.63. Found: C, 51.16; H, 3.48; N, 4.52.

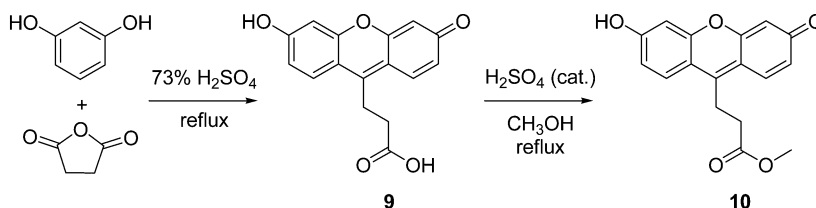
**(6-Hydroxy-3-oxo-3H-xanthen-9-yl)methyl Acetate-DDQ Complex (1b-DDQ).** (3,6-Dimethoxy-9H-xanthen-9-yl)methyl Acetate (7b). A mixture of (3,6-dimethoxy-9H-xanthen-9-yl)methanol (6, 0.336 g, 1.9 mmol), triethylamine (0.8 mL, 5.7 mmol), 4-dimethylaminopyridine (0.0179 g, 0.15 mmol), and acetic anhydride (0.7 mL, 7.4 mmol) was stirred at

20 °C for 14 h under an Ar atmosphere. The reaction mixture was shaken with diethyl ether (10 mL) and hydrochloric acid (2 M, 10 mL). The organic layer was washed twice with saturated aq NaHCO<sub>3</sub> (2  $\times$  20 mL), dried over Na<sub>2</sub>SO<sub>4</sub>, filtered, and the solvent was removed under reduced pressure to give a slightly brownish oil which was purified by thin-layer chromatography (CHCl<sub>3</sub>/ethyl acetate, 30:1, v/v) to obtain a pure title product. Yield: 0.38 g (98%). Slightly yellow oil.  $^1\text{H}$  NMR (400 MHz, DMSO- $d_6$ ):  $\delta$  (ppm) 1.90 (s, 3H), 3.76 (s, 6H), 4.06 (d, 2H,  $J = 5.9$  Hz), 4.20 (t, 1H,  $J = 5.8$  Hz), 6.67 (d, 2H,  $J = 2.5$  Hz), 6.71 (dd, 2H,  $J_1 = 8.4$  Hz,  $J_2 = 2.6$  Hz), 7.26 (d, 2H,  $J = 8.5$  Hz) (Supplementary Figure S15).  $^{13}\text{C}$  NMR (126 MHz, DMSO- $d_6$ ):  $\delta$  (ppm) 20.5, 36.1, 55.2, 68.9, 101.0, 109.9, 113.2, 129.9, 152.2, 159.2, 169.9 (Supplementary Figure S16). MALDI-MS: (negative mode):  $m/z = 313.358$ , 314.341. MS (FAB):  $m/z = 314.0$  (M, 3.08), 315.1 (M + H $^+$ , 9.56), 316.1 (M + 2H $^+$ , 2.24), 317.0 (M + 3H $^+$ , 0.67). FTIR (cm $^{-1}$ ): 3000, 2943, 2908, 2836, 2365, 1735 (C=O), 1693, 1650, 1631, 1612, 1599, 1573, 1499, 1462, 1436, 1425, 1377, 1358, 1327, 1286, 1250 (O-CH<sub>2</sub>), 1224, 1195, 1160, 1120, 1100, 1028, 974, 926, 830, 806, 736, 716, 659, 645. UV-vis (CHCl<sub>3</sub>):  $\lambda_{\text{max}}/\text{nm}$  (relative intensity) = 241 (100), 278 (67). Anal. Calcd for C<sub>18</sub>H<sub>18</sub>O<sub>5</sub>: C 68.78; H 5.77; O 25.45. Found: C 68.66; H 5.96; O 25.38.

**(3,6-Dihydroxy-9H-xanthen-9-yl)methyl Acetate (8b).** This compound was synthesized from (3,6-dimethoxy-9H-xanthen-9-yl)methyl acetate (7b) by the same procedure as that used for (3,6-dihydroxy-9H-xanthen-9-yl)methyl diethyl phosphate (8a). Yield: 97%. Beige powder. Mp 150 °C (decomp).  $^1\text{H}$  NMR (600 MHz, DMSO- $d_6$ ):  $\delta$  (ppm) 1.92 (s, 3H), 4.00 (d, 2H,  $J = 6.0$  Hz), 4.07 (t, 1H,  $J = 5.9$  Hz), 6.46 (d, 2H,  $J = 2.0$  Hz), 6.52 (dd, 2H,  $J_1 = 8.2$  Hz,  $J_2 = 2.1$  Hz), 7.11 (d, 2H,  $J = 8.3$  Hz), 9.56 (s, 2H, -OH) (Supplementary Figure S17).  $^{13}\text{C}$  NMR (126 MHz, DMSO- $d_6$ ):  $\delta$  (ppm) 20.4, 36.0, 68.9, 102.3, 110.7, 111.6, 129.7, 152.0, 157.1, 169.7 (Supplementary Figure S18). MS (ESI $^-$ ; CH<sub>3</sub>OH/H<sub>2</sub>O, 1:1 (v/v) + 5 mM NH<sub>4</sub>OAc,  $\gamma \sim 0.1$  mg cm $^{-3}$ ):  $m/z = 285.0$  (M - H $^+$ , 100), 286.0 (M $^-$ , 16). FTIR (cm $^{-1}$ ): 3353, 2359, 2341, 1739 (C=O), 1725, 1700, 1608, 1558, 1506, 1456, 1446, 1374, 1358, 1280, 1272, 1256, 1239, 1226, 1217, 1209, 1166, 1148, 1109, 1036, 989, 955, 840, 668, 660. UV-vis (C<sub>2</sub>H<sub>5</sub>OH,  $c$  1.16  $\times 10^{-5}$  mol dm $^{-3}$ ):  $\lambda_{\text{max}}/\text{nm}$  ( $\epsilon/\text{M}^{-1}$  cm $^{-1}$ ) = 211 (48400), 278 (4700). Anal. Calcd for C<sub>16</sub>H<sub>14</sub>O<sub>5</sub>: C 67.13; H 4.93. Found: C 67.01; H 5.13.

**(6-Hydroxy-3-oxo-3H-xanthen-9-yl)methyl Acetate-DDQ Complex (1b-DDQ).** This compound was synthesized from (3,6-dihydroxy-9H-xanthen-9-yl)methyl acetate (8b) by the same procedure as that used for diethyl (6-hydroxy-3-oxo-3H-xanthen-9-yl)methyl phosphate-DDQ complex (1a-DDQ). Yield: 44%. Dark brown powder. Mp 190 °C (decomp).  $^1\text{H}$  NMR (600 MHz, DMSO- $d_6$ ):  $\delta$  (ppm) 1.94 (s, 3H), 6.24 (s, 1H), 6.47 (dd, 2H,  $J_1 = 4.8$  Hz,  $J_2 = 2.3$  Hz), 6.63 (m, 2H), 7.57 (m, 2H), 9.67 (s, 2H, -OH) (Supplementary Figure S19).  $^{13}\text{C}$  NMR (126 MHz, DMSO- $d_6$ ):  $\delta$  (ppm) 20.2, 67.6, 98.7, 101.2, 109.8, 110.5, 112.9, 114.1, 128.6, 129.3, 151.4, 151.7, 157.9, 158.1, 169.4. FTIR (cm $^{-1}$ ): 2513, 2360, 2331, 2229, 2221 (C $\equiv$ N), 1755 (C=O), 1643, 1593, 1556, 1446, 1402, 1272, 1253, 1199, 1176, 1114, 1068, 1041, 991, 946, 927, 839, 818, 650, 613, 590 (Supplementary Figure S21). UV-vis (aq phosphate buffer, pH = 7.0,  $I = 0.1$  M):  $\lambda_{\text{max}}/\text{nm}$  ( $\epsilon/\text{M}^{-1}$  cm $^{-1}$ ) = 244 (53200), 328 (7300), 375 (11200), 495 (35700), 524 (40900) (Supplementary Figure S20). HRMS (TOF MS ESI $^-$ ): calcd for C<sub>24</sub>H<sub>11</sub>Cl<sub>2</sub>N<sub>2</sub>O<sub>7</sub> (M - H $^+$ ) 508.9943



Scheme 4. Synthesis of Succinylfluorescein **9** and Its Methyl Ester **10**

( $C_{24}H_{12}^{35}Cl^{35}ClN_2O_7 - H^+$ ), 510.9914 ( $C_{24}H_{12}^{35}Cl^{37}ClN_2O_7 - H^+$ ), found 508.9943, 510.9951 (Supplementary Figure S22).

**9-(Bromomethyl)-6-hydroxy-3H-xanthen-3-one-DDQ Complex (1c-DDQ).** 9-(Bromomethyl)-3,6-dimethoxy-9H-xanthene (**7c**). Triphenylphosphine (0.59 g, 2.25 mmol) and carbon tetrabromide (1.63 g, 4.92 mmol) were added to a solution of **6** (0.51 g, 1.86 mmol) in dichloromethane (12 mL). The reaction mixture was stirred under Ar atmosphere at 20 °C for 10 h, and subsequently washed with aq NaHCO<sub>3</sub> (2 × 20 mL, satd) and brine (2 × 20 mL). The organic layer was dried over Na<sub>2</sub>SO<sub>4</sub> and filtered, and the solvent was removed under reduced pressure. The residue was purified by column chromatography (CHCl<sub>3</sub>/MeOH, 20:1, v/v). Yield: 0.61 g (97%). Yellow greenish solid. Mp 134.3–135.3 °C. <sup>1</sup>H NMR (400 MHz, DMSO-*d*<sub>6</sub>): δ (ppm) 3.75 (s, 6H), 3.78 (d, 2H, *J* = 4.1 Hz), 4.49 (t, 1H, *J* = 4.0 Hz), 6.63 (d, 1H, *J* = 2.6 Hz), 6.70 (dd, 2H, *J*<sub>1</sub> = 8.5 Hz, *J*<sub>2</sub> = 2.6 Hz), 7.31 (d, 2H, *J* = 8.6 Hz) (Supplementary Figure S23). <sup>13</sup>C NMR (126 MHz, DMSO-*d*<sub>6</sub>): δ (ppm) 37.4, 44.3, 55.2, 100.7, 109.9, 113.7, 129.7, 152.1, 159.2 (Supplementary Figure S24). MS (FAB): *m/z* = 334.0 ( $C_{16}H_{15}^{79}BrO_3$ , 22), 334.9 ( $C_{16}H_{15}^{79}BrO_3 + H^+$ , 100), 335.9 ( $C_{16}H_{15}^{81}BrO_3$ , 31), 336.9 ( $C_{16}H_{15}^{81}BrO_3 + H^+$ , 68). FTIR (cm<sup>-1</sup>): 2359, 2336, 1656, 1631, 1604, 1566, 1551, 1502, 1469, 1462, 1437, 1422, 1327, 1291, 1257, 1201, 1185, 1168, 1149, 1097, 1029, 980, 845, 830, 821, 806, 800, 788, 668 (C–Br), 626, 618. UV–vis (CHCl<sub>3</sub>): λ<sub>max</sub>/nm (relative intensity) = 241 (100), 278 (59). Anal. Calcd for C<sub>16</sub>H<sub>15</sub>BrO<sub>3</sub>: C, 57.33; H, 4.51. Found: C, 57.37; H, 4.75.

**9-(Bromomethyl)-9H-xanthene-3,6-diol (8c).** This compound was synthesized from **7c** according to the same procedure as that used for (3,6-dihydroxy-9H-xanthen-9-yl)methyl diethyl phosphate (**8a**). Yield: 99%. Ochre powder. Mp 120 °C (decomp). <sup>1</sup>H NMR (400 MHz, DMSO-*d*<sub>6</sub>): δ (ppm) 3.70 (d, 2H, *J* = 4.3 Hz), 4.34 (t, 1H, *J* = 4.2 Hz), 6.42 (d, 1H, *J* = 2.4 Hz), 6.51 (dd, 2H, *J*<sub>1</sub> = 8.3 Hz, *J*<sub>2</sub> = 2.4 Hz), 7.16 (d, 2H, *J* = 8.4 Hz), 9.57 (s, 2H, –OH) (Supplementary Figure S25). <sup>13</sup>C NMR (126 MHz, DMSO-*d*<sub>6</sub>): δ (ppm) 37.6, 44.3, 102.2, 110.9, 112.3, 129.6, 152.1, 157.3 (Supplementary Figure S26). MALDI-MS (positive mode): *m/z* = 305.073, 307.084. MS (ESI<sup>-</sup>; CH<sub>3</sub>OH/H<sub>2</sub>O, 1:1 (v/v) + 5 mM NH<sub>4</sub>OAc, γ ~ 0.1 mg cm<sup>-3</sup>): *m/z* = 305.0 ( $C_{14}H_{11}^{79}BrO_3 - H^+$ , 30), 306.0 ( $C_{14}H_{11}^{79}BrO_3^-$ , 6.0), 307.0 ( $C_{14}H_{11}^{81}BrO_3 - H^+$ , 32.6), 308.0 ( $C_{14}H_{11}^{81}BrO_3^-$ , 5.5). FTIR (cm<sup>-1</sup>): 3348, 3217, 2360, 2341, 1612, 1589, 1504, 1450, 1296, 1265 (CH<sub>2</sub>), 1172, 1095, 987, 933, 840, 756, 648 (C–Br). UV–vis (C<sub>2</sub>H<sub>5</sub>OH, *c* 1.22 × 10<sup>-5</sup> mol dm<sup>-3</sup>): λ<sub>max</sub>/nm (ε/M<sup>-1</sup> cm<sup>-1</sup>) = 203 (54800), 211 (54500), 279 (14000). Anal. Calcd for C<sub>14</sub>H<sub>11</sub>BrO<sub>3</sub>: C, 54.75; H, 3.62. Found: C, 54.84; H, 3.99.

**9-(Bromomethyl)-6-hydroxy-3H-xanthen-3-one-DDQ Complex (1c-DDQ).** This compound was synthesized from 9-(bromomethyl)-9H-xanthene-3,6-diol (**8c**) by the procedure used for the preparation of diethyl (6-hydroxy-3-oxo-3H-xanthen-9-yl)methyl phosphate-DDQ complex (**1a-DDQ**).

Yield: 55%. Crimson powder. Mp >105 °C (decomp). <sup>1</sup>H NMR (400 MHz, DMSO-*d*<sub>6</sub>): δ (ppm) 6.53 (d, 1H, *J* = 2.4 Hz), 6.60 (m, 2H, *J*<sub>1</sub> = 2.4 Hz, *J*<sub>2</sub> = 2.4 Hz, *J*<sub>3</sub> = 2.3 Hz), 6.67 (s, 1H), 6.68 (dd, 1H, *J*<sub>1</sub> = 8.8 Hz, *J*<sub>2</sub> = 2.5 Hz), 7.51 (d, 1H, *J* = 8.7 Hz), 8.32 (d, 1H, *J* = 8.8 Hz), 9.97 (bs, 1H), 10.12 (bs, 1H) (Supplementary Figure S27). <sup>13</sup>C NMR (126 MHz, DMSO-*d*<sub>6</sub>): δ (ppm) 94.2, 102.3, 102.0, 110.4, 112.0, 113.8, 113.9, 124.8, 127.8, 128.1, 150.5, 152.6, 158.6, 158.9 (Supplementary Figure S28). FTIR (cm<sup>-1</sup>): 2970, 2359, 2334, 1736 (C=O), 1364, 1601, 1575, 1568, 1456, 1418, 1404, 1318, 1267, 1209, 1188, 1129, 1118, 1083, 1048, 931, 848, 826, 815, 771, 764, 668, 653 (C–Br), 633. UV–vis (aq phosphate buffer, pH = 7.0, *I* = 0.1 M): λ<sub>max</sub>/nm (ε/M<sup>-1</sup> cm<sup>-1</sup>) = 243 (44300), 329 (5200), 517 (44900) (Supplementary Figure S29). HRMS (TOF MS ESI<sup>-</sup>): calcd for C<sub>22</sub>H<sub>8</sub>BrCl<sub>2</sub>N<sub>2</sub>O<sub>5</sub> (M – H<sup>+</sup>) 528.8999 ( $C_{22}H_9^{79}Br^{35}Cl^{35}ClN_2O_5 - H^+$ ), 530.8979 ( $C_{22}H_9^{81}Br^{35}Cl^{35}ClN_2O_5 - H^+$ ), found 528.8995, 530.8986 (Supplementary Figures S30 and S31).

**6-Hydroxy-3-oxo-3H-xanthene-9-propanoic Acid (Succinylfluorescein, **9**; Scheme 4).** A stirred mixture of succinic acid anhydride (2.50 g, 25 mmol) and resorcinol (2.75 g, 25 mmol) in aq sulfuric acid (30 mL, 73% (v/v)) was heated to 140 °C for 6 h. The reaction mixture was cooled to 20 °C and poured into water (500 mL). The stirred solution was alkalinized with aq NaOH (50%) to pH = 13, while the temperature was kept at ~20 °C. Acetic acid was added to the solution until pH = 4 was obtained, and the brown precipitate was filtered. The filtrate was washed with water (3 × 25 mL), dried under reduced pressure, washed with hot 1,4-dioxane (15 mL) and hot methanol (15 mL), and dried under reduced pressure to give pure **9**. Yield: 5.7 g (80%). Dark brown solid. Mp 300 °C (decomp) (lit. 155–160 °C (decomp)).<sup>10</sup> <sup>1</sup>H NMR (300 MHz, DMSO-*d*<sub>6</sub>): δ (ppm) 3.40 (d, 2H, *J* = 7.2 Hz), 5.81 (t, 1H, *J* = 7.3 Hz), 6.50 (d, 1H, *J* = 2.3 Hz), 6.56 (d, 1H, *J* = 2.3 Hz), 6.62 (dt, 2H, *J*<sub>1</sub> = 8.6 Hz, *J*<sub>2</sub> = 2.3 Hz), 7.43 (dd, 2H, *J*<sub>1</sub> = 8.6 Hz, *J*<sub>2</sub> = 2.0 Hz), 9.74 (s, 1H, –OH), 9.89 (s, 1H, –OH), 12.36 (bs, 1H, –COOH) (Supplementary Figure S32). <sup>13</sup>C NMR (75.5 MHz, DMSO-*d*<sub>6</sub>): δ (ppm) 34.6, 66.2, 102.2, 102.6, 110.8, 111.8, 111.9, 112.7, 115.8, 124.3, 126.5, 128.3, 151.2, 152.9, 157.9, 158.1, 172.9 (Supplementary Figure S33). MS (EI<sup>+</sup>, 70 eV): *m/z* = 284 (35), 255 (1), 239 (100), 229 (50), 223 (7), 213 (10), 200 (3), 181 (5), 165 (6), 152 (11), 137 (7), 115 (9). FTIR (KBr, cm<sup>-1</sup>) = 3450 (br), 3053, 2968, 1745, 1633, 1599, 1463, 1391, 1329, 1250, 1202, 1159, 1116, 1037, 846. UV–vis (aq phosphate buffer, pH = 7.0, *I* = 0.1 M), (*c* 1.00 × 10<sup>-5</sup> mol dm<sup>-3</sup>): λ<sub>max</sub>/nm (ε/M<sup>-1</sup> cm<sup>-1</sup>) = 238 (53800), 486 (95000) (Supplementary Figure S34). HRMS (ESI<sup>+</sup>): calcd for C<sub>16</sub>H<sub>13</sub>O<sub>5</sub> (M + H<sup>+</sup>) 285.0757. Found: 285.0758. This compound has also been characterized elsewhere.<sup>10</sup>

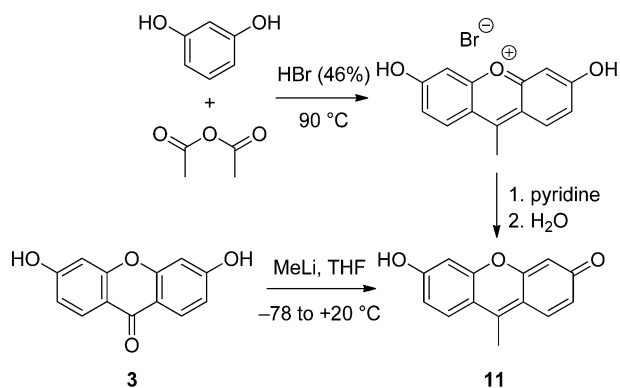
**Methyl 3-(6-Hydroxy-3-oxo-3H-xanthene-9-yl)propanoate (**10**).** A stirred mixture of succinylfluorescein (**9**, 1.00 g, 4.0 mmol) and H<sub>2</sub>SO<sub>4</sub> (0.15 mL, 95% (v/v)) in



MeOH (300 mL) was heated to 65 °C for 7 days. The reaction mixture was then cooled to 20 °C. The stirred solution was neutralized to pH = 6 with aq Na<sub>2</sub>CO<sub>3</sub> (satd). A reddish precipitate was formed, filtered, and purified by column chromatography (CHCl<sub>3</sub>/MeOH, 9:1, v/v). The purified product was redissolved in cold aq NaOH (0.2 M) keeping pH = 9 and then was reprecipitated by adjusting pH to 4 with aq HCl (0.2 M). The precipitate was filtered, washed with water (3 × 15 mL), and dried under reduced pressure to give a red solid. Yield: 150 mg (13%). Mp 187–189 °C (decomp) (lit. 187–190 °C (decomp)<sup>10</sup>). Note: A product of methanolysis was also identified simultaneously in a freshly prepared solution in methanol (Supplementary Figures S35 and S36); a tautomeric form containing an exocyclic double bond was then formed overnight, and it was the only form present in DMSO-*d*<sub>6</sub> (Supplementary Figures S37 and S38). <sup>1</sup>H NMR (500 MHz, CD<sub>3</sub>OD): δ (ppm) 1.81 (t, 2H, *J* = 7.9 Hz), 2.35 (t, 2H, *J* = 7.7 Hz), 2.76 (t, 0.75H, *J* = 7.8 Hz), 3.43 (s, 3H), 3.64 (t, 0.75H, *J* = 7.9 Hz), 3.66 (s, 1.13H), 6.50 (d, 2H, *J* = 1.8 Hz), 6.64 (d, 0.75H, *J* = 1.7 Hz), 6.66 (d, 2H, *J* = 2.0 Hz), 6.87 (d, 1H, *J* = 8.6 Hz), 7.30 (d, 2H, *J* = 8.5 Hz), 7.99 (d, 1H, *J* = 9.3 Hz) (Supplementary Figure S35). <sup>1</sup>H NMR (500 MHz, DMSO-*d*<sub>6</sub>): δ (ppm) 3.51 (d, 2H, *J* = 7.2 Hz), 3.65 (s, 3H), 5.79 (t, 1H, *J* = 7.2 Hz), 6.50 (d, 1H, *J* = 2.2 Hz), 6.56 (d, 1H, *J* = 2.2 Hz), 6.58–6.65 (m, 2H), 7.41 (d, 1H, *J* = 8.5 Hz), 7.44 (d, 1H, *J* = 8.6 Hz), 9.76 (s, 1H, –OH), 9.90 (s, 1H, –OH) (Supplementary Figure S37). <sup>13</sup>C NMR (126 MHz, CD<sub>3</sub>OD): δ (ppm) 23.8, 30.8, 35.5, 41.7, 52.1, 52.5, 76.0, 103.1, 104.4, 113.0, 113.2, 129.1, 130.3, 154.7, 156.1, 159.7, 173.7, 175.2 (Supplementary Figure S36). <sup>13</sup>C NMR (126 MHz, DMSO-*d*<sub>6</sub>): δ (ppm) 34.3, 51.6, 102.2, 102.6, 110.8, 110.9, 111.9, 112.6, 115.6, 124.4, 127.0, 128.3, 151.2, 152.9, 157.9, 158.2, 171.9 (Supplementary Figure S38). MS (EI<sup>+</sup>, 70 eV): *m/z* = 298 (38), 299 (8), 240 (17), 239 (100), 238 (6), 237 (8), 213 (14). FTIR (KBr, cm<sup>-1</sup>) = 3045 (br), 2949, 1737, 1641, 1596, 1459, 1395, 1330, 1274, 1207, 1116, 847. UV–vis (aq phosphate buffer, pH = 7.0, *I* = 0.1 M/CH<sub>3</sub>OH, 1:1, (v/v), (*c* 1.00 × 10<sup>-5</sup> mol dm<sup>-3</sup>): λ<sub>max</sub>/nm (ε/M<sup>-1</sup> cm<sup>-1</sup>) = 241 (43500), 498 (77000) (Supplementary Figure S39). HRMS (ESI<sup>+</sup>): calcd for C<sub>17</sub>H<sub>14</sub>O<sub>5</sub> (M + H<sup>+</sup>) 299.0914. Found: 299.0915. This compound has also been characterized elsewhere.<sup>10</sup>

**6-Hydroxy-9-methyl-3*H*-xanthen-3-one (11; Scheme 5). Method A.** Hydrobromic acid (6.7 mL, aq, 46%, 57 mmol) was added dropwise to stirred acetic anhydride (28 mL, 294 mmol) at 0 °C over a period of 20 min. Resorcinol (11.0 g, 100 mmol) was then added to the reaction mixture in one portion.

**Scheme 5. Synthesis of 6-Hydroxy-9-methyl-3*H*-xanthen-3-one 11**



The solution was heated to 90 °C (the reaction mixture became red and a red precipitate appeared). The reaction mixture was then cooled to 0 °C and filtered. The solid precipitate was washed with glacial acetic acid (3 × 5 mL) and ice-cold propan-2-ol (5 mL), and the remaining solid was dried under vacuum over phosphorus pentoxide to an afford orange solid of 3,6-dihydroxy-9-methylxanthenium bromide. Yield 4.86 g (32%). Mp >170 °C (decomp). <sup>1</sup>H NMR (600 MHz, CF<sub>3</sub>COOD): δ (ppm) 3.25 (s, 3H) 7.42 (d, 2H, *J* = 2.2 Hz), 7.45 (dd, 2H, *J*<sub>1</sub> = 9.3 Hz, *J*<sub>2</sub> = 2.2 Hz), 8.40 (d, 2H, *J* = 9.3 Hz). <sup>13</sup>C NMR (126 MHz, CF<sub>3</sub>COOD): δ (ppm) 16.7, 105.0, 119.8, 122.4, 132.8, 161.4, 170.6, 171.9. MS (EI): 226.2 (100), 227.2 (14) 228.2 (2), 229.2 (0.1). FTIR (KBr, cm<sup>-1</sup>) = 2916, 2721, 2582, 2359, 1721, 1632, 1599, 1551, 1530, 1474, 1469, 1461, 1410, 1356, 1310, 1269, 1228, 1206, 1168, 1124, 866, 838, 821, 702, 648. UV–vis (1 M aq HCl): λ<sub>max</sub>/nm (relative intensity) = 205 (46), 226 (69), 249 (51), 291 (8), 426 (100). Anal. Calcd for C<sub>14</sub>H<sub>11</sub>BrO<sub>3</sub>: C, 54.75; H, 3.61. Found: C, 54.49; H, 3.62. All obtained 3,6-dihydroxy-9-methylxanthenium bromide (4.52 g, 1.47 mmol) was suspended in dry pyridine (80 mL) by sonication and left at 20 °C for an additional 90 min. Water (400 mL) was then added to the slowly stirred solution, and a precipitate was formed. The precipitate was filtered, washed with water (5 × 50 mL), and dried under vacuum over phosphorus pentoxide to a crimson solid. Yield: 3.08 g (93%).

**Method B.** MeLi (4.80 mL, 1.6 M solution in hexane, 7.7 mmol) was added dropwise to a stirred solution of 3,6-dihydroxy-9*H*-xanthen-9-one (3, 0.50 g, 2.2 mmol) in dry THF (100 mL) at –78 °C under inert atmosphere. After 30 min of stirring at –78 °C another portion of MeLi (1.37 mL, 1.6 M solution in hexane, 2.20 mmol) was added dropwise. The reaction mixture was stirred for an additional 45 min at –78 °C, allowed to slowly warm up to 20 °C (in 30 min) and then was stirred at 20 °C for 1 h. The solvents were removed under reduced pressure. The solid residue was dissolved in dichloromethane (20 mL), washed with acidic water (10 mL, pH = 3) and brine (10 mL), dried over MgSO<sub>4</sub>, and filtered, and the solvent was removed under reduced pressure to give a deep red solid. Yield: 451 mg (91%). <sup>1</sup>H NMR (400 MHz, DMSO-*d*<sub>6</sub>): δ (ppm) 5.25 (s, 2H), 6.49 (d, 2H, *J* = 2.4 Hz), 6.60 (dd, 2H, *J*<sub>1</sub> = 8.7 Hz, *J*<sub>2</sub> = 2.4 Hz), 7.65 (d, 2H, *J* = 8.7 Hz), 9.92 (s, 2H, –OH) (Supplementary Figure S40). <sup>13</sup>C NMR (126 MHz, DMSO-*d*<sub>6</sub>): δ (ppm) 95.3, 102.3, 112.0, 112.1, 125.2, 131.0, 150.8, 158.1 (Supplementary Figure S41). MS (ESI<sup>-</sup>; CH<sub>3</sub>OH + 5 mM NH<sub>3</sub>, γ ~0.1 mg cm<sup>-3</sup>): *m/z* = 223.5 (M – H<sup>+</sup>, 100), 226.3 (M<sup>-</sup>, 15.8), 450.8 (M<sub>2</sub> – H<sup>+</sup>, 35.2), 451.9 (M<sub>2</sub><sup>-</sup>, 9.9). MS (EI<sup>+</sup>, 70 eV, *m/z*, %): 226 (100), 211 (25). FTIR (KBr, cm<sup>-1</sup>) = 3257, 2359, 2336, 1558, 1447, 1387, 1315, 1268, 1251, 1198, 1178, 1109, 1040, 927, 839, 814, 806, 778, 654. UV–vis (0.1 M aq NaOH): λ<sub>max</sub>/nm (relative intensity) = 238 (60), 279 (14), 312 (9), 481 (100). UV–vis (C<sub>2</sub>H<sub>5</sub>OH), (*c* 1.55 × 10<sup>-5</sup> mol dm<sup>-3</sup>): λ<sub>max</sub>/nm (ε/M<sup>-1</sup> cm<sup>-1</sup>) = 211 (25456), 232 (30733), 274 (9570), 497 (26312). HRMS (ESI<sup>+</sup>): calcd for C<sub>14</sub>H<sub>11</sub>O<sub>3</sub> (M + H<sup>+</sup>) 227.0703. Found: 227.0694. HRMS (ESI<sup>-</sup>): calcd for C<sub>14</sub>H<sub>9</sub>O<sub>3</sub> (M – H<sup>+</sup>) 225.0557. Found: 225.0556.

**2,3-Dichloro-5-cyano-6-hydroxy-1,4-benzoquinone (12).** Water (5 mL) was added to a solution of 2,3-dichloro-5,6-dicyano-1,4-benzoquinone (DDQ, 15 mg) in methanol (5 mL) in one portion at 20 °C; the solution changed color from yellow to red while released HCN was detected by the corresponding analytic techniques or sensorically. Methanol was removed under reduced pressure, and remaining water was lyophilized to give a yellow powder. No further purification was

performed. Yield: 13 mg (90%). Mp 196–199 °C.  $^{13}\text{C}$  NMR (75.5 MHz, 0.1 M  $\text{D}_2\text{O}$  phosphate buffer with 5%  $\text{CD}_3\text{CN}$  (v/v)):  $\delta$  (ppm) 89.1, 117.5, 137.7, 144.9, 173.3, 175.7, 175.8 (Supplementary Figure S42). FTIR (KBr,  $\text{cm}^{-1}$ ) = 3009, 2970, 2950, 2227, 1739, 1698, 1589, 1577, 1369, 1219, 1109, 889, 822, 746, 600, 528. HRMS (ESI $^-$ ): calcd for  $\text{C}_7\text{Cl}_2\text{NO}_3$  ( $\text{M} - \text{H}^+$ ) 215.9261 ( $\text{C}_7^{35}\text{Cl}^{35}\text{ClNO}_3$ ), 217.9231 ( $\text{C}_7^{37}\text{Cl}^{35}\text{ClNO}_3$ ). Found: 215.9258, 217.9229.

**Photochemical Experiments. Irradiation in UV Cuvettes (General Procedure).** Solutions of **1a–c-DDQ** ( $c \sim 1 \times 10^{-5}$  mol  $\text{dm}^{-3}$ ) in 0.1 M phosphate buffer (4 mL, pH = 7.0) were irradiated with a medium pressure 40-W mercury lamp through a band-pass optical filter ( $\lambda_{\text{irr}} = 546$  nm). The progress of the reaction was monitored using by UV–vis spectrometry.

**Irradiation in NMR Tubes (General Procedure).** Small amounts of **1a–c-DDQ** (2–3 mg) were dissolved in 0.1 M phosphate buffer ( $\text{D}_2\text{O}$  based, pH = 7.4) or methanol- $d_4$  or methanol- $d_4$ /water- $d_2$  1:1 (v/v) mixture (500  $\mu\text{L}$ ) in an NMR tube. The solutions were irradiated with the same irradiation source as described above. The reaction progress was monitored by  $^1\text{H}$  NMR and  $^{31}\text{P}$  NMR.

**Characterization of the Photoproducts.** Diethyl phosphoric acid, acetic acid, and 3,6-dihydroxy-9H-xanthen-9-one (**3**) were characterized by their  $^1\text{H}$ ,  $^{13}\text{C}$ , and  $^{31}\text{P}$  (when applicable) NMR, MS and/or HRMS (for photoproducts from **1a** only), and comparison of the data to those of the authentic samples.

**6-Hydroxy-3-oxo-3H-xanthen-9-carboxylic Acid (13).** Compound **13** was obtained upon irradiation of **1a** in aqueous phosphate buffer. A  $\sim 10$  mmol  $\text{dm}^{-3}$  solution of **1a-DDQ** in 0.1 M phosphate buffer ( $\text{D}_2\text{O}$ , pH = 7.4) was irradiated in an NMR tube. Part (40%) of the starting material precipitated and was filtered off. The filtrate was acidified with aq  $\text{CF}_3\text{COOH}$  to form a red precipitate, which was filtered, washed with aq  $\text{CF}_3\text{COOH}$  ( $3 \times 1$  mL), and dried. Yield: 50% (calculated on the basis of the starting material consumed). Dark red powder.  $^1\text{H}$  NMR (300 MHz, 0.1 M phosphate buffer in  $\text{D}_2\text{O}$ , pH = 7.4):  $\delta$  (ppm) 6.67 (d, 1H,  $J = 2.0$  Hz), 6.84 (dd, 2H,  $J_1 = 9.0$  Hz,  $J_2 = 2.0$  Hz), 7.63 (d, 2H,  $J = 9.0$  Hz) (Supplementary Figure S51).  $^1\text{H}$  NMR (300 MHz,  $\text{CD}_3\text{OD}/\text{CD}_3\text{CN}$ , 1:1, v/v): 6.56 (d, 2H,  $J = 2.6$  Hz), 6.64 (dd, 2H,  $J_1 = 8.6$  Hz,  $J_2 = 2.6$  Hz), 7.23 (d, 2H,  $J = 8.6$  Hz).  $^{13}\text{C}$  NMR (126 MHz, 0.1 M phosphate buffer in  $\text{D}_2\text{O}$ , pH = 7.4):  $\delta$  (ppm) 104.2, 108.5, 123.6, 131.1, 154.0, 159.7, 171.9 (–COOH), 180.5 ( $\text{C}_{\text{ar}}=\text{O}$ ) (Supplementary Figure S52). HRMS (TOF MS ES $^+$ ): calcd for  $\text{C}_{14}\text{H}_9\text{O}_5$  ( $\text{M} + \text{H}^+$ ) 257.0444, found 257.0452 (Figure S53). UV–vis ( $\text{CH}_3\text{OH}$ ):  $\lambda_{\text{max}}/\text{nm}$  (relative intensity) = 491 (100), 321 (16), 242 (101); UV–vis (0.1 M aq phosphate buffer, pH = 7.4):  $\lambda_{\text{max}}/\text{nm}$  (relative intensity) = 489 (100), 318 (11), 241 (81) (Supplementary Figure S50). According to claims in the literature, this compound has also been prepared before.<sup>31,42</sup> These procedures were reproduced to give solid samples with the described characteristics (color and appearance), but they were found to be complex mixtures.

**Characterization of the 9-DDQ and 10-DDQ Complexes.** Succinylfluorescein (**9**) or methyl 3-(6-hydroxy-3-oxo-3H-xanthen-9-yl)propanoate (**10**) was mixed with 2,3-dichloro-5,6-dicyano-1,4-benzoquinone (DDQ) in methanol in the 1:1 molar ratio while keeping the concentration of **9/10** equal to  $1.0 \times 10^{-5}$  mol  $\text{dm}^{-3}$ . The solutions were left for 2 h at 20 °C, and the solvent was evaporated to yield a dark brown solid that was analyzed by HRMS.

**9-DDQ.** HRMS (ESI $^-$ ): calcd for  $\text{C}_{24}\text{H}_{11}\text{Cl}_2\text{N}_2\text{O}_7$  508.9943 ( $\text{C}_{24}\text{H}_{12}^{35}\text{Cl}^{35}\text{ClN}_2\text{O}_7 - \text{H}^+$ ), 510.9914 ( $\text{C}_{24}\text{H}_{12}^{35}\text{Cl}^{37}\text{ClN}_2\text{O}_7$

–  $\text{H}^+$ ). Found 508.9945, 510.9913 (Supplementary Figure S43).

**10-DDQ.** HRMS (ESI $^-$ ): calcd for  $\text{C}_{25}\text{H}_{13}\text{Cl}_2\text{N}_2\text{O}_7$  523.0100 ( $\text{C}_{25}\text{H}_{14}^{35}\text{Cl}^{35}\text{ClN}_2\text{O}_7 - \text{H}^+$ ), 525.0070 ( $\text{C}_{25}\text{H}_{14}^{35}\text{Cl}^{37}\text{ClN}_2\text{O}_7 - \text{H}^+$ ). Found 523.0106, 525.0087 (Supplementary Figure S44).

## ■ ASSOCIATED CONTENT

### 📄 Supporting Information

UV, NMR, IR and HRMS spectra. This material is available free of charge via the Internet at <http://pubs.acs.org>.

## ■ AUTHOR INFORMATION

### ✉ Corresponding Author

\*E-mail: [klan@sci.muni.cz](mailto:klan@sci.muni.cz); [J.Wirz@unibas.ch](mailto:J.Wirz@unibas.ch).

### Notes

The authors declare no competing financial interest.

## ■ ACKNOWLEDGMENTS

Support for this work was provided by the Swiss National Science Foundation, the Grant Agency of the Czech Republic (GA203/09/0748), and the project CETOCOEN (CZ.1.05/2.1.00/01.0001) granted by the European Regional Development Fund (P.S., P.K.). The authors express their thanks to Jaromír František, Blanka Vrbková, Lubomír Prokeš, Michal Čajan, Otakar Humpa, Daniel Häussinger, Heinz Nadig, and Robert Vícha for their help with the mass spectrometry, NMR measurements, and elemental analyses. We thank Prof. Reinhard Schmidt for providing us the mDPH actinometer and Miloš Černík, Radek Marek, Lukáš Maier, Jan Taimr, and Kamil Paruch for fruitful discussions.

## ■ DEDICATION

This paper is dedicated to the memory of Professor Howard E. Zimmerman, University of Wisconsin, Madison (July 5, 1926 – February 11, 2012).

## ■ REFERENCES

- (1) Goeldner, M.; Givens, R. S. *Dynamic Studies in Biology*; Wiley-VCH: Weinheim, Germany, 2006.
- (2) Pelliccioli, A. P.; Wirz, J. *Photochem. Photobiol. Sci.* **2002**, *1*, 441.
- (3) Givens, R. S.; Rubina, M.; Wirz, J. *Photochem. Photobiol. Sci.* **2012**, *11*, 472.
- (4) Zimmerman, H. E.; Sandel, V. R. *J. Am. Chem. Soc.* **1963**, *85*, 915.
- (5) Seiler, P.; Wirz, J. *Helv. Chim. Acta* **1972**, *55*, 2693.
- (6) Dela Cruz, J. L.; Blanchard, G. J. *J. Phys. Chem. A* **2002**, *106*, 10718.
- (7) Klimtchuk, E.; Rodgers, M. A. J.; Neckers, D. C. *J. Phys. Chem.* **1992**, *96*, 9817.
- (8) Müller, R.; Zander, C.; Sauer, M.; Deimel, M.; Ko, D.-S.; Siebert, S.; Arden-Jacob, J.; Deltau, G.; Marx, N. J.; Drexhage, K. H.; Wolfrum, J. *Chem. Phys. Lett.* **1996**, *262*, 716.
- (9) Timpe, H. J.; Kronfeld, K. P.; Mahlow, R. *Z. Chem.* **1990**, *30*, 55.
- (10) Amat-Guerri, F.; Martin, M. E.; Martinez-Utrilla, R.; Pascual, C. *J. Chem. Res., Synop.* **1988**, 1411.
- (11) Casalnuovo, A. L.; Calabrese, J. C. *J. Am. Chem. Soc.* **1990**, *112*, 4324.
- (12) Turk, S.; Kovac, A.; Boniface, A.; Bostock, J. M.; Chopra, I.; Blanot, D.; Gobec, S. *Bioorg. Med. Chem.* **2009**, *17*, 1884.
- (13) Shi, J. M.; Zhang, X. P.; Neckers, D. C. *J. Org. Chem.* **1992**, *57*, 4418.
- (14) Alberola, A.; Andres, C.; Ortega, A. G.; Pedrosa, R.; Vicente, M. *J. Heterocycl. Chem.* **1986**, *23*, 1781.

- (15) Höfle, G.; Steglich, W.; Vorbrüggen, H. *Angew. Chem., Int. Ed.* **1978**, *17*, 569.
- (16) Ohno, M.; Miyamoto, M.; Hoshi, K.; Takeda, T.; Yamada, N.; Ohtake, A. *J. Med. Chem.* **2005**, *48*, 5279.
- (17) Bhatt, M. V.; Kulkarni, S. U. *Synthesis* **1983**, 249.
- (18) Shi, J. M.; Zhang, X. P.; Neckers, D. C. *Tetrahedron Lett.* **1993**, *34*, 6013.
- (19) Walker, D.; Hiebert, J. D. *Chem. Rev.* **1967**, *67*, 153.
- (20) Hammond, P. R. *J. Chem. Soc.* **1963**, 3113.
- (21) Ottenberg, A.; Brandon, R. L.; Browne, M. E. *Nature* **1964**, *201*, 1119.
- (22) Misra, V. S.; Tewari, D. C.; Tripathi, P. N. *Electrochim. Acta* **1984**, *29*, 1335.
- (23) Mann, C. K.; Barnes, K. K. *Electrochemical Reactions in Non-Aqueous Systems*; Marcel Dekker: New York, 1970.
- (24) Neumann, M.; Fuldner, S.; König, B.; Zeitler, K. *Angew. Chem., Int. Ed.* **2011**, *50*, 951.
- (25) Saleh, G. A.; Askal, H. F.; Radwan, M. F.; Omar, M. A. *Talanta* **2001**, *54*, 1205.
- (26) Porto, R. S.; Vasconcellos, M.; Ventura, E.; Coelho, F. *Synthesis* **2005**, 2297.
- (27) Burstein, S. H.; Ringold, H. J. *J. Am. Chem. Soc.* **1964**, *86*, 4952.
- (28) Seybold, P. G.; Gouterman, M.; Callis, J. *Photochem. Photobiol.* **1969**, *9*, 229.
- (29) Amat-Guerri, F.; Martin, M. E.; Sanz, J.; Martinez-Utrilla, R. *Talanta* **1989**, *36*, 704.
- (30) Frisch, M. J. et al., *Gaussian 03, Revision D.02*; Gaussian, Inc.: Wallingford, CT, 2004.
- (31) Sen, R. N.; Sinha, N. N. *J. Am. Chem. Soc.* **1923**, *45*, 2984.
- (32) Schmidt, R.; Brauer, H. D. *J. Photochem.* **1984**, *25*, 489.
- (33) Alvarez-Pez, J. M.; Ballesteros, L.; Talavera, E.; Yguerabide, J. J. *Phys. Chem. A* **2001**, *105*, 6320.
- (34) Patel, G. N.; Patolia, R. J.; Trivedi, K. N. *Indian J. Chem., Sect. B* **1987**, *26*, 1035.
- (35) Noro, T.; Ueno, A.; Mizutani, M.; Hashimoto, T.; Miyase, T.; Kuroyanagi, M.; Fukushima, S. *Chem. Pharm. Bull.* **1984**, *32*, 4455.
- (36) Janjic, N.; Schloeder, D.; Tramontano, A. *J. Am. Chem. Soc.* **1989**, *111*, 6374.
- (37) Finnegan, R. A.; Merkel, K. E. *J. Pharm. Sci.* **1977**, *66*, 884.
- (38) Khan, M. S. Y.; Khan, M. H.; Javed, K. *Indian J. Chem., Sect. B* **1990**, *29*, 1101.
- (39) Lin, C. N.; Liou, S. S.; Ko, F. N.; Teng, C. M. *J. Pharm. Sci.* **1993**, *82*, 11.
- (40) Poronik, Y. M.; Shandura, M. P.; Kovtun, Y. P. *Zh. Org. Pharm. Khim.* **2005**, *2*, 38.
- (41) Poronik, Y. M.; Shandura, M. P.; Kovtun, Y. P. *Dyes Pigments* **2007**, *72*, 199.
- (42) Hewitt, J. T.; Pope, F. G. *Ber. Dtsch. Chem. Ges.* **1896**, *29*, 2824.

# Caged Fluoride: Photochemistry and Applications of 4-Hydroxyphenacyl Fluoride

Tomáš Slanina,<sup>†</sup> Peter Šebej,<sup>†</sup> Alexander Heckel,<sup>‡</sup> Richard S. Givens,<sup>§</sup> and Petr Klán<sup>\*,†</sup>

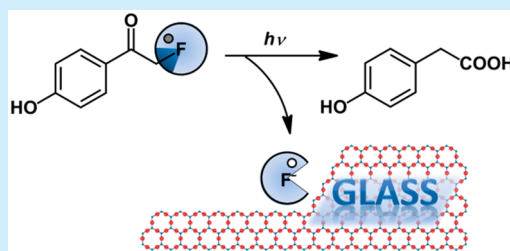
<sup>†</sup>Department of Chemistry and RECETOX, Faculty of Science, Masaryk University, Kamenice 5, 625 00 Brno, Czech Republic

<sup>‡</sup>Institute for Organic Chemistry and Chemical Biology, Goethe-University Frankfurt, Max-von-Laue-Str. 9, 60438 Frankfurt, Germany

<sup>§</sup>Department of Chemistry, University of Kansas, 1251 Wescoe Hall Drive, 5010 Malott Hall, Lawrence, Kansas 66045, United States

**S** Supporting Information

**ABSTRACT:** The quantitative, efficient ( $\Phi = 0.8$ ) photorelease of the fluoride ion upon UV-irradiation in aqueous media is introduced. The 4-hydroxyphenacyl chromophore is simultaneously transformed into UV-transparent 4-hydroxyphenylacetate via a photo-Favorskii rearrangement. The application of this process is demonstrated by photoinduced etching of mica and silicon by AFM.



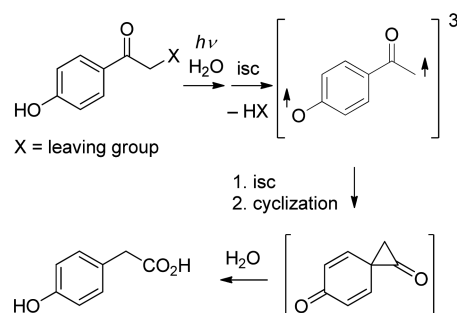
Targeted delivery by release of reactive chemical species with precise spatial and temporal resolution is highly sought after in many technologically driven fields. The fluoride ion, for example, has been recognized as a key effector in the growth and function of mammal hard tissues, such as teeth and bones,<sup>1</sup> cell metabolism,<sup>2</sup> and recently as a key component in fluoride-selective riboswitches in gene regulation.<sup>3</sup> Fluoride is used in dental medicine applications<sup>4</sup> and in organic synthesis, especially for deprotection of silyl protecting groups.<sup>5</sup> Both HF and  $\text{NH}_4\text{F}$  have been widely used for etching of silicon oxide (e.g., glass) and silicon surfaces, especially for microarchitecture fabrication in computer chip production. Normally, a surface is covered with a protective layer or a temporary inhibitor (e.g., photoresist in microchip fabrication)<sup>6a,b</sup> which is subsequently removed by irradiation allowing a chemical agent to modify (etch) the exposed areas.<sup>7a,b</sup> The mechanism of surface etching with fluorides has been thoroughly studied, and fluoride has been found to successfully insert into the Si–H, Si–OH, and Si–Si bonds to form monomeric and small oligomeric molecules of general structure  $\text{H}_x\text{Si}_y\text{F}_z$ .<sup>8a–c</sup>

The controlled release of reagents from photoremovable protecting groups (PPGs) has been demonstrated to afford exquisite spatial and temporal delivery of biologically active reagents.<sup>9</sup> To our knowledge, only one fluoride-releasing PPG, a 3',5'-dimethoxydesyl derivative, has been reported,<sup>10</sup> but poor water solubility and a highly absorbing byproduct (causing substantial internal filter effect) have precluded further development.

The 4-hydroxyphenacyl (pHP) group photoreleases a wide variety of reagents, possesses excellent water solubility, and efficiently ( $\Phi = 0.1–1.0$ ) and rapidly ( $k_{\text{obs}} = (7–100) \times 10^8 \text{ s}^{-1}$ ) releases the reagent or leaving group. The chromophore is transformed via a photo-Favorskii rearrangement into a

phenylacetic acid through rearrangement of the short-lived triplet biradical intermediate (Scheme 1).<sup>11a–d</sup>

## Scheme 1. Photochemistry of pHP Derivatives



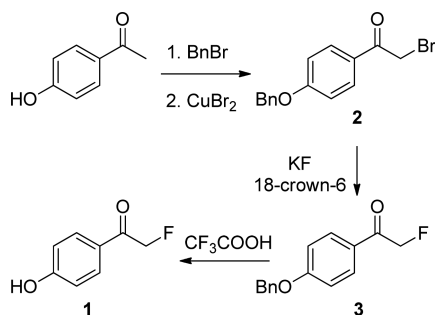
In this work, we introduce 4-hydroxyphenacyl as a photoremovable protecting group for release of the fluoride ion. The chemical yields, quantum efficiencies, and kinetics for  $\text{F}^-$  release and mechanistic considerations from time-resolved transient absorption measurements are provided along with several surface etching applications.

**Synthesis.** 4-Hydroxyphenacyl fluoride (**1**) was prepared from 4-hydroxyacetophenone in four steps in 55% chemical yield (Scheme 2). The absorption spectra of **1** in water (pH = 5.0;  $\lambda_{\text{max}} = 281 \text{ nm}$ ,  $\epsilon = 1.12 \times 10^4 \text{ dm}^3 \text{ mol}^{-1} \text{ cm}^{-1}$ ; Figure S7) and acetonitrile ( $\lambda_{\text{max}} = 271 \text{ nm}$ ,  $\epsilon = 1.17 \times 10^4 \text{ dm}^3 \text{ mol}^{-1} \text{ cm}^{-1}$ ; Figure S7) are similar, and the bands are assigned to the neutral form. In basic aqueous solutions (pH = 10.0), the major absorption band at  $\lambda_{\text{max}} = 331 \text{ nm}$  ( $\epsilon = 1.74 \times 10^4 \text{ dm}^3 \text{ mol}^{-1}$

Received: August 17, 2015

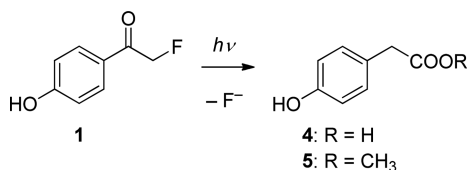


## Scheme 2. Synthesis of 4-Hydroxyphenacyl Fluoride (1)



$\text{cm}^{-1}$ ; Figure S7), similar to that of unsubstituted 4-hydroxyacetophenone,<sup>12</sup> corresponds to the phenolate form of 1. Only a very weak fluorescence of 1 was observed (Figure S12) in acetonitrile. The  $\text{p}K_{\text{a}} = (7.59 \pm 0.06)$  of the OH group of 1 was determined by spectrophotometric titration using global analysis of the spectra (see Supporting Information for details; Figure S11). Deconvolving the data provided the individual spectra of 1 and its conjugate base, identical to those measured at pH 5 and 10. *p*HP fluoride 1 is chemically stable in aqueous solutions at pH = 5 in the dark for at least 7 days, and less than 10% is consumed in 7 days at pH = 10 ( $^1\text{H}$  NMR).

**Photochemistry.** Exhaustive irradiation of *p*HP fluoride 1 in aqueous solutions at  $\lambda_{\text{irr}} = 313$  nm led to the release of the fluoride ion, determined by  $^{19}\text{F}$  NMR, in very high chemical yields with a disappearance quantum efficiency ( $\Phi_{\text{dis}}$ ) of  $0.84 \pm 0.02$  (Scheme 3, Table 1). 4-Hydroxyphenylacetic acid (4),

Scheme 3. Photoinduced Release of the Fluoride Ion from 1<sup>a</sup>

<sup>a</sup>5 is formed only in aqueous methanolic solutions.

Table 1. Photochemistry of 1<sup>a</sup>

solvent	yield (F <sup>-</sup> )/%	yield (4)/%	yield (5)/%	$\Phi_{\text{dis}}$
acetate buffer <sup>b</sup> pH = 5.0	98	95	n.r. <sup>d</sup>	$0.84 \pm 0.02^c$
phosphate buffer <sup>b</sup> pH = 10.0	95	95	n.r. <sup>d</sup>	$0.051 \pm 0.005^c$
CD <sub>3</sub> CN/D <sub>2</sub> O 1:1 (v/v)	96	93	n.r. <sup>d</sup>	$0.75 \pm 0.05^e$
CD <sub>3</sub> OD/D <sub>2</sub> O 1:1 (v/v)	98	59	37	$0.84 \pm 0.05^e$
CD <sub>3</sub> OD/D <sub>2</sub> O 3:1 (v/v)	95	39	59	$0.79 \pm 0.05^e$

<sup>a</sup>Aerated solutions of 1 ( $c = 10$  mmol dm<sup>-3</sup>) irradiated at  $(314 \pm 2)$  nm (Figure S27). Each experiment was run at least in duplicate. <sup>b</sup>D<sub>2</sub>O-based buffers with 5% of CH<sub>3</sub>CN (v/v) as cosolvent ( $I = 50$  mmol dm<sup>-3</sup>). <sup>c</sup>Solutions ( $c \approx 5 \times 10^{-5}$  mol dm<sup>-3</sup>) irradiated to <15% conversion. Ferrioxalate ( $\Phi = 1.24$  in water)<sup>16</sup> was used as an actinometer. All measurements were accomplished at least five times. <sup>d</sup>Not relevant. <sup>e</sup>Solutions ( $c \approx 4 \times 10^{-2}$  mol dm<sup>-3</sup>) in NMR tubes irradiated to ~15% conversion; the concentrations were determined by  $^1\text{H}$  NMR.

which typifies a photo-Favorskii rearrangement,<sup>13a,b</sup> was the exclusive byproduct in aqueous acetonitrile or buffered solutions. Methyl-*d*<sub>3</sub> ester of 4-hydroxyphenylacetic acid (5) was produced along with 4 when 1 was irradiated in CD<sub>3</sub>OD solutions. Formation of 4-hydroxybenzyl alcohol, which in some cases<sup>14</sup> accompanies photolysis of *p*HP derivatives, was not observed. *p*HP fluoride was unreactive when photolyzed in acetonitrile (<0.1% water).

The quantum efficiency of 1 in aqueous buffer at pH = 5.0 was approximately 16-fold higher than that at pH = 10.0, similar to that observed in unbuffered aqueous media (Table 1). This is in accord with a substantially lower reactivity of the 4-hydroxyphenacyl anion compared to that of the neutral form as demonstrated by Givens, Wirz and co-workers before<sup>14</sup> and reflects the energy difference between the neutral triplet of 4-hydroxyacetophenone and its corresponding triplet anion.<sup>11c,15</sup>

**Transient Kinetic Study.** The transient absorption spectra of 1 ( $c = 2$  mmol dm<sup>-3</sup>) were recorded in acetate buffer ( $I = 33$  mmol dm<sup>-3</sup>, 40% aqueous acetonitrile, v/v, pH = 5.0) in 0.15 ps steps up to a 18 ps delay (Figure S13). Immediately after excitation, the transient absorption signal was relatively weak, but its intensity increased at longer delays. Fitting the single exponential kinetics to the data using global analysis<sup>17</sup> gave spectra of two species, which are attributed to the lowest excited singlet ( $^1\text{I}^*$ ,  $\lambda_{\text{max}}(\text{abs}) = 315$  nm; the deconvolved spectrum is shown in Figure S14) and the triplet excited state ( $^3\text{I}^*$ ,  $\lambda_{\text{max}}(\text{abs}) = 405$  nm; for the deconvolved spectrum, see Figure S14). The singlet lifetime of  $^1\text{I}^*$  was  $2.50 \pm 0.05$  ps (Figure S15) and corresponds to the appearance of the neutral triplet  $^3\text{I}^*$  with an intersystem crossing rate constant of  $k_{\text{isc}} = (3.98 \pm 0.10) \times 10^{11} \text{ s}^{-1}$ .<sup>11d</sup>

A strong absorbance of  $^3\text{I}^*$  at 405 nm was observed at longer delays after the excitation (>20 ps). The corresponding rate constant for decay of the triplet,  $^3k_{\text{decay}} = (3.20 \pm 0.08) \times 10^9 \text{ s}^{-1}$  (Figures 1 and S17), was assigned to F<sup>-</sup> release.

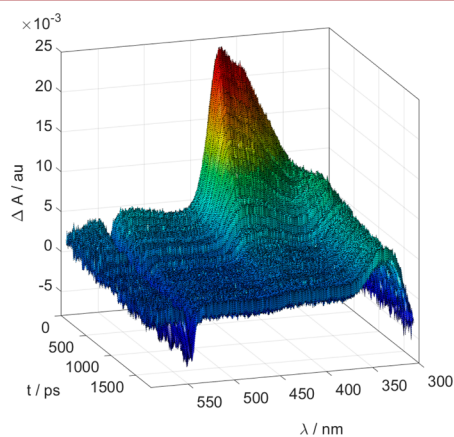
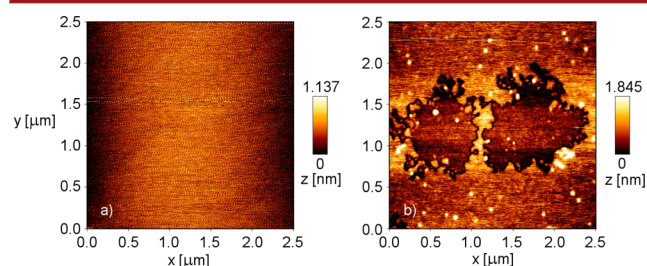


Figure 1. Pump-probe spectra of 1 ( $c = 2$  mmol dm<sup>-3</sup>) in acetate buffer (pH = 5.0,  $I = 33$  mmol dm<sup>-3</sup>, with 40% (v/v) of acetonitrile as a cosolvent) reconstructed after global analysis (the time frame <1.7 ns; 10 ps steps).

Concomitant with triplet decay, a weaker signal ( $\lambda_{\text{max}}(\text{abs}) = 330, 420, \text{ and } 445$  nm) arose whose spectrum was obtained from global analysis (Figure S16) and assigned to the 4-oxophenacyl triplet biradical as a short-lived intermediate<sup>14</sup> previously encountered with other photo-Favorskii rearrangements (Scheme 1). The triplet biradical decays with a rate constant of  $k_{\text{dirad}} \approx (2.3 \pm 0.2) \times 10^9 \text{ s}^{-1}$  (Figure S17). The

observed rate constant for  $F^-$  release from  $^3I^*$  is similar to other  $pHP$  decaying rates nicely fitting the correlation of a Brønsted linear free energy relationship for release rate vs  $pK_a$  of several other nucleofuge conjugate acids<sup>11d</sup> (Figure S18).

**Surface Etching.** We performed the following experiments to demonstrate applicability of the fluoride release for surface modifications of silicon-based materials. A freshly prepared surface of mica was covered with a drop of the solution of **1** ( $c = 22 \text{ mmol dm}^{-3}$ ) in a 7:3 (v/v) mixture of aqueous acetate buffer ( $c = 0.1 \text{ mol dm}^{-3}$ ,  $pH = 5$ ) and  $CH_3CN$ . The samples were either kept in the dark or irradiated using a LED source at  $\lambda_{em} = (281 \pm 6) \text{ nm}$  for 2 h, and subsequently kept in the dark for 14 h. Afterward, the solution was removed, and the surface was inspected by tapping-mode atomic force microscopy (AFM). Nonirradiated surfaces exhibited surface roughness below 300 pm (Figure S21) similar to a fresh mica surface (Figures 2a and S19). The sample exposed to UV light showed



**Figure 2.** Representative AFM images ( $2.5 \mu\text{m} \times 2.5 \mu\text{m}$ ) of (a) a fresh and untreated mica surface and (b) a mica surface treated with **1** ( $c = 22 \text{ mmol dm}^{-3}$ , in a 7:3 (v/v) mixture of  $CH_3CN$  and aqueous acetate buffer ( $c = 0.1 \text{ mol dm}^{-3}$ ,  $pH = 5$ )) irradiated with LEDs ( $\lambda_{em} = 281 \pm 6 \text{ nm}$ ) for 2 h and then left in the dark for 14 h.

distinct flat surface dents of  $\sim 2 \text{ nm}$  depth (Figures 2b and S20) suggesting that partial etching of the surface layer(s) occurred. A similar type of etching has been observed upon exposure of the mica surface to HF vapors<sup>18</sup> or HF solutions<sup>19</sup> and has also been suggested as a calibration method for AFM.<sup>20</sup> For this work, the mica surface was also exposed to an aqueous solution of KF ( $c = 22 \text{ mmol dm}^{-3}$ ) in the dark, and the resulting changes of the surface (Figure S22) were identical to those found upon irradiation shown in Figure 2b.

In addition, the monocrystalline silicon surface was treated by fluoride released by irradiation of **1** under the same experimental conditions as described above. The silicon surface covered by a solution of **1**, whose original roughness was below 400 pm (Figure S23), remained the same in the dark (Figure S25) but was substantially etched upon UV irradiation. A porous structure evoking small potholes with a height difference up to 1 nm appeared (Figure S24), resembling structural changes observed upon treatment of silicon with aq KF (Scheme S26), aq  $KOH$ <sup>21</sup> or upon electrochemical etching using a HF-based electrolyte solution.<sup>22</sup>

**Conclusions.** 4-Hydroxyphenacyl fluoride (**1**), a caged fluoride, upon exposure to 280–330 nm irradiation efficiently and rapidly releases the fluoride ion while simultaneously converting the phenacyl chromophore into 4-hydroxyphenylacetic acid. A photo-Favorskii mechanism is consistent with the transient absorption experiments. The photorelease of  $F^-$  provides a readily available protocol for a temporally and spatially controlled etching of the mica and silicon surfaces by the released fluoride ion from **1**. This protocol has additional

potential for application in engineering, material science, and biochemical related applications.

## ■ ASSOCIATED CONTENT

### Supporting Information

The Supporting Information is available free of charge on the ACS Publications website at DOI: 10.1021/acs.orglett.5b02374.

Material and methods; Synthetic details;  $pK_a$  determination; Irradiation procedures; Time-resolved spectroscopy details; Absorption and emission spectra; NMR spectra; AFM results (PDF)

## ■ AUTHOR INFORMATION

### Corresponding Author

\*E-mail: klan@sci.muni.cz.

### Notes

The authors declare no competing financial interest.

## ■ ACKNOWLEDGMENTS

Support for this work was provided by the Czech Science Foundation (GA13-25775S) (P.K.) and the Deutsche Forschungsgemeinschaft (INST 161/761-1) (A.H.). The RECEPTOX research infrastructure was supported by the projects of the Czech Ministry of Education (LO1214) and (LM2011028). The authors express their thanks to Dr. Kenneth F. Stensrud (University of Kansas) for performing preliminary experiments. Luboř Jílek is acknowledged for his help with the time-resolved measurements, and Thomas Halbritter (Goethe-University Frankfurt), for his help with AFM. We thank Pavel Friš (Masaryk University) for developing the software for manipulation of the time-resolved data.

## ■ REFERENCES

- Ozsvath, D. *Rev. Environ. Sci. Bio/Technol.* **2009**, *8*, 59–79.
- Barbier, O.; Arreola-Mendoza, L.; Del Razo, L. M. *Chem.-Biol. Interact.* **2010**, *188*, 319–333.
- Ren, A.; Rajashankar, K. R.; Patel, D. J. *Nature* **2012**, *486*, 85–89.
- Wiegand, A.; Buchalla, W.; Attin, T. *Dent. Mater.* **2007**, *23*, 343–362.
- Wuts, P. G. M.; Greene, T. W. *Greene's Protective Groups in Organic Synthesis*; John Wiley & Sons, Inc.: 2006.
- (a) Nakagawa, T.; Tanaka, T.; Niwa, D.; Osaka, T.; Takeyama, H.; Matsunaga, T. *J. Biotechnol.* **2005**, *116*, 105–111. (b) Tsai, Y.-C.; Jen, H.-P.; Lin, K.-W.; Hsieh, Y.-Z. *J. Chromatogr. A* **2006**, *1111*, 267–271.
- (a) French, R. H.; Tran, H. V. *Annu. Rev. Mater. Res.* **2009**, *39*, 93–126. (b) Moon, S.-Y.; Kim, J.-M. *J. Photochem. Photobiol. C* **2007**, *8*, 157–173.
- (a) Kolasinski, K. W. *Phys. Chem. Chem. Phys.* **2003**, *5*, 1270–1278. (b) Knotter, D. M. *J. Am. Chem. Soc.* **2000**, *122*, 4345–4351.
- Trucks, G. W.; Raghavachari, K.; Higashi, G. S.; Chabal, Y. J. *Phys. Rev. Lett.* **1990**, *65*, 504–507.
- Klán, P.; Šolomek, T.; Bochet, C. G.; Blanc, A.; Givens, R.; Rubina, M.; Popik, V.; Kostikov, A.; Wirz, J. *Chem. Rev.* **2013**, *113*, 119–191.
- Boudebous, H.; Košmrlj, B.; Šket, B.; Wirz, J. *J. Phys. Chem. A* **2007**, *111*, 2811–2813.
- (a) Givens, R. S.; Jung, A.; Park, C. H.; Weber, J.; Bartlett, W. J. *Am. Chem. Soc.* **1997**, *119*, 8369–8370. (b) Givens, R. S.; Park, C. H. *Tetrahedron Lett.* **1996**, *37*, 6259–6262. (c) Givens, R. S.; Weber, J. F. W.; Conrad, P. G.; Orosz, G.; Donahue, S. L.; Thayer, S. A. *J. Am. Chem. Soc.* **2000**, *122*, 2687–2697. (d) Givens, R. S.; Rubina, M.; Wirz, J. *Photochem. Photobiol. Sci.* **2012**, *11*, 472–488.

- (12) Klíčová, L.; Šebej, P.; Šolomek, T.; Hellrung, B.; Slavíček, P.; Klán, P.; Heger, D.; Wirz, J. *J. Phys. Chem. A* **2012**, *116*, 2935–2944.
- (13) (a) Stensrud, K.; Noh, J.; Kandler, K.; Wirz, J.; Heger, D.; Givens, R. S. *J. Org. Chem.* **2009**, *74*, 5219–5227. (b) Sebej, P.; Lim, B. H.; Park, B. S.; Givens, R. S.; Klan, P. *Org. Lett.* **2011**, *13*, 644–647.
- (14) Givens, R. S.; Heger, D.; Hellrung, B.; Kamdzhilov, Y.; Mac, M.; Conrad, P. G.; Cope, E.; Lee, J. I.; Mata-Segreda, J. F.; Schowen, R. L.; Wirz, J. *J. Am. Chem. Soc.* **2008**, *130*, 3307–3309.
- (15) Conrad, P. G.; Givens, R. S.; Hellrung, B.; Rajesh, C. S.; Ramseier, M.; Wirz, J. *J. Am. Chem. Soc.* **2000**, *122*, 9346–9347.
- (16) Hatchard, C. G.; Parker, C. A. P. *Proc. R. Soc. London, Ser. A* **1956**, *235*, 518–536.
- (17) Gampp, H.; Maeder, M.; Meyer, C. J.; Zuberbuhler, A. D. *Talanta* **1985**, *32*, 95–101.
- (18) Patel, A. R.; Tolansky, S. *Proc. R. Soc. London, Ser. A* **1957**, *243*, 33–40.
- (19) Rufe, E.; Hochella, M. F. *Science* **1999**, *285*, 874–876.
- (20) Nagahara, L. A.; Hashimoto, K.; Fujishima, A.; Snowden-Ifft, D.; Price, P. B. *J. Vac. Sci. Technol., B: Microelectron. Process. Phenom.* **1994**, *12*, 1694–1697.
- (21) Miyake, S.; Wang, M.; Kim, J. *J. Nanotechnol.* **2014**, *2014*, 1–19.
- (22) Nayef, U. M.; Muayad, M. W. *Int. J. Basic Appl. Sci.* **2013**, *13*, 15–17.

# Fluorescein Analogue Xanthene-9-Carboxylic Acid: A Transition-Metal-Free CO Releasing Molecule Activated by Green Light

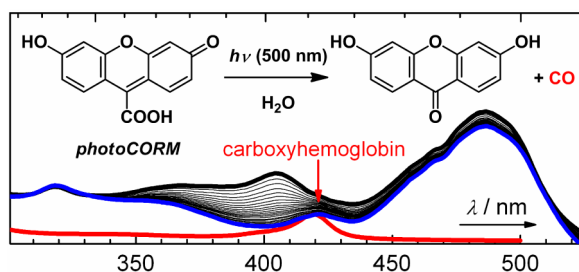
Lovely Angel Panamparambil Antony,<sup>†,§</sup> Tomáš Slanina,<sup>†,‡,§</sup> Peter Šebej,<sup>†,‡</sup>  
Tomáš Šolomek,<sup>†,‡</sup> and Petr Klán<sup>\*,†,‡</sup>

Department of Chemistry, Faculty of Science, Masaryk University, Kamenice 5, 625 00 Brno, Czech Republic, and Research Centre for Toxic Compounds in the Environment, Faculty of Science, Masaryk University, Kamenice 5, 625 00 Brno, Czech Republic

klan@sci.muni.cz

Received July 25, 2013

## ABSTRACT



6-Hydroxy-3-oxo-3H-xanthene-9-carboxylic acid is introduced as the first transition-metal-free carbon monoxide releasing molecule activated by visible light (photoCORM). This water-soluble fluorescein analogue releases carbon monoxide in both water and methanol upon irradiation at 500 nm. When selectively irradiated in the presence of hemoglobin (Hb) under physiological conditions, released CO is quantitatively trapped to form carboxyhemoglobin (COHb). The reaction progress can be accurately monitored by characteristic absorption and emission properties of the reactants and products.

Carbon monoxide, one of the byproducts of the enzymatic heme catabolism by heme oxygenase, has been recognized as an essential physiological signaling molecule.<sup>1</sup> CO acts as an agent for tissue protection via its anti-inflammatory, antiproliferative, and antiapoptotic effects at cellular concentrations ranging from 10 to 250 ppm.

Various metal-based carbon monoxide releasing molecules (CORMs) that can be used to elicit various biological activities and for therapeutic applications have been introduced in the past decade.<sup>2</sup> Low toxicity, water solubility, and stability prior to the application are the most desirable properties of CORMs. Contrary to

various small organic molecules, such as cyclopropanones,<sup>3</sup> 1,3-cyclobutanediones,<sup>4</sup> or 1,2-dioxolane-3,5-diones,<sup>5</sup> which liberate CO upon biologically adverse UV or near-UV (below 420 nm) irradiation, some transition-metal containing photoactivatable<sup>6</sup> CORMs (photoCORMs) that can be triggered by visible light<sup>7</sup> have been introduced recently. Mn-based photoCORMs, for example, polypyridyl metallodendrimers<sup>8</sup> and complexes

(3) (a) Kuzmanich, G.; Gard, M. N.; Garcia-Garibay, M. A. *J. Am. Chem. Soc.* **2009**, *131*, 11606. (b) Poloukhine, A.; Popik, V. V. *J. Org. Chem.* **2003**, *68*, 7833. (c) Poloukhine, A.; Popik, V. V. *J. Phys. Chem. A* **2006**, *110*, 1749. (d) Poloukhine, A. A.; Mbua, N. E.; Wolfert, M. A.; Boons, G.-J.; Popik, V. V. *J. Am. Chem. Soc.* **2009**, *131*, 15769.  
(4) Kuzmanich, G.; Garcia-Garibay, M. A. *J. Phys. Org. Chem.* **2011**, *24*, 883.

(5) Chapman, O. L.; Wojtkowski, P. W.; Adam, W.; Rodriguez, O.; Rucktaeschel, R. *J. Am. Chem. Soc.* **1972**, *94*, 1365.

(6) Klan, P.; Wirz, J. *Photochemistry of organic compounds: From concepts to practice*; John Wiley & Sons: Chichester, 2009.

(7) (a) Klan, P.; Šolomek, T.; Bochet, C. G.; Blanc, A.; Givens, R.; Rubina, M.; Popik, V.; Kostikov, A.; Wirz, J. *Chem. Rev.* **2012**, *113*, 119. (b) Schatzschneider, U. *Inorg. Chim. Acta* **2011**, *374*, 19. (c) Rimmer, R. D.; Pierri, A. E.; Ford, P. C. *Coord. Chem. Rev.* **2012**, *256*, 1509.

<sup>†</sup> Department of Chemistry.

<sup>‡</sup> Research Centre for Toxic Compounds in the Environment.

<sup>§</sup> These authors contributed equally to this work.

(1) Verma, A.; Hirsch, D.; Glatt, C.; Ronnett, G.; Snyder, S. *Science* **1993**, *259*, 381.

(2) (a) Mann, B. E. In *Medicinal Organometallic Chemistry*; Jaouen, G., Metzler-Nolte, N., Eds.; Springer: Heidelberg, 2010; Vol. 32, p 247. (b) Mann, B. E. *Organometallics* **2012**, *31*, 5728.

10.1021/ol4021089 © 2013 American Chemical Society

Published on Web 08/19/2013

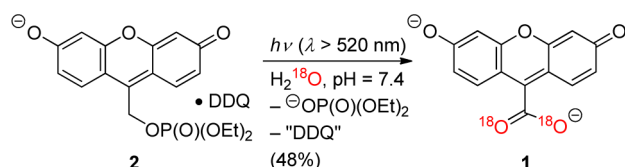


of various azaheteroaromatic ligands,<sup>9</sup> can release CO upon irradiation at 410 and > 500 nm, respectively.

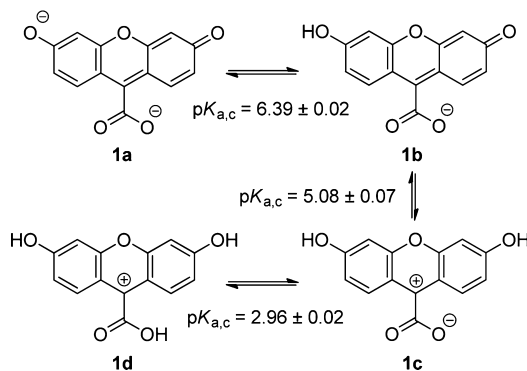
In this work, we introduce the first water-soluble, transition-metal-free CORM that can be activated by visible light. Released CO is shown to be quantitatively trapped by hemoglobin (Hb) under physiological conditions.

**Synthesis and Physico-Chemical Properties of 1.** 6-Hydroxy-3-oxo-3*H*-xanthene-9-carboxylic acid (**1**) is a fluorescein analogue possessing a nonaromatic substituent attached to the C9-position. The synthesis of this compound has been reported long ago.<sup>10</sup> However, following these procedures we obtained complex mixtures that did not contain any substantial amount of **1**. We also attempted to prepare this compound by several alternative synthetic pathways which were, unfortunately, unsuccessful (Scheme S2). Recently, some of us have shown that **1** is formed from the diethyl (6-hydroxy-3-oxo-3*H*-xanthen-9-yl)methyl phosphate·2,3-dichloro-5,6-dicyano-1,4-benzoquinone (DDQ) complex (**2**) upon irradiation at 520 nm (Scheme 1).<sup>11</sup> We further optimized and scaled up this photochemical procedure to produce tens of milligrams of **1** in high purity (Supporting Information).

**Scheme 1.** Synthesis of **1** (the incorporation of <sup>18</sup>O from water is shown in red)<sup>11</sup>



**Scheme 2.** Four Acid–Base Forms of **1** and the Corresponding  $pK_{a,c}$  Values



(8) Govender, P.; Pai, S.; Schatzschneider, U.; Smith, G. S. *Inorg. Chem.* **2013**, *52*, 5470.

(9) Gonzalez, M. A.; Carrington, S. J.; Fry, N. L.; Martinez, J. L.; Mascharak, P. K. *Inorg. Chem.* **2012**, *51*, 11930.

(10) (a) Hewitt, J. T.; Pope, F. G. *Ber. Dtsch. Chem. Ges.* **1896**, *29*, 2824. (b) Sen, R. N.; Sinha, N. N. *J. Am. Chem. Soc.* **1923**, *45*, 2984.

(11) Šebelj, P.; Wintner, J.; Müller, P.; Slanina, T.; Al Anshori, J.; Antony, L. A. P.; Klán, P.; Wirz, J. *J. Org. Chem.* **2013**, *78*, 1833.

Four pH-dependent forms of **1** (**1a–d**; Scheme 2) and the corresponding  $pK_{a,c}$  values were determined spectrometrically in aq buffer solutions ( $K_{a,c}$  are concentration quotients at ionic strength  $I \approx 0.1$  M; see Supporting Information and Figures S14–S15; the zwitterionic form of **1c** was predicted to be lower in energy (DFT,  $\sim 5$  kcal mol<sup>-1</sup>) than the corresponding charge-neutral tautomer). A dianion form **1a** ( $\lambda_{\max} = 488$  nm, Figure 1) is present at physiological pH (7.4) at > 90%. Spectroscopic properties of **1** in methanol (Figure S13) are similar to those in an aq solution. The fluorescence quantum yield in aq buffer at pH = 7.4 was found to be relatively high ( $0.39 \pm 0.03$ ;  $\lambda_{\text{em}} \sim 530$  nm; the single-exponential fluorescence lifetime is  $\tau = 2.43 \pm 0.08$  ns; Figure 1; Table S1). The compound is stable in aq buffer at pH = 7.4 in the dark at 4 °C for at least a month.

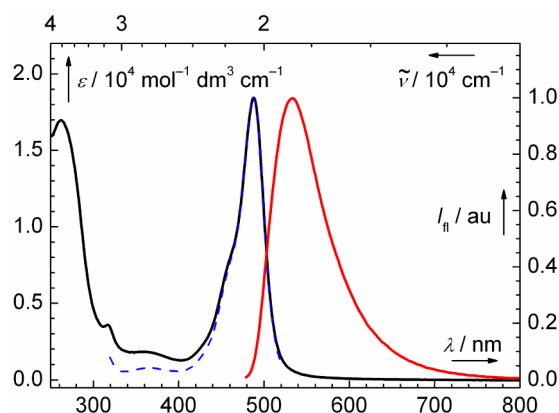
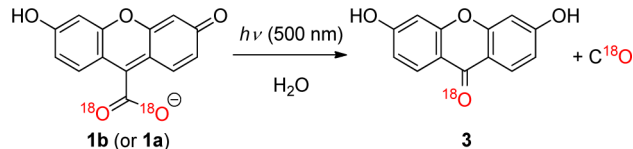


**Figure 1.** Absorption (black solid line), normalized emission (red solid line), and excitation (blue dashed line) spectra of **1** ( $c \approx 1 \times 10^{-5}$  M) in 0.1 M aq phosphate buffer at pH = 7.4.

**Photochemistry.** Irradiation of **1** in water, methanol, and their mixtures at 500 nm gave an exclusive and isolable product, 3,6-dihydroxy-9*H*-xanthen-9-one (**3**, Scheme 3). The decomposition quantum yield ( $\Phi$ ) of **1**, determined using **2** as an actinometer,<sup>11</sup> was  $(6.8 \pm 3.0) \times 10^{-4}$  in aq phosphate buffer (pH = 7.4,  $I = 0.1$  M; **1a** was the major (> 97%) light-absorbing form present; see Figures S14 and S15). A higher  $\Phi$  by a factor of  $\sim 6$  ( $(3.9 \pm 1.3) \times 10^{-3}$ ) was obtained at pH = 5.7, at which the monoanion **1b** and the dianion **1a** possess an equal absorbance at the excitation wavelength (Figures S14 and S15; the spectra of pure forms were obtained by the single value decomposition analysis; see Supporting Information). **3** was the sole photoproduct found at both pH's. The product of the molar absorption coefficient and the quantum yield,  $\epsilon\Phi$ , which is proportional to the extent of release,<sup>7a</sup> was relatively large (on the order of 1–10) at  $\lambda_{\text{irr}} \approx 500$  nm and pH = 7.4 due to large molar absorption coefficients of the corresponding forms. Therefore, the phototransformation of **1** was fast even when LEDs were used as an irradiation source.

Using the deconvoluted spectra (Figure S15) and the observed quantum yields at two different pH's (5.7 and 7.4),

**Scheme 3.** Photochemistry of **1a** or **1b** at pH 5.7–7.4 (isotopically labeled  $^{18}\text{O}$  is shown in red; the presence of  $^{18}\text{O}$  in CO is only a presumption)



the decomposition quantum yield of the individual form **1b** was estimated to be higher by approximately 1 order of magnitude compared to that of **1a**, provided that  $\Phi$  for each of the species is not affected by pH in this pH range.

The reaction efficiency at pH = 7.4 was not affected by the presence of oxygen. Thus either a triplet state was not involved or its lifetime was too short.

In contrast, an undetermined product with a  $\lambda_{\text{max}}$  of 430 nm (Figure S21) was formed in an aq solution at pH = 9.5 (the dianion **1a** was present exclusively) probably via a new concomitant (photo)reaction at such high hydroxide ion concentrations. Practically no photochemistry was observed at pH = 4.5, at which **1c** was the major absorbing species. **1** precipitated at pH = 2.5; thus the quantum yield could not be determined.

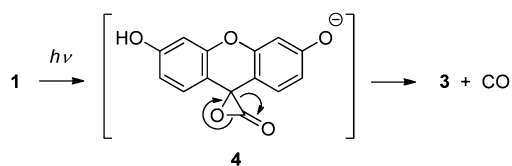
As a result, we conclude that both **1a** and **1b** are the only reactive species which undergo the phototransformation shown in Scheme 3 in the pH range 5.7–7.4.

Formation of two plausible gaseous side photoproducts, carbon monoxide and carbon dioxide, was considered. Irradiation of isotopically labeled **1** ( $-\text{C}^{18}\text{O}_2\text{H}$  in the C9-position), prepared photochemically from **2** in  $\text{D}_2^{18}\text{O}$  (Scheme 1),<sup>11</sup> in  $\text{H}_2^{16}\text{O}$ -based buffer (pH = 7.4; Scheme 3) gave **3** possessing the  $\text{C}=\text{O}^{18}$  group (Figure S23). No isotopic incorporation to **3** occurred when **1** with the  $-\text{C}^{16}\text{O}_2\text{H}$  group was irradiated in  $\text{D}_2^{18}\text{O}$  (Figure S22). These experiments thus ruled out the direct involvement of the solvent in the phototransformation and suggested that carbon monoxide is the second photoproduct, most probably containing the oxygen atom from the parent carboxylic moiety (thermal decomposition of **1** leads to decarboxylation; Scheme S1).

**Photorelease Mechanism.** Based on the results of our isotopic labeling experiments, we hypothesized that the  $\alpha$ -lactone **4**, which would further decarboxylate to form **3** (Scheme 4), might be formed as a primary product. It is known that  $\alpha$ -lactones (oxiranones) are short-lived intermediates<sup>12</sup> that decompose efficiently by decarboxylation; the most stable known  $\alpha$ -lactone has a half-life of  $\sim 8$  h at 24 °C.<sup>13</sup> Our TD-DFT calculations showed that vertical excitation of **1** at the wavelengths of irradiation used ( $\sim 500$  nm) populates the lowest singlet excited state ( $\text{S}_1$ ) for both the **1a** and **1b** forms (Tables S3–S5 and

Figure S1). The relaxed  $\text{S}_1$  potential energy surface (PES) scan along the coordinate of the C9–O bond length starting from the  $\text{S}_1$  energy minimum of both forms led to an intermediate similar to **4** that was, however,  $> 40$  kcal mol<sup>-1</sup> higher in energy (Figure S2). The calculations did not indicate involvement of a conical intersection along the scanned coordinate, and we were unable to locate any local minimum for **4** on the ground state PES using various methods (Supporting Information). It is in agreement with the fact that  $\alpha$ -lactone formation is favored only in systems that possess strong electron-withdrawing groups.<sup>14</sup> In addition, a ground-state transition state that connects **1** to both **3** and CO was found (Figure S3), but its high energy ( $> 50$  kcal mol<sup>-1</sup>) prevents a spontaneous decarboxylation of **1** at 20 °C. We also could not find a transition state for the CO release on the triplet hypersurface. Although our DFT calculations did not provide any evidence that the process involves **4**, its intermediacy should not be ruled out. Additional experiments and theoretical multiconfigurational models must be employed to fully understand the CO photorelease mechanism from **1**.

**Scheme 4.** Formation of a Putative Intermediate **4**



**CO Trapping with Hemoglobin.** A fast and sensitive method for determination of CO present in blood<sup>15</sup> or photoreleased from CORMs<sup>16</sup> often involves its complexation with hemoglobin (Hb) to form carboxyhemoglobin (COHb). In this work, an aqueous solution of uncomplexed Hb ( $\text{Fe}^{\text{II}}$ ) was prepared by reduction of bovine methemoglobin (MetHb,  $\text{Fe}^{\text{III}}$ ;  $c = 2.3 \times 10^{-5}$  M) by sodium dithionite.<sup>17</sup> It was subsequently mixed with a solution of **1** ( $c = 1.3 \times 10^{-4}$  M in 0.1 M aq phosphate buffer, pH = 7.4, purged with  $\text{N}_2$ ), and **1** was irradiated at  $503 \pm 15$  nm until complete conversion of Hb to COHb was observed. Formation of COHb was followed by absorption spectroscopy (Figure 2), although specific fluorescence signals of both **1** and **3** also allowed monitoring the course of the reaction. The distinct absorption characteristics of all species involved, **1a** ( $\lambda_{\text{max}} = 488$  nm), Hb ( $\lambda_{\text{max}} = 405$  nm), and COHb ( $\lambda_{\text{max}} = 419$  nm) (Figure S17), therefore provide unique advantages for simultaneous observation of the CO complexation by using a

(14) Showalter, B. M.; Toscano, J. R. *J. Phys. Org. Chem.* **2004**, *17*, 743.

(15) Widdop, B. *Ann. Clin. Biochem.* **2002**, *39*, 378.

(16) (a) Pfeiffer, H.; Rojas, A.; Niesel, J.; Schatzschneider, U. *Dalton Trans.* **2009**, 4292. (b) Zijlstra, W. G.; Buursma, A. *Comp. Biochem. Phys. B* **1997**, *118*, 743.

(17) Rodkey, F. L.; Hill, T. A.; Pitts, L. L.; Robertson, R. F. *Clin. Chem.* **1979**, *25*, 1388.

(12) L'Abbé, G. *Angew. Chem., Int. Ed.* **1980**, *19*, 276.

(13) (a) Adam, W.; Liu, J.-C.; Rodriguez, O. *J. Org. Chem.* **1973**, *38*, 2269. (b) Coe, P. L.; Sellars, A.; Tatlow, J. C.; Whittaker, G.; Fielding, H. C. *J. Chem. Soc., Chem. Commun.* **1982**, *0*, 362.

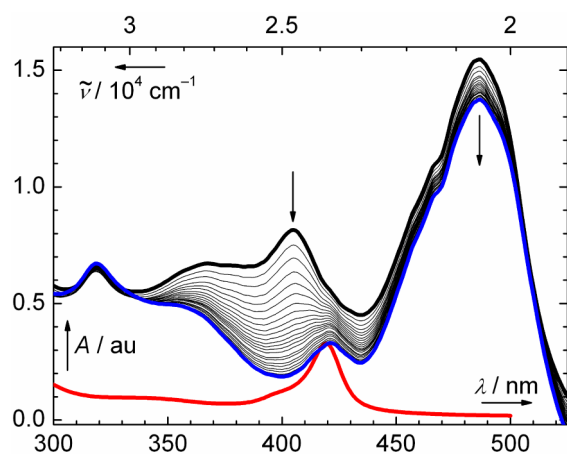


**Figure 2.** Absorption spectra (black lines) measured following irradiation of **1** ( $c \approx 1.3 \times 10^{-4}$  M; the total irradiation time was 4.6 h) in the presence of MetHb ( $c \approx 2.3 \times 10^{-5}$  M) and  $\text{Na}_2\text{S}_2\text{O}_4$  ( $c = 2.5 \times 10^{-5}$  M) in 0.1 M aq phosphate buffer at pH = 7.4 purged with  $\text{N}_2$  at  $503 \pm 15$  nm. The initial (black bold line) and final (blue bold line) spectra are highlighted. The spectrum of pure COHb formed from Hb and CO dissolved in water (red line) is shown for comparison.

selective excitation of the photoCORM **1** without spectral interference of the present hemoglobin derivatives.

In conclusion, 6-hydroxy-3-oxo-3*H*-xanthene-9-carboxylic acid (**1**) is the first representative of a transition-metal-free

carbon monoxide releasing molecule activatable by visible light (photoCORM) that allows precise spatio-temporal control over the CO release in the presence of hemoglobin. Its favorable spectroscopic properties, good aqueous solubility, and transformation to a noninterfering photoproduct project possible applications in biology and medicine.

**Acknowledgment.** Support for this work was provided by the Grant Agency of the Czech Republic (13-25775S) and the project CETOCOEN (CZ.1.05/2.1.00/01.0001) granted by the European Regional Development Fund (P. K.). The authors express their thanks to Jaroslav František (Ratiochem, Brno), Lukáš Maier, Zdeněk Moravec, Petr Kukučka, Miroslava Bittová (Masaryk University, Brno), and Robert Vícha (Tomas Bata University, Zlin) for their help with the mass spectrometry, NMR, thermogravimetry, and elemental analyses. The authors also thank Jakob Wirz (University of Basel) for fruitful discussions. University of Fribourg is acknowledged for computational resources.

**Supporting Information Available.** Materials and methods; synthesis and photophysical properties of the compounds; determination of  $\text{p}K_a$  of **1**; trapping of CO by hemoglobin; quantum chemical calculations; NMR, HRMS, UV-vis, and fluorescence data of new compounds. This material is available free of charge via the Internet at <http://pubs.acs.org>.

The authors declare no competing financial interest.

# Transition-Metal-Free CO-Releasing BODIPY Derivatives Activatable by Visible to NIR Light as Promising Bioactive Molecules

Eduardo Palao,<sup>†,||</sup> Tomáš Slanina,<sup>†,||</sup> Lucie Muchová,<sup>‡</sup> Tomáš Šolomek,<sup>†</sup> Libor Víttek<sup>‡,§</sup> Petr Klán<sup>†,\*</sup>

<sup>†</sup> Department of Chemistry and RECETOX, Masaryk University, Kamenice 5, 625 00 Brno, Czech Republic

<sup>‡</sup> Institute of Medical Biochemistry and Laboratory Diagnostics, 1<sup>st</sup> Faculty of Medicine, Charles University in Prague, Na Bojišti 3, 121 08 Praha 2, Czech Republic

<sup>§</sup> 4<sup>th</sup> Department of Internal Medicine, 1<sup>st</sup> Faculty of Medicine, Charles University in Prague, Na Bojišti 3, 121 08 Praha, Czech Republic

**ABSTRACT:** Carbon monoxide-releasing molecules (CORMs) are chemical agents used to administer CO as an endogenous, biologically active molecule. A precise spatial and temporal control over the CO release is the major requirement for their applications. Here we report the synthesis and properties of a new generation of transition-metal-free carbon monoxide-releasing molecules based on BODIPY chromophores (COR-BDPs) activatable by visible-to-NIR (up to 730 nm) light. We demonstrate their performance both for *in vitro* and *in vivo* experimental settings, and we propose the mechanism of the CO release based on steady-state and transient spectroscopy experiments and quantum chemical calculations.

## Introduction

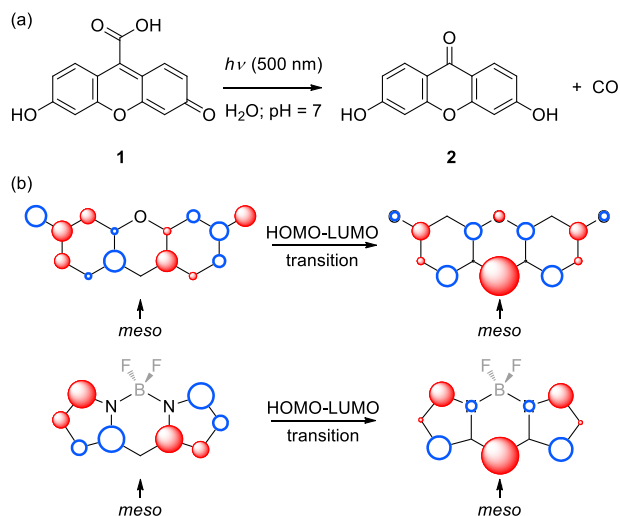
Carbon monoxide is known for its lethal effects in mammals because it binds to hemoglobin more strongly than oxygen.<sup>1</sup> However, it is now evident that CO is an important cell-signaling molecule with substantial therapeutic potential protecting from vascular, inflammatory or even cancer diseases.<sup>2-6</sup>

Carbon monoxide-releasing molecules (CORMs) have been developed to deliver CO into the cell.<sup>3,7-11</sup> The most important criteria for designing CORMs are chemical stability when stored as well as aqueous solubility, temporal control over the CO release and low toxicity in their *in vivo* applications. Unlike other signaling molecules, such as NO or H<sub>2</sub>S, CO is a stable and inert molecule that reacts only with transition metals.<sup>1</sup> Thus, with a few exceptions, such as boranocarbonates<sup>12</sup> or an interesting “click and release” pro-drug system,<sup>13</sup> metal-carbonyl complexes are used as CORMs.<sup>3,4,7-10</sup> The most common activation of CO release from these compounds is hydrolysis in aqueous media that starts immediately upon CORM administration.

Light-triggered CO liberation from a photochemically active CORM (photoCORM<sup>14</sup>) is an alternative activation strategy that allows for a precise spatial and temporal control over the CO release.<sup>15</sup> Transition metal-based complexes offer a relatively good flexibility and diversity in terms of their chemical composition and release efficiencies,<sup>7,9,16</sup> however, only a few such photoCORMs, e.g. polypyridyl metal-lodendrimers,<sup>17</sup> Mn-complexes of azaheteroaromatic ligands<sup>18</sup> or azopyridine,<sup>19,20</sup> absorb biologically benign visible light. CO release upon irradiation with 980 nm from a Mn-based nanocarrier *via* upconversion has also been recently shown.<sup>21</sup> Nevertheless, the design of new photoCORMs, which are chemically stable, nontoxic and release CO efficiently upon visible light exposure, is still a major challenge.

PhotoCORMs based on organic compounds offer a great promise to address this challenge. Several examples of organic molecules, such as cyclopropanones,<sup>22-25</sup> 1,3-cyclobutanediones,<sup>26</sup> or 1,2-dioxolane-3,5-diones,<sup>27</sup> liberate CO upon biologically adverse UV or near-UV (< 420 nm) light. To our knowledge, only two purely organic photoCORMs can be activated by visible light. Liao and coworkers have developed a system based on a cyclic aromatic  $\alpha$ -diketone chromophore that liberates CO upon irradiation with light below ~500 nm.<sup>28</sup> The molar absorption coefficients of such chromophores are however relatively low (only ~1000 dm<sup>3</sup> mol<sup>-1</sup> cm<sup>-1</sup> at 458 nm<sup>29</sup>). Some of us have introduced a fluorescein analogue, 6-hydroxy-3-oxo-3*H*-xanthen-9-carboxylic acid (**1**; Scheme 1a), as a photoCORM that liberates CO along with the formation of 3,6-dihydroxy-9*H*-xanthen-9-one (**2**) upon irradiation below 520 nm in aqueous solutions at pH ~ 7.<sup>30</sup> Although the CO-release quantum efficiency is low ( $\Phi \sim 7 \times 10^{-4}$ ), the uncaging cross-section<sup>15</sup> evaluated as the product of  $\Phi$  and the decadic molar absorption coefficient at the wavelength of irradiation ( $\lambda_{\text{irr}}$ ),  $\Phi \epsilon$ , is large (on the order of 1–10). Unfortunately, the synthesis of this compound is very difficult<sup>30</sup> and we could not find an alternative pathway to produce it in sufficient quantities for further mechanistic studies that would allow us to modify the chromophore properties and shift its absorption to longer wavelengths. We therefore decided to find an alternative chromophore that can be easily synthesized and exhibits similar photoreactivity as **1**.





**Scheme 1.** (a) 6-Hydroxy-3-oxo-3H-xanthene-9-carboxylic acid (**1**) as a photoCORM. (b) A comparison of the frontier MOs (left: HOMO, right: LUMO) of 6-hydroxy-3-oxo-3H-xanthene (top) and BODIPY (bottom; Figure 1) chromophores using the Hückel MO theory. The *meso* position in both chromophores is indicated by an arrow. The BF<sub>2</sub> group of BODIPY (in grey) was not explicitly considered in the Hückel calculation.

Herein, we report the synthesis and properties of the *meso*-carboxy BODIPY (COR-BDP) derivatives **3a,b** (Figure 1) and demonstrate their ability to efficiently release CO. We tested their bioavailability and potential toxicity in both *in vitro* and *in vivo* experimental settings, and we propose the mechanism of the CO release based on steady-state and transient spectroscopy experiments and DFT calculations.

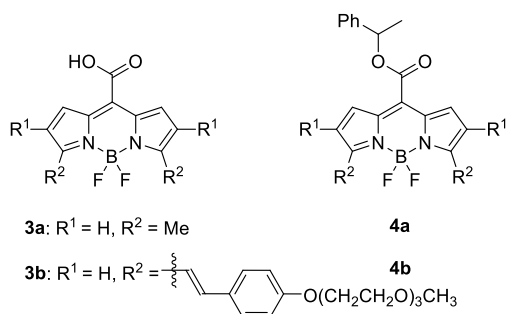


**Figure 1.** Structures of the BODIPY-based photoCORMs (COR-BDPs) **3a–c** and the synthetic precursors **4a,b**.

## Results and Discussion

In our previous work, we hypothesized that an  $\alpha$ -lactone is formed in the *meso* position prior to the CO-release step

upon irradiation of **1**.<sup>30</sup> Such an intermediate should be formed by a formal addition of the carboxylate oxygen to the *meso* position in an excited singlet or triplet state, possibly involving a photoinduced one-electron reduction step. Therefore, an alternative chromophore that preserves the photoreactivity of **1** should possess frontier molecular orbitals (MOs) with similar nodal properties at the *meso* position.<sup>31</sup>

Using Hückel molecular orbital (HMO) calculations, we screened the frontier molecular orbitals (MOs) of several well-known chromophores with strong absorption in the visible region, and we identified that the boron-dipyrromethene (BODIPY) molecule has a similar antisymmetric highest occupied MO (HOMO) compared to that of **1** (Scheme 1b). HMO predicts an increase in electronic density on the *meso* carbon atom upon the HOMO-LUMO excitation for both systems. Therefore, we deduced that *meso*-carboxy BODIPY derivatives (**3**, Figure 1) are promising photoCORM candidates. Many BODIPY derivatives have already received considerable attention in the past decade due to their distinctive and easily tunable optical properties.<sup>32–34</sup>

We first synthesized the model COR-BDP **3a** to evaluate its properties and ability to release CO. The preparation of a *meso*-carboxy BODIPY derivative analogous to **3a** has been recently reported.<sup>35</sup> The benzyl ester **4a** (Figure 1) was prepared as a synthetic precursor from benzyl chlorooxalate and 2-methylpyrrole.<sup>36</sup> This compound was then hydrogenated on Pd/C to obtain **3a** in 82% yield. The compound **3a** is soluble in aqueous solutions (>5 mM) and the pK<sub>a</sub> of its carboxylic group in an aqueous solution, determined by potentiometric titration was found to be (3.0 ± 0.2) (Figure S30). This value corresponds well with the pK<sub>a</sub>s of coumarine-3-carboxylic acid<sup>37</sup> or xanthene-9-carboxylic acid (**1**).<sup>30</sup> Compound **3a** therefore exists as its conjugate base at physiological pH. Another protonation step occurs at a lower pH with pK<sub>a</sub>' = (1.69 ± 0.02) that affects the absorption properties of the chromophore (Figure S31). It is possible that a BF<sub>2</sub> moiety is displaced at such a low pH as observed in the case of other BODIPY derivatives.<sup>38</sup> The compound quickly decomposes at pH < 0.5. It is stable in the crystalline state (>3 weeks) as well as in aqueous solutions (pH = 7.4, >2 weeks) in the dark. The absorption spectrum of an aqueous solution of **3a** (phosphate buffered saline, PBS; pH = 7.4; the ionic strength, *I* = 0.15 mol dm<sup>-3</sup>) shows a major band with  $\lambda_{\max}$  = 502 nm (Figure 2). The compound exhibits a bright fluorescence (Figure 2) with a quantum yield  $\Phi_f$  of 67%. The corresponding excitation spectrum matches that of the absorption (Figure S17).

The compound **3a** underwent a complete decomposition upon irradiation at ~500 nm (Figure 3a) with quantum yields of (2.7 ± 0.4) × 10<sup>-4</sup> and (1.1 ± 0.1) × 10<sup>-4</sup> in degassed and aerated PBS solutions (pH = 7.4), respectively (Table 1).<sup>39</sup> The product of  $\Phi_{\epsilon_{\max}}$  on the order of 10 is comparable to that of some of common caged compounds, especially those absorbing near 400 nm.<sup>15</sup> The quantum yields were independent on the concentration of **3a** (Figures S27–S29). Our GC/RGA analysis of CO released into the headspace of septum-sealed

vials containing an irradiated sample evidenced that the decomposition of **3a** was accompanied by the formation of CO. Its total chemical yield reached 87% upon complete conversion, that is, the quantum yield of decomposition corresponds reasonably to that of CO release. Only UV-light absorbing photoproducts were formed in the solution upon exhaustive irradiation. This is a great advantage as the photoproducts do not interfere with the photochemical process as internal filters.<sup>15</sup> HRMS analysis showed that the major products were 2-methylpyrrol and 2*H*-pyrrole-4-carbaldehyde (Figure S16) in accord with the reports that describe photochemical degradation of other BODIPY derivatives.<sup>40</sup> For comparison, the ester **4a** was irradiated under the same condition as **3a**. This compound was photochemically stable and no CO release was detected. The carboxylic functional group is therefore essential for the reaction.

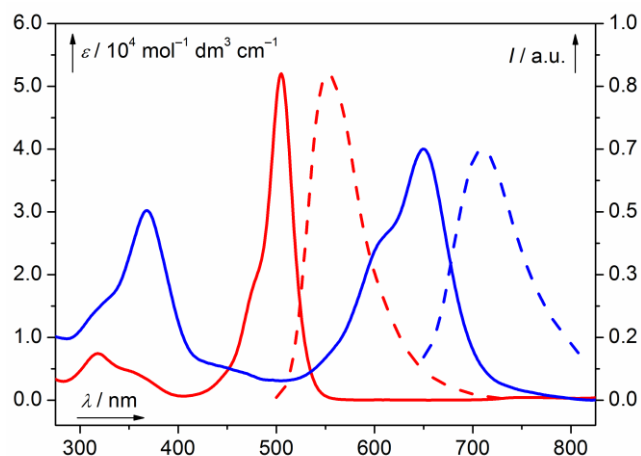


**Figure 2.** Absorption (solid lines) and normalized emission (dashed lines) spectra of **3a** (red) and **3b** (blue) ( $c = 1 \times 10^{-5}$  mol dm<sup>-3</sup>; phosphate buffered saline pH = 7.4;  $I = 0.15$  mol dm<sup>-3</sup>).

Encouraged with the results, we decided to design COR-BDP with a  $\pi$ -extended chromophore to shift the absorption to the phototherapeutic (or tissue-transparent) window (the region of 650–950 nm),<sup>41</sup> desired for biological and medical applications. There is currently no transition-metal-free caged compound that can be directly activated by light in this wavelength region. Only a few chemical systems releasing a chemical species upon irradiation with wavelengths above 450 but below ~600 nm are known,<sup>15</sup> e.g. the (6-hydroxy-3-oxo-3*H*-xanthen-9-yl)methyl<sup>30</sup> or pyronin<sup>42</sup> derivatives introduced by our laboratory, 4-aryloxy BODIPY derivatives proposed by Urano and coworkers,<sup>43</sup> and the *meso*-methylhydroxy BODIPY scaffold designed simultaneously by the groups of Weinstain<sup>44</sup> and Winter.<sup>45</sup>

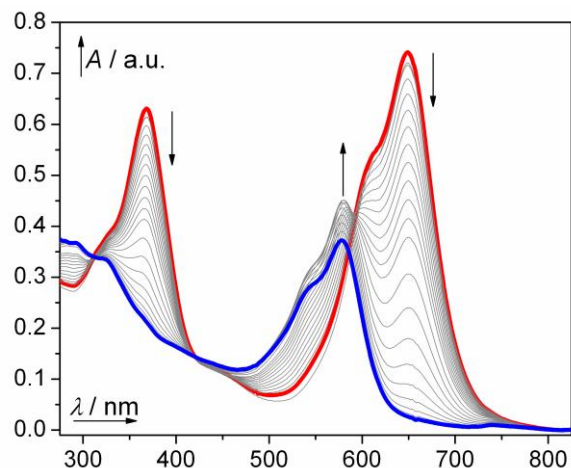
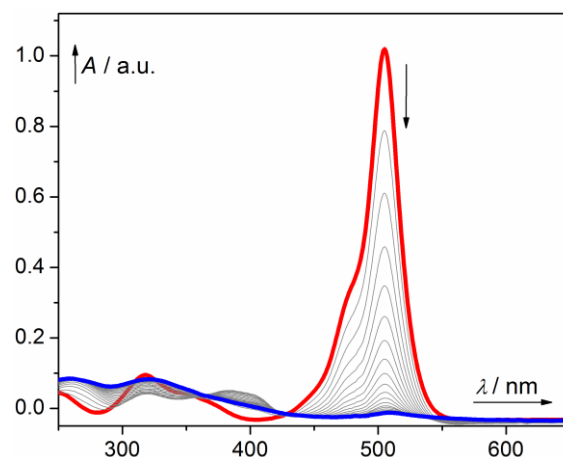


**Figure 3.** Irradiation of **3a** at 500 nm (top) and **3b** at 625 nm (bottom) in aerated phosphate buffer solutions (pH = 7.4). The spectra prior to (red line) and after (blue line) the irradiation are highlighted.

**Table 1. Photochemistry of 3a–c**

compd <sup>a</sup>	$\Phi_{\text{decomp}}/\%$ <sup>b</sup>	yield/ $\%$ <sup>c</sup>	$\epsilon_{\text{max}}$ <sup>d</sup>	$\Phi\epsilon_{\text{max}}$ <sup>e</sup>
<b>3a</b> (deg)	$(2.7 \pm 0.4) \times 10^{-2}$	87	49500	13
<b>3a</b> (aer)	$(1.1 \pm 0.1) \times 10^{-2}$	44		5
<b>3b</b> (deg)	$(1.2 \pm 0.4) \times 10^{-3}$	91	52000	0.6
<b>3b</b> (aer)	$(1.4 \pm 0.4) \times 10^{-3}$	42		0.7

<sup>a</sup> In deg = degassed, aer = aerated phosphate buffer solutions ( $I = 0.1$  M, pH = 7.4). <sup>b</sup> **130** was used as an actinometer for **3a** and **3b**; ferrioxalate actinometer was also used for **3b**. Compound **3b** was irradiated at  $\lambda_{\text{irr}} = 365$  nm (the second major absorption band). <sup>c</sup> The total maximum chemical yields of released CO monitored by a GC/RGA head-space analysis, obtained upon exhaustive irradiation. <sup>d</sup> The molar absorption coefficient,  $\epsilon_{\text{max}}$  / (mol<sup>-1</sup> dm<sup>-3</sup> cm<sup>-1</sup>). <sup>e</sup> The uncaging cross-section at  $\lambda_{\text{max}}$ . n.r. = not relevant for CO release.

We synthesized COR-BDP **3b** by condensation of **4a** with the corresponding PEG-substituted benzaldehyde in the presence of piperidine in glacial acetic acid and subsequent hydrogenation on Pd/C in 56% yield. The 3,5-distyryl groups in **3b** affect the absorption properties of the BODIPY chromophore by extending the  $\pi$ -conjugation, whereas PEG chains enhance its aqueous solubility. The major absorption band of this compound (652 nm, tails to  $\sim$  750 nm; Figure 2) is bathochromically shifted by  $\sim$ 150 nm compared to that of **3a**. Excitation of **3b** at either of the main absorption bands ( $\lambda_{\text{max}} = 368$  and 652 nm) resulted in the same fluorescence spectrum (Figure 2), that is, in the same emitting excited state. The presence of two styryl groups in **3b** are probably responsible for its lower fluorescence quantum yield ( $\Phi_f = 12\%$ ) as compared to that of **3a** due to enhanced radiationless decay of the singlet excited state.<sup>46,47</sup>

Two protonation steps with  $\text{p}K_{\text{a}}' = (4.71 \pm 0.01)$  and  $\text{p}K_{\text{a}} = (3.0 \pm 0.2)$ , respectively, have been identified, thus the conjugate base of **3b** is present at physiological pH (Figure S32). Irradiation of **3b** in an aqueous solution (PBS, pH = 7.4) released CO not only upon excitation at the major absorption band maxima (368 and 652 nm) but also at the absorption tail in the near-infrared region (732 nm). To our knowledge, COR-BDP **3b** is therefore the first caged compound that efficiently releases a molecule upon direct irradiation with near-infrared photons. Although the product of  $\Phi_{\text{E}}$  decreases at longer wavelengths (see Table 1), it is still suitable for biological applications because the light penetrates deeply into the tissue.

This premise was confirmed by an *in vivo* experiment with a nude SKH1 mouse strain (Table 2). Hairless mice were used to facilitate light penetration through the cutaneous barrier. One group of mice that was not treated with **3b** served as a control group. Two other groups received intraperitoneal application of **3b** (50  $\mu\text{mol}$  per kg of body weight). One group was left in the dark while the other was irradiated with white light focused to the abdominal area of mice for 4 h. Irradiation resulted in a substantial increase in both the carbonyl-hemoglobin (COHb) concentration in blood and the CO content in hepatic and kidney tissues, when compared to both non-treated and non-irradiated control groups. It should be noted that although non-irradiated mice treated with **3b** were carefully kept in the dark, inadvertent light exposure of biological material (blood, liver), still containing unreacted **3b** during sampling, resulted in increased levels of COHb. Nevertheless, statistically unequivocal increase in the CO levels in both blood and tissues of irradiated mice compared to both control groups (by factors of 1.5–2) clearly demonstrate that CO was photoreleased *in vivo*. Heme oxygenase induction, a possible source of CO overproduction, was excluded by a direct determination of heme oxygenase activity (Figure S49). In addition, an *in vitro* sample of blood containing **3b** was irradiated with white light, and the production of CO was detected by GC (Table S2).

The CO release from **3b** is accompanied by the concomitant formation of a yet-unidentified primary photoproduct that remains in the solution even after a prolonged photolysis (<10% conversion after 24 hours) at wavelengths close to its absorption maximum ( $\lambda_{\text{max}} = 578$  nm; Figure 3b). Based on the absorption spectrum, this compound still probably contains a BODIPY chromophore, but it does not represent an internal filter when the irradiation is conducted at wavelengths longer than the  $\lambda_{\text{max}}$  of **3b**. The decomposition quantum yields, yields of CO release upon exhaustive irradiation, and the uncaging cross-sections,  $\Phi_{\text{E}_{\text{max}}}$ , of **3b** when aerated or degassed samples were used are summarized in Table 1.

**Table 2. CO Release from **3b** upon Irradiation *in vivo***

group	$w_{\text{COHb}}^{\text{blood}} / \%$ <sup>d</sup>	$c_{\text{CO}}^{\text{liver}} / \text{pmol}^e$	$c_{\text{CO}}^{\text{kidney}} / \text{pmol}^f$
control <sup>a</sup>	$0.36 \pm 0.06$	$5.6 \pm 1.2$	$7.1 \pm 1.7$
dark <sup>b</sup>	$0.57 \pm 0.04^g$	$7.1 \pm 1.1$	$7.0 \pm 0.8$
irradiated <sup>c</sup>	$0.78 \pm 0.18^{g,h}$	$11.3 \pm 2.7^{g,h}$	$10.1 \pm 0.8^{g,h}$

<sup>a</sup>A control group of 6 animals (no **3b** application). Another group of 12 animals received an intraperitoneal injection of **3b** in saline (50  $\mu\text{mol}$  per kg of body weight), from which <sup>b</sup> 6 mice were kept in the dark and <sup>c</sup> 6 mice were irradiated with white light focused to the abdominal area. <sup>d</sup> $w_{\text{COHb}}^{\text{blood}}$ : the relative amounts of COHb in the total amount of Hb in blood (in %); <sup>e</sup> $c_{\text{CO}}^{\text{liver}}$  and <sup>f</sup> $c_{\text{CO}}^{\text{kidney}}$ : the amounts of CO in pmol per 1 mg of a fresh liver and kidney tissue, respectively. The statistical significance: <sup>g</sup> *P*-value  $\leq 0.05$  vs. “control group”. <sup>h</sup> *P*-value  $\leq 0.05$  vs. “dark group”; *n* = 6 in each mice group.

A controlled, steady and long-lasting CO production is crucial for biologic applications. Our GC/RGA analysis revealed a steady CO release for 100 h and 26 h using **3a** (e.g., Figure 4) and **3b**, respectively. The release rate depends on the intensity of the incident light. The formation of CO ceased immediately when the irradiation was interrupted, allowing for complete control over the CO release.

Neither of **3a,b** nor their photoproducts displayed toxicity<sup>48</sup> in our *in vitro* experiments on hepatoblastoma HepG2 and/or neuroblastoma SH-SY5Y cell lines up to concentrations of 100  $\mu\text{mol l}^{-1}$  (Figure S39).

The influence of oxygen on the photolysis quantum yield of **3a** ( $\Phi_{\text{decomp}}$  is lower by a factor of 2 in an aerated sample; Table 1) suggested that its triplet state might be involved in the CO release. The formation of a triplet state in **3a** is apparently not efficient due to fluorescence ( $\Phi_f = 67\%$ ) and perhaps other radiationless processes, and this may also partially explain the rather low decomposition quantum yields. We thus synthesized a diiodo derivative **3c** (the synthesis and its photochemical properties are described in

Supporting Information) to enhance the intersystem crossing (isc) rate via a heavy-atom effect as demonstrated on other BODIPY derivatives. For example, the isc quantum yield can reach 0.66 in a hexabromo-substituted BODIPY.<sup>49</sup> The absorption properties of **3c** are similar to those of **3a** (Figures 2 and S23), however, its fluorescence quantum yield dropped to  $\Phi_f = 2\%$  as expected. Unfortunately, the total chemical yield of released CO was very low ( $\sim 3\%$ ) in the case of **3c**. We concluded that the triplet excited **3c** undergoes a photoreaction that does not lead to the CO production (see Supporting Information) either due to an alternative reaction pathway (i.e., a C–I bond fission) or bleaching by the generated singlet oxygen.

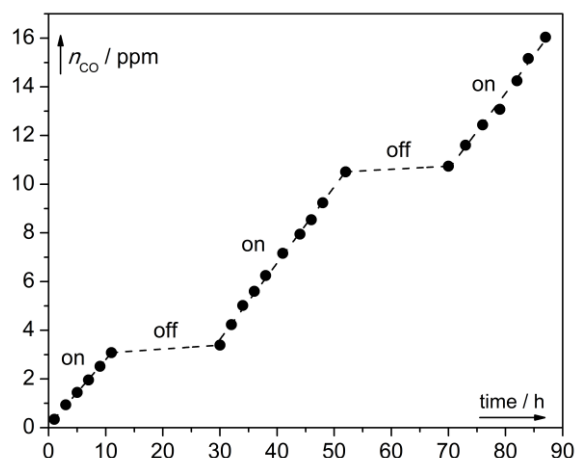


**Figure 4.** CO Production from **3a**. **3a** (500  $\mu\text{M}$ , PBS solution) was irradiated at 510 nm ( $11.6 \text{ mW cm}^{-2}$ ). The CO released to the vial headspace was measured by GC/RGA in 2–4 h intervals and expressed as the amount of CO (in ppm) released from **3a**. When irradiation (on) was interrupted (off), the vial was kept in dark at 4  $^{\circ}\text{C}$ .

Nevertheless, laser flash spectroscopy of the compound **3c** helped us to assign the transient absorption signals of triplet **3a** that are of low intensity due to its inefficient isc. The transient triplet-triplet absorption spectrum of **3c** possesses three absorption maxima at 325, 415 and 660 nm (Figures S36–S38) which exhibit the same decay kinetics. Triplet-state absorption bands in the region of 410–450 nm have already been reported for analogous brominated BODIPY derivatives.<sup>49</sup> The lifetimes of the triplet **3c** under different conditions are shown in Table S1. The triplet state is markedly quenched by oxygen; the lifetime of ( $34.5 \pm 0.62$ )  $\mu\text{s}$  in a degassed aqueous buffer solution at pH = 7.4 dropped to ( $0.50 \pm 0.02$ )  $\mu\text{s}$  in an oxygen-saturated sample. The triplet of **3a** possesses absorption maxima at 430 and 640 nm with a lifetime of  $\sim (5 \pm 1)$   $\mu\text{s}$  in an aerated solution (Figure S35).

Final evidence that a triplet state is involved in the CO release was provided by irradiation of **3a** in a degassed aqueous solution containing CsCl (1 M aqueous solution; an analogous NaCl-containing sample was used as a reference) as a

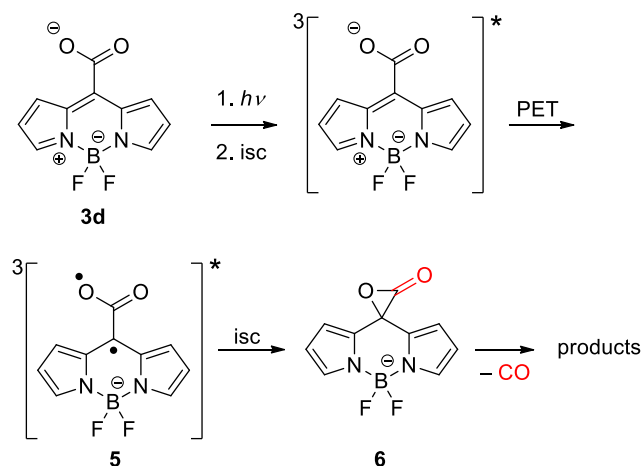
heavy-atom effect mediator<sup>50</sup> (Figure S34). We monitored the major absorption band of **3a** and observed that  $\Phi_{\text{decomp}}$  increased by the factor of 1.6 in the presence of Cs<sup>+</sup> ions due to the isc-rate enhancement, while the fluorescence quantum yield decreased from 67% to 53%. The rate of the CO release monitored by a GC/RGA head-space analysis increased accordingly and matched that of **3a** decomposition.

This result has motivated us to further explore the reaction mechanism. When a solution of **3a** was irradiated at pH = 2.5 where only 25% of **3a** exist in the form of the conjugate base, a decrease in  $\Phi_{\text{decomp}}$  by a factor of  $\sim 4$  was observed (Figure S29). This suggests that the negative charge on the carboxyl group is essential for the reaction. The proton dissociation strongly influences the redox properties. For example, carboxylic acids have redox potentials which are more positive than those of the corresponding carboxylates by  $\sim 0.5$  V.<sup>51</sup> The ground state redox potential for **3a** was determined by cyclic voltammetry ( $-1.02$  V vs SCE; the one-electron oxidation of **3a** (as a conjugate base) occurs at  $+0.13$  V vs. SCE; Figure S33). The former value corresponds well to the published data for other BODIPY derivatives.<sup>52–53</sup> The energy of the triplet-excited state of a BODIPY can be estimated from the phosphorescence spectra of the dibromo ( $\lambda_{\text{phos}} = 740$  nm, 1.68 eV)<sup>54</sup> or diiodo derivatives ( $\lambda_{\text{phos}} = 795$  nm, 1.56 eV).<sup>55</sup> Using the latter value, the triplet state redox potential equals to  $+0.54$  V vs SCE. As a result,  $\Delta G_{\text{ET}}$  of an intramolecular electron transfer between the carboxylate anion attached to an aromatic system and the excited triplet BODIPY moiety equals to  $\sim -0.41$  eV ( $-9.5 \text{ kcal mol}^{-1}$ ). In contrast, electron transfer between the protonated carboxylic acid and the BODIPY would be slightly endothermic ( $\sim +0.09$  eV;  $+2 \text{ kcal mol}^{-1}$ ). Therefore, we assumed that a photoinduced intramolecular electron transfer (PET) takes place between the carboxylate and the BODIPY system in the triplet excited state.

Such PET would result in the formation of a triplet diradical **5** (Scheme 2) with one electron on the carboxylate moiety and the other largely localized in the *meso* position of the BODIPY core (see HMOs in Scheme 1b). Such a structure resembles the oxyallyl diradical, formation of which via photolysis of *p*-hydroxyphenacyl derivatives in aqueous solution was recently studied by some of us.<sup>56</sup> Its decay from a triplet to an open-shell singlet state is followed by the formation of an intermediate with a three-membered ring that can readily decarbonylate, and that can be considered as a structural analogue of the  $\alpha$ -lactone **6** (Scheme 2). Liberation of CO from  $\alpha$ -lactones in the dark has previously been described.<sup>57,58</sup> In our previous study on 6-hydroxy-3-oxo-3*H*-xanthene-9-carboxylic acid (**1**),<sup>39</sup> the density functional theory (DFT) calculations failed to provide an evidence for the existence of the related  $\alpha$ -lactone. We therefore decided to examine whether **6** may be formed prior to the CO release (Scheme 2). Here, we attempted to find a potential energy minimum that would correspond to the structure of **6** on the singlet ground state potential energy surface. By screening a series of well-performing functionals (see Supporting Information for a detailed technical description), we found that



the heterolysis of the  $\alpha$ -lactone ring represents a difficult case to DFT methods. Thorough test calculations with a smaller but structurally similar model to **6** (Supporting Information), which allowed the use of accurate perturbation and coupled-cluster methods, showed that the Mo6HF functional, which predicted that an energy minimum for **6** does exist, performs best of all the DFT methods. We therefore conclude that the formation of **6** is feasible.



**Scheme 2.** The proposed mechanism of COR-BDP photo-transformation to release CO

Based on our experimental and computational evidence, we propose the mechanism of CO release from COR-BDPs **3** (Scheme 2). Upon excitation, a strongly fluorescent, lowest excited singlet state of **3** undergoes relatively inefficient intersystem crossing to the triplet state where an exergonic PET from the carboxylate to the BODIPY chromophore takes place, resulting in the formation of an oxallyl-type triplet diradical **5**. The subsequent intersystem crossing leads to the formation of  $\alpha$ -lactone **6** on the singlet ground-state potential energy surface. The compound **6** then undergoes a non-photochemical fragmentation to release CO.

## Conclusions

We report a straightforward synthesis of a new generation of transition-metal-free CORMs based on BODIPY chromophores (COR-BDPs) that are activatable by visible-to-NIR (up to 730 nm) light. Such wavelengths are highly advantageous due to a better penetration of the light into biological tissues. We show the ability of COR-BDPs to efficiently release CO in a fully controllable way, and demonstrate their performance in both *in vitro* and *in vivo* experimental settings. The fluorescent nature of the chromophores is also desirable for simultaneous *in vivo* imaging. We propose a mechanism of the CO release based on steady-state and transient absorption spectroscopy experiments and quantum chemical calculations. The BODIPY molecular scaffold allows for fine-tuning of the physico-chemical properties of COR-BDPs (such as optical properties or aqueous solubility) using

simple structural modification and promises a rapid development of improved CORM molecules. Further biological studies to prove the therapeutic potential of the COR-BDPs are under investigation in our laboratories.

## Experimental Section

**Synthesis of 4a.** Benzyl chlorooxalate (556 mg, 2.8 mmol) was added to a solution of 2-methylpyrrole (500 mg, 6.16 mmol) in dichloromethane at 0 °C, and the mixture was stirred for 4 h at 0 °C. Triethylamine (1.96 mL, 14 mmol) was added, followed by an addition of  $\text{BF}_3 \cdot \text{Et}_2\text{O}$  (1.68 mL, 14 mmol). The solution was warmed to room temperature and stirred for 2 h. The reaction was quenched with aq HCl (10%), and the crude product was extracted with ethyl acetate. The organic layers were washed with water, dried with  $\text{MgSO}_4$ , filtered and the solvents were evaporated to dryness. The compounds were purified by flash chromatography on silica gel using hexane/ethyl acetate (9 : 1) to give the pure compound **4a**. Yield: 110 mg (11%). Purple solid. Mp: >300 °C (decomp.).  $^1\text{H}$  NMR (500 MHz,  $\text{CDCl}_3$ ):  $\delta$  (ppm) 7.48–7.40 (m, 5H, 5 CH), 7.19 (d,  $J = 3.8$  Hz, 2H, 2CH), 6.30 (d,  $J = 3.9$  Hz, 2H, 2CH), 5.45 (s, 2H,  $\text{CH}_2$ ), 2.64 (s, 6H, 2 $\text{CH}_3$ ) (Figure S1).  $^{13}\text{C}$  NMR (125 MHz,  $\text{CDCl}_3$ ):  $\delta$  (ppm) 163.7 (C), 160.7 (C), 134.7 (C), 133.5 (C), 130.8 (CH), 128.8 (CH), 128.6 (CH), 128.0 (C), 120.7 (CH), 120.6 (CH), 68.2 ( $\text{CH}_2$ ), 15.2 ( $\text{CH}_3$ ) (Figure S2). FTIR (neat): 3065, 1725, 1567, 1458, 1374, 1163, 1101  $\text{cm}^{-1}$ . HRMS (APCI): calcd for ( $\text{C}_{19}\text{H}_{17}\text{BF}_2\text{N}_2\text{O}_2$ ) 353.1460, found 353.1459 (Figure S11).

**Synthesis of 4b.** 4-{2-[2-(2-methoxyethoxy)ethoxy]-ethoxy}benzaldehyde (66 mg, 0.22 mmol), glacial acetic acid (0.08 mL, 1.8 mmol), piperidine (0.12 mL, 1.8 mmol) and a small amount of molecular sieves were added to a solution of **4a** (40 mg, 0.11 mmol) dissolved in anhydrous benzene (10 mL) in a round-bottomed flask equipped with a Dean-Stark head under argon atmosphere. The mixture was refluxed for 1 h. The solvent was then removed under reduced pressure, and the residue was diluted with ethyl acetate and washed with water. The organic layer was dried with  $\text{MgSO}_4$ , filtered and concentrated under reduced pressure. The crude mixture was purified by flash chromatography on silica gel using hexane/dichloromethane (2 : 8) to give **4b**. Yield: 66 mg (70%). Green solid. Mp: >280 °C (decomp.).  $^1\text{H}$  NMR (500 MHz,  $\text{CDCl}_3$ ):  $\delta$  (ppm) 7.55–7.49 (m, 6H, 6CH), 7.39–7.30 (m, 5H, 5CH), 7.25–7.22 (m, 4H, 4CH), 6.88 (d,  $J = 8.8$  Hz, 4H, 4CH), 6.29 (d,  $J = 4.6$  Hz, 2H, 2CH), 5.35 (s, 2H,  $\text{CH}_2$ ), 4.11 (t,  $J = 4.8$  Hz, 4H, 2- $\text{OCH}_2$ ), 3.82 (t,  $J = 4.9$  Hz, 4H,  $\text{OCH}_2$ ), 3.69–3.67 (m, 4H,  $\text{OCH}_2$ ), 3.63–3.58 (m, 8H,  $\text{OCH}_2$ ), 3.49–3.47 (m, 4H,  $\text{OCH}_2$ ), 3.31 (s, 6H,  $\text{OCH}_3$ ) (Figure S3).  $^{13}\text{C}$  NMR (125 MHz,  $\text{CDCl}_3$ ):  $\delta$  (ppm) 164.2 (C), 160.2 (C), 156.5 (C), 138.1 (CH), 136.0 (C), 135.0 (C), 129.6 (CH), 129.5 (CH), 129.4 (CH), 128.8 (CH), 128.7 (CH), 128.6 (CH), 122.6 (C), 117.4 (CH), 115.1 (CH), 72.0 ( $\text{CH}_2$ ), 70.9 ( $\text{CH}_2$ ), 70.7 ( $\text{CH}_2$ ), 70.6 ( $\text{CH}_2$ ), 69.7 ( $\text{CH}_2$ ), 67.6 ( $\text{CH}_2$ ), 59.0 ( $\text{CH}_3$ ) (Figure S4). FTIR (neat): 3085, 2920, 2851, 1717, 1593, 1349, 1158, 949  $\text{cm}^{-1}$ ; HRMS

(ESI): calcd for (C<sub>47</sub>H<sub>53</sub>BF<sub>2</sub>N<sub>2</sub>O<sub>10</sub>) 854.3761, found 854.3756 (Figure S12).

**Synthesis of 3a.** **4a** (50 mg, 0.14 mmol) was dissolved in dichloromethane (20 mL), and 10% Pd/C powder (5 mol%) was added under argon atmosphere, followed by addition of methanol (20 mL). The mixture was saturated with hydrogen, and stirred at 25 °C for 2 h until no starting material remained. Pd/C was removed through filtration, and the solvent was evaporated under reduced pressure. The products were purified using flash chromatography using dichloromethane/methanol (8 : 2) on silica gel to give **3a**. Yield: 32 mg (82%). Yellow-orange solid. Mp: 250 °C (decomp.). <sup>1</sup>H NMR (500 MHz, D<sub>2</sub>O):  $\delta$  (ppm) 7.13 (d,  $J$  = 4.1 Hz, 2H, 2CH), 6.43 (d,  $J$  = 4.1 Hz, 2H, 2CH), 2.53 (s, 6H, 2CH<sub>3</sub>) (Figure S5). <sup>13</sup>B NMR (125 MHz, D<sub>2</sub>O):  $\delta$  (ppm) 170.5 (C), 158.6 (C), 139.0 (C), 131.2 (C), 129.7 (CH), 120.1 (CH), 14.2 (CH<sub>3</sub>) (Figure S6). FTIR (neat): 3321, 3065, 1725, 1567, 1261, 1101, 1007, 945 cm<sup>-1</sup>. HRMS (APCI): calcd for (C<sub>12</sub>H<sub>11</sub>BF<sub>2</sub>N<sub>2</sub>O<sub>2</sub>) 262.0845, found 262.0844 (Figure S13).

**Synthesis of 3b.** **3b** was synthesized according to the same procedure as **3a** from **4c** (40 mg, 0.047 mmol). Yield: 19 mg (53%). Blue solid. Mp: >255 °C (decomp.). <sup>1</sup>H NMR (500 MHz, CD<sub>3</sub>OD):  $\delta$  (ppm) 7.62–7.57 (m, 6H, 6CH), 7.46 (d,  $J$  = 16.4 Hz, 2H, 2CH=CH), 7.28 (d,  $J$  = 4.4 Hz, 2H, 2CH), 7.06–7.02 (m, 6H, 6CH), 4.24 (t,  $J$  = 4.5 Hz, 4H, OCH<sub>2</sub>), 3.89 (t,  $J$  = 4.6 Hz, 4H, OCH<sub>2</sub>), 3.74–3.72 (m, 4H, OCH<sub>2</sub>), 3.69–3.64 (m, 8H, OCH<sub>2</sub>), 3.56–3.54 (m, 4H, OCH<sub>2</sub>), 3.37 (s, 6H, OCH<sub>3</sub>) (Figure S7). <sup>13</sup>B NMR (125 MHz, CD<sub>3</sub>OD):  $\delta$  (ppm) 169.6 (C), 159.9 (C), 154.6 (C), 135.7 (CH), 133.8 (C), 129.7 (C), 128.5 (CH), 116.9 (CH), 115.3 (CH), 114.8 (CH), 71.5 (CH<sub>2</sub>), 70.4 (CH<sub>2</sub>), 70.2 (CH<sub>2</sub>), 70.0 (CH<sub>2</sub>), 69.4 (CH<sub>2</sub>), 67.4 (CH<sub>2</sub>), 57.7 (CH<sub>3</sub>) (Figure S8). FTIR (neat): 3331, 3075, 1721, 1575, 1302, 1132, 1007, 944 cm<sup>-1</sup>; HRMS (ESI): calcd for (C<sub>40</sub>H<sub>47</sub>BF<sub>2</sub>N<sub>2</sub>O<sub>10</sub>) 764.3292, found 764.3291 (Figure S14).

**General Procedure for Irradiation in UV Cuvettes.** A solution of a compound in the given solvent (3 mL) in a matched 1.0 cm quartz PTFE screw-cap cuvette equipped with a stir bar was stirred and irradiated with a light source of 32 LEDs emitting at the selected wavelength:  $\lambda_{\text{max}}$  = 365, 503, 525, 590, or 625 nm (the bandwidths at half height = 30 nm). Light pulses (425.6 Hz repetition rate,  $\leq$  150 fs pulse length and energy of  $\sim$ 7.5  $\pm$  0.3 mW) from a Ti:Sapphire laser coupled to a noncollinear optical parametric amplifier (NOPA) with the wavelength set to 505 (bandwidth at half height of  $\sim$ 15 nm) were used to irradiate samples at 505 nm. A 400 W broad-band halogen lamp with a filter (transmittance spectrum is shown in Figure S23) was used to irradiate samples at 732 nm. The progress of reactions was monitored by UV-vis spectrometry using a diode-array spectrophotometer in a kinetic mode.

**Quantum Yield Determination.** The decomposition quantum yields of **3a** and **3b** were determined using a solution of xanthene-9-carboxylic acid (**1**,  $c$  = 1.0  $\times$  10<sup>-5</sup> M in aq phosphate buffered saline (PBS,  $I$  = 0.1 M, pH = 7.4;  $\Phi_{\text{disapp.}}$  = (6.8  $\pm$  3.0)  $\times$  10<sup>-4</sup>)<sup>30</sup> as an actinometer and light pulses at 505

$\pm$  7 nm (see above). The quantum yield of photodegradation of **3b** was determined at 365 nm with ferrioxalate actinometer<sup>59</sup> according to the published procedure.<sup>60</sup> The data were processed using a single value decomposition (SVD) software.

**Determination of the Photoproducts.** **3a** (500 mL,  $c \sim$  1  $\times$  10<sup>-5</sup> M, aq. solution) was irradiated in a large Petri dish (50 cm diameter) with a halogen lamp (500 W, Pyrex filter) for 38 hours to reach a full conversion (the solution is photo-bleached). The resulting mixture was lyophilized to give the photoproducts which were analyzed by HRMS (Figure S16).

**Spectrophotometric Determination of pK<sub>a</sub>s.** A freshly prepared solution of **3a-c** ( $c$  = 2.5  $\times$  10<sup>-5</sup> M) in PBS (3 mL,  $I$  = 0.1 M, pH  $\sim$  7.4) was transferred into a matched 1.0 cm quartz cuvette, and its UV-vis absorption spectrum was recorded. The solution was acidified with HCl to pH  $\sim$  1 (10  $\mu$ L of a 1 M solution) and was titrated with small additions of aq NaOH (typically 10  $\mu$ L; 0.1 M, 0.01 M or 0.001 M;  $I$  = 0.1 M, adjusted by NaCl) and the pH and UV-vis absorption spectra were monitored after each addition (Figures S31-S32).

**Potentiometric Determination of pK<sub>a</sub>s.** A freshly prepared solution of **3a-c** ( $c$  = 1  $\times$  10<sup>-3</sup> M) in distilled water (5 mL) was stirred in a 25 mL beaker. The pH was measured potentiometrically, and the solution was acidified by HCl to pH  $\sim$  1 (10  $\mu$ L, 1 M solution). The acidified solution was titrated with small additions of aq NaOH (typically 10  $\mu$ L; 0.1 M, 0.01 M or 0.001 M;  $I$  = 0.1 M, adjusted by NaCl), and the pH was measured after each addition. The volume of the added aq NaOH corresponding to every change in pH was recorded and the titration curve constructed (Figure S30).

**Cyclic Voltammetry.** Electrochemical studies were carried out with compounds dissolved in acetonitrile containing 0.1 M tetra-*n*-butylammonium hexafluorophosphate as a conducting salt using the ferrocene/ferrocenium (Fc/Fc<sup>+</sup>) couple as an internal standard under argon atmosphere (Figure S33). The measurements were carried out in an optically transparent thin-layer electrochemical cell (0.1 mm optical length). A Pt minigrad working electrode, Pt minigrad reference electrode and silver wire pseudo-reference electrode were used. The measured potentials were recalculated to potentials vs SCE according to the published procedure.<sup>61</sup>

**Determination of CO Concentrations.** A solution of **3a-c** (0.25–2 mM) in PBS (20–150  $\mu$ L,  $I$  = 0.1 M, pH  $\sim$  7.4) was added into CO-free septum-sealed glass vials. After irradiation with white light (433 mW cm<sup>-2</sup>; 10 cm from the light source) or (510  $\pm$  5) nm (11.6 mW cm<sup>-2</sup>; Edmund Optics Barrington filter No. 65152), the CO amount released into the vial headspace was determined by gas chromatography with a reduction gas analyzer described previously.<sup>62</sup>

**In Vitro Toxicity Determination.** Human neuroblastoma SHSY5Y and hepatoblastoma HepG2 cell lines were grown according to the manufacturer's protocol in a 96-well plate with solutions of **3a** and **3b** or their photoproducts in the concentration range of 10–100  $\mu$ M for 4, 24 or 48 h. The via-

bility of cell lines was determined by a 3-(4,5-dimethylthiazol-2-yl)-2,5-diphenyltetrazolium bromide assay (MTT). After 2 h incubation period with MTT, the absorbance of a formazan-reduction product was measured at 545 nm with a standard ELISA reader. The compounds **3a** and **3b** were found not to interfere with the reduction of MTT.

**In Vivo Experiments.** Male nude SKH1 mice, were allowed water and standard granulated diet *ad libitum*. All studies in this work met the criteria for the care and use of animals, and were approved by the Animal Research Committee of the 1<sup>st</sup> Faculty of Medicine, Charles University in Prague. Mice were anesthetized and then received an intraperitoneal injection of saline (a control group) or a solution of **3b** in saline (50  $\mu\text{mol}$  per 1 kg of body weight). An experimental group of mice was irradiated with a lamp focused to the abdominal area for 4 h while a control group was kept in the dark. Subsequently, the animals were sacrificed. Blood from superior vena cava of each animal was transferred to the test tubes containing aq solution of EDTA (2  $\mu\text{L}$ ; 0.5 M). The CO (as COHb) and total hemoglobin concentrations in the sample of blood (1  $\mu\text{L}$ ) were determined using GC and a Drabkin cyanmethemoglobin method described previously.<sup>63</sup> Liver and kidneys of each animal were then harvested, washed, put into an ice-cold potassium phosphate buffer ( $c = 0.1$  M,  $\text{pH} = 7.4$ ) in a ratio 1:4 (w/w) and homogenized by sonication. The liver/kidneys homogenate (40  $\mu\text{L}$ ) was added to CO-free septum-sealed vials containing 5  $\mu\text{L}$  of 60% (v/w) sulfosalicylic acid. After incubation on ice (30 min), the amount of the CO released into the vial headspace was determined by GC/RGA as reported previously.<sup>64</sup>

**Statistical Analyses.** The data from *in vivo* experiments are expressed as mean  $\pm$  standard deviation. The Student's t-test was used to determine the significance of the differences among the study mice groups. The resulting *P*-values  $\leq 0.05$  (Table 2) are considered as statistically significant.

**Quantum Chemical Calculations.** The Hückel molecular orbital theory calculations were done with a freeware program HULIS.<sup>65,66</sup> The structure of the BODIPY chromophore was approximated with dipyrin because Hückel theory applies only to  $\pi$ -systems. The density functional theory (DFT) and *ab initio* calculations were performed with the Gaussian 09 package<sup>67</sup> of electronic structure programs. Gas-phase constrained geometry optimizations to compute the potential energy surfaces along the *meso*-carbon of BODIPY and the oxygen of  $\alpha$ -lactone bond length were performed with a series of DFT (B3LYP, CAM-B3LYP, BMK, Mo6HF, Mo6-2X and  $\omega$ B97X) and perturbation theory (MP2 and MP4(SDQ)) methods with a 6-311+G(d) basis set. Full geometry optimization were performed with selected DFT methods with 6-31G(d) or 6-311+G(d) basis sets using the polarizable continuum model (PCM) as implemented in Gaussian to mimic the solvation effects (acetonitrile or water) or the gas phase. Harmonic vibrational frequencies were computed for the stationary points. Single point energies on the geometries

obtained by the constrained geometry optimization at the MP4(SDQ)/6-311+G(d) or Mo6HF/6-311+G(d) level of theory were computed by MP4(SDQ), QCISD(T) and CCSD(T) *ab initio* methods with the use of cc-pVTZ basis set.

## ASSOCIATED CONTENT

### Supporting Information

Materials and methods; synthesis of **3c**; spectroscopy results; toxicity and heme oxygenase activity measurements; details of quantum chemical calculations and additional characterization data. The Supporting Information is available free of charge on the ACS Publications website at DOI: 10.1021/

## AUTHOR INFORMATION

### Corresponding Author

\* klan@sci.muni.cz

### Author Contributions

|| These authors contributed equally to this work.

### Notes

The authors declare no competing financial interests.

## ACKNOWLEDGMENT

Support for this work was provided by the Czech Science Foundation (GA13-25775S) (P. K.) and Czech Ministry of Health (RVO-VFN64165/2015) (L. V.). The RECETOX research infrastructure was supported by the projects of the Czech Ministry of Education (LO1214) and (LM2011028). The authors also thank Marie Zadinová and Jakub Šuk for their technical assistance with *in vivo* experiments, Jana Vaníková for performing MTT assays, Kateřina Klánová for her help with TOC, and Jakob Wirz for fruitful discussions.

## References

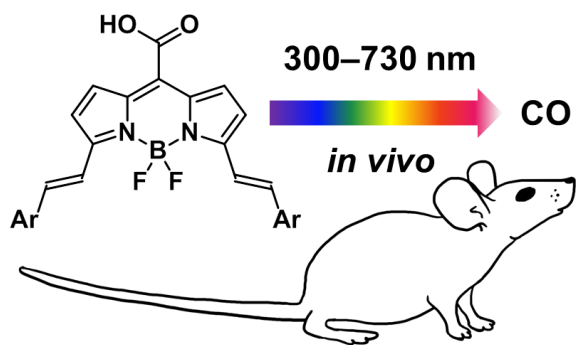
- (1) Boczkowski, J.; Poderoso, J. J.; Motterlini, R. *Trends Biochem. Sci.* **2006**, *31*, 614.
- (2) Motterlini, R.; Otterbein, L. E. *Nat. Rev. Drug Discov.* **2010**, *9*, 728.
- (3) Romao, C. C.; Blattler, W. A.; Seixas, J. D.; Bernardes, G. J. L. *Chem. Soc. Rev.* **2012**, *41*, 3571.
- (4) Garcia-Gallego, S.; Bernardes, G. J. L. *Angew. Chem. Int. Ed.* **2014**, *53*, 9712.
- (5) Ahmad, S.; Hewett, P. W.; Fujisawa, T.; Sissaoui, S.; Cai, M.; Gueron, G.; Al-Ani, B.; Cudmore, M.; Ahmed, S. F.; Wong, M. K. K.; Wegiel, B.; Otterbein, L. E.; Vitek, L.; Ramma, W.; Wang, K. Q.; Ahmed, A. *Thromb. Haemostasis* **2015**, *113*, 329.
- (6) Vitek, L.; Gbelcova, H.; Muchova, L.; Vanova, K.; Zelenka, J.; Konickova, R.; Suk, J.; Zadinova, M.; Knejzlik, Z.; Ahmad, S.; Fujisawa, T.; Ahmed, A.; Ruml, T. *Digest. Liver Dis.* **2014**, *46*, 369.
- (7) Schatzschneider, U. *Br. J. Pharmacol.* **2015**, *172*, 1638.

- (8) Heinemann, S. H.; Hoshi, T.; Westerhausen, M.; Schiller, A. *Chem. Commun.* **2014**, *50*, 3644.
- (9) Schatzschneider, U. *Eur. J. Inorg. Chem.* **2010**, 1451.
- (10) Mann, B. E. *Organometallics* **2012**, *31*, 5728.
- (11) Motterlini, R.; Mann, B. E.; Foresti, R. *Expert Opin. Inv. Dr.* **2005**, *14*, 1305.
- (12) Motterlini, R.; Sawle, P.; Hammad, J.; Bains, S.; Alberto, R.; Foresti, R.; Green, C. J. *FASEB J.* **2005**, *19*, 284.
- (13) Wang, D. Z.; Viennois, E.; Ji, K.; Damera, K.; Draganov, A.; Zheng, Y. Q.; Dai, C. F.; Merlin, D.; Wang, B. H. *Chem. Commun.* **2014**, *50*, 15890.
- (14) Rimmer, R. D.; Richter, H.; Ford, P. C. *Inorg. Chem.* **2010**, *49*, 1180.
- (15) Klan, P.; Solomek, T.; Bochet, C. G.; Blanc, A.; Givens, R.; Rubina, M.; Popik, V.; Kostikov, A.; Wirz, J. *Chem. Rev.* **2013**, *113*, 119.
- (16) Schatzschneider, U. *Inorg. Chim. Acta* **2011**, *374*, 19.
- (17) Govender, P.; Pai, S.; Schatzschneider, U.; Smith, G. S. *Inorg. Chem.* **2013**, *52*, 5470.
- (18) Gonzalez, M. A.; Carrington, S. J.; Fry, N. L.; Martinez, J. L.; Mascharak, P. K. *Inorg. Chem.* **2012**, *51*, 11930.
- (19) Carrington, S. J.; Chakraborty, I.; Mascharak, P. K. *Chem. Commun.* **2013**, *49*, 11254.
- (20) Chakraborty, I.; Carrington, S. J.; Mascharak, P. K. *Acc. Chem. Res.* **2014**, *47*, 2603.
- (21) Pierrri, A. E.; Huang, P. J.; Garcia, J. V.; Stanfill, J. G.; Chui, M.; Wu, G.; Zheng, N.; Ford, P. C. *Chem. Commun.* **2015**, *51*, 2072.
- (22) Kuzmanich, G.; Gard, M. N.; Garcia-Garibay, M. A. *J. Am. Chem. Soc.* **2009**, *131*, 11606.
- (23) Poloukhine, A.; Popik, V. V. *J. Org. Chem.* **2003**, *68*, 7833.
- (24) Poloukhine, A.; Popik, V. V. *J. Phys. Chem. A* **2006**, *110*, 1749.
- (25) Poloukhine, A. A.; Mbua, N. E.; Wolfert, M. A.; Boons, G.-J.; Popik, V. V. *J. Am. Chem. Soc.* **2009**, *131*, 15769.
- (26) Kuzmanich, G.; Garcia-Garibay, M. A. *J. Phys. Org. Chem.* **2011**, *24*, 883.
- (27) Chapman, O. L.; Wojtkowski, P. W.; Adam, W.; Rodriguez, O.; Rucktaeschel, R. *J. Am. Chem. Soc.* **1972**, *94*, 1365.
- (28) Peng, P.; Wang, C. M.; Shi, Z.; Johns, V. K.; Ma, L. Y.; Oyer, J.; Copik, A.; Igarashi, R.; Liao, Y. *Org. Biomol. Chem.* **2013**, *11*, 6671.
- (29) Birnbaum, H.; Cookson, R. C.; Lewin, N. J. *Chem. Soc.* **1961**, 1224.
- (30) Antony, L. A. P.; Slanina, T.; Sebej, P.; Solomek, T.; Klan, P. *Org. Lett.* **2013**, *15*, 4552.
- (31) Similar nodal properties of frontier MOs is a necessary but not sufficient condition for predicting the same type of a photoreaction of two, seemingly unrelated chromophores.
- (32) Boens, N.; Leen, V.; Dehaen, W. *Chem. Soc. Rev.* **2012**, *41*, 1130.
- (33) Bessette, A.; Hanan, G. S. *Chem. Soc. Rev.* **2014**, *43*, 3342.
- (34) Lu, H.; Mack, J.; Yang, Y. C.; Shen, Z. *Chem. Soc. Rev.* **2014**, *43*, 4778.
- (35) Ni, Y.; Zeng, L. T.; Kang, N. Y.; Huang, K. W.; Wang, L.; Zeng, Z. B.; Chang, Y. T.; Wu, J. S. *Chem. Eur. J.* **2014**, *20*, 2301.
- (36) Lo, M. M. C.; Fu, G. C. *J. Am. Chem. Soc.* **2002**, *124*, 4572.
- (37) Varlan, A.; Hillebrand, M. *Cent. Eur. J. Chem.* **2011**, *9*, 624.
- (38) Yu, M. F.; Wong, J. K. H.; Tang, C.; Turner, P.; Todd, M. H.; Rutledge, P. J. *Beilstein J. Org. Chem.* **2015**, *11*, 1.
- (39) The benzyl ester **4a** is stable upon irradiation in both degassed and aerated methanolic solutions (Figure S29).
- (40) Mula, S.; Ray, A. K.; Banerjee, M.; Chaudhuri, T.; Dasgupta, K.; Chattopadhyay, S. *J. Org. Chem.* **2008**, *73*, 2146.
- (41) Konig, K. *J. Microsc.* **2000**, *200*, 83.
- (42) Stacko, P.; Sebej, P.; Veetil, A. T.; Klán, P. *Org. Lett.* **2012**, *14*, 4918.
- (43) Umeda, N.; Takahashi, H.; Kamiya, M.; Ueno, T.; Komatsu, T.; Terai, T.; Hanaoka, K.; Nagano, T.; Urano, Y. *ACS Chem. Biol.* **2014**, *9*, 2242.
- (44) Rubinstein, N.; Liu, P.; Miller, E. W.; Weinstain, R. *Chem. Commun.* **2015**, *51*, 6369.
- (45) Goswami, P. P.; Syed, A.; Beck, C. L.; Albright, T. R.; Mahoney, K. M.; Unash, R.; Smith, E. A.; Winter, A. H. *J. Am. Chem. Soc.* **2015**, *137*, 3783.
- (46) Ortiz, M. J.; Garcia-Moreno, I.; Agarrabeitia, A. R.; Duran-Sampedro, G.; Costela, A.; Sastre, R.; Arbeloa, F. L.; Prieto, J. B.; Arbeloa, I. L. *Phys. Chem. Chem. Phys.* **2010**, *12*, 7804.
- (47) Costela, A.; Garcia-Moreno, I.; Pintado-Sierra, M.; Amat-Guerri, F.; Liras, M.; Sastre, R.; Arbeloa, F. L.; Prieto, J. B.; Arbeloa, I. L. *J. Photochem. Photobiol. A* **2008**, *198*, 192.
- (48) Kostova, I. *Curr. Med. Chem.* **2006**, *13*, 1085.
- (49) Zhang, X. F.; Yang, X. D. *J. Chem. Phys. B* **2013**, *117*, 5533.
- (50) Saito, F.; Tobita, S.; Shizuka, H. *J. Chem. Soc., Faraday Trans.* **1996**, *92*, 4177.
- (51) Perkins, R. J.; Xu, H. C.; Campbell, J. M.; Moeller, K. D. *Beilstein J. Org. Chem.* **2013**, *9*, 1630.
- (52) Palao, E.; Agarrabeitia, A. R.; Banuelos-Prieto, J.; Lopez, T. A.; Lopez-Arbeloa, I.; Armesto, D.; Ortiz, M. *J. Org. Lett.* **2013**, *15*, 4454.
- (53) Nepomnyashchii, A. B.; Bard, A. J. *Acc. Chem. Res.* **2012**, *45*, 1844.
- (54) Banerjee, S.; Kuznetsova, R. T.; Papkovsky, D. B. *Sensors Actuat. B-Chem.* **2015**, *212*, 229.
- (55) Zhang, X. F.; Yang, X. D.; Niu, K.; Geng, H. *J. Photochem. Photobiol. A* **2014**, *285*, 16.
- (56) Solomek, T.; Heger, D.; Ngoy, B. P.; Givens, R. S.; Klan, P. *J. Am. Chem. Soc.* **2013**, *135*, 15209.
- (57) Labbe, G. *Angew. Chem. Int. Ed.* **1980**, *19*, 276.
- (58) Showalter, B. M.; Toscano, J. R. *J. Phys. Org. Chem.* **2004**, *17*, 743.
- (59) Hatchard, C. G.; Parker, C. A. *P. Roy. Soc. Lond. A Mat.* **1956**, *235*, 518.



- (60) Klan, P.; Wirz, J. *Photochemistry of organic compounds: From concepts to practice*; 1<sup>st</sup> ed.; John Wiley & Sons Ltd.: Chichester, 2009.
- (61) Pavlishchuk, V. V.; Addison, A. W. *Inorg. Chim. Acta* **2000**, *298*, 97.
- (62) Vreman, H. J.; Stevenson, D. K. *Anal. Biochem.* **1988**, *168*, 31.
- (63) Vreman, H. J.; Kwong, L. K.; Stevenson, D. K. *Clinical Chemistry* **1984**, *30*, 1382.
- (64) Vreman, H. J.; Wong, R. J.; Kadotani, T.; Stevenson, D. K. *Anal. Biochem.* **2005**, *341*, 280.
- (65) Hagebaum-Reignier, D.; Girardi, R.; Carissan, Y.; Humbel, S. *THEOCHEM* **2007**, *817*, 99.
- (66) Carissan, Y.; Hagebaum-Reignier, D.; Goudard, N.; Humbel, S. *J. Phys. Chem. A* **2008**, *112*, 13256.
- (67) Frisch, M. J.; Trucks, G. W.; Schlegel, H. B.; Scuseria, G. E.; Robb, M. A.; Cheeseman, J. R.; Scalmani, G.; Barone, V.; Mennucci, B.; Petersson, G. A.; Nakatsuji, H.; Caricato, M. L., X.; Hratchian, H. P. I., A. F.; Bloino, J.; Zheng, G.; Sonnenberg, J. L.; Hada, M.; Ehara, M.; Toyota, K.; Fukuda, R.; Hasegawa, J. I., M.; Nakajima, T.; Honda, Y.; Kitao, O.; Nakai, H.; Vreven, T.; Montgomery, J. A., Jr.; Peralta, J. E.; Ogliaro, F.; Bearpark, M.; Heyd, J. J.; Brothers, E.; Kudin, K. N.; Staroverov, V. N.; Kobayashi, R.; Normand, J.; Raghavachari, K.; Rendell, A.; Burant, J. C.; Iyengar, S. S.; Tomasi, J.; Cossi, M.; Rega, N.; Millam, J. M.; Klene, M.; Knox, J. E.; Cross, J. B.; Bakken, V.; Adamo, C.; Jaramillo, J.; Gomperts, R.; Stratmann, R. E.; Yazyev, O.; Austin, A. J. C., R.; Pomelli, C.; Ochterski, J. W.; Martin, R. L.; Morokuma, K.; Zakrzewski, V. G.; Voth, G. A.; Salvador, P.; Dannenberg, J. J.; Dapprich, S.; Daniels, A. D.; Farkas, O.; Foresman, J. B.; Ortiz, J. V.; Cioslowski, J.; Fox, D. J.; Gaussian, Inc., Wallingford, CT, 2009.

TOC



Cite this: *Chem. Sci.*, 2015, 6, 2027

# Visible light photocatalytic reduction of aldehydes by Rh(III)–H: a detailed mechanistic study†

T. Ghosh,‡<sup>a</sup> T. Slanina‡<sup>abc</sup> and B. König\*<sup>a</sup>

The chemoselective photoreduction of aldehydes in the presence of ketones was achieved using triethanolamine (TEOA) as sacrificial electron donor, proflavine (PF) as photocatalyst and [Cp\*Rh(III)(bpy)Cl]Cl (Rh<sub>cat</sub>) as mediator. The reducing agent, which reacts with the carbonyl group was found to be [Cp\*Rh(III)(bpy)H]Cl (Rh(III)–H). Contrary to formate-based reduction, its slow photochemical *in situ* generation enables to kinetically distinguish aldehydes from ketones. The inherent reactivity difference of the carbonyl compounds is transferred by the method into synthetically useful reaction selectivities. The substrate scope is broad with excellent yields. A detailed study of the reaction mechanism reveals that the photoreduction of the PF triplet and the subsequent reduction of the Rh<sub>cat</sub> leading to Rh(III)–H represents the major reaction pathway, which is highly oxygen sensitive. The oxidative quenching of the PF singlet state by Rh<sub>cat</sub> is a competing mechanism, which prevails in non-degassed systems.

Received 30th November 2014  
Accepted 6th January 2015

DOI: 10.1039/c4sc03709j

www.rsc.org/chemicalscience

## Introduction

Aldehydes and ketones are similar in reactivity. The development of methods for the chemoselective reduction of aldehydes in the presence of ketones has therefore received considerable attention.<sup>1,2</sup> Employing NaBH<sub>4</sub> as reduction reagent, selectivity can be achieved only at very low temperatures (–78 °C)<sup>3,4</sup> or by using additives such as thiols,<sup>5</sup> metal salts,<sup>6</sup> resins,<sup>7</sup> PEG<sup>8</sup> or Na<sub>2</sub>CO<sub>3</sub> in water.<sup>9</sup> Various modified borohydrides are known to allow chemoselective reduction of aldehydes in the presence of ketones. For example, tetraalkylammonium borohydride can reduce aldehydes in the presence of ketones to its corresponding alcohol, but with only low selectivity.<sup>10</sup> Na(AcO)<sub>3</sub>BH<sup>11</sup> and *n*-Bu<sub>4</sub>N(AcO)<sub>3</sub>BH<sup>12</sup> were used to reduce aldehydes in the presence of ketones with a high selectivity, but rather harsh reduction conditions, such as reflux in benzene, are required. In recent past, chemists started to modify borohydrides<sup>13</sup> with sterically hindered substituents and different electron-withdrawing groups, which are then able to distinguish between the carbonyl groups of aldehydes and ketones. Most of these modified borohydrides require special reagents and methods to prepare.

Moreover, in all these hydride reductions the reducing agent was used stoichiometrically. In 2006 Casey *et al.* introduced the catalytic chemoselective hydrogenation of aldehydes over ketones in non-polar solvent at elevated temperature, which was demonstrated with only one example: the reduction of benzaldehyde in the presence of acetophenone.<sup>14</sup> In 2012 McCulla *et al.* reported<sup>15</sup> photo-chemical chemoselectivity of aryl aldehydes in the presence of alkyl aldehydes and aryl ketones. They used a polymeric heterogeneous photocatalyst with a tail absorption (400–440 nm) in the visible part of the spectrum. However, by this method they were able to achieve only low conversion of starting materials with low overall yields of the corresponding alcohols for both neutral and electron rich aldehydes. Moreover, they often observed the benzoin condensation as a side reaction.

Herein, we report the chemoselective visible light induced photocatalytic hydride reduction of aldehydes in the presence of ketones. Our photocatalytic system offers, in comparison to previously published methods, a robust selectivity, which can differentiate aldehydes from ketones over a broad reactivity range. Park and Nam have introduced<sup>16</sup> a photocatalytic system using PF (3,6-diaminoacridine) as photocatalyst and Rh<sub>cat</sub> as a mediator for the regeneration of NADH from NAD<sup>+</sup> produced by enzymatic synthesis of L-glutamate demonstrating an artificial photosynthetic approach. We modified the system for synthetic purposes. The schematic mechanism is shown in Fig. 1, upper part. PF is a well-known acridine dye studied in detail for its ability to bind with DNA.<sup>17</sup> It has also been used as a promising molecule for the photogeneration of hydrogen.<sup>18</sup> Rh<sub>cat</sub> has been first described by Youinou and Ziesel in 1989.<sup>19</sup> Since then it has frequently been used as a hydride transferring agent for cofactor regeneration.<sup>20</sup> Unlike other hydrides, it exhibits an

<sup>a</sup>Institute of Organic Chemistry, University of Regensburg, D-93040 Regensburg, Germany. E-mail: Burkhard.Koenig@ur.de

<sup>b</sup>Department of Chemistry, Faculty of Science, Masaryk University, Kamenice 5, 62500 Brno, Czech Republic

<sup>c</sup>Research Centre for Toxic Compounds in the Environment, Faculty of Science, Masaryk University, Kamenice 5, 62500 Brno, Czech Republic

† Electronic supplementary information (ESI) available: Detailed experimental procedures of the photocatalytic reactions, additional spectral data, calculations, photochemical measurements and mechanistic studies and schemes. See DOI: 10.1039/c4sc03709j

‡ These authors contributed equally to this work.



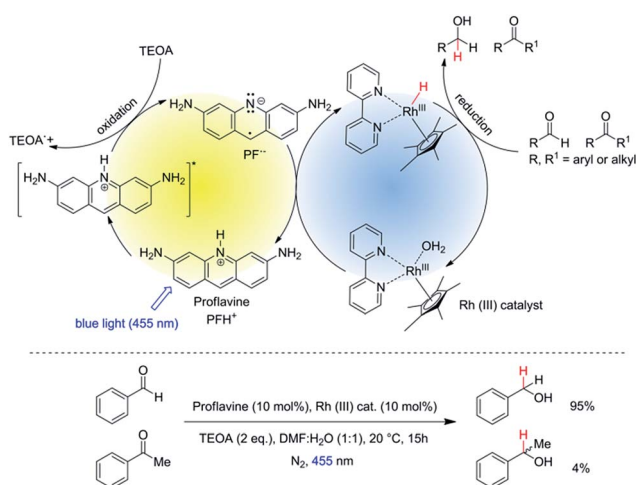


Fig. 1 Top: schematic representation of the photocatalytic cycle with mediator cycle involving PF as photocatalyst and  $[\text{Cp}^*\text{Rh}(\text{III})(\text{bpy})\text{Cl}]\text{Cl}$  as mediator. Bottom: high chemo-selectivity for benzaldehyde in the presence of acetophenone.

outstanding regioselectivity in the reduction of  $\text{NAD}^+$ .<sup>21</sup> It has also been used for the chemical reduction of both aldehydes and ketones by hydride transfer from formic acid.<sup>22,23</sup> We photochemically generate the same hydride reducing agent,  $\text{Rh}(\text{III})\text{-H}$  as in the formate-based reduction. However, due to its slow *in situ* generation, we maintain a low concentration of  $\text{Rh}(\text{III})\text{-H}$  in the reaction medium, which then kinetically distinguishes between aldehydes and ketones with a high selectivity (Fig. 1, bottom).

## Results and discussion

### Synthetic investigations

The reaction conditions were optimized using benzaldehyde as a substrate. The selected results are summarized in the Table 1. The yields were determined by GC/FID after 15 hours of irradiation at 455 nm. The reactions in anhydrous organic solvent (Table 1, entries 1 and 2) did not yield a significant amount of product as water is required as a proton source for generation of

$\text{Rh}(\text{III})\text{-H}$ .<sup>24</sup> Both aqueous acetonitrile and DMF gave good yields and DMF/ $\text{H}_2\text{O}$  (1 : 1, v/v) was chosen for further studies as the aliphatic substrates dissolve better in the reaction medium. The yields of benzyl alcohol were highest in case of 10 mol% of both PF and  $\text{Rh}_{\text{cat}}$  (Table 1, entry 5). Using 5 mol% of both PF and  $\text{Rh}_{\text{cat}}$  we obtained a similar result for the benzaldehyde reduction (Table 1, entry 9), but we increased the catalysts loading to 10 mol% to accelerate the reduction rate of aliphatic substrates.

To investigate the role of each component of the photocatalytic system we performed a series of control experiments. The results are summarized in Table S1.† The data clearly show that each component is essential for the reaction progress. The reaction without degassing (Table S1,† entry 6) yields about 30% of the product. This has been further studied and will be discussed in the mechanistic part. Reactions in hydrogen atmosphere did not yield any product (Table S1,† entries 7 and 8) from which it is evident that no direct hydrogenation occurs.

Various aromatic and aliphatic aldehydes and ketones were tested as substrates in our catalytic system (Table 2). For all substrates the optimized reaction conditions were used (Table 2, entry 5). The reaction rate could be accelerated by a factor of 5, without affecting the selectivity (Table 2, entries 1–3) using a flow reactor, which delivers the incident light more efficiently to the whole volume of the reaction mixture. Excellent yields were obtained for neutral, electron rich and electron poor aldehydes, whereas the corresponding ketones remained unreacted. Using an activated ketone as one reactant, we performed the reduction reactions varying the other reactant from electron-poor to electron-neutral to electron-rich aldehyde with notable selectivity (Table 2, entry 8–10). The selectivity was observed not only for a mixture of aldehyde and ketone, but also for a bifunctional molecule (Table 2, entry 11). Somewhat lower yield in entry 11 is caused by a side reaction leading to a pinacol-type product (detected by HPLC-MS, see Fig. S44†). In entry 12 a lower yield was obtained, because of decomposition of the substrate, which is not related to the photoreaction.

The rate of reduction is partially dependent on the electron density of the aldehyde functionality. That indicates that the hydride transfer from  $\text{Rh}(\text{III})\text{-H}$  to the carbonyl compound is the rate-determining step. The correlation of reaction yields,

Table 1 Optimization of reaction conditions

Entry	Proflavine (mol%)	$\text{Rh}_{\text{cat}}$ (mol%)	TEOA (eq.)	Solvent	Yield after 15 <sup>a</sup> h (%)
1	10	10	2	Dry MeCN	<1
2	10	10	2	Dry DMF	7
3	10	10	2	DMF/ $\text{H}_2\text{O}$ (1 : 2)	83
4	10	10	2	DMF/ $\text{H}_2\text{O}$ (2 : 1)	61
5	10	10	2	<b>DMF/<math>\text{H}_2\text{O}</math> (1 : 1)</b>	<b>97</b>
6	10	10	2	MeCN/ $\text{H}_2\text{O}$ (1 : 1)	80
7	5	10	2	DMF/ $\text{H}_2\text{O}$ (1 : 1)	86
8	10	5	2	DMF/ $\text{H}_2\text{O}$ (1 : 1)	73
9	5	5	2	DMF/ $\text{H}_2\text{O}$ (1 : 1)	95
10	10	10	1	DMF/ $\text{H}_2\text{O}$ (1 : 1)	35
11	10	10	3	DMF/ $\text{H}_2\text{O}$ (1 : 1)	81

<sup>a</sup> GC/FID determined yield with appropriate internal standard.





Table 2 Substrate scope

Entry	Substrate	Reaction type	Time (h)	Yield
1		Batch Flow	15 3.5	97 91
2		Batch Flow	15 3.5	7 4
3		Batch Flow	15 3.5	95 (4) <sup>a</sup> 82 (<1) <sup>a</sup>
4		Batch	25	95
5		Batch	25	83
6		Batch	32	84
7		Batch	32	3
8		Batch	18	76 (2) <sup>a</sup>
9		Batch	16	91 (2) <sup>a</sup>
10		Batch	25	93 (4) <sup>a</sup>
11		Batch	16	51 (<1) <sup>b</sup>
12		Batch	42	56 (3) <sup>a</sup>

<sup>a</sup> Yields of ketone reductions. <sup>b</sup> Yield of doubly reduced product.

reduction potentials and Hammett's sigma values is shown in Fig. S8.† Generally, the photoreduction is slower for electron-rich aldehydes, but no clear trend was observed. Ketones are almost unreacted, which is mainly caused by steric effects. Rh<sub>cat</sub> is sufficiently crowded to create selectivity even between similar substrates, which was demonstrated on various NAD<sup>+</sup> model compounds.<sup>21</sup>

The catalytic system also reduces imines (see Table S3†). Dry DMSO was found to be the most suitable solvent and the addition of thiourea (1 eq.) accelerated the reaction significantly by hydrogen bond activation of the imine.<sup>25</sup>

The reaction selectivity was compared with known systems. Rh<sub>cat</sub> has been recently used for chemical reductions of both aldehydes and ketones.<sup>22,23</sup> The selectivity is reported only marginally.<sup>22</sup> The reactions were accomplished in biphasic conditions without any phase transfer catalyst. The reduction was fast even with low catalyst loadings (~0.5 mol%). We therefore examined the selectivity of Rh(III)-H generated chemically using formate aqueous buffer as a hydride source. The results are shown in Table S2.† After 15 minutes the benzaldehyde is efficiently reduced, whereas the conversion of acetophenone is only 32%. Contrary to the formate-based system our photocatalytic reduction is slower and the reaction can be easily stopped after the aldehyde is reduced and the ketone is almost intact. The aldehyde–ketone selectivity depends on the reaction conversion and therefore the ratio of reduction products is influenced by the reaction time. The kinetics of the reaction is described in more detail in the ESI (Scheme S3 and Fig. S12†).

### Mechanistic investigations

The photophysical properties of PF have been studied in detail. In solution the dye is prone to dimerization ( $K_D = 500 \text{ M}^{-1}$ ) and its molar absorptivity is concentration dependent from  $c \sim 10^{-4} \text{ M}$ .<sup>26</sup> At physiological pH, PF is protonated at the central nitrogen atom N-10; PFH<sup>+</sup> ( $pK_a = 9.5$ ).<sup>27</sup> PFH<sup>+</sup> absorbs at 443 nm and has a strong fluorescence ( $\Phi_{fl} = 0.39$ ,  $\lambda_{em} = 508 \text{ nm}$ )<sup>28</sup> whereas the neutral form (PF) absorbs at 393 nm and exhibits no fluorescence§ (see Fig. S13 and S16†). PFH<sup>+</sup> has interesting emission properties. It exhibits strong prompt fluorescence from the singlet state,  $^1[\text{PFH}^+]^*$  (Fig. S45†), thermally dependent delayed E-type fluorescence (fl<sup>E</sup>) originating from thermal repopulation of  $^1[\text{PFH}^+]^*$  from  $^3[\text{PFH}^+]^*$ , concentration dependent delayed P-type fluorescence (fl<sup>P</sup>) caused by triplet–triplet annihilation with energy transfer,¶ and light intensity dependent photoionization recombination delayed fluorescence (fl<sup>PIR</sup>) which occurs after recombination of ion pair  $[\text{PFH}^+]^{2+} \dots e^-$  (solv.) created by photoionization from  $^1[\text{PFH}^+]^*$ .<sup>29</sup> Phosphorescence from the triplet state is the most significant emission with maximum intensity at 570 nm till 197 K and is negligible above 253 K.<sup>29</sup>

Photoinduced electron transfer (PET) occurs between  $^3[\text{PFH}^+]^*$  and an appropriate electron donor. The redox potential of  $^3[\text{PFH}^+]^*$  can be estimated using the Rehm–Weller equation from the measured ground state redox potential ( $E_0 = -0.74 \text{ V vs. SCE}$ , Fig. S6†) and its triplet energy ( $\lambda_{\text{phosph.}} = 570 \text{ nm}$ ,  $\sim 2.17 \text{ eV}$ ) resulting in  $+1.44 \text{ V vs. SCE}$ .|| Electron-rich compounds like amines can serve as electron donors for PET. TEOA ( $E_0 = +0.76 \text{ V vs. SCE}$ )<sup>30</sup> is easily†† oxidized by  $^3[\text{PFH}^+]^*$  creating TEOA<sup>+</sup> and a reduced proflavine radical (PFH<sup>•</sup>). The back electron transfer does not occur due to the fast deprotonation of TEOA<sup>+</sup>.<sup>31</sup>

Interaction of PF with TEOA in aqueous media has been studied by measuring its fluorescence. Titration of PF solution (aq.,  $c = 5.0 \times 10^{-6} \text{ M}$ ) with TEOA or TEA resulted in a decrease in fluorescence intensity as observed by Basu *et al.*<sup>32</sup> This would indicate that TEOA is quenching the singlet excited state by PET



and would be in contradiction with the well-established PET from PF triplet.<sup>31</sup> The UV spectra (Fig. S15†) indicate the formation of a new species with an absorption peak at 393 nm, which corresponds to PF formed by a simple acidobasic equilibrium, which is also supported by the UV pH titration (Fig. S13†) and fluorescence pH titration (Fig. 2, upper part). The distribution of the respective acidobasic forms calculated from both pH and TEOA titration corresponds to each other (Fig. S20†). We did not observe the formation of PFH<sup>+</sup>⋯TEA ground-state complex as proposed by Basu *et al.*<sup>32</sup>

Fluorescence quenching of PF with Rh<sub>cat</sub> is shown in Fig. 2, lower part. Unlike TEOA, the Rh catalyst does not interact with PF in the ground state. Fluorescence was quenched at relatively high concentrations.†† The quenching constant was dependent on the excitation beam intensity. This indicates that Rh<sub>cat</sub> is quenched by photoionized electrons, which are originally responsible for the photoionization recombination delayed fluorescence (fl<sup>PIR</sup>). The contribution of the photoionization recombination delayed fluorescence to the overall emission was determined by measuring the dependence of the relative fluorescence yield on the intensity of excitation light. The light intensity was kept below the saturation limit so that all of the excitation light was absorbed by the sample. Increasing

intensity of the excitation light leads to a non-linear increase of the fluorescence intensity, which corresponds to the fl<sup>PIR</sup> (Fig. S22†).

The properties of rhodium mediator were studied in detail. Rh<sub>cat</sub> is a water-soluble air-stable d<sup>6</sup> metal complex, which undergoes a ligand exchange after its dissolution in water. The catalytic active form [Cp<sup>\*</sup>Rh(III)(bpy)(H<sub>2</sub>O)]Cl<sub>2</sub> has its maximum absorption at 355 nm and a tail absorption in the visible region (λ<sub>tail</sub> ~ 420 nm, Fig. S25†). Its absorption in the blue region (λ = 455 nm) is weak§§ and it does not interfere with PFH<sup>+</sup>. The reducing species has been described as a metal hydride complex, Rh(III)–H. It was confirmed as a key intermediate in the formate-based reductive catalytic system generated by direct hydride transfer from HCOO<sup>-</sup>.<sup>33</sup> It has also been proposed as a reducing agent in photocatalytic systems coupled with various dyes.<sup>16,34,35</sup> To identify Rh(III)–H in our reduction system we prepared Rh(III)–H independently from the reaction with formate ions. After dissolution of Rh<sub>cat</sub> in formate buffer (2 M; pH = 3.5) bubbles of CO<sub>2</sub> and H<sub>2</sub> were generated vigorously. The yellow solution turned blue and could be slowly re-oxidized back by O<sub>2</sub>. A new absorption peak at 612 nm is observed (Fig. S25†) corresponding to the previously published spectra of Rh(III)–H (Fig. 3). Due to the vigorous gas evolution we were not able to measure the NMR spectrum for structural characterization. EPR analysis showed that the hydride complex is diamagnetic, which corresponds to the previous findings. In the UV-vis spectrum of the typical reaction mixture without substrate (Fig. 1) irradiated for 15 hours with 455 nm LED the shoulder at 612 nm corresponding to the Rh(III)–H was observed. After purging with air the peak vanished and the spectrum changed to the initial state before irradiation (Fig. 3). This is a clear evidence for the presence of Rh(III)–H in the reaction mixture.

Rh(III)–H is known to produce dihydrogen upon its protonation by the solvent.<sup>24</sup> We therefore examined if the hydrogen is produced in the catalytic system. We measured the composition

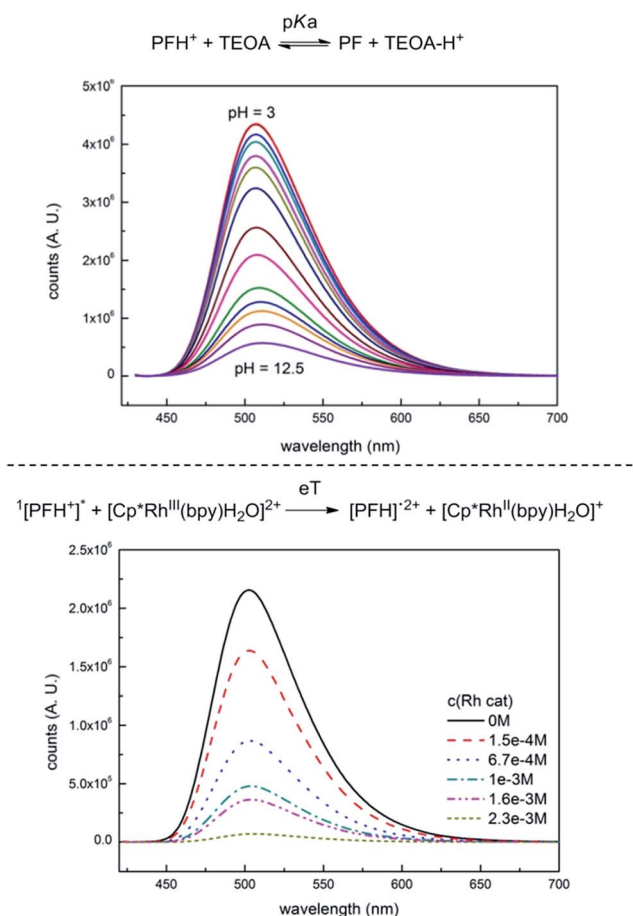


Fig. 2 Fluorescence quenching of PF with TEOA (upper part) and Rh<sub>cat</sub> (lower part).

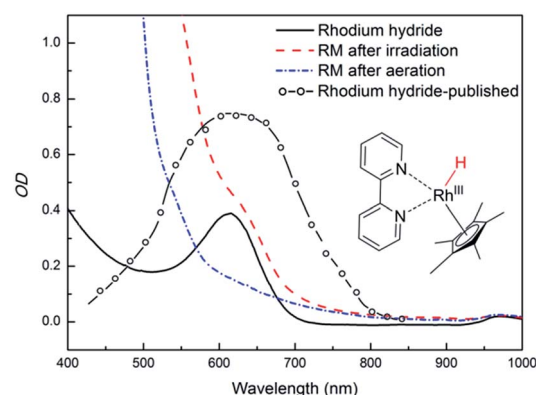


Fig. 3 Spectroscopic evidence of presence of Rh(III)–H in the photocatalytic system (left side). Spectra of a typical reaction mixture after irradiation (dashed red line), after bubbling with air (dash – dotted blue line), of a prepared Rh(III)–H standard (solid black line), and a published<sup>24</sup> spectrum (open circles + dashed line; redrawn from the original) are shown.



of the gas phase above the typical reaction mixture after 15 hours of irradiation by head-space GC. Dihydrogen was present together with nitrogen used for degassing (Fig. S9†). We also examined if the presence of H<sub>2</sub> in the reaction mixture could be responsible for the course of the reaction. The typical reaction mixture without TEOA was purged with oxygen-free H<sub>2</sub> (Table S1,† entries 7 and 8) and was irradiated for 15 h. No product formation was observed, which indicates that the decomposition of Rh(III)-H is an irreversible process and that carbonyls cannot be reduced by dihydrogen itself in the presence of the Rh catalyst.

To have a better insight into the mechanism we measured the kinetics of the evolution of H<sub>2</sub> using benzaldehyde or acetophenone as a substrate (benzaldehyde is being reduced by Rh(III)-H efficiently whereas acetophenone is not). The result is shown in Fig. S10.† In the photo-reduction of benzaldehyde the amount of H<sub>2</sub> produced is lower (approx. by the factor of 2) than when acetophenone is used. In the first case a fraction of Rh(III)-H (ca. 50%) is consumed for the reduction and the rest is decomposed by protonation.¶ In the case of the ketone, where no reduction was observed, the Rh(III)-H is solely decomposed to dihydrogen.¶¶ This behavior corresponds to the side reaction kinetics shown in the Fig. S12.†

Based on the literature data and our experimental results we suggest the mechanism of the rhodium catalytic cycle depicted in the Fig. 4. The aqueous solution of Rh<sub>cat</sub> contains [Cp\*Rh<sup>III</sup>(bpy)H<sub>2</sub>O]Cl<sub>2</sub>, formed after the ligand exchange of Cl<sup>-</sup>

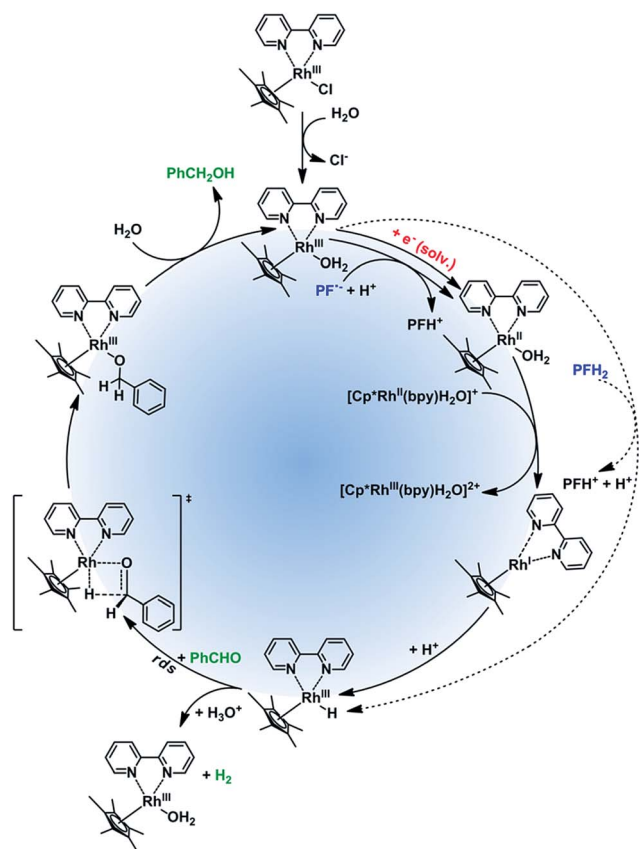


Fig. 4 Proposed rhodium catalytic cycle, rds = rate determining step.

to H<sub>2</sub>O. This process is important for the catalytic activity making the central metal ion more accessible.<sup>36</sup> In the next step, the rhodium aqua-complex is reduced. In principle, two different mechanisms are possible: the one electron reduction<sup>24</sup> or a hydride transfer from a suitable hydrogen donor (e.g. HCOO<sup>-</sup>)<sup>36</sup> have both been described in detail. The first mechanism applies for PF<sup>•+</sup> generated by PET from <sup>3</sup>[PFH<sup>+</sup>]\* and TEOA and subsequent deprotonation\*\*\* (for pK<sub>a</sub> values of PF species in various oxidation and excitation states see Fig. S45†). The deprotonation of PFH<sup>+</sup> to PF<sup>•-</sup> is further proved by CV and spectroelectrochemistry (Fig. S6 and S7†). From the rate constants of dimerization and disproportionation<sup>37</sup> of PF<sup>•-</sup> we can estimate the rate constant for electron transfer ( $k_{\text{red}} \sim 5 \times 10^9 \text{ s}^{-1} \text{ M}^{-1}$ , Fig. S46†). The photoreduction with solvated electrons generated by photo-ionization of PF occurs at a rate close to the diffusion limit.<sup>37</sup> The d<sup>7</sup> complex [Cp\*Rh<sup>II</sup>(bpy)H<sub>2</sub>O]<sup>+</sup> created after the one electron reduction is not stable and disproportionates fast ( $k_{\text{disp}} = 3.7 \times 10^8 \text{ s}^{-1} \text{ M}^{-1}$ )<sup>33</sup> to a rhodium(I) complex. This d<sup>8</sup> complex, [Cp\*Rh<sup>I</sup>(bpy)], is then protonated††† by a protic solvent to give Rh(III)-H. In case of a possible direct hydride transfer between [Cp\*Rh<sup>III</sup>(bpy)H<sub>2</sub>O]Cl<sub>2</sub> and PFH<sub>2</sub>, Rh(III)-H is formed directly.

Rh(III)-H can either reduce the corresponding carbonyl (productive reaction) or can be protonated again to produce dihydrogen regenerating the catalyst.††† In case of the hydride reduction the carbonyl group is reduced to an alkoxy ligand, which is easily hydrolyzed<sup>22</sup> giving the respective alcohol.

To investigate the fate of PF in the solution we examined the photoproducts formed from PF. The irradiation of degassed solutions of PF ( $c = 6.67 \text{ mmol}$ ) and TEOA ( $c = 133 \text{ mmol}$ ) provided a mixture of 2 photoproducts. The spectral characterization is provided in the ESI (Fig. S27 and S29†). A product absorbing at 340 nm was assigned to “leuco PF” whereas the second product absorbing at 424 nm was assigned to “diacridine” in accordance with published data.<sup>38</sup> The first product is only observed when irradiating a degassed sample, whereas the second product is oxygen insensitive. Therefore we assume that leuco PF is formed from PF<sup>•-</sup> (triplet reductive pathway) and diacridine is formed from PF<sup>•+</sup> (singlet ionization pathway).

Based on our mechanistic experiments and literature reports we propose the overall catalytic mechanism depicted in Fig. 5. After absorption of a blue photon PFH<sup>+</sup> is excited to the first excited singlet state. Fluorescence (prompt and delayed) is a significant deactivation pathway with an overall quantum yield of 39%.<sup>28</sup> Intersystem crossing (isc) gives the triplet state which accepts an electron from TEOA. The radical PFH<sup>•</sup> is deprotonated to the radical anion PF<sup>•-</sup>, which is then oxidized by Rh<sub>cat</sub> back to PFH<sup>+</sup>. In the absence of the metal complex the radical anion forms leuco PF and disproportionates to PFH<sub>2</sub>.<sup>37</sup> The reduced Rh<sub>cat</sub> reacts according to the catalytic cycle depicted in Fig. 4.

The control experiment without degassing (Table S1,† line 6) unexpectedly gave 30% of the product. As oxygen can efficiently quench both <sup>3</sup>[PFH<sup>+</sup>]\* and PF<sup>•-</sup> (for the rate constants see Fig. S45†), the product cannot be formed in this case through the triplet reductive pathway (Fig. 5, right side). We propose that another, oxygen-insensitive, pathway is present. PF is known for



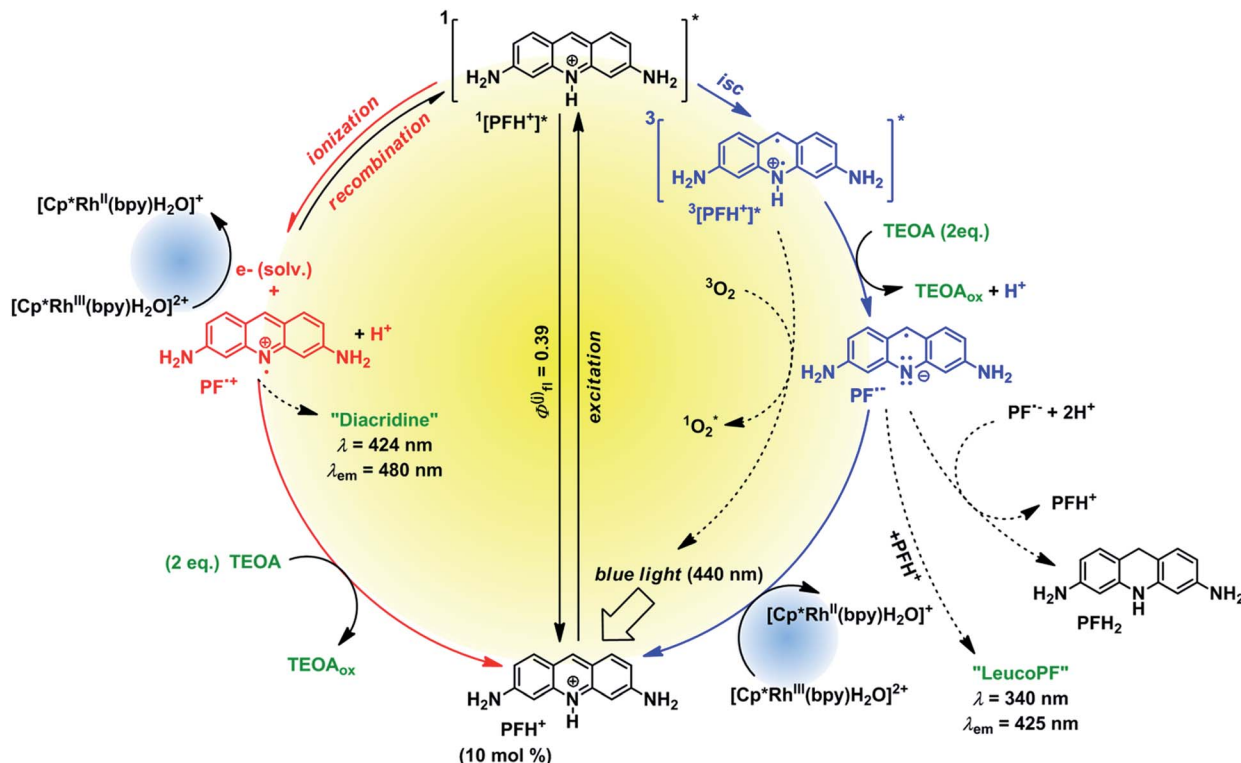


Fig. 5 Proposed proflavine catalytic cycle.

its photoionization from  $^1[\text{PFH}^+]^*$  after excitation.<sup>31</sup> Pileni and Grätzel<sup>31</sup> reported that the photoionization is a single-photon process, whereas Hussein and Goetz examined the process in more detail and revealed that the photoionization is caused by multiple photon process (*i.e.* absorption of the excited state).<sup>39</sup> The photoionization produces solvated electrons<sup>40</sup> which react either with  $\text{PFH}^+$  to form  $\text{PF}^{\bullet+}$  or with  $\text{Rh}_{\text{cat}}$  to form  $\text{Rh}(\text{II})$  species.<sup>37</sup> Unlike the triplet pathway, the PET from the singlet state is obviously an outer-sphere process. The oxidized PF radical cation  $[\text{PF}^{\bullet+}]^+$  is then reduced back by TEOA present in the system.<sup>41</sup> These two parallel mechanisms (oxidative and reductive quenching) have been recently found in an iridium-based photocatalytic system.<sup>41</sup>

To further prove our mechanistic proposal, we performed a series of experiments using transient pump-probe spectroscopy (Fig. 6 and S32–S36†). The solution of PF ( $c = 2.2 \times 10^{-4}$  M) in DMF/water mixture exhibited a strong fluorescence negative peak directly after the excitation flash (Fig. S32†). After  $\sim 50$  ns, when the fluorescence decays (the fluorescence lifetime was reported to be  $\sim 5$  ns)<sup>31</sup> three peaks were observed at 550, 610 and 670 nm, respectively (Fig. 6). This was assigned to the  $^3[\text{PFH}^+]^*$ . The lifetime of the PF triplet was approx. 2  $\mu\text{s}$  in aerated solution. The triplet spectrum and lifetime corresponds to the previously published data.<sup>40</sup> The solution of PF and  $\text{Rh}_{\text{cat}}$  ( $c_{\text{Rh}} = 2.0 \times 10^{-4}$  M) showed partially quenched fluorescence and the intensity of the PF triplet peak was significantly lowered (Fig. S34†). This finding corresponds to the Stern–Volmer experiment discussed previously and indicates that  $\text{Rh}_{\text{cat}}$  partially quenches the excited singlet state, which also leads to a diminished triplet yield.

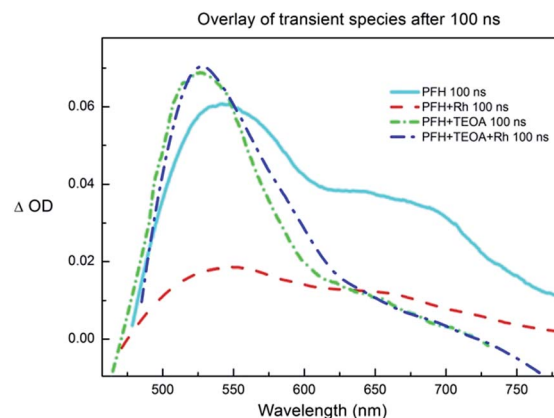


Fig. 6 The overlay of the transient signal of proflavine ( $c = 2.24 \times 10^{-4}$  M), TEOA ( $c = 2.58 \times 10^{-2}$  M) and rhodium catalyst ( $c = 2.0 \times 10^{-4}$  M) in DMF/water 1 : 1, bubbled with nitrogen, excitation wavelength  $\lambda_{\text{ex}} = 355$  nm; time window 50 ns, 10 $\times$  accumulated, 100 ns after the pulse, smoothed; the single peak at  $\sim 530$  nm corresponds to  $\text{PF}^{\bullet+}$  and the peak at  $\sim 550$  nm with a broad shoulder at  $\sim 670$  nm corresponds to  $^3[\text{PFH}^+]^*$ .

The transient spectra of the solution of PF and TEOA ( $c_{\text{TEOA}} = 25.8 \times 10^{-3}$  M) exhibited a new peak with an absorption maximum at  $\sim 530$  nm and with a lifetime of approx. 8  $\mu\text{s}$  in aerated solution (Fig. S33†). The observed peak was oxygen-sensitive and corresponds to the  $\text{PF}^{\bullet+}$ ,<sup>40</sup> confirming the PET from TEOA to  $^3[\text{PFH}^+]^*$ .

The transient spectrum of the solution of PF, TEOA and  $\text{Rh}_{\text{cat}}$  exhibited the absorption peak of  $\text{PF}^{\bullet+}$  (Fig. S35†). The intensity





of the peak was lower than in the case of PFH<sup>+</sup> and TEOA solution and its lifetime shortened to ~3 μs caused by the electron transfer from the PF<sup>•-</sup> to Rh<sub>cat</sub>.

Rh<sub>cat</sub> itself does not exhibit any transient species and no product from PET with TEOA is detected. Unlike its iridium analogue, Rh(III)-H is not photoactive.<sup>42</sup>

The quantum yield of the product formation was determined to be  $\Phi = (0.14 \pm 0.05)\%$  at 455 nm measured at low light intensity ( $P_{\text{absorbed}} = 9.3$  mW, see ESI† for details). The low quantum yield is caused by loss of excitation by fluorescence (~39%),<sup>28</sup> low triplet yield (~10%),<sup>29</sup> disproportionation of the Rh<sup>II</sup> species (two moles of PF<sup>•-</sup> for one mole of Rh<sup>I</sup>)<sup>33</sup> and partial Rh(III)-H decomposition (~50% of Rh(III)-H lost to H<sub>2</sub>).

## Conclusions

In summary, the selective photocatalytic reduction of aldehydes over ketones was achieved employing *in situ* generated Rh(III)-H as the reduction reagent. Contrary to a formate-based aqueous reduction, the Rh(III)-H is formed in the photocatalytic protocol slowly and allows therefore to kinetically distinguish between aldehydes and ketones. The photoreduction proceeds both *via* photoinduced electron transfer from the proflavine triplet and by oxidative quenching with Rh<sub>cat</sub>. The former pathway is oxygen sensitive and the latter is light intensity dependent. The light intensity influences directly the reaction mechanism and the reaction rate. A change of the light source (high-power LED vs. fluorescence light bulb) affects the product yield and the photocatalytic mechanism.

## Acknowledgements

We thank the Deutsche Forschungsgemeinschaft (GRK 1626) for financial support. We thank the Laboratory of Organic Photochemistry of Faculty of Science at Masaryk University in Brno, Czech Republic for transient absorption spectroscopic measurements, which were supported by the Czech Ministry of Education (LO1214). We thank Malte Hansen for help in preparation the graphical abstract and Prof. O. Reiser for helpful discussions.

## Notes and references

§ PF is weakly fluorescent till pH = 11.5 which corresponds to the pK<sub>a</sub> of the singlet excited state. K. Kalyanasundaram; D. Dung, *J. Phys. Chem.*, 1980, **84**, 2551.

¶  $^3[\text{PFH}^+]^* + ^3[\text{PFH}^+]^* \rightarrow ^1[\text{PFH}^+]^* + ^1[\text{PFH}^+]$ .

|| This value corresponds well with the published potential (+1.36 V). M. P. Pileni; M. Grätzel, *J. Phys. Chem.*, 1980, **84**, 2402.

\*\*  $E_0 = +0.80$  V vs. Ag/AgCl.

††  $\Delta G^\circ = -e \times (-0.76 \text{ V} + 1.44 \text{ V}) - 0.08 \text{ eV} = -0.76 \text{ eV} \sim -73.3 \text{ kJ mol}^{-1}$ , according to *J. Am. Chem. Soc.*, 1999, **121**, 1681–1687.

‡‡ 300 eq. of Rh catalyst vs. PFH<sup>+</sup>, Stern-Volmer quenching constant is (2260 ± 30) M<sup>-1</sup>.

§§ Measured molar absorptivities are:  $\epsilon^{455}(\text{PFH}^+) = 28 \text{ 600}$ ;  $\epsilon^{455}(\text{Rh}^{\text{III}}\text{cat}) = 120$ .

¶¶ These side reactions have similar rate constants.

||| The ketone reduction does not efficiently compete with the decomposition.

\*\*\* pK<sub>a</sub>(PFH<sup>+</sup>) = 4.5; *J. Chem. Soc., Chem. Comm.*, 1979, 1137–1138.

†††  $k_{\text{prot}} = 1.6 \times 10^6 \text{ s}^{-1} \text{ M}^{-1}$ ; U. Kölle; M. Grätzel, *Angew. Chem.*, 1987, **99**, 572.

‡‡‡ Protonation:  $k_{\text{dec}} = 1.8 \times 10^3 \text{ s}^{-1} \text{ M}^{-1}$ ; *Angew. Chem.*, 1987, **99**, 572; reduction:  $k_{\text{red}} \sim 2 \times 10^3 \text{ s}^{-1} \text{ M}^{-1}$ .

§§§ And partially (10%) from  $^3[\text{PFH}^+]^*$ ; *Chem. Phys. Lett.*, 1980, **69**, 61–65.

¶¶¶  $k_{\text{red}} = 2.5 \times 10^{10} \text{ s}^{-1} \text{ M}^{-1}$ ; S. Solar; W. Solar; N. Getoff, *Z. Naturforsch., A: Phys., Phys. Chem., Kosmophys.*, 1982, **37**, 1077.

||||  $k_{\text{red}} \sim 10^{10} \text{ s}^{-1} \text{ M}^{-1}$ ; estimated value, based on: S. Solar; W. Solar; N. Getoff, *Z. Naturforsch., A: Phys., Phys. Chem., Kosmophys.*, 1982, **37**, 1077.

\*\*\*\* Redox potential of [PFH<sup>+</sup>]<sup>2+</sup> is  $E_0 = +1.07$  V vs. SCE, Fig. S6.†  $\Delta G^\circ = -e \times (-0.76 \text{ V} + 1.07 \text{ V}) - 0.08 \text{ eV} = -0.39 \text{ eV} \sim -37 \text{ kJ mol}^{-1}$ .

- G. A. Tolstikov, V. N. Odinokov, R. I. Galeeva, R. S. Bakeeva and V. R. Akhunova, *Tetrahedron Lett.*, 1979, **20**, 4851–4854.
- R. O. Hutchins and D. Kandasamy, *J. Am. Chem. Soc.*, 1973, **95**, 6131–6133.
- D. E. Ward and C. K. Rhee, *Synth. Commun.*, 1988, **18**, 1927–1933.
- D. E. Ward and C. K. Rhee, *Can. J. Chem.*, 1989, **67**, 1206–1211.
- Y. Maki, K. Kikuchi, H. Sugiyama and S. Seto, *Tetrahedron Lett.*, 1977, **18**, 263–264.
- C. Adams, *Synth. Commun.*, 1984, **14**, 1349–1353.
- B. Zeynizadeh and F. Shirini, *J. Chem. Res.*, 2003, **2003**, 334–339.
- K. Tanemura, T. Suzuki, Y. Nishida, K. Satsumabayashi and T. Horaguchi, *Synth. Commun.*, 2005, **35**, 867–872.
- S. Chandrasekhar and A. Shrinidhi, *Synth. Commun.*, 2014, **44**, 2051–2056.
- D. J. Raber, W. C. Guida and D. C. Shoenberger, *Tetrahedron Lett.*, 1981, **22**, 5107–5110.
- G. W. Gribble and D. C. Ferguson, *J. Chem. Soc., Chem. Commun.*, 1975, 535–536.
- C. F. Nutaitis and G. W. Gribble, *Tetrahedron Lett.*, 1983, **24**, 4287–4290.
- Y. Kuroiwa, S. Matsumura and K. Toshima, *Synlett*, 2008, **2008**, 2523–2525.
- C. P. Casey, N. A. Strotman, S. E. Beetner, J. B. Johnson, D. C. Priebe and I. A. Guzei, *Organometallics*, 2006, **25**, 1236–1244.
- M. Zhang, W. D. Rouch and R. D. McCulla, *Eur. J. Org. Chem.*, 2012, **2012**, 6187–6196.
- D. H. Nam and C. B. Park, *ChemBioChem*, 2012, **13**, 1278–1282.
- R. W. Armstrong and N. M. Panzer, *J. Am. Chem. Soc.*, 1972, **94**, 7650–7653.
- A. I. Krasna, *Photochem. Photobiol.*, 1979, **29**, 267–276.
- M. T. Youinou and R. Ziessel, *J. Organomet. Chem.*, 1989, **363**, 197–208.
- F. Hollmann, A. Schmid and E. Steckhan, *Angew. Chem., Int. Ed.*, 2001, **40**, 169–171.
- H. C. Lo, O. Buriez, J. B. Kerr and R. H. Fish, *Angew. Chem., Int. Ed.*, 1999, **38**, 1429–1432.
- C. Leiva, H. C. Lo and R. H. Fish, *J. Organomet. Chem.*, 2010, **695**, 145–150.
- Y. Himeda, N. Onozawa-Komatsuzaki, H. Sugihara, H. Arakawa and K. Kasuga, *J. Mol. Catal. A: Chem.*, 2003, **195**, 95–100.
- U. Kölle and M. Grätzel, *Angew. Chem., Int. Ed. Engl.*, 1987, **99**, 572–574.



- 25 D. Menche, J. Hassfeld, J. Li, G. Menche, A. Ritter and S. Rudolph, *Org. Lett.*, 2006, **8**, 741–744.
- 26 G. R. Haugen and W. H. Melhuish, *Trans. Faraday Soc.*, 1964, **60**, 386.
- 27 N. Mataga, Y. Kaifu and M. Koizumi, *Bull. Chem. Soc. Jpn.*, 1956, **29**, 373–379.
- 28 C. A. Parker and T. A. Joyce, *Photochem. Photobiol.*, 1973, **18**, 467–474.
- 29 W. E. Lee and W. C. Galley, *Biophys. J.*, 1988, **54**, 627–635.
- 30 P. Kurz, B. Probst, B. Spingler and R. Alberto, *Eur. J. Inorg. Chem.*, 2006, **2006**, 2966–2974.
- 31 M. P. Pileni and M. Grätzel, *J. Phys. Chem.*, 1980, **84**, 2402–2406.
- 32 B. Chakraborty and S. Basu, *Chem. Phys. Lett.*, 2009, **477**, 382–387.
- 33 E. Steckhan, S. Herrmann, R. Ruppert, E. Dietz, M. Frede and E. Spika, *Organometallics*, 1991, **10**, 1568–1577.
- 34 S. H. Lee, D. H. Nam, J. H. Kim, J.-O. Baeg and C. B. Park, *ChemBioChem*, 2009, **10**, 1621–1624.
- 35 S. H. Lee, D. H. Nam and C. B. Park, *Adv. Synth. Catal.*, 2009, **351**, 2589–2594.
- 36 H. C. Lo, C. Leiva, O. Buriez, J. B. Kerr, M. M. Olmstead and R. H. Fish, *Inorg. Chem.*, 2001, **40**, 6705–6716.
- 37 S. Solar, W. Solar and N. Getoff, *Z. Naturforsch., A: Phys. Sci.*, 1982, **37**, 1077–1082.
- 38 G. Oster, J. S. Bellin, R. W. Kimball and M. E. Schrader, *J. Am. Chem. Soc.*, 1959, **81**, 5095–5099.
- 39 B. H. M. Hussein and M. Goetz, Ph.D. Dissertation, Universität Halle-Wittenberg, Germany, 2005.
- 40 K. Kalyanasundaram and D. Dung, *J. Phys. Chem.*, 1980, **84**, 2551–2556.
- 41 H. Lv, W. Guo, K. Wu, Z. Chen, J. Bacsá, D. G. Musaev, Y. V. Geletii, S. M. Lauinger, T. Lian and C. L. Hill, *J. Am. Chem. Soc.*, 2014, **136**, 14015–14018.
- 42 S. M. Barrett, C. L. Pitman, A. G. Walden and A. J. M. Miller, *J. Am. Chem. Soc.*, 2014, **136**, 14718–14721.





Cite this: *Chem. Commun.*, 2015, 51, 6568

Received 24th February 2015,  
Accepted 10th March 2015

DOI: 10.1039/c5cc01580d

www.rsc.org/chemcomm

## Visible light photooxidation of nitrate: the dawn of a nocturnal radical†

T. Hering,<sup>a</sup> T. Slanina,<sup>a</sup> A. Hancock,<sup>b</sup> U. Wille\*<sup>b</sup> and B. König\*<sup>a</sup>

**Highly oxidizing nitrate radicals (NO<sub>3</sub>•) are easily accessed from readily available nitrate salts by visible light photoredox catalysis using a purely organic dye as the catalyst and oxygen as the terminal oxidant. The interaction of the excited catalyst and nitrate anions was studied by spectroscopic methods to elucidate the mechanism, and the method was applied to the NO<sub>3</sub>• induced oxidation of alkynes and alcohols.**

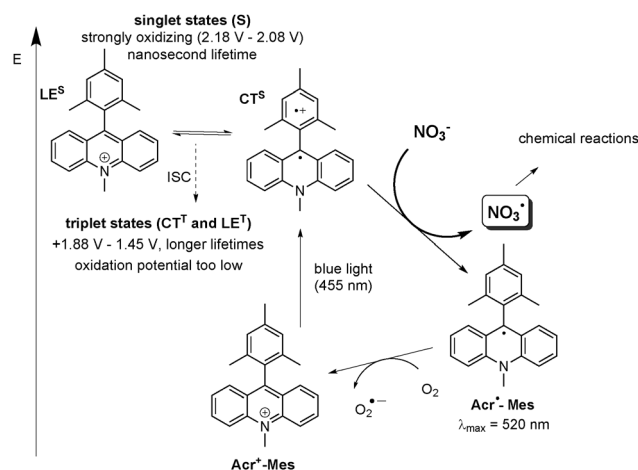
The nitrate radical (NO<sub>3</sub>•) is the most important nocturnal free radical oxidant in the troposphere and thus accounts for the majority of the oxidative reactions at night-time.<sup>1</sup> In the atmosphere NO<sub>3</sub>• oxidizes a broad scope of volatile organic species including alkenes,<sup>2,3</sup> alcohols,<sup>4,5</sup> terpenes,<sup>1</sup> esters,<sup>6</sup> and sulfides.<sup>1</sup> It is a highly reactive and chemically versatile O-centered radical<sup>7</sup> with an oxidation potential of +2.00 V (vs. SCE in MeCN).<sup>8</sup> Apart from electron transfer (ET),<sup>9,10</sup> NO<sub>3</sub>• also reacts by addition to π systems<sup>1,11</sup> and by hydrogen atom abstraction (HAT).<sup>8,12,13</sup> Overall, the reactivity of NO<sub>3</sub>• with organic molecules can be seen in between that of hydroxyl radicals (OH•) and sulfate radical anions (SO<sub>4</sub>•<sup>-</sup>).<sup>14</sup>

Despite its high chemical versatility, it is surprising that only limited synthetic applications of NO<sub>3</sub>• are available so far. Shono reported the addition of electrochemically generated NO<sub>3</sub>• to alkenes.<sup>11</sup> The reaction of NO<sub>3</sub>• with cyclic alkynes and alkynones was employed to obtain *cis*-fused bicyclic ketones in self-terminating oxidative radical cyclizations.<sup>15,16</sup> This concept was later extended to alkyne ethers yielding tetrasubstituted tetrahydrofurans.<sup>17,18</sup> One reason for the limited use of NO<sub>3</sub>• as a reagent in organic transformations is its rather difficult accessibility. Common methods for NO<sub>3</sub>• generation on preparative scale in solution are the reaction of nitrogen dioxide and ozone,<sup>1,19</sup> electrooxidation of nitrate anions<sup>11</sup> or the photolysis of (NH<sub>4</sub>)<sub>2</sub>Ce(NO<sub>3</sub>)<sub>6</sub> (CAN) with UV light (λ = 350 nm)<sup>14,20</sup>

However, the use of toxic gases, high electrode potentials,<sup>8</sup> or UV irradiation are so far limiting the applications and lead to undesired side reactions.

We were pleased to observe that, upon excitation of the organic photocatalyst 9-mesityl-10-methylacridinium perchlorate (**1**) with blue light, oxidation of nitrate anions to NO<sub>3</sub>•, readily occurs (Scheme 1), thus providing a convenient access to NO<sub>3</sub>• on a preparative scale. 9-Mesityl-10-methylacridinium perchlorate (**1**) was chosen, because it is known to have a strong oxidizing capacity in the excited state.<sup>21,22</sup> To the best of our knowledge, this is the first visible light mediated generation of nitrate radicals.

In order to elucidate the mechanism of the NO<sub>3</sub>• formation, we monitored the generation of reduced catalyst **Acr<sup>•</sup>-Mes** in the presence of LiNO<sub>3</sub> upon continuous irradiation of a 5 μM solution of **Acr<sup>+</sup>-Mes** (**1**) in MeCN with 455 nm light under



**Scheme 1** Proposed mechanism of visible light mediated generation of NO<sub>3</sub>• via photocatalytic oxidation by **Acr<sup>+</sup>-Mes** (**1**). The electron transfer from NO<sub>3</sub><sup>-</sup> occurs from the short-lived singlet state (LE<sup>S</sup> or CT<sup>S</sup>) with sufficient oxidative capacity to generate the reduced catalyst **Acr<sup>•</sup>-Mes** and NO<sub>3</sub>•, the longer lived transient triplet species (CT<sup>T</sup> or LE<sup>T</sup>) is not reactive towards NO<sub>3</sub><sup>-</sup>. The reduced catalyst **Acr<sup>•</sup>-Mes** is regenerated by oxygen. (All oxidation potentials are given vs. SCE in MeCN or PhCN).<sup>23,25,26</sup>

<sup>a</sup> Institut für Organische Chemie, Universität Regensburg, Universitätsstrasse 31, D-93053 Regensburg, Germany. E-mail: burkhard.koenig@ur.de

<sup>b</sup> School of Chemistry and BIO21 Molecular Science and Biotechnology Institute, The University of Melbourne, 30 Flemington Road, Parkville, VIC 3010, Australia. E-mail: uwille@unimelb.edu.au

† Electronic supplementary information (ESI) available. See DOI: 10.1039/c5cc01580d

anaerobic conditions. The differential absorption spectrum shows the appearance of **Acr<sup>•</sup>-Mes** with a maximum at 520 nm<sup>21,23</sup> after irradiation for 120 s and 240 s. (see ESI,† Fig. S6) This observation suggests a direct oxidation of NO<sub>3</sub><sup>-</sup> by the excited catalyst thus demonstrating that NO<sub>3</sub><sup>-</sup> can act as an electron donor to the excited catalyst. The reduced catalyst **Acr<sup>•</sup>-Mes** is stable under argon, however, the signal vanishes completely after aeration of the reaction mixture due to reoxidation of **Acr<sup>•</sup>-Mes** to the ground state catalyst **Acr<sup>+</sup>-Mes** by oxygen (see Scheme 1).<sup>24</sup> The negative signal at λ < 460 nm in the differential absorption spectrum is caused mainly by the decrease of the ground state absorption of **Acr<sup>+</sup>-Mes** as a result of **Acr<sup>•</sup>-Mes** formation and partial photobleaching of **Acr<sup>+</sup>-Mes**.<sup>‡</sup> The long-lived triplet state with a microsecond lifetime is generally discussed as the reactive state in most oxidative reactions.<sup>25,26</sup> The exact nature of this state is controversial and could be both a CT<sup>T</sup> state with an oxidation potential of +1.88 V vs. SCE, as reported by Fukuzumi<sup>25</sup> or a locally excited triplet state, LE<sup>T</sup>, with an oxidation potential of +1.45 V vs. SCE as reported by Verhoeven.<sup>26</sup> However, neither would have the oxidative capacity to oxidize NO<sub>3</sub><sup>-</sup>. Recent detailed mechanistic investigations by the group of Nicewicz revealed that for substrates with oxidation potentials exceeding +1.88 V (vs. SCE), a reaction should occur out of the short-lived excited singlet state (mainly CT<sup>S</sup>), which has an estimated oxidation potential of 2.08 V (Scheme 1).<sup>23</sup> Since both singlet states are fluorescent (φ<sub>F</sub> ~ 8%), whereas the triplet states do not emit,<sup>23</sup> we performed fluorescence quenching experiments to explore the nature of the reactive state involved in NO<sub>3</sub><sup>-</sup> oxidation. A clear quenching of the fluorescence by LiNO<sub>3</sub> confirms that oxidation of NO<sub>3</sub><sup>-</sup> occurs from the singlet excited state of **1** (see ESI,† Fig. S6). Moreover, laser flash photolysis experiments confirmed that no interaction of the long lived triplet state and NO<sub>3</sub><sup>-</sup> can be observed (Fig. S8 in the ESI†). Based on these findings, we suggest that the reaction proceeds *via* a singlet excited state as depicted in Scheme 1.

Having demonstrated the pathway for photocatalytic NO<sub>3</sub><sup>•</sup> generation, we selected the well-studied reaction of NO<sub>3</sub><sup>•</sup> with diphenylacetylene (**2**) yielding benzil (**3**) and benzophenone (**4**) to explore the synthetic application of this new method and to compare it with the previously reported methods. The results are compiled in Table 1. Under photocatalytic conditions using 5 mol% of **Acr<sup>+</sup>-Mes** (**1**), 0.25 mmol of alkyne **2** and 2 eq. of LiNO<sub>3</sub>, diketone **3** and ketone **4** were obtained after 2 h of irradiation with blue light (λ = 455 nm) with yields comparable to previous methods.<sup>27</sup> When oxygen was replaced by ammonium persulfate as the electron acceptor in a degassed system, the yield and product ratio were not changed significantly (entry 5). This shows that potential interfering reactions by singlet oxygen could be excluded. In the absence of light or catalyst no reaction occurred (entries 7 and 9). However, small amounts of diketone **3** were formed in the direct reaction of **2** with the excited catalyst in the absence of nitrate ions (entry 8).

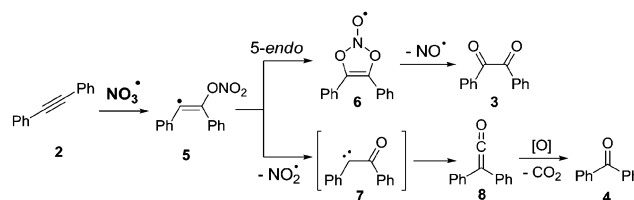
According to computational studies, the mechanism for the NO<sub>3</sub><sup>•</sup> induced oxidation of diphenylacetylene suggests formation of diketone **3** and benzophenone (**4**) through competing pathways in the initial vinyl radical adduct **5** (Scheme 2). While diketone **3** results from a 5-*endo* cyclization, followed by loss

Table 1 Oxidation of diphenylacetylene **2** by NO<sub>3</sub><sup>•a</sup>

Entry	Conditions	Yield <sup>b</sup> <b>3</b> + <b>4</b> (%)
1	5 mol% <b>1</b> , air	50 (30 + 20)
2	5 mol% <b>1</b> , O <sub>2</sub>	55 (31 + 24)
3	NaNO <sub>3</sub>	41 (27 + 15)
4	10 mol% <b>1</b>	38 (24 + 14)
5	(NH <sub>4</sub> ) <sub>2</sub> S <sub>2</sub> O <sub>8</sub> , N <sub>2</sub> atmosphere	46 (27 + 19)
6	DCM	52 (32 + 20)
7	Without light	0
8	Without NO <sub>3</sub> <sup>-</sup>	13 (3 only)
9	Without <b>1</b>	0

<sup>a</sup> Reactions were carried out using diphenylacetylene (**2**, 0.25 mmol) and the respective amount of 9-mesityl-10-methylacridinium perchlorate (**1**) in 1 mL of MeCN unless otherwise noted with an irradiation time of 2 h.

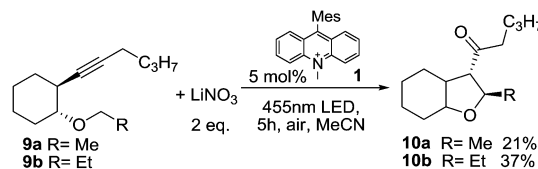
<sup>b</sup> Quantitative GC yields using acetophenone as internal standard.



Scheme 2 Proposed mechanism for the oxidation of aromatic alkynes by NO<sub>3</sub><sup>•</sup>.<sup>27</sup>

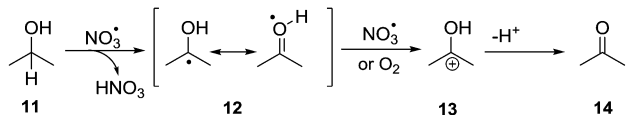
of NO<sup>•</sup>, the key-step in the formation of benzophenone (**4**) is γ-fragmentation with elimination of NO<sub>2</sub><sup>•</sup>, and subsequent Wolff-rearrangement of the carbene intermediate **7** followed by oxidative decarboxylation.<sup>27</sup>

Next, we applied the photocatalytic NO<sub>3</sub><sup>•</sup> formation to the synthesis of tetrasubstituted tetrahydrofurans, which proceeds *via* a self-terminating radical cascade that is initiated by NO<sub>3</sub><sup>•</sup> addition to the triple bond in alkyne **9**. The reaction was described previously using either anodic oxidation of lithium nitrate or CAN photolysis.<sup>17,18</sup> The starting material **9** (Scheme 3) contains an aliphatic alkyne, which is more difficult to oxidize compared to **2** and thus decreases the background reaction that is caused by direct oxidation of **9** by the photocatalyst. The reaction of **9b** with 2 eq. of LiNO<sub>3</sub> and 5 mol% **1** gave the anticipated product **10b** in a yield of 37% (67% based on conversion), with 45% of the starting material **9b** being recovered. Methyl ether **9a** gave lower yields and



Scheme 3 Self-terminating radical oxidative cyclization to tetrasubstituted tetrahydrofurans **10**.<sup>17,18</sup>





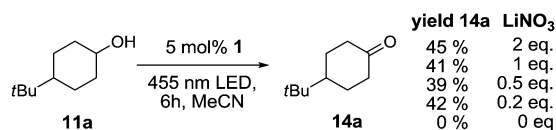
Scheme 4 General mechanism of the nitrate mediated alcohol oxidation via initial hydrogen abstraction followed by oxidation and loss of a proton.

an incomplete conversion, which can be rationalized by a non-regioselective addition of  $\text{NO}_3^\bullet$  to both ends of the alkyne,<sup>§</sup> in accordance with previous reports. The low conversion (and resulting low product yield) is likely due to the fact that  $\text{NO}_3^\bullet$  leads to degradation of catalyst **1**. This effect could also be observed in UV/Vis measurements of the reaction mixture, which showed considerable photobleaching of the ground state during irradiation (see Fig. S7 in the ESI<sup>†</sup>). It is likely that the observed degradation proceeds via oxidation of the methyl groups on the mesityl moiety of the catalyst,<sup>8</sup> which is a known degradation pathway that leads to loss of catalytic activity.<sup>28</sup> The problem of low conversion could be partly overcome through slow addition of the catalyst via syringe pump.

Apart from addition to  $\pi$  systems,  $\text{NO}_3^\bullet$  also reacts through hydrogen abstraction,<sup>8,12,13</sup> which was explored in the catalytic oxidation of non-activated alcohols. In this reaction,  $\text{NO}_3^\bullet$  acts as a redox mediator, which is regenerated during the catalytic cycle, according to the mechanism in Scheme 4. Initial HAT from the alcohol carbon atom by  $\text{NO}_3^\bullet$ <sup>29</sup> leads to the regeneration of  $\text{NO}_3^-$  as nitric acid and formation of radical **12**. The latter is subsequently oxidized by either  $\text{NO}_3^\bullet$  or oxygen to give cationic intermediate **13**, which deprotonates to yield ketone **14**. The mechanism is similar to the indirect anodic oxidation of alcohols by nitrate.<sup>30</sup> Donaldson and Styler reported the enhanced gas phase oxidation of propanol under UV irradiation using  $\text{TiO}_2$  co-embedded with  $\text{KNO}_3$ . The finding was explained by formation of  $\text{NO}_3^\bullet$  and its ability to abstract hydrogen atoms from the alcohol carbon atom.<sup>31</sup>

The reaction was explored using *tert*-butyl cyclohexanol (**11a**) and the results are compiled in Scheme 5. To our delight, oxidation into the corresponding ketone **14a** occurred upon irradiation with blue light in the presence of  $\text{LiNO}_3$  using 5 mol% of **1** in acetonitrile. No reaction was observed in the absence of nitrate, which clearly confirms the role of  $\text{NO}_3^\bullet$  in this reaction. Stepwise reduction of the amount of  $\text{LiNO}_3$  from 2 eq. to 20 mol% did not affect the outcome, showing that  $\text{NO}_3^\bullet$  can act as mediator in this reaction (Scheme 5). An acidification of the solution due to formation of nitric acid was observed, but no apparent influence on the reaction or the stability of the catalyst was found.¶

The scope of this method was explored towards other non-activated alcohols and electron deficient benzyl alcohols.



Scheme 5 Experimental conditions and results for the  $\text{NO}_3^\bullet$  mediated oxidation of alcohols.

Table 2 Experimental conditions and results for the  $\text{NO}_3^\bullet$  mediated oxidation of alcohols<sup>a</sup>

Entry	Alcohol	Product	Yield product <sup>b</sup> (%)	Recovered starting material <sup>b</sup> (%)
1			45 (79)	44
2			42 (95)	56
3			40 (40)	—
4 <sup>c</sup>			55 (100)	45
5 <sup>d</sup>			— <sup>d</sup>	— <sup>d</sup>
6			16 (20)	17

<sup>a</sup> Reactions carried out using 0.25 mmol of the alcohol **11**, 1 eq. of  $\text{LiNO}_3$  and 10 mol% of **1** (two subsequent additions of 5 mol%) in 1 mL of MeCN with an irradiation time of 6 h. <sup>b</sup> Isolated yields, in brackets yield based on conversion. <sup>c</sup> Background reaction without  $\text{LiNO}_3$  is 9%. <sup>d</sup> Decomposition of substrate **11e**.

All reactions were carried out by two sequential additions of 5 mol% of **1** in order to counteract the loss of catalytic activity caused by degradation of the catalyst. The reactions proceed with good selectivity (see Table 2, entries 1, 2, 4), but the conversion was incomplete and unreacted starting material was recovered. Aliphatic (entries 1–3) and benzylic alcohols (entries 4 and 6) were converted.

In the oxidation of isomenthol (**11b**) (entry 2) the configuration of the stereocenter remained unchanged, while the basic substrate **11e** gave no product, which is most likely due to an acid–base reaction of pyridine with nitric acid that is generated during this reaction|| by the H-abstraction by  $\text{NO}_3^\bullet$  or a possible direct oxidation of the nitrogen of pyridine by the photocatalyst or  $\text{NO}_3^\bullet$  (entry 5).<sup>32</sup>

In conclusion, we described a new and simple access to highly reactive nitrate radicals using visible light photocatalysis with an organic dye as the photoredox catalyst. This method avoids the use of toxic compounds, or high electrochemical potentials and is, to the best of our knowledge, the first method yielding  $\text{NO}_3^\bullet$  in a catalytic process using visible light. We verified the formation of nitrate radicals by observation of the reduced catalyst **Ac<sup>r</sup>-Mes** and showed that the mechanism is proceeding via the singlet excited state of the catalyst. By investigating the addition to aromatic alkynes, a previously well studied model reaction of  $\text{NO}_3^\bullet$ , we showed that the photocatalytic procedure is as efficient as the previously employed methods.

Financial support by the Deutsche Forschungsgemeinschaft (DFG), the GRK 1626 and the Australian Research Council is acknowledged. TH thanks the Fonds der Deutschen Chemischen Industrie for a fellowship.

## Notes and references

‡ After aeration the ground state absorption of Acr<sup>+</sup>-Mes cannot be fully recovered (see ESI†).

§ For the mechanism of this reaction see ESI†.

¶ The addition of different bases (LiNO<sub>3</sub>, LiOAc, pyridine, lutidine) did not influence the outcome of the reaction or the stability of the catalyst.

|| Based on the assumption that both the initial hydrogen abstraction and the oxidation of 12 are done by nitrate radicals.

- 1 R. P. Wayne, I. Barnes, P. Biggs, J. P. Burrows, C. E. Canosa-Mas, J. Hjorth, G. Le Bras, G. K. Moortgat, D. Perner, G. Poulet, G. Restelli and H. Sidebottom, *Atmos. Environ., Part A*, 1991, **25**, 1–203.
- 2 M. P. Pérez-Casany, I. Nebot-Gil, J. Sánchez-Marín, F. Tomás-Vert, E. Martínez-Ataz, B. Cabañas-Galán and A. Aranda-Rubio, *J. Org. Chem.*, 1998, **63**, 6978–6983.
- 3 H. Gong, A. Matsunaga and P. J. Ziemann, *J. Phys. Chem. A*, 2005, **109**, 4312–4324.
- 4 J. C. Harrison and J. R. Wells, *Int. J. Chem. Kinet.*, 2012, **44**, 778–788.
- 5 D. Rousse and C. George, *Phys. Chem. Chem. Phys.*, 2004, **6**, 3408–3414.
- 6 S. Langer, E. Ljungstrom and I. Wangberg, *J. Chem. Soc., Faraday Trans.*, 1993, **89**, 425–431.
- 7 O. Ito, S. Akiho and M. Iino, *J. Phys. Chem.*, 1989, **93**, 4079–4083.
- 8 E. Baciocchi, T. D. Giacco, S. M. Murgia and G. V. Sebastiani, *J. Chem. Soc., Chem. Commun.*, 1987, 1246–1248.
- 9 H. Suzuki and T. Mori, *J. Chem. Soc., Perkin Trans. 2*, 1996, 677–683.
- 10 E. Baciocchi, I. Del Giacco, C. Rol and G. V. Sebastiani, *Tetrahedron Lett.*, 1985, **26**, 541–544.
- 11 T. Shono, M. Chuankamnerdkarn, H. Maekawa, M. Ishifune and S. Kashimura, *Synthesis*, 1994, 895–897.
- 12 A. A. Fokin, S. A. Peleshanko, P. A. Gunchenko, D. V. Gusev and P. R. Schreiner, *Eur. J. Org. Chem.*, 2000, 3357–3362.
- 13 M. Mella, M. Freccero, T. Soldi, E. Fasani and A. Albini, *J. Org. Chem.*, 1996, **61**, 1413–1422.
- 14 U. Wille, *Chem. – Eur. J.*, 2002, **8**, 340–347.
- 15 U. Wille, *J. Am. Chem. Soc.*, 2001, **124**, 14–15.
- 16 U. Wille, *Chem. Rev.*, 2012, **113**, 813–853.
- 17 U. Wille and L. Lietzau, *Tetrahedron*, 1999, **55**, 11465–11474.
- 18 U. Wille and L. Lietzau, *Tetrahedron*, 1999, **55**, 10119–10134.
- 19 L. F. Gamon, J. M. White and U. Wille, *Org. Biomol. Chem.*, 2014, **12**, 8280–8287.
- 20 D. C. E. Sigmund and U. Wille, *Chem. Commun.*, 2008, 2121–2123.
- 21 S. Fukuzumi, H. Kotani, K. Ohkubo, S. Ogo, N. V. Tkachenko and H. Lemmetyinen, *J. Am. Chem. Soc.*, 2004, **126**, 1600–1601.
- 22 K. Ohkubo, K. Mizushima, R. Iwata, K. Souma, N. Suzuki and S. Fukuzumi, *Chem. Commun.*, 2010, **46**, 601–603.
- 23 N. A. Romero and D. A. Nicewicz, *J. Am. Chem. Soc.*, 2014, **136**, 17024–17035.
- 24 K. Ohkubo, K. Mizushima and S. Fukuzumi, *Res. Chem. Intermed.*, 2013, **39**, 205–220.
- 25 S. Fukuzumi, K. Ohkubo and T. Suenobu, *Acc. Chem. Res.*, 2014, **47**, 1455–1464.
- 26 A. C. Benniston, A. Harriman, P. Li, J. P. Rostron, H. J. van Ramesdonk, M. M. Groeneveld, H. Zhang and J. W. Verhoeven, *J. Am. Chem. Soc.*, 2005, **127**, 16054–16064.
- 27 U. Wille and J. Andropof, *Aust. J. Chem.*, 2007, **60**, 420–428.
- 28 A. C. Benniston, K. J. Elliott, R. W. Harrington and W. Clegg, *Eur. J. Org. Chem.*, 2009, 253–258.
- 29 S. Langer and E. Ljungstrom, *J. Chem. Soc., Faraday Trans.*, 1995, **91**, 405–410.
- 30 D. Kyriacou, *Modern Electroorganic Chemistry*, Springer-Verlag, Berlin, Heidelberg, 1994.
- 31 S. A. Styler and D. J. Donaldson, *Environ. Sci. Technol.*, 2011, **45**, 10004–10012.
- 32 A. Thellend, P. Battioni, W. Sanderson and D. Mansuy, *Synthesis*, 1997, 1387–1388.

# Metal-Free Perfluoroarylation by Visible Light Photoredox Catalysis

Andreas U. Meyer,<sup>a§</sup> Tomáš Slanina,<sup>a,b§</sup> Chang-Jiang Yao,<sup>a,c§</sup> and Burkhard König<sup>a,\*</sup>

<sup>a</sup> Institut für Organische Chemie, Universität Regensburg, Universitätsstrasse 31, 93053 Regensburg, Germany. Fax: (+49)-941-943-1717; phone: (+49)-941-943-4575; e-mail: Burkhard.Koenig@chemie.uni-regensburg.de

<sup>b</sup> Department of Chemistry and RECETOX, Masaryk University, Kamenice 5, 625 00 Brno, Czech Republic

<sup>c</sup> Beijing National Laboratory for Molecular Sciences, CAS Key Laboratory of Photochemistry, Institute of Chemistry, Chinese Academy of Sciences, Beijing 100190, People's Republic of China

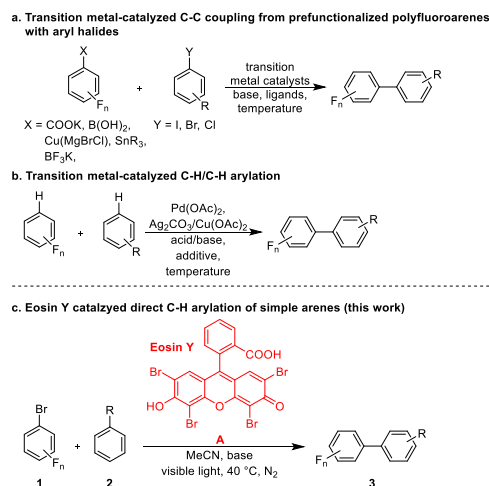
*Perfluorophenyl; photocatalysis; visible light; metal-free conditions; C-H arylation*

**ABSTRACT:** Visible light and eosin Y catalyze the direct arylation of simple arenes with fluorinated aryl bromides by a photoredox process. The reaction scope is broad in fluorinated compounds and arenes and the general and simple procedure provides a metal-free alternative for the synthesis of synthetically valuable polyfluorinated biaryl structures. The mild reaction conditions allow a selective reaction with the alkaloid brucine without protection of functional groups illustrating the potential of the process for late stage functionalization. Mechanistic investigations reveal the photoreduction of eosin Y via its triplet state by triethylamine, and subsequent electron transfer from the eosin Y radical anion to the polyfluorinated bromoarene, which fragments into the polyfluorinated aryl radical and a bromide anion. A radical chain reaction mechanism was excluded by a quenching factor analysis.

## ■ INTRODUCTION

Polyfluorobiaryl structures are important motifs in medicinal chemistry,<sup>1</sup> in functional materials, such as organic light emitting diodes (OLEDs),<sup>2</sup> in electron-transport devices,<sup>3</sup> as sensitizers for the photo-splitting of water,<sup>4</sup> or in liquid crystals.<sup>5</sup> As substructure of ligands in metal catalysis or organocatalysis they often enhance the catalytic performance.<sup>2b,6</sup> Polyfluorinated biaryls are found in binding sites for molecular recognition<sup>7</sup> and are used as starting materials in synthesis.<sup>8</sup> Most syntheses of polyfluorinated biaryls require transition metals, typically palladium<sup>9</sup> or copper,<sup>10</sup> and often the use of organometallic starting materials, such as boronic acids,<sup>11</sup> borate salts,<sup>12</sup> benzoates,<sup>13</sup> copper species,<sup>14</sup> or stannanes (Scheme 1, a).<sup>15</sup> Beside these methods the transition metal-catalyzed C–H arylation of arenes with aryl halides<sup>16</sup> or sodium arylsulfonates,<sup>17</sup> and the C–H/C–H arylation of arenes (Scheme 1, b)<sup>18</sup> are used. Syntheses without transition metal catalysts are rare. Two examples are the photoinduced electron-transfer reaction of arenes with pentafluorophenylsulfonates<sup>19</sup> or pentafluoriodobenzene<sup>20</sup> reported by Chen *et al.* in 1993, and the thermal (iodide) and photoinduced electron-transfer catalysis with diazonium salts by Kochi *et al.* from 1997.<sup>21</sup> However, the early examples require either the use of UV irradiation, addition of iodine or unstable diazonium salt reagents. Visible light photoredox catalysis may provide a valuable alternative avoiding the use of transition metal catalysts, ligands, or high temperatures and unstable reagents. Many recent reports have shown the formation of C–C,<sup>22</sup> C–P,<sup>23</sup> C–N,<sup>24</sup> and C–S<sup>25</sup> bonds using visible light and iridium or ruthenium complexes<sup>26</sup> or organic dyes<sup>27</sup> as photoredox catalysts. Weaver *et al.* have shown the hydrodefluorination of perfluoroarenes using visible light and iridium complexes.<sup>28</sup> We report here the visible light-mediated, metal-free direct

arylation of simple arenes with fluorinated aryl bromides using green light, the organic dye eosin Y (**A**) as photocatalyst and triethylamine as sacrificial electron donor (Scheme 1, c).



**Scheme 1.** Transition metal-catalyzed and photocatalytic reactions for the synthesis of polyfluorobiphenyls **3**

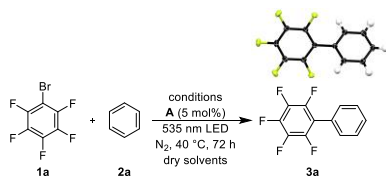
## ■ RESULTS AND DISCUSSION

### Synthesis

The reaction conditions were optimized by irradiating a mixture of 1-bromo-2,3,4,5,6-pentafluorobenzene (**1a**), benzene (**2a**), eosin Y (**A**) and triethylamine with green LED light under nitrogen atmosphere. Using one equivalent of triethylamine as electron donor, eosin Y (**A**) as photoca-

lyst yielded 53% of the product (**3a**, Table 1, entry 1) compared to Ru(bpy)<sub>3</sub>Cl<sub>2</sub> and rose bengal, which gave 39% (Table 1, entries 2 and 3). The best product yield of 63% was achieved with two equivalents of the electron donor in acetonitrile as solvent (Table 1, entry 4). The use of other solvents, like DMSO and DMF, and different electron donors, such as DIPEA, decreased the product yield (Table 1, entries 5-7). Control experiments without base, catalyst or light, confirmed that all components are necessary for product formation (Table 1, entries 8-10). In non-degassed reaction mixtures the yield of product decreased drastically (6%, Table 1, entry 11), most likely due to the competing quenching of the eosin excited triplet state by molecular oxygen.<sup>29</sup> This corresponds to the mechanistic findings (*vide infra*). An attempt to use benzene (**2a**) as solvent led to a significant decrease in product yield (13%, Table 1, entry 12).

**Table 1.** Optimization of the reaction conditions



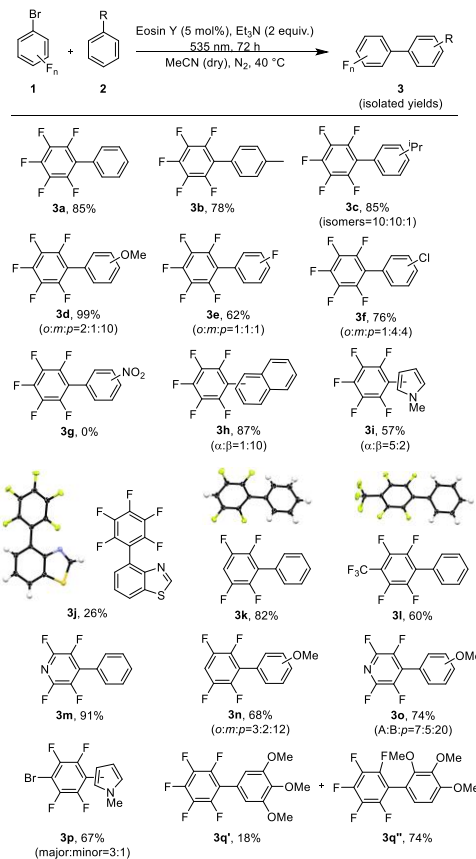
Entry	Conditions	Yield [%] <sup>[a]</sup>
1	<b>A</b> (5), <b>2a</b> (20 equiv.), Et <sub>3</sub> N (1 equiv.), MeCN	53%
2	Ru(bpy) <sub>3</sub> Cl <sub>2</sub> (5), 455 nm, <b>2a</b> (20 equiv.), Et <sub>3</sub> N (1 equiv.), MeCN	39%
3	rose bengal (5), <b>2a</b> (20 equiv.), Et <sub>3</sub> N (1 equiv.), MeCN	39%
4	<b>A</b> (5), <b>2a</b> (20 equiv.), Et <sub>3</sub> N (2 equiv.), MeCN	63%
5	<b>A</b> (5), <b>2a</b> (20 equiv.), Et <sub>3</sub> N (2 equiv.), DMSO	46%
6	<b>A</b> (5), <b>2a</b> (20 equiv.), Et <sub>3</sub> N (2 equiv.), DMF	17%
7	<b>A</b> (5), <b>2a</b> (20 equiv.), <sup>1</sup> Pr <sub>2</sub> EtN (2 equiv.), MeCN	15%
8	<b>A</b> (5), <b>2a</b> (20 equiv.), no base, MeCN	-
9	no catalyst, <b>2a</b> (20 equiv.), MeCN	-
10	<b>A</b> (5), <b>2a</b> (20 equiv.), Et <sub>3</sub> N (2 equiv.), MeCN, no light	-
11	<b>A</b> (5), <b>2a</b> (20 equiv.), Et <sub>3</sub> N (2 equiv.), MeCN, air	6%
12	<b>A</b> (5), <b>2a</b> (1 mL) as solvent, Et <sub>3</sub> N (2 equiv.)	13%

<sup>[a]</sup> Determined by GC analysis with naphthalene as internal standard.

The scope of the reaction was explored using the optimized reaction conditions (Table 1, entry 4): various fluorinated aryl bromides (**1**), simple arenes (**2**), 5 mol% eosin Y (**A**), green light LED irradiation, triethylamine (2 equiv.) and acetonitrile as a solvent. As shown in the *molecular* structures of compounds **3a**, **3j**, **3k** and **3l** were confirmed by X-ray single crystal analysis. Electron donating or electron withdrawing substituents are generally well tolerated. The chloride substituent allows further synthetic modifications of the coupling products. The two C-H arylation products **3q'** (para 18%) **3q''** (meta 74%) were obtained from the reaction with 1,2,3-trimethoxybenzene and could be separated by chromatography. In addition, a minor amount of a methoxy ipso substitution product (**3q'''**) was detected.<sup>32</sup> The methoxy group has been described as a leaving group in radical reactions, but examples are very rare.<sup>33</sup>

**Table 2**, all expected products **3a-3p** were obtained in moderate to excellent yields. Reactions with benzene (**2a**) led to the single isomers **3a** (85%), **3k** (82%), **3l** (60%) and **3m** (91%). Likewise the reactions with toluene (**2b**) and benzothiazole (**2j**) gave **3b** (78%) and **3j** (26%) as the only products. All other mono-substituted arenes **2** gave mixtures of *ortho:meta:para* isomers **3c** (85%), **3d** (99%), **3e** (62%), **3f** (76%), **3n** (68%) and **3o** (74%)<sup>30</sup> in relative ratios as indicated in Table 2. Naphthalene (**2h**) and *N*-methyl-pyrrole (**2i**) yield mixtures of  $\alpha:\beta$  substitution **3h** (87%), **3i** (57%) and **3p** (67%) in different relative ratios as given. The reaction with nitrobenzene (**2g**) yields no product, because **2g** is an excellent electron acceptor and can be photocatalytically reduced to aniline under the reaction conditions.<sup>31</sup> The molecular structures of compounds **3a**, **3j**, **3k** and **3l** were confirmed by X-ray single crystal analysis. Electron donating or electron withdrawing substituents are generally well tolerated. The chloride substituent allows further synthetic modifications of the coupling products. The two C-H arylation products **3q'** (para 18%) **3q''** (meta 74%) were obtained from the reaction with 1,2,3-trimethoxybenzene and could be separated by chromatography. In addition, a minor amount of a methoxy ipso substitution product (**3q'''**) was detected.<sup>32</sup> The methoxy group has been described as a leaving group in radical reactions, but examples are very rare.<sup>33</sup>

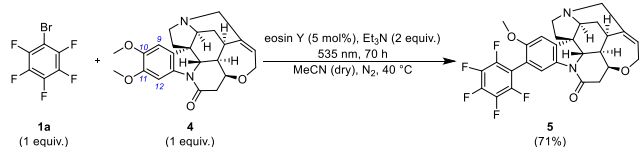
**Table 2.** Substrate scope



Next the complex non-protected natural product brucine (**4**) was used in a late stage functionalization (LSF) to demonstrate the functional group tolerance of the reaction. In 2012 Davies *et al.* functionalized brucine (**4**) by a metal-free carbene ap-



proach.<sup>34</sup> Recently Beckwith *et al.* achieved a selective functionalization at the  $\alpha$ -amino carbon moiety *via* an intermolecular rhodium-carbenoid insertion.<sup>35</sup> Brucine (**4**) is a toxic alkaloid found in *Strychnos nux-vomica*<sup>36</sup> and used as chiral base for the resolution of racemates.<sup>37</sup> Brucine (**4**) has analgesic and anti-inflammatory properties, behaves as a morphine-like analgesic drug<sup>38</sup> and positively cooperates with acetylcholine.<sup>39</sup> Allosteric enhancers of acetylcholine binding and function are regarded as useful targets for drug development for the treatment of Alzheimer's disease.<sup>39</sup> Substitution of the aromatic core of **4** may lead to derivatives with altered pharmacologic properties.



**Scheme 2.** Aromatic functionalization of brucine (**4**)

The standard conditions were used for the reaction of **1a** with **4** (1 equiv.) yielding product **5** in 71%.<sup>40</sup> Surprisingly, the C<sub>6</sub>F<sub>5</sub> radical substituted the brucine methoxy group in position 11.

### Mechanistic investigations

The photocatalytic system using eosin Y (EY, triethylammonium salt, for preparation see supporting information) as a photocatalyst and triethylamine (TEA) as electron donor enables the generation of a pentafluorophenyl radical, which is trapped by non-activated arenes resulting in polyfluorinated biaryls. The optimized conditions are shown in Figure 1; substrate concentration is 0.1 M and the reaction is performed under nitrogen.

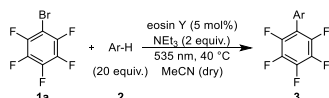


**Figure 1.** Optimized conditions for the C–H arylation

Eosin Y is a xanthene dye with ambivalent reactivity as photocatalyst. It was used in oxidative quenching cycles as photoreductant of diazonium salts<sup>27a</sup> as well as for the photoinduced reduction of nitrobenzenes, where eosin enters the reductive quenching cycle with a suitable sacrificial electron donor.<sup>31</sup> Based on the known eosin Y photoreactivity, two plausible mechanisms for the here described photocatalytic reaction of fluorinated aryl bromides **1** can be proposed (Figure 2).

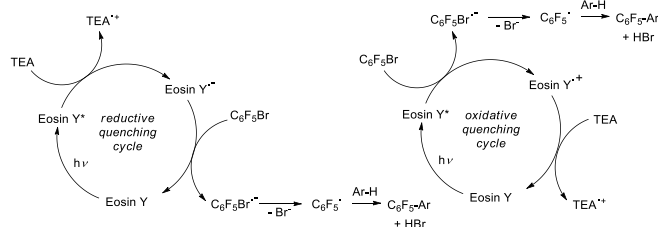


**Figure 2.** Two proposed catalytic reaction cycles

The reductive quenching cycle involves a photoinduced electron transfer from TEA to the excited eosin Y and subsequent

re-oxidation of the generated eosin radical anion by bromopentafluorobenzene. The reduced fluorinated arene cleaves the C<sub>Ar</sub>–Br bond yielding the pentafluorophenyl radical, which reacts to the product.<sup>41</sup>

The oxidative quenching cycle is based on photoinduced electron transfer from excited eosin Y to bromopentafluorobenzene.

In both cases hydrobromic acid is produced, which is neutralized by one equivalent of TEA present in the reaction mixture. Another equivalent of TEA is needed for the efficient quenching of the triplet excited state of eosin Y and also partially as a base for deprotonation of the lactone isomer of eosin Y used for the reactions. The photocatalytically active forms are the anion and dianion of EY.<sup>42</sup>

The mechanism of the photocatalytic reaction was elucidated by steady-state (UV-vis, fluorimetry) and transient spectroscopy (nanosecond pump-probe spectroscopy) and electrochemical measurements.

### Thermodynamics of the electron transfer

The electrochemical analysis of **1a** showed an irreversible reduction peak at  $-1.39$  V vs SCE (see supporting information for details). After the one-electron reduction the arene radical anion loses a bromide ion yielding the pentafluorophenyl radical.<sup>22c</sup> This explains the irreversibility of the reduction peak. The redox potential of TEA<sup>+</sup>/TEA is  $\sim +0.7$  V vs SCE.<sup>43</sup>

Eosin Y has been thoroughly studied as a photocatalyst and its redox potentials are well known. The redox potential of eosin Y in the ground state is EY/EY<sup>•-</sup> =  $-1.06$  V vs SCE, the excited triplet state of eosin Y was estimated to be <sup>3</sup>EY\*/EY<sup>•-</sup> =  $+0.83$  V vs SCE<sup>26a</sup>, and the redox potential of the oxidation of the excited state is EY<sup>•+</sup>/<sup>3</sup>EY\* =  $-1.1$  V vs SCE.<sup>42</sup>

The  $\Delta G_{eT}$  between the eosin triplet state and bromopentafluorobenzene (**1a**) estimated by the Rehm-Weller equation is  $+0.29$  eV ( $+6.7$  kcal/mol). This reaction is a key step in the oxidative quenching cycle and rather endothermic. The  $\Delta G_{eT}$  between the eosin triplet state and triethylamine (reductive quenching cycle) is  $-0.13$  eV ( $-3$  kcal/mol) and is thermodynamically feasible. The next step, re-oxidation of the eosin radical anion by the fluorinated arene **1a** has an estimated endothermic  $\Delta G_{eT}$  of  $+0.33$  eV ( $+7.6$  kcal/mol). In the case of two stable species, the endothermic reaction equilibrium is shifted towards the products by the subsequent irreversible fission of the bromide anion from the fluorinated arene.<sup>41</sup> This might result in a low quantum yield of the product formation corresponding to the required long reaction times of up to 72 h.

From the thermodynamic point of view, only the reductive quenching cycle is feasible. The radical adduct of the pentafluorophenyl radical and the arene is easily re-oxidized to the product. The driving force for this step is the restoration of the aromaticity of the system.

### Steady state spectroscopy

The interaction of fluorinated arene **1** and eosin Y (**A**) has been studied by means of UV-vis and fluorescence spectroscopy (see supporting information for details). It was found that bromopentafluorobenzene (**1a**) interacts neither with the ground state (UV-vis measurements, see supporting information for details) nor with the singlet state of eosin Y (fluorescence titration, see supporting information for details).

In analogy to previous reports the interaction of TEA and EY was studied by steady-state spectroscopy.<sup>42</sup> No changes in the absorption spectra and no quenching of fluorescence were observed. This proves that TEA does not interact with the ground state or with the excited singlet state of eosin Y. Slight changes in the absorption (see supporting information for details) and emission (see supporting information for details) spectra are caused by the acid-base equilibrium (deprotonation of the eosin Y lactone).<sup>42</sup>

### Transient spectroscopy

To elucidate the full mechanism a transient spectroscopy study was performed. Both excited state absorption spectra and kinetics of their respective decays have been measured in nanosecond to microsecond time-scale.

The transient spectra of a solution of EY measured after different times after excitation are shown in Figure 3. Immediately after excitation the singlet absorption peak ( $\lambda_S = 440$  nm), ground state bleach ( $\lambda_{GS} = 550$  nm) and fluorescence ( $\lambda_{FI} = 645$  nm) can be observed. The singlet state corresponds to the literature data.<sup>44</sup> Ground state bleach and fluorescence signal correspond to the absorption and emission spectra of eosin Y. The singlet decays with  $\tau_S = 6$  ns, which corresponds to the measured fluorescence lifetime (rise at 645 nm). After the intersystem crossing the triplet is formed with its characteristic absorption peak at 580 nm corresponding to published data.<sup>45</sup> The triplet lifetime of EY in non-degassed acetonitrile is  $\tau_T = 320$  ns. The triplet is quenched by oxygen present in the system as well as triplet-triplet interactions (T-T annihilation and T-T electron transfer), but the bimolecular processes do not play an important role and the decay can be reasonably well fitted with a mono-exponential function (Figure 4).

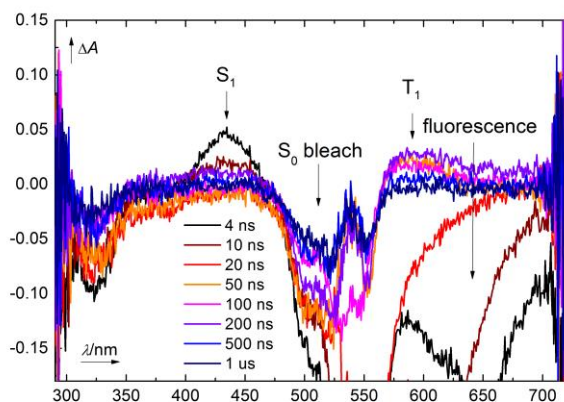


**Figure 3.** Transient absorption spectra of EY ( $10^{-4}$  M in acetonitrile, non-degassed, excitation wavelength 532 nm) at different times after excitation

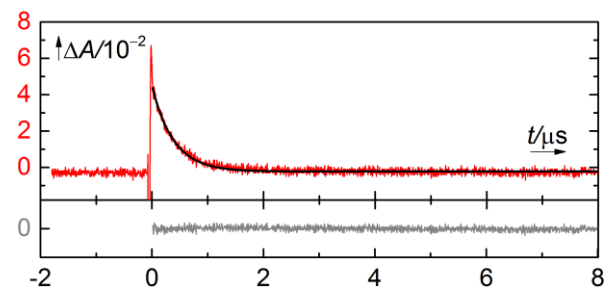


**Figure 4.** Decay trace of the triplet state of EY at 580 nm (top, red), mono-exponential fit (black curve) and the residuals of the fit (bottom, gray)

To investigate the interaction of EY with bromopentafluorobenzene the transient spectra of the solution of eosin Y ( $10^{-4}$  M) and the fluorinated arene ( $10^{-2}$  M in acetonitrile, non-degassed) were measured. The transient spectra measured after different times after excitation are shown in Figure 5.

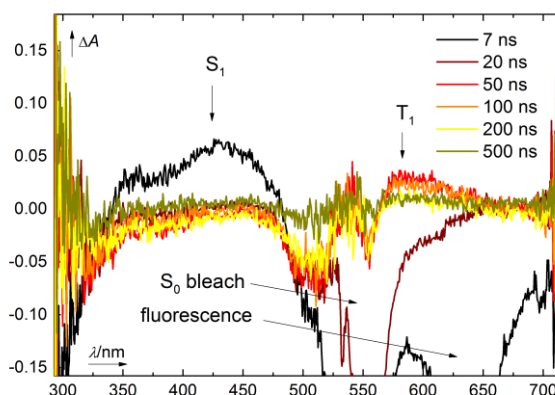


**Figure 5.** Transient absorption spectra of EY ( $10^{-4}$  M in acetonitrile, non-degassed, excitation wavelength 532 nm) and bromopentafluorobenzene ( $10^{-2}$  M) at different times after excitation

The intermediates correspond to the EY solution spectra (singlet absorption peak at  $\lambda_S = 440$  nm, ground state bleach at  $\lambda_{GS} = 550$  nm, fluorescence at  $\lambda_{FI} = 645$  nm and triplet at  $\lambda_T = 680$  nm).

The singlet ( $\tau_S = 6$  ns) and triplet lifetime ( $\tau_T = 320$  ns) remain unchanged in the presence of bromopentafluorobenzene. This indicates that there is no interaction between the ground or excited state of eosin Y and the arene.

The transient spectra of a solution of EY and triethylamine measured after different times after excitation are shown in Figure 6. The singlet absorption peak ( $\lambda_S = 440$  nm), ground state bleach ( $\lambda_{GS} = 550$  nm) and fluorescence ( $\lambda_{FI} = 645$  nm) are observed. After intersystem crossing ( $\tau_{isc} = 6$  ns) the triplet is formed with its characteristic absorption peak at 580 nm. The triplet lifetime of EY under these conditions is  $\tau_T = 280$  ns, which is lower than in pure EY solution indicating the quenching of the triplet state by TEA. Moreover, a new transient appears at 405 nm, which is assigned to the radical anion according to literature data.<sup>31</sup> The lifetime of the radical anion is 500 ns in non-degassed solution and is quenched mainly by re-oxidation by oxygen. The bimolecular dismutation of two

radicals is not significant, which can be derived from the mono-exponential fit of its decay (Figure 7, lower part).

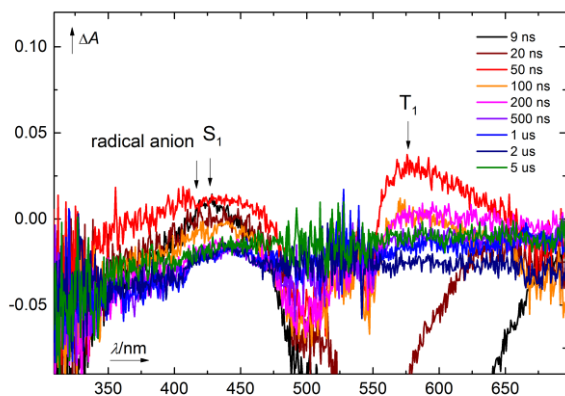


**Figure 6.** Transient absorption spectra of EY ( $10^{-4}$  M in acetonitrile, non-degassed, excitation wavelength 532 nm) and TEA ( $10^{-2}$  M) at different times after excitation

The comparison of the decay at 435 nm (singlet and shoulder of the radical anion) for solutions containing EY + TEA or EY + arene is shown in Figure 7. In the upper part the fast decay corresponds to the singlet state and in the lower part the singlet is observed together with the radical anion (slow decay).

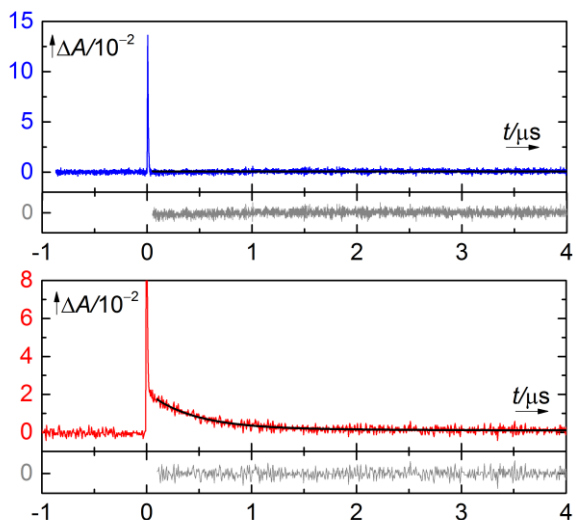


**Figure 7.** Decay traces of solutions of EY + arene (top, blue) and EY + TEA (bottom, red) ( $10^{-4}$  M EY and  $10^{-2}$  M TEA/arene) at 435 nm and the corresponding fits (black) and residuals (gray) after mono-exponential fit. The decay of singlet (fast decay, both spectra) and of the radical anion (slow decay, bottom) can be observed

The transient spectra of solutions of EY, bromopentafluorobenzene (**1a**) and triethylamine measured after different times after excitation are shown in Figure 8. After excitation the singlet absorption peak ( $\lambda_S = 440$  nm), ground state bleach ( $\lambda_{GS} = 550$  nm) and fluorescence ( $\lambda_{FI} = 645$  nm) can be observed. After the intersystem crossing ( $\tau_{isc} = 6$  ns) the triplet is formed with a characteristic absorption peak at 580 nm. The triplet lifetime of EY in non-degassed acetonitrile is  $\tau_T = 280$  ns, which corresponds to the triplet quenched by TEA. The radical anion of EY has a transient at 405 nm and its lifetime is signif-

icantly shortened by quenching with bromopentafluorobenzene to 250 ns.

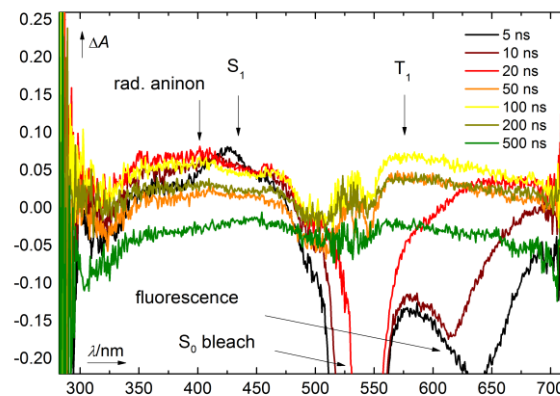


**Figure 8.** Transient absorption spectra of EY ( $10^{-4}$  M in acetonitrile, non-degassed, excitation wavelength 532 nm), TEA ( $10^{-2}$  M) and bromopentafluorobenzene ( $10^{-2}$  M) at different times after excitation

The results of the laser flash experiments are summarized in Table 3. The triplet state is reductively quenched by TEA to create the radical anion of EY, which transfers an electron to pentafluorobromobenzene.

**Table 3.** Transient species of EY and its lifetimes under various conditions; n. o. = not observed

transient		singlet	fluorescence	triplet	radical anion
wavelength [nm]		440	645	580	405
lifetime [ns]	EY	6	6	320	n. o.
	EY+arene	6	6	320	n. o.
	EY+TEA	6	6	280	500
	EY+TEA+arene	6	6	280	250

The overall proposed mechanism corresponds to the left part of Figure 2. EY undergoes a photoinduced single-electron reduction by TEA from the triplet state. The created anion radical is re-oxidized by the fluorinated arene **1a**, which cleaves forming the pentafluorophenyl radical. This species is trapped by an arene **2** leading to the radical adduct. The restoration of the aromaticity of this adduct, which leads to the product **3**, involves a one-electron oxidation and deprotonation (formally H-dissociation). The process is very facile as previously illustrated by the very low bond dissociation energies (BDE) of similar systems.<sup>46</sup>

The radical intermediates were trapped by the persistent radical TEMPO and the structure of adducts were determined by LC-MS (**6**, see supporting information). This further confirms the proposed mechanism.

#### Quantum yield determination

The quantum yield of the model photocatalytic reaction (see supporting information for details) was determined to be  $\Phi = (0.15 \pm 0.07) \%$ . This value corresponds to the long reaction times. The mechanism was tested if it contains any radical chain propagation by a method recently published by Yoon et al (see supporting information for details).<sup>47</sup> The quenching

constant was determined to be 0.74 and the corresponding radical chain length to be  $1.44 \times 10^{-2}$ . This indicates that the reaction mechanism does not involve radical chain processes and requires photoexcitation for each conversion.

## ■ CONCLUSION

The organic dye eosin Y is photoreduced by TEA via its triplet state by green light irradiation. The corresponding radical anion is then re-oxidized by bromopentafluorobenzene or bromotetrafluoro arenes. The radical anion of the halogenated arene fragments to give the corresponding fluorinated aryl radical and a bromine anion. The aryl radical reacts with simple arenes to give C–H arylation, but can also substitute a methoxy group in the complex structure of the alkaloid brucine. Very mild conditions of the radical generation by green light irradiation of 535 nm ensure good functional group tolerance. However, with several equally reactive positions for the C–H arylation, such as in naphthalene, mixtures of isomers are obtained. Such lack of selectivity may be of use in the non-specific late stage functionalization of active compounds in medicinal chemistry. The quantum yield of the reaction is low, due to significant energy loss by fluorescence and a rather small triplet quantum yield. Each catalytic cycle requires photoexcitation and a photoinduced radical chain mechanism can be excluded.

The simple and mild reaction conditions of the C–H / C–OME arylation of arenes with polyfluorinated benzenes make the described method suitable for the synthesis of bioactive molecules, organic materials or ligands for metal complexes.

## ASSOCIATED CONTENT

**Supporting Information.** For full experimental data see the Supporting Information. This material is available free of charge via the Internet at <http://pubs.acs.org>.

## AUTHOR INFORMATION

### Corresponding Author

\* Burkhard.Koenig@ur.de

### Notes

§ These authors contributed equally to the scientific results of the manuscript and appear in alphabetic order. All authors declare no competing financial interest.

## ACKNOWLEDGMENT

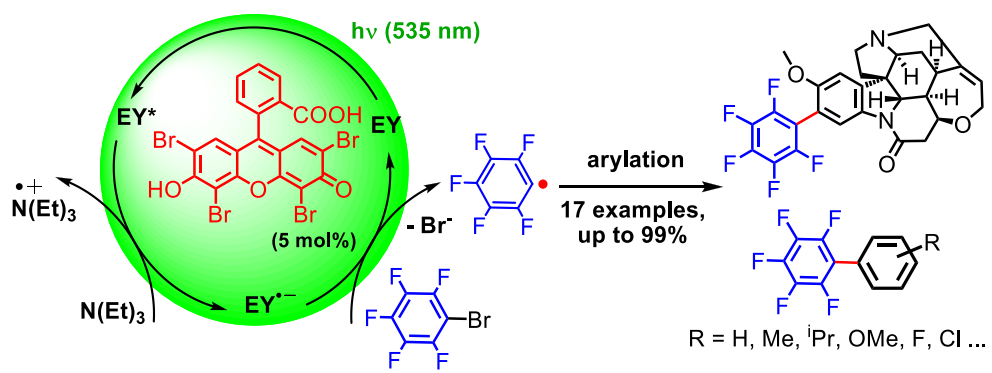
This work was supported by the German Science Foundation (DFG) (GRK 1626, Chemical Photocatalysis). A.U.M. thanks the Fonds der Chemischen Industrie for a scholarship. We thank Dr. Rudolf Vasold (University of Regensburg) for his assistance in GC-MS measurements, Regina Hoheisel (University of Regensburg) for her assistance in cyclic voltammetry measurements, and the Laboratory of Organic Photochemistry of Faculty of Science at Masaryk University in Brno, Czech Republic for transient absorption spectroscopic measurements. The RECETOX research infrastructure used for these measurements was supported by the projects of the Czech Ministry of Education (LO1214) and (LM2011028). C.J.Y. thanks the Sino-German Center for a Lindau fellowship.

## REFERENCES

- (1) (a) Zahn, A.; Brotschi, C.; Leumann, C. J. *Chem. Eur. J.* **2005**, *11*, 2125. (b) Purser, S.; Moore, P. R.; Swallow, S.; Gouverneur, V. *Chem. Soc. Rev.* **2008**, *37*, 320.
- (2) (a) Hwang, D.-H.; Song, S. Y.; Ahn, T.; Chu, H. Y.; Do, L.-M.; Kim, S. H.; Shim, H.-K.; Zyung, T. *Synth. Met.* **2000**, *111–112*, 485. (b) Tsuzuki, T.; Shirasawa, N.; Suzuki, T.; Tokito, S. *Adv. Mater.* **2003**, *15*, 1455. (c) Montes, V. A.; Li, G.; Pohl, R.; Shinar, J.; Anzenbacher, P. *Adv. Mater.* **2004**, *16*, 2001.
- (3) (a) Sakamoto, Y.; Suzuki, T.; Miura, A.; Fujikawa, H.; Tokito, S.; Taga, Y. *J. Am. Chem. Soc.* **2000**, *122*, 1832. (b) Babudri, F.; Farinola, G. M.; Naso, F.; Ragni, R. *Chem. Commun.* **2007**, 1003.
- (4) Kitamura, T.; Wada, Y.; Yanagida, S. *J. Fluorine Chem.* **2000**, *105*, 305.
- (5) (a) Weck, M.; Dunn, A. R.; Matsumoto, K.; Coates, G. W.; Lobkovsky, E. B.; Grubbs, R. H. *Angew. Chem. Int. Ed.* **1999**, *38*, 2741. (b) Nitschke, J. R.; Tilley, T. D. *J. Am. Chem. Soc.* **2001**, *123*, 10183.
- (6) Baragwanath, L.; Rose, C. A.; Zeitler, K.; Connon, S. J. *J. Org. Chem.* **2009**, *74*, 9214.
- (7) Meyer, E. A.; Castellano, R. K.; Diederich, F. *Angew. Chem. Int. Ed.* **2003**, *42*, 1210.
- (8) (a) Amii, H.; Uneyama, K. *Chem. Rev.* **2009**, *109*, 2119. (b) Senaweera, S. M.; Singh, A.; Weaver, J. D. *J. Am. Chem. Soc.* **2014**, *136*, 3002.
- (9) (a) Smith, R. C.; Bodner, C. R.; Earl, M. J.; Sears, N. C.; Hill, N. E.; Bishop, L. M.; Sizemore, N.; Hehemann, D. T.; Bohn, J. J.; Protasiewicz, J. D. *J. Organomet. Chem.* **2005**, *690*, 477. (b) Zhao, H.; Wei, Y.; Xu, J.; Kan, J.; Su, W.; Hong, M. *J. Org. Chem.* **2011**, *76*, 882.
- (10) Xiao, J.-C.; Ye, C.; Shreeve, J. n. M. *Org. Lett.* **2005**, *7*, 1963.
- (11) (a) Korenaga, T.; Kosaki, T.; Fukumura, R.; Ema, T.; Sakai, T. *Org. Lett.* **2005**, *7*, 4915. (b) Wei, Y.; Kan, J.; Wang, M.; Su, W.; Hong, M. *Org. Lett.* **2009**, *11*, 3346. (c) Kinzel, T.; Zhang, Y.; Buchwald, S. L. *J. Am. Chem. Soc.* **2010**, *132*, 14073.
- (12) (a) Frohn, H. J.; Adonin, N. Y.; Bardin, V. V.; Starichenko, V. F. *Tetrahedron Lett.* **2002**, *43*, 8111. (b) Frohn, H.-J.; Adonin, N. Y.; Bardin, V. V.; Starichenko, V. F. *J. Fluorine Chem.* **2002**, *117*, 115.
- (13) (a) Shang, R.; Fu, Y.; Wang, Y.; Xu, Q.; Yu, H.-Z.; Liu, L. *Angew. Chem. Int. Ed.* **2009**, *48*, 9350. (b) Shang, R.; Xu, Q.; Jiang, Y.-Y.; Wang, Y.; Liu, L. *Org. Lett.* **2010**, *12*, 1000.
- (14) DePasquale, R. J.; Tamborski, C. J. *J. Org. Chem.* **1969**, *34*, 1736.
- (15) Coe, P. L.; Pearl, G. M. *J. Organomet. Chem.* **1971**, *31*, 55.
- (16) (a) Lafrance, M.; Rowley, C. N.; Woo, T. K.; Fagnou, K. *J. Am. Chem. Soc.* **2006**, *128*, 8754. (b) René, O.; Fagnou, K. *Org. Lett.* **2010**, *12*, 2116.
- (17) Miao, T.; Wang, L. *Adv. Synth. Catal.* **2014**, *356*, 429.
- (18) (a) Wei, Y.; Su, W. *J. Am. Chem. Soc.* **2010**, *132*, 16377. (b) Li, H.; Liu, J.; Sun, C.-L.; Li, B.-J.; Shi, Z.-J. *Org. Lett.* **2011**, *13*, 276.
- (19) Chen, Q. Y.; Li, Z. T. *J. Org. Chem.* **1993**, *58*, 2599.
- (20) Chen, Q.-Y.; Li, Z.-T. *J. Chem. Soc., Perkin Trans. 1* **1993**, 1705.
- (21) (a) Kosynkin, D.; Bockman, T. M.; Kochi, J. K. *J. Am. Chem. Soc.* **1997**, *119*, 4846. (b) Kosynkin, D.; Bockman, T. M.; Kochi, J. K. *J. Chem. Soc., Perkin Trans. 2* **1997**, 2003.
- (22) (a) Hari, D. P.; Schroll, P.; König, B. *J. Am. Chem. Soc.* **2012**, *134*, 2958. (b) Hari, D. P.; König, B. *Angew. Chem. Int. Ed.* **2013**, *52*, 4734. (c) Ghosh, I.; Ghosh, T.; Bardagi, J. I.; König, B. *Science* **2014**, *346*, 725. (d) Nicewicz, D. A.; MacMillan, D. W. C. *Science* **2008**, *322*, 77. (e) Du, J.; Espelt, L. R.; Guzei, I. A.; Yoon, T. P. *Chem. Sci.* **2011**, *2*, 2115. (f) Wallentin, C.-J.; Nguyen, J. D.; Finkbeiner, P.; Stephenson, C. R. J. *J. Am. Chem. Soc.* **2012**, *134*, 8875.
- (23) (a) Hari, D. P.; König, B. *Org. Lett.* **2011**, *13*, 3852. (b) Rueping, M.; Zhu, S.; Koenigs, R. M. *Chem. Commun.* **2011**, 47, 8679.
- (24) (a) Hari, D. P.; Hering, T.; König, B. *Angew. Chem. Int. Ed.* **2014**, *53*, 725. (b) Nguyen, T. M.; Manohar, N.; Nicewicz, D. A. *Angew. Chem. Int. Ed.* **2014**, *53*, 6198.
- (25) (a) Meyer, A. U.; Jäger, S.; Hari, D. P.; König, B. *Adv. Synth. Catal.* **2015**, *357*, 2050. (b) Keylor, M. H.; Park, J. E.; Wallentin, C.-J.; Stephenson, C. R. J. *Tetrahedron* **2014**, *70*, 4264.



- (26) (a) Prier, C. K.; Rankic, D. A.; MacMillan, D. W. C. *Chem. Rev.* **2013**, *113*, 5322. (b) Schultz, D. M.; Yoon, T. P. *Science* **2014**, *343*, 1239176.
- (27) (a) Hari, D. P.; König, B. *Chem. Commun.* **2014**, *50*, 6688. (b) Fukuzumi, S.; Kotani, H.; Ohkubo, K.; Ogo, S.; Tkachenko, N. V.; Lemmetyinen, H. *J. Am. Chem. Soc.* **2004**, *126*, 1600.
- (28) Weaver, J. *Synlett* **2014**, *25*, 1946.
- (29) Redmond, R. W.; Gamlin, J. N. *Photochem. Photobiol.* **1999**, *70*, 391.
- (30) The two minor isomers are the ortho and meta products. There exact assignement was not possible because of the lack of literature NMRs.
- (31) Yang, X.-J.; Chen, B.; Zheng, L.-Q.; Wu, L.-Z.; Tung, C.-H. *Green Chem.* **2014**, *16*, 1082.
- (32) See GC/MS data in the supporting information. The product amount was too small for preparative isolation and characterization.
- (33) (a) Aihara, K.; Urano, Y.; Higuchi, T.; Hirobe, M. *J. Chem. Soc., Perkin Trans. 2* **1993**, 2165. (b) Rosa, A. M.; Lobo, A. M.; Branco, P. S.; Sundaresan, P. *Tetrahedron* **1997**, *53*, 285. (c) Zhang, W.; Pugh, G. *Tetrahedron Lett.* **2001**, *42*, 5613. (d) Ohno, H.; Wakayama, R.; Maeda, S.-i.; Iwasaki, H.; Okumura, M.; Iwata, C.; Mikamiyama, H.; Tanaka, T. *J. Org. Chem.* **2003**, *68*, 5909.
- (34) Hansen, S. R.; Spangler, J. E.; Hansen, J. H.; Davies, H. M. L. *Org. Lett.* **2012**, *14*, 4626.
- (35) He, J.; Hamann, L. G.; Davies, H. M. L.; Beckwith, R. E. J. *Nat. Commun.* **2015**, *6*, 5943.
- (36) Frédérich, M.; Choi, Y. H.; Verpoorte, R. *Planta Med.* **2003**, *69*, 1169.
- (37) Bhushan, R.; Ali, I. *Chromatographia* **1987**, *23*, 141.
- (38) Yin, W.; Wang, T.-S.; Yin, F.-Z.; Cai, B.-C. *J. Ethnopharmacol.* **2003**, *88*, 205.
- (39) Gharagozloo, P.; Lazareno, S.; Popham, A.; Birdsall, N. J. M. *J. Med. Chem.* **1999**, *42*, 438.
- (40) A second minor isomer was isolated in a yield of 8%. The HRMS of 561.1816 ( $[M + H]^+$  ( $C_{29}H_{26}F_5N_2O_4$ ) calc.: 561.1807) indicates the incorporation of  $C_6F_5$  in position 9 or 12, the limited amount of material and overlapping resonances in the NMR prevent the exact structure assignment of the byproduct.
- (41) Costentin, C.; Robert, M.; Savéant, J.-M. *J. Am. Chem. Soc.* **2004**, *126*, 16051.
- (42) Majek, M.; Filace, F.; Wangelin, A. J. v. *Beilstein J. Org. Chem.* **2014**, *10*, 981.
- (43) Ghosh, T.; Slanina, T.; König, B. *Chem. Sci.* **2015**, *6*, 2027.
- (44) Penzkofer, A.; Beidoun, A.; Speiser, S. *Chem. Phys.* **1993**, *170*, 139.
- (45) Liu, Q.; Li, Y.-N.; Zhang, H.-H.; Chen, B.; Tung, C.-H.; Wu, L.-Z. *Chem. Eur. J.* **2012**, *18*, 620.
- (46) Anamimoghadam, O.; Symes, M. D.; Busche, C.; Long, D.-L.; Caldwell, S. T.; Flors, C.; Nonell, S.; Cronin, L.; Bucher, G. *Org. Lett.* **2013**, *15*, 2970.
- (47) Cismesia, M. A.; Yoon, T. P. *Chem. Sci.* **2015**, *6*, 5426.

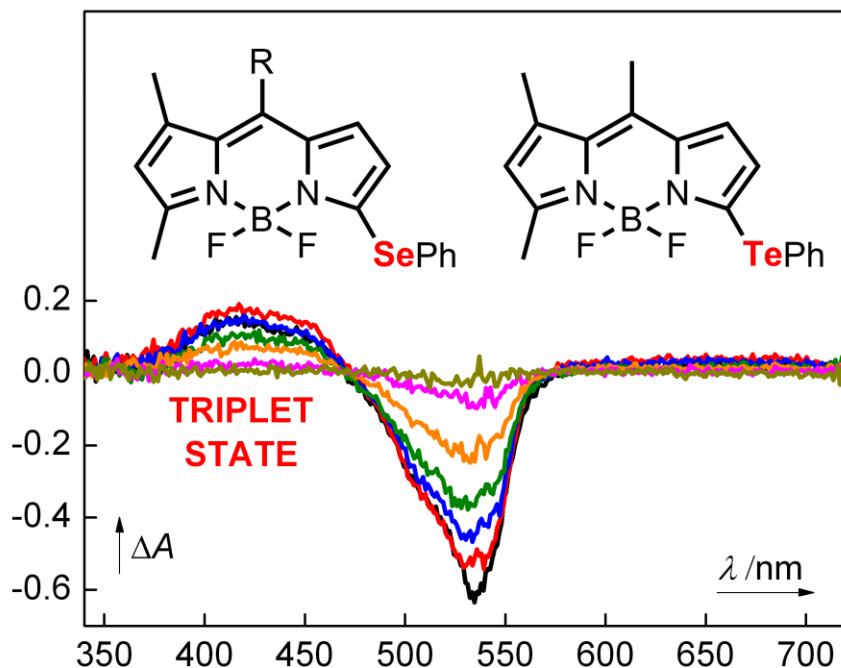


# Internal Heavy-Atom Effect in 3-Phenylselanyl and 3-Phenyltellanyl BODIPY Derivatives Studied by Transient Absorption Spectroscopy

Jamaludin Al Anshori, Tomáš Slanina, Eduardo Palao, Petr Klán\*

RECETOX, Faculty of Science, Masaryk University, Kamenice 5, 625 00, Brno

\* E-mail: klan@sci.muni.cz; Phone: +420-54949-4856; Fax: +420-54949-2443



## Abstract

Three monosubstituted 3-phenylselanyl and 3-phenyltellanyl BODIPY derivatives were synthesized and their spectroscopic properties were characterized and compared to those of iodine and chlorine-atom containing analogues as well as an unsubstituted BODIPY derivative. The fluorescence quantum yields were found to decrease, whereas the intersystem crossing quantum yields ( $\Phi_{\text{ISC}}$ ), determined by transient spectroscopy, increased in the order of the H→Cl→Se/I→Te substitution. The maximum  $\Phi_{\text{ISC}}$ , found for the 3-phenyltellanyl derivative, was 59%. The results are interpreted in terms of the internal heavy-atom effect of the substituents.

## Introduction

4,4-Difluoro-4-bora-3a,4a-diaza-*s*-indacene (BODIPY) derivatives have found extensive applications as fluorescent dyes and biological probes due to their robust and easily tunable photophysical properties.<sup>1-8</sup> BODIPY chromophores typically exhibit very high quantum yields of fluorescence; the intersystem crossing (ISC) quantum yield in most derivatives is negligible. This prevents their use as triplet photosensitizers in photocatalysis, photovoltaics, photodynamic therapy (singlet oxygen generation), or triplet–triplet annihilation upconversion.<sup>9</sup>

Nagano and his collaborators were first to prepare a 2,6-diiodo BODIPY derivative.<sup>10</sup> The presence of the iodine atoms enhances intersystem crossing due to a strong spin-orbit coupling between singlet and triplet states (heavy atom effect).<sup>11, 12</sup> High photoinduced cytotoxicity of this compound redirected the investigations, and various bromo and iodo analogues with different substituents<sup>5</sup> as well as those bearing alternative ISC promoters, such as heavy metal containing units, were designed and studied.<sup>6, 13, 14</sup> Such structural variations improved the physico-chemical properties of the chromophores and their cytotoxicities only in some cases.<sup>5, 15</sup> Heavy atom-free BODIPY dimers represent an alternative solution in the design of triplet sensitizers.<sup>16-20</sup> Structural variations of this type as well as extension of the BODIPY  $\pi$ -system by styryl or thiophene substituents shifts the absorption band maxima bathochromically to the spectral region called the phototherapeutic (tissue-transparent) window (650–950 nm).<sup>21</sup> Several aza-BODIPY analogues have also been introduced as triplet photosensitizers.<sup>5</sup>

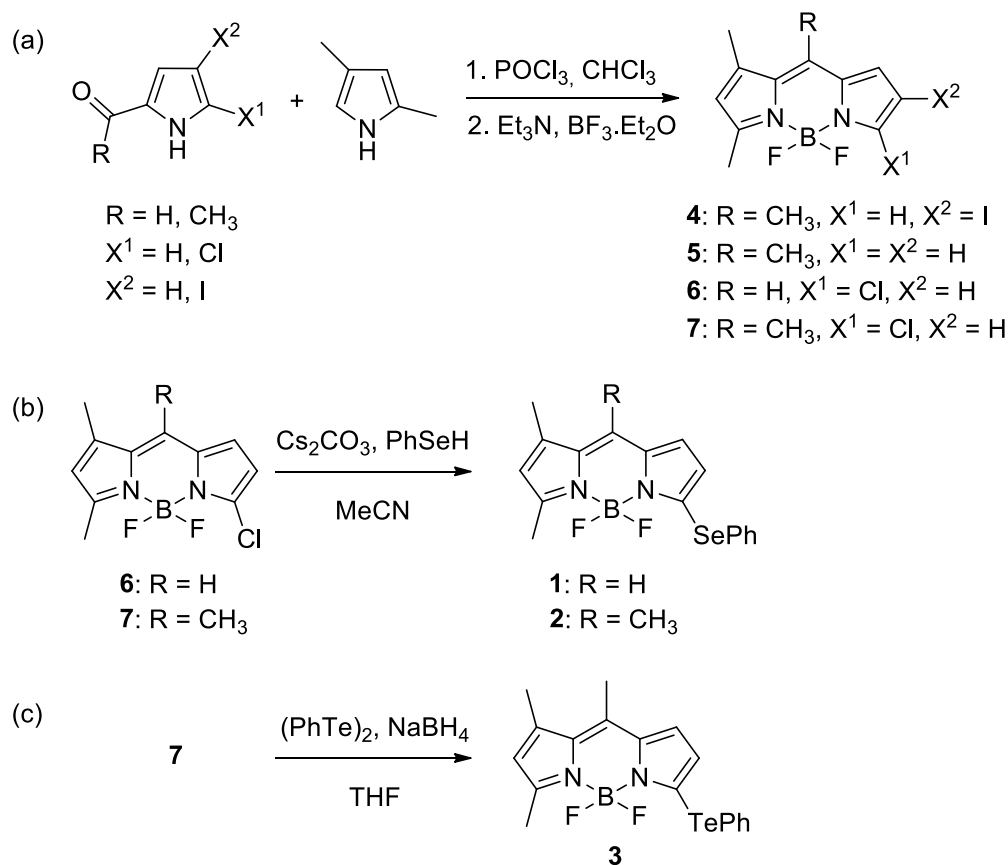
Important advances in the chemistry of selenium- and tellurium-containing organic compounds have been made in the past years due to their promising pharmacological properties and low toxicity.<sup>22-24</sup> These compounds can be used for sensing of reactive oxygen species (ROS), reactive nitrogen species (RNS), and bioorganic thiols.<sup>25-27</sup> Several examples of Se- and Te-BODIPY ROS sensors, based on turning off-on fluorescence in different oxidation states, have been reported.<sup>28, 29</sup> In most of these examples, the Se- and Te-atom containing groups are separated from the BODIPY chromophore by a linker that still permits an efficient intramolecular charge-transfer (ICT) in their reduced form. As far as we know, only two studies describe the synthesis of compounds that have either Se or Te directly attached to the BODIPY core.<sup>30, 31</sup> In one of those works, Vosch and coworkers used transient spectroscopy and fluorescence single-photon timing experiments to conclude that the presence of one or two of these atoms dramatically reduces the fluorescence due to efficient ISC.<sup>30</sup> The triplet lifetimes and ISC quantum yields have not been determined. In addition, the authors suggested that ICT from chalcogen to the BODIPY core can be responsible for deactivation of the locally excited state.

In this work, we present the synthesis and spectroscopic characterization of several novel 3-phenylselanyl and 3-phenyltellanyl BODIPY derivatives. Transient absorption spectroscopy was used to determine the triplet lifetimes and ISC quantum yields to evaluate the effect of chalcogen

substituents as heavy atoms. The spectroscopic results are compared to those obtained with some other reference BODIPY derivatives.

## Results and Discussion

**Synthesis.** The 3-phenylselenanyl BODIPY derivatives **1** and **2** were synthesized from the corresponding chlorides **6** and **7**, prepared by the condensation of two pyrrole derivatives according to Dehaen and coworkers<sup>32</sup> (Scheme 1a; see also Experimental Part), via an S<sub>N</sub>Ar reaction of benzeneselenolate generated from benzeneselenol and Cs<sub>2</sub>CO<sub>3</sub> in good chemical yields (~70%; Scheme 1b), analogous to the procedure of Vosch and coworkers.<sup>30</sup> The 3-phenyltellanyl BODIPY derivative **3** was obtained from **7** and benzenetelluroate generated from diphenyl ditelluride in the presence of NaBH<sub>4</sub> in 68% (Scheme 1c). The BODIPY derivatives **4** and **5** were again synthesized according the condensation method<sup>32</sup> (Scheme 1a) described above in 65 and 14% yields, respectively.



**Scheme 2.** Synthesis of the BODIPY Derivatives **1**–**7**.

**Photophysical Properties.** The absorption spectra of the BODIPY derivatives **1–7** in acetonitrile possess a major absorption band in the region of  $\lambda_{\max} = 482\text{--}540$  nm (Figure 1, Table 1). The absorption bands are bathochromically shifted for the derivatives **1–3** compared to those of **4–7**. Their values are affected by the solvent polarity (Figure S1; aggregation of **1** was excluded by a concentration dependence study, Figure S2). For example,  $\lambda_{\max}$  of **1** in water is 540 nm, and a new shoulder appears at 576 nm (Figure S1). The compounds **5–7** exhibit bright fluorescence, whereas the heavy atom (I, Se, Te) containing derivatives **1–4** are only weakly fluorescent at room temperature (Figure 2; Table 1). The higher signal-to-noise ratio in the emission signal of **3** is a consequence of its very low fluorescence quantum yield,  $\Phi_f$ . The bathochromic shifts caused by the heavy atoms in the absorption spectra of **1–3** is also apparent in their emission spectra. The fluorescence lifetimes,  $\tau_f$ , of **1**, **2** and **4** were shorter than those of the BODIPY derivatives **5–7**. We were unable to determine  $\tau_f$  of **3** because the compound photochemically degraded during the fluorescence measurement, and a new signal of a photoproduct (see below) overlapped that of **3**.

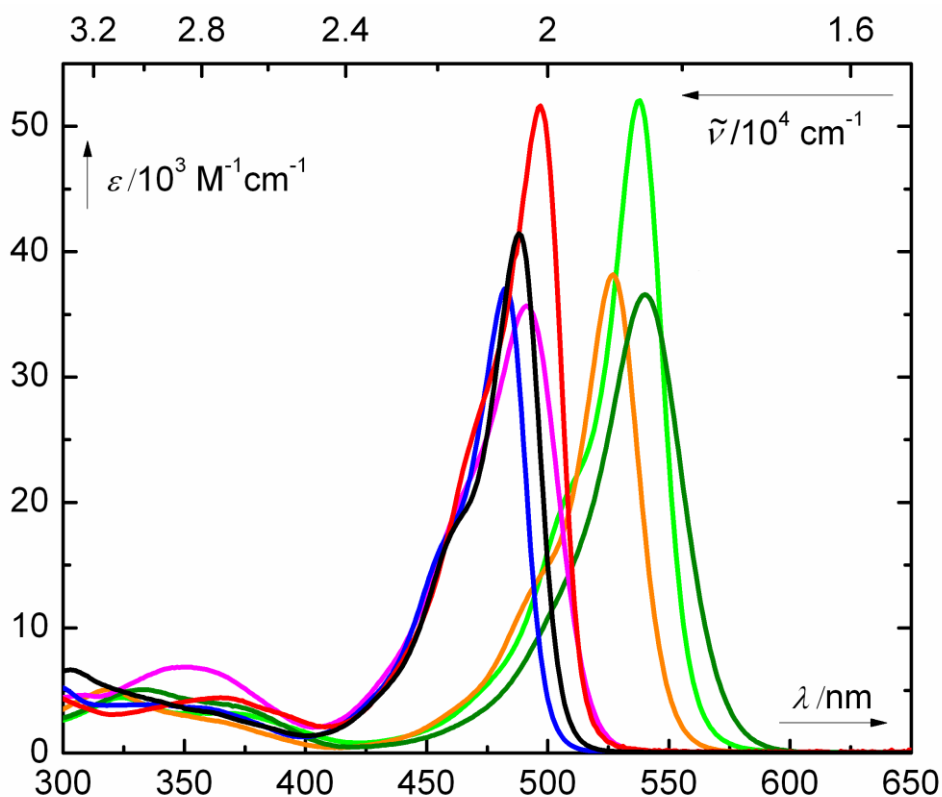


**Figure 1.** Absorption spectra of **1–7** in acetonitrile (**1**: light green; **2**: orange; **3**: dark green; **4**: magenta; **5**: blue; **6**: red; **7**: black).

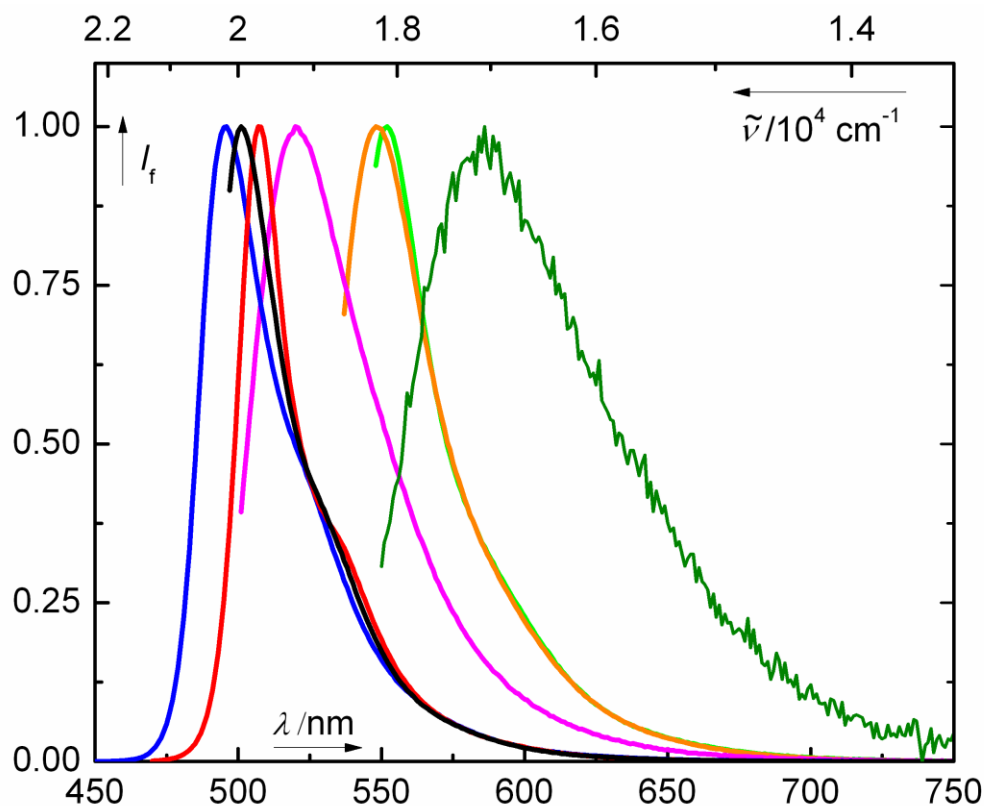


**Figure 2.** Normalized emission spectra of the BODIPY derivatives **1–7** in acetonitrile (**1**: light green; **2**: orange; **3**: dark green; **4**: magenta; **5**: blue; **6**: red; **7**: black).

**Table 1.** Absorption Photophysical Properties of **1–7** in Acetonitrile

compound	$\lambda_{\max}/\text{nm}$	$\epsilon_{\max}/\text{mol}^{-1} \text{ dm}^3 \text{ cm}^{-1}$	$\lambda_f/\text{nm}^a$	$\Phi_f/\%^b$	$\tau_f/\text{ns}^c$
<b>1</b>	538	52000	551	$6.3 \pm 0.4$	$0.53 \pm 0.01$
<b>2</b>	527	38200	545	$20 \pm 1$	$1.23 \pm 0.01$
<b>3</b>	540	36600	585	$0.09 \pm 0.03$	n. d. <sup>e</sup>
<b>4</b>	493	35400	521	$4.8 \pm 0.2$	$0.34 \pm 0.01$
<b>5</b>	483	37100	496	$92 \pm 3$	$5.98 \pm 0.01$
<b>6</b>	497	51640	507	$74^d$	$5.46 \pm 0.01$
<b>7</b>	488	37840	501	$73^d$	$5.60 \pm 0.01$

<sup>a</sup> **1–4** and **7**:  $\lambda_{\text{exc}} = \lambda_{\text{max}}$ ; **5**:  $\lambda_{\text{exc}} = 452 \text{ nm}$ ; **6**:  $\lambda_{\text{exc}} = 460 \text{ nm}$ . <sup>b</sup> The standard deviations were calculated from 5 independent measurements. <sup>c</sup> The standard deviations were calculated from 3 independent measurements. <sup>d</sup> From the ref. <sup>33</sup> <sup>e</sup> n. d. = not determined.



**Chemical Stability.** The compounds **1–5** were found to be stable when kept in acetonitrile solutions ( $c = 1\text{--}3 \times 10^{-5} \text{ mol dm}^{-3}$ ) in the dark at 22 °C. Their concentrations decreased only 3–4% in 10 days. When the same solutions were irradiated at  $\lambda_{\text{em}} = 525.5 \text{ nm}$ , the Se-BODIPY derivatives **1** and **2** were found to be more stable than the Te- and I-analogues **3,4** (Table 2). As expected, **5** was the most photostable of all studied derivatives, which may imply that photochemical activity is directly connected to the presence of a heavy heteroatom. Upon irradiation of **1–3**, a new emission band at  $\sim 496 \text{ nm}$  appeared (Figures S3–S5). We identified the photoproduct as compound **5** using HPLC using the authentic compound as a standard; therefore the cleavage of the C–Se or C–Te bonds occurs in the first photochemical step. As the compound **5** has a substantially higher fluorescence quantum yield (Table 1) than those of **1–3**, even trace amounts of this compound gives a strong emission signal.

**Table 2.** Photostability of **1–5** in Acetonitrile<sup>a</sup>

compound	$\tau_{1/2}/\text{h}$
<b>1</b>	24
<b>2</b>	101
<b>3</b>	0.2
<b>4</b>	7.7
<b>5</b>	650

<sup>a</sup> Irradiated using 32 high-energy LEDs emitting at  $\lambda_{\text{em}} = 525.5 \text{ nm}$  at the distance of  $\sim 1 \text{ cm}$  from the cuvette window. The same initial absorbance at  $\lambda = 525.2 \text{ nm}$  was adjusted for all samples.

**Transient Spectroscopy.** Transient absorption spectra of **1** obtained 8 ns–50  $\mu\text{s}$  after excitation at 532 nm were measured in both aerated and degassed acetonitrile ( $c = 1.10 \times 10^{-5} \text{ mol dm}^{-3}$ ; Figures 3 and S6). Absorption maxima at 420 and  $\sim 650 \text{ nm}$  as well as a ground state bleach at 535 nm, resembling its absorption spectrum (Figure 1), were observed. The decay or rise of the signals at the corresponding wavelengths followed the same monoexponential kinetics, and we attribute the signal to the lowest triplet state of **1**. Similar transient absorption of the triplet state of BODIPY derivatives has been reported before.<sup>30, 34</sup> A representative kinetic trace of the triplet state of **1** in both aerated and degassed acetonitrile solutions (Figure 4) gave the triplet lifetimes of  $\tau_{\text{T}} = 0.24$  and  $7.3 \mu\text{s}$ , respectively (Table 3). Transient spectra of the analogue **2** in both aerated and degassed acetonitrile solutions are shown in Figures S7 and S8. The absorption maximum ( $\lambda_{\text{max}}^{\text{T}} = 436 \text{ nm}$ ) and that of the ground state bleach at 520 nm are similar to those of **1**. A weak absorption band in the red part of the spectra seems to be somewhat shifted to longer wavelengths (Figures S6 and S7). The decay measured at the corresponding wavelengths followed the same monoexponential kinetics (Table 3). As the transient lifetime increased considerably (from  $\tau_{\text{T}} = 0.24$  to  $7.1 \mu\text{s}$ ) upon degassing the solution, we also assign it to the triplet state. Although the presence of tellurium in **3** is responsible for a bathochromic shift of its emission band maximum compared to those of **1** and **2** (Figure 2), it is not apparent in the

transient spectra of **1** and **2** (Figures S9 and S10;  $\lambda_{\text{max}} = 440$  and  $\sim 620$  nm). The rate constants of the triplet decay ( $k_d^T$ ) in aerated and degassed solutions are also shown in Table 3.

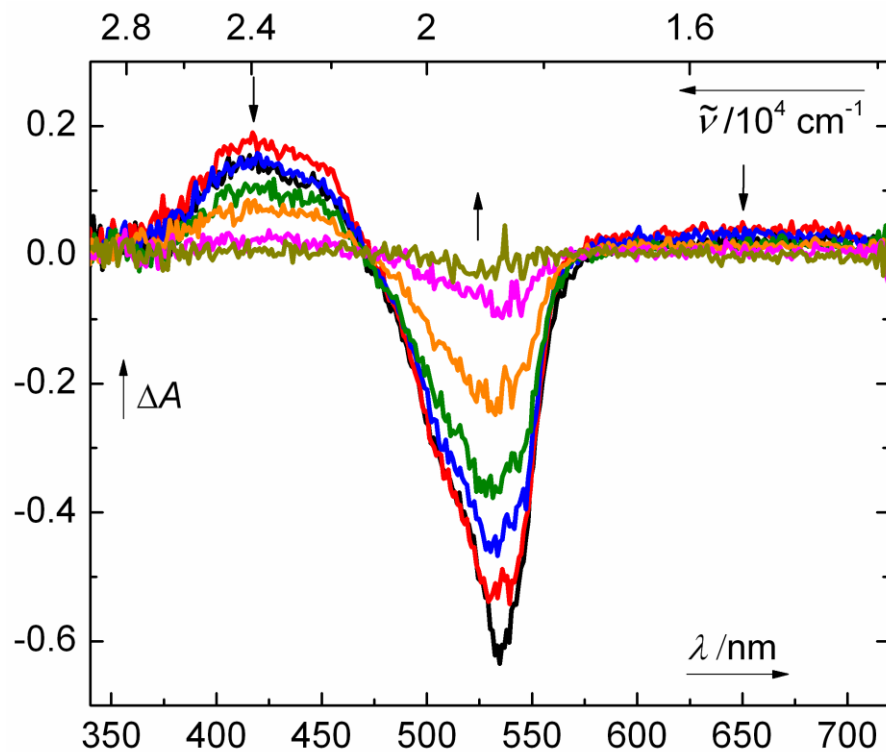


**Figure 3:** Transient spectra ( $\lambda_{\text{exc}} = 532$  nm) of **1** in non-degassed acetonitrile ( $c = 1.10 \times 10^{-5}$  mol dm $^{-3}$ ) obtained 8 ns-50  $\mu$ s after excitation.

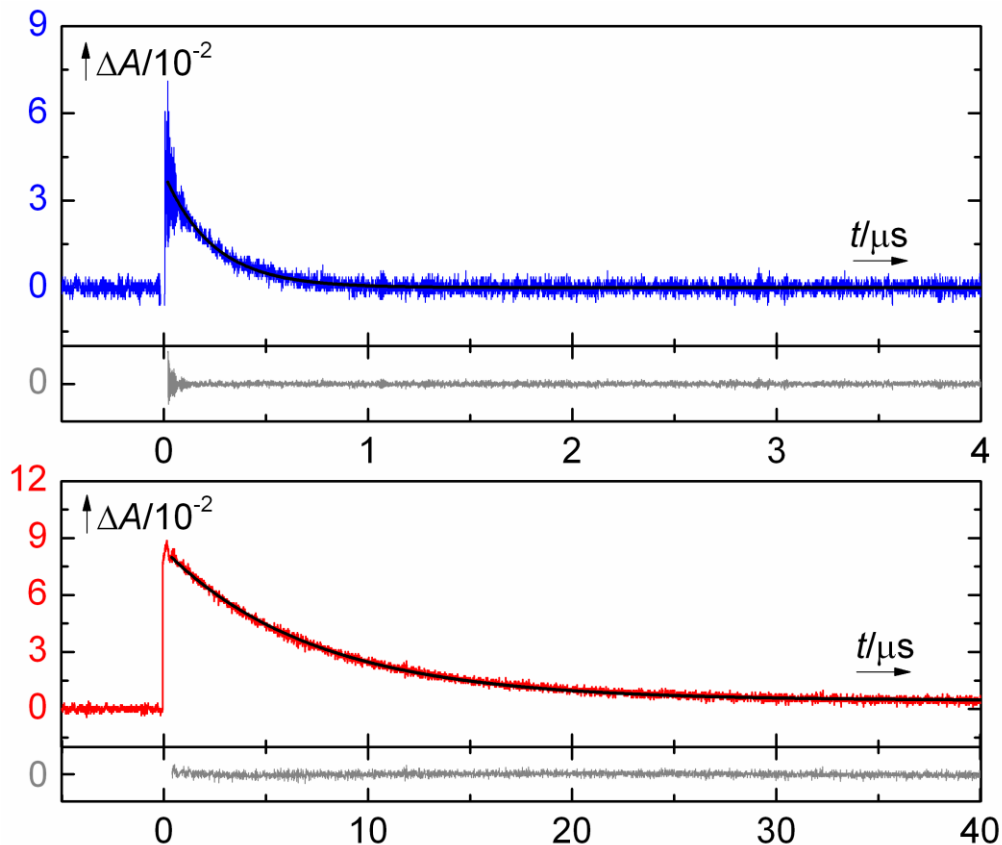


**Figure 4.** Representative kinetic traces and the residuals with a single-exponential fit of the signal for **1** excited at  $\lambda_{\text{exc}} = 532$  nm in aerated (top, kinetic trace: blue, exponential fit: black, sum of the residuals: gray) and degassed (bottom, kinetic trace: red, exponential fit: black, sum of the residuals: gray) acetonitrile ( $c = 1.10 \times 10^{-5}$  mol dm $^{-3}$ ) obtained at  $\lambda_{\text{exc}} = 650$  nm (top) and  $\lambda_{\text{exc}} = 420$  nm (bottom).

**Table 3.** Transient Absorption Data for **1–4**.

compd <sup>a</sup>	$\lambda_{\text{exc}}/\text{nm}^b$	cond <sup>c</sup>	$k_d^T/\text{s}^{-1}$ <sup>d</sup>	$\Phi_{\text{ISC}}^e$	$\lambda_{\text{max}}^T$ <sup>f</sup>	$\epsilon_{\text{max}}^T/\text{mol}^{-1} \text{dm}^3 \text{cm}^{-1}$ <sup>g</sup>
<b>1</b>	532	deg	$(1.4 \pm 0.1) \times 10^5$	$0.40 \pm 0.02$	418	$16400 \pm 1700$
		air	$(4.2 \pm 0.2) \times 10^6$			
<b>2</b>		deg	$(1.4 \pm 0.1) \times 10^5$	$0.44 \pm 0.02$	435	$6500 \pm 500$
		air	$(4.3 \pm 0.1) \times 10^6$			
<b>3</b>		deg	$(1.2 \pm 0.1) \times 10^5$	$0.59 \pm 0.02$	437	$9900 \pm 800$
		air	$(4.2 \pm 0.2) \times 10^6$			
<b>4</b>	355	deg	$(1.4 \pm 0.1) \times 10^5$	$0.54 \pm 0.03$	417	$11800 \pm 1300$
		air	$(4.4 \pm 0.1) \times 10^6$			

<sup>a</sup> Solutions in acetonitrile: **1–3**:  $c = \sim 1.5 \times 10^{-5}$  mol dm $^{-3}$ ; **4**:  $c = \sim 4.5 \times 10^{-5}$  mol dm $^{-3}$ . <sup>b</sup> Laser pulses of  $\leq 170$  ps;  $E_{\text{pulse}} = 240$  mJ at  $\lambda_{\text{exc}} = 532$  nm or  $E_{\text{pulse}} = 160$  mJ at  $\lambda_{\text{exc}} = 355$  nm. <sup>c</sup> deg: degassed; air: aerated. <sup>d</sup> Rate constants of triplet decay; a monoexponential fit based on 6

measurements. <sup>e</sup> Quantum yields of intersystem crossing (determined by a previously published method<sup>35</sup>), averaged from  $\geq 6$  measurements. <sup>f</sup> The maximum of triplet-triplet absorption and <sup>g</sup> its molar absorption coefficient (the standard deviation was calculated from  $\geq 6$  independent measurements).

The model 3-iodo BODIPY derivative **4**<sup>32</sup> does not absorb at 532 nm; therefore, 355-nm excitation was used for the transient spectroscopy measurements (Figures S11 and S12). The triplet spectrum exhibits similar characteristic absorption peaks ( $\lambda_{\text{max}}^{\text{T}} = 414$  and 667 nm) to those of **1–3**. The ground state bleach is masked by a high absorption of **4** in the region of 450–500 nm. We also attempted to investigate the model compounds **5** (no heavy atom) and **7** (Cl-atom containing derivative). However, we did not observe any triplet transient under the same experimental conditions, which points to a significantly lower quantum yield of ISC (Figure S13). This was expected as the compounds have very high fluorescence quantum yields (Table 1).

Table 3 shows that the compounds **1–4** possess nearly identical triplet lifetimes (7–8 and 0.2  $\mu\text{s}$  for degassed and aerated acetonitrile solutions, respectively), thus the Se, Te and I atoms must be responsible for efficient ISC (0.4–0.66). The superimposed transient spectra of **1–4** obtained at 2 ns after the excitation are shown in Figure 5. The molar absorption coefficients were calculated using the Lambert-Beer law from  $\Delta A$  of the ground state bleach signal taken at 2 ns after excitation and a cuvette optical pathway determined using a solution of eosin Y as a standard at  $c = 1 \times 10^{-5} \text{ mol dm}^{-3}$  (see Supporting Information). Compound **1** has the highest molar absorption coefficient at  $\lambda_{\text{max}}$  in both the triplet-triplet (Table 3) and  $S_0 \rightarrow S_1$  absorption (Table 1) spectra. The shape of the ground state bleach of **4** differs somewhat from its absorption spectrum, which indicates that the triplet state partially absorbs in the region of 440–480 nm.

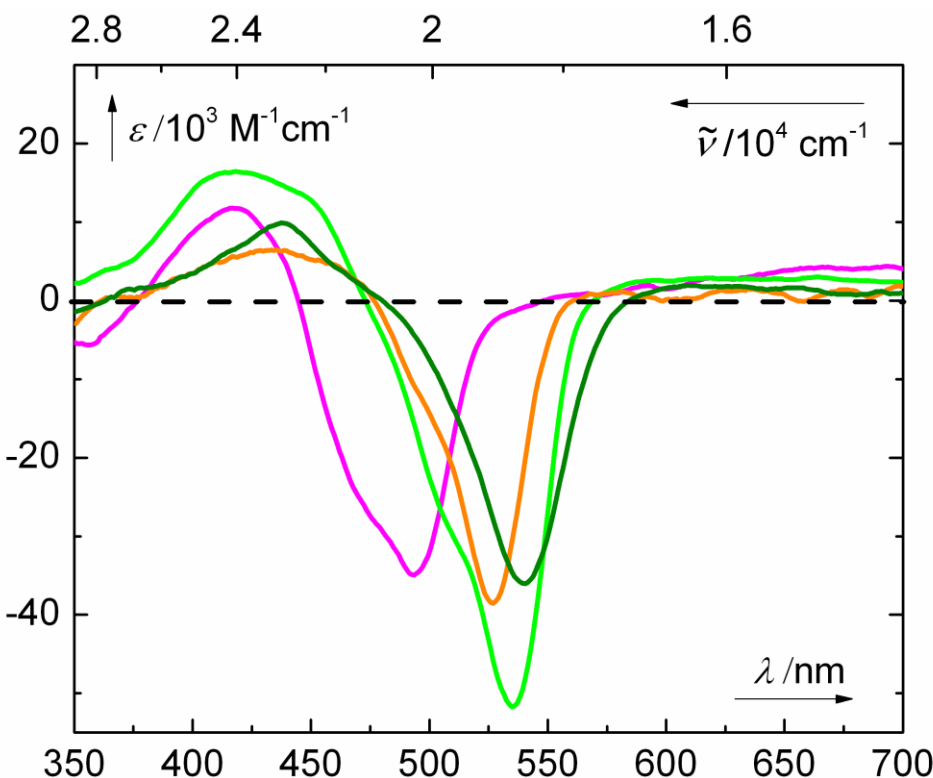


**Figure 5.** Transient spectra ( $\lambda_{\text{exc}} = 532 \text{ nm}$ ) of **1–4** in aerated acetonitrile solutions obtained at 2 ns after the excitation (the molar absorption coefficients are shown; **1**: light green; **2**: orange; **3**: dark green; **4**: magenta).

The aim of this work was to design and study BODIPY derivatives that exhibit efficient ISC as a consequence of the internal heavy-atom effect.<sup>12</sup> This effect is a short-distance phenomenon. For example, installation of the iodine atom to the *para*-position of the *meso*-phenyl group of BODIPY exhibits only very efficient fluorescence;<sup>36</sup> however, when iodine is attached directly to the chromophore core, ISC becomes dominant.<sup>34</sup> In contrast, 2-iodothieryl BODIPY derivatives have been introduced as efficient triplet photosensitizers due to an extended  $\pi$ -conjugation of the 2-iodothieryl and BODIPY moieties.<sup>37</sup> Several heavy-atom-containing BODIPY derivatives have already been made and studied. Iodine-substituted derivatives indeed possess high ISC quantum yields but the compounds were found to be rather photolabile and induce cytotoxicity upon photoproduct formation.<sup>5, 10</sup> Only two studies have introduced Se- or Te-substituted BODIPY derivatives,<sup>30, 31</sup> and the effect of heavy atoms on the ISC quantum yields have not been evaluated. Therefore, we prepared monosubstituted Se- and Te-atom containing derivatives **1–3** to compare their photophysical properties to those of the iodo or chloro analogues **4, 6** and **7** and an unsubstituted derivative **5**.

Alkyl groups at the *meso* position are known to have no special effect on the absorption and emission spectra.<sup>6</sup> However, the presence of a phenyl group in the *meso* position of BODIPY was found to decrease the fluorescence efficiency due to a more efficient radiationless decay induced by a ring rotation.<sup>38</sup> This group can also impose a considerable steric hindrance for substituents in the positions 1 and 7, which then enhances the fluorescence.<sup>39</sup> When we compared the properties of the *meso* H- and methyl-analogues **1** and **2**, the fluorescence efficiency increased for **2** compared to those of **1** by a factor of 3 (Table 1). Nevertheless, the photostability of **2** was ~4 times higher than of **1** (Table 2); therefore, the *meso* methyl group was installed in all remaining compounds studied (**3–5**). The Se and Te atoms were installed to the position 3 because the syntheses via nucleophilic substitution are straightforward<sup>40</sup> (unlike the positions 2 and 6 that bear the least positive charge and are rather susceptible to an electrophilic attack).<sup>6</sup> Finally, the model 2-iodo BODIPY analogue **4** was used because the synthetic protocol was readily available.<sup>32</sup>

The absorption and emission spectra of all compounds **1–7** in acetonitrile (Figures 1 and 2) possess characteristic features of the basic BODIPY chromophore.<sup>41</sup> A sharp peak and its shoulder in the absorption spectra is a manifestation of the allowed  $S_0 \rightarrow S_1$  transition of the delocalized  $\pi$ -conjugated system. Smaller molar absorption coefficients ( $35\text{--}55 \times 10^3 \text{ mol}^{-1} \text{ dm}^3 \text{ cm}^{-1}$ ) than those of unsubstituted symmetrical BODIPY derivatives ( $80\text{--}120 \times 10^3 \text{ mol}^{-1} \text{ dm}^3 \text{ cm}^{-1}$ )<sup>8</sup> are probably caused by an asymmetric substitution pattern, leading to charge separation between the pyrrole rings.<sup>39</sup> A second, less pronounced band observed in the region of 225–400 nm is attributed to the  $S_0 \rightarrow S_2$  transition. A bathochromic shift observed in both absorption and emission spectra in the order of the substituents H/Cl  $\rightarrow$  I  $\rightarrow$  Se  $\rightarrow$  Te (Figures 1 and 2) is clearly a consequence of an increasing electron-donating ability of the substituent. The relatively small Stokes shifts (13–45 nm) observed in all derivatives are related to the rigidity of the BODIPY system.

The fluorescence quantum yields decreased with the heavy-atom substitution; nevertheless, residual fluorescence was still detected (Table 1). The heavy-atom effect must be responsible for fluorescence quenching but also for shortening of the phosphorescence lifetimes.<sup>11</sup> Examples of compounds bearing the chalcogen atoms that exhibit enhanced ISC in various chromophores have already been reported. For example, furan, thiophene, selenophene, or tellurophene and their derivatives exhibited a linear correlation with the atomic spin-orbit constant of the corresponding chalcogen in the series of O  $\rightarrow$  S  $\rightarrow$  Se  $\rightarrow$  Te.<sup>42, 43</sup>

In most of the literature reports, indirect measurements of the quantum yield (QY) of singlet oxygen ( $^1\text{O}_2$ ) generation serves as a tool to determine the ISC efficiency in BODIPY derivatives.<sup>5</sup> In this work, we identified the triplet state and determined the triplet lifetimes and ISC quantum yields for all compounds using nanosecond transient absorption measurements (Table 3). Unfortunately, we could not evaluate the rate constants of the triplet state formation because the process was too fast for our ns apparatus. Similar transient spectra of the BODIPY

triplets have also been reported for several BODIPY derivatives containing Se, Te,<sup>30</sup> and I<sup>39</sup> atoms. As expected, tellurium in **3** enhanced the triplet state more efficiently than selenium in the derivatives **1** and **2** and iodine in **4** (by a factor below 1.4), whereas the decay of the corresponding triplets was essentially the same for all degassed samples (~7  $\mu$ s), perhaps due to competition of other radiationless processes or a cleavage of the carbon–chalcogen bond occurring in the triplet state (see above). A 2<sup>nd</sup> order kinetic model, such as triplet-triplet annihilation, could not be fitted with the experimental data.

In addition, Churchill and coworkers provided evidence for the photoinduced electron transfer (PET) from a phenyl tellurium group attached to the BODIPY core (they reported that the fluorescence quantum yield increased from 0.06 to 0.2 when the Te atom was oxidized to the corresponding tellurium oxide) in their search for selective sensing of hypochlorite ion in aqueous solutions.<sup>23, 31</sup> As the sum of the quantum yields of fluorescence and ISC never reached 100% in compounds studied in this work (Tables 1 and 3), other (radiationless) processes must contribute to the overall excitation decay. It is thus possible that PET from the chalcogens<sup>44</sup> to the S<sub>1</sub> excited BODIPY core<sup>45</sup> in **1–3** competes with ISC.

If the applicability of the compounds **1–3** as triplet sensitizers is considered, all derivatives have the same magnitude of  $\Phi_{ISC}$  but their photostability is profoundly different (Table 2). The Te-atom substituted BODIPY is photochemically rather unstable, whereas the Se-derivative **2** exhibits a very high photochemical stability; its half-life under the identical irradiation conditions is almost two orders of magnitude longer than that of the 2-iodo BODIPY derivative **4**.

## Conclusions

Steady-state and transient spectroscopy studies of three novel monosubstituted 3-phenylselenanyl and 3-phenyltellanyl BODIPY derivatives were used to evaluate the extent of intersystem crossing related to the heavy-atom effect of the Se and Te atoms. It was found that its magnitude is comparable to that of the corresponding monosubstituted 2-iodo derivative. As the photostability of the selenium atom-containing derivatives was found relatively high, they could be considered as triplet sensitizers in various applications.

## Experimental Part

**Material and Methods.** The reagents and solvents of the highest purity available were used as purchased, or they were purified/dried using standard procedures and kept over activated 3 Å molecular sieves (8–12 mesh) under dry N<sub>2</sub>. The synthetic steps were performed under ambient atmosphere unless stated otherwise. The following synthetic intermediates, 5-chloro-1*H*-pyrrole-2-carbaldehyde, 1-(5-chloro-1*H*-pyrrol-2-yl)ethanone, 1-(4-iodo-1*H*-pyrrol-2-yl)ethanone, were



synthesized using the procedure reported before.<sup>32</sup> All glassware was oven-dried prior to use. All purification procedures were performed using silica gel column or preparative thin layer chromatography.

<sup>1</sup>H and <sup>13</sup>C NMR spectra were recorded on 300 or 500 MHz spectrometers in chloroform-*d*, acetone-*d*<sub>6</sub>, or dichloromethane-*d*<sub>2</sub>. The NMR signals were referenced to the residual peak of the (major) solvent. The deuterated solvents were kept over activated 3 Å molecular sieves (8–12 mesh) under dry N<sub>2</sub>. UV absorption spectra and the molar absorption coefficients were obtained on a UV-vis spectrometer with matched 1.0-cm quartz cells. Fluorescence spectra were recorded on an automated luminescence spectrometer in 1.0 cm quartz fluorescence cuvettes at 25 ± 1 °C; the sample concentration was set to keep the absorbance below 0.1 at λ<sub>max</sub>; each sample was measured five times and the spectra were averaged. Emission and excitation spectra are normalized; they were corrected using standard correction files. A nanosecond flash lamp (filled with H<sub>2</sub>) was used for measuring the fluorescence lifetimes. The data obtained were deconvolved from the measured decay curves of the sample and the instrumental response function. HPLC (a reverse phase column C-8; UV and fluorescence detectors) was used to check the purity of the final synthetic products. Exact masses were obtained using a triple quadrupole electrospray ionization mass spectrometer in positive or negative ion mode. The melting points were determined on a non-calibrated Kofler's hot stage or in open-end capillary tubes using a non-calibrated melting point apparatus.

The nanosecond laser flash photolysis (LFP) setup was operated in a right-angle arrangement of the pump and probe beams. Laser pulses of 170 ps duration at 532 nm (240 mJ; the compounds **1–3**) or at 355 nm (160 mJ; the compound **4**) were obtained from a Nd:YAG laser. The laser beam was dispersed on a 40 mm long and 10 mm wide modified fluorescence cuvette (a 40 mm optical path). The probe light from a xenon lamp was filtered as necessary. The full description of the apparatus has been published before.<sup>46</sup> The measurements were performed at ambient temperature (20 ± 2 °C). Kinetic traces were fitted using the Levenberg-Marquard algorithm. All measurements were performed at least three times unless stated otherwise. All samples were irradiated by a single laser flash (all BODIPY derivatives are photoactive); the cuvette was filled with a fresh solution after each measurement. The samples were degassed by purging the solutions with oxygen-free nitrogen for 20 minutes in a modified Schlenk fluorescence quartz cuvette. Our degassing method was compared with a freeze-pump-thaw technique (3 cycles): the triplet lifetimes determined by both methods did not differ by more than 5%. In addition, the procedure is highly reproducible as can be seen from standard deviations for the measured triplet lifetimes (Table 3).

**General Procedure for the Synthesis of the Compounds 4-7.** The synthesis was accomplished according to the reported procedure.<sup>32</sup> A solution of POCl<sub>3</sub> (1.1 equiv.) was added into a stirred solution of 1-(5-halo-1*H*-pyrrol-2-yl)ethanone derivative (1 equiv.) in chloroform (50 mL) (Scheme 1). The reaction mixture was stirred at 23 °C for 1 h. 2,4-Dimethyl-1*H*-pyrrole (1.1 equiv.) was added in to the reaction mixture which was further stirred at room temperature

overnight. Triethylamine (1.1 equiv.) was then added to the solution and followed by the addition of  $\text{BF}_3 \cdot \text{Et}_2\text{O}$  (1.1 equiv.). The reaction mixture was stirred for 2.5 h. The reaction mixture was quenched with 10% of HCl (10 mL) and extracted with ethyl acetate. The organic layer was washed with water ( $3 \times 10$  mL), dried over  $\text{MgSO}_4$  and filtered. The solvent was removed under reduced pressure. Column chromatography was used to purify the title compounds.

**Synthesis of 2-Iodo-4,4-difluoro-5,7,8-trimethyl-4-bora-3a,4a-diaza-s-indacene (4).** The following starting material was used: 1-(4-iodo-1*H*-pyrrol-2-yl)ethanone (500 mg, 2.13 mmol),  $\text{POCl}_3$  (360 mg, 0.21 mL, 2.34 mmol), 2,4-dimethyl-1*H*-pyrrole (223 mg, 0.23 mL, 2.34 mmol), triethylamine (236 g, 0.32 mL, 2.34 mmol),  $\text{BF}_3 \cdot \text{Et}_2\text{O}$  (332 mg, 0.30 mL, 2.34 mmol). Column chromatography: silica gel; *n*-hexane/dichloromethane, 1 : 1, v/v. Orange solid. Yield: 500 mg (65%).  $^1\text{H}$  NMR (500 MHz, acetone- $d_6$ ):  $\delta$  (ppm) 7.54 (s, 1H), 7.37 (s, 1H), 6.43 (s, 1H), 2.64 (s, 3H), 2.54 (s, 3H), 2.49 (s, 3H). The compound was characterized elsewhere.<sup>32</sup>

**Synthesis of 4,4-Difluoro-5,7,8-trimethyl-4-bora-3a,4a-diaza-s-indacene (5).** The following starting material was used: 1-(1*H*-pyrrol-2-yl)ethanone (100 mg, 0.92 mmol),  $\text{POCl}_3$  (169 mg, 0.10 mL, 1.10 mmol), 2,4-dimethyl-1*H*-pyrrole (105 mg, 0.11 mL, 1.10 mmol), triethylamine (111 mg, 0.15 mL, 1.10 mmol),  $\text{BF}_3 \cdot \text{Et}_2\text{O}$  (156 mg, 0.14 mL, 1.10 mmol). Column chromatography: silica gel; *n*-hexane/dichloromethane, 6 : 4, v/v. Mp 163–164 °C. Orange solid. Yield: 29 mg (14%).  $^1\text{H}$  NMR (500 MHz,  $\text{CD}_2\text{Cl}_2$ ):  $\delta$  (ppm) 7.56 (s, 1H), 7.14 (s, 1H), 6.45 (s, 1H), 6.21 (s, 1H), 2.59 (s, 3H), 2.54 (s, 3H), 2.44 (s, 3H).  $^{13}\text{C}$  NMR (126 MHz,  $\text{CD}_2\text{Cl}_2$ ):  $\delta$  (ppm) 160.9, 146.7, 143.0, 138.0, 134.9, 134.8, 124.3, 123.5, 116.0, 17.27, 17.0, 15.2. HRMS (APCI)  $m/z$ :  $[\text{M} - \text{H}]^-$  calcd. for  $\text{C}_{12}\text{H}_{13}\text{BF}_2\text{N}_2$  233.1069; found 233.1067.

**Synthesis of 3-Chloro-4,4-difluoro-5,7-dimethyl-4-bora-3a,4a-diaza-s-indacene (6).** The following starting material was used: 5-chloro-1*H*-pyrrole-2-carbaldehyde (500 mg, 3.86 mmol),  $\text{POCl}_3$  (651 mg, 0.40 mL, 4.2 mmol), 2,4-dimethyl-1*H*-pyrrole (400 mg, 0.44 mL, 4.2 mmol), triethylamine (427 mg, 0.59 mL, 4.2 mmol),  $\text{BF}_3 \cdot \text{Et}_2\text{O}$  (0.60 g, 0.52 mL, 4.2 mmol). Column chromatography: silica gel; *n*-hexane/dichloromethane, 6 : 4, v/v. Red crimson solid. Yield: 400 mg (40%).  $^1\text{H}$  NMR (500 MHz,  $\text{CD}_2\text{Cl}_2$ ):  $\delta$  (ppm) 7.16 (s, 1H), 6.94 (d, 1H,  $J = 4.0$  Hz), 6.35 (d, 1H,  $J = 4.0$  Hz), 6.26 (s, 1H), 2.61 (s, 3H), 2.31 (s, 3H). The compound was characterized elsewhere.<sup>32</sup>

**Synthesis of 3-Chloro-4,4-difluoro-5,7,8-dimethyl-4-bora-3a,4a-diaza-s-indacene (7).** The following starting material was used: 1-(5-chloro-1*H*-pyrrol-2-yl)ethanone (500 mg, 3.48 mmol),  $\text{POCl}_3$  (593 mg, 0.36 mL, 3.83 mmol), 2,4-dimethyl-1*H*-pyrrole (364 mg, 0.40 mL, 3.83 mmol), triethylamine (389 mg, 0.54 mL, 3.83 mmol),  $\text{BF}_3 \cdot \text{Et}_2\text{O}$  (550 mg, 0.47 mL, 3.83 mmol). Column chromatography: silica gel; *n*-hexane/dichloromethane, 6 : 4, v/v. Red crimson solid. Yield: 550 mg (59%).  $^1\text{H}$  NMR (300 MHz,  $\text{CDCl}_3$ ):  $\delta$  (ppm) 7.03 (d, 1H,  $J=3.63$  Hz), 6.29 (d, 1H,  $J=3.66$  Hz), 6.17 (s, 1H), 2.58 (s, 3H), 2.50 (s, 3H), 2.40 (s, 3H). The compound was characterized elsewhere.<sup>32</sup>

**General Procedure for the Synthesis of the Compounds 1 and 2.** This synthesis is a modification of the method Vosch and coworkers (Scheme 1).<sup>30</sup> A BODIPY precursor (1 molar equiv.) was added to a solution of benzeneselenol (1.5 equiv.) and Cs<sub>2</sub>CO<sub>3</sub> (1.5 equiv.) in dry acetonitrile under nitrogen atmosphere, and the reaction mixture was stirred at 20 °C. After disappearance of the starting material (TLC; ~10 min), water was added and the crude product was extracted with dichloromethane. The organic phases were dried over MgSO<sub>4</sub>, filtered and concentrated to dryness. The resulting product was purified by preparative TLC (silica gel; *n*-hexane/ethyl acetate, 8 : 2, v/v).

**Synthesis of 3-Phenylselanyl-4,4-difluoro-5,7-dimethyl-4-bora-3a,4a-diaza-s-indacene (1).**

The following starting material was used: **6** (50 mg, 0.20 mmol), benzeneselenol (46 mg, 31.3 μL, 0.29 mmol) and Cs<sub>2</sub>CO<sub>3</sub> (96 mg, 0.29 mmol), and dry acetonitrile (10 mL). Red solid. Yield: 50 mg (67%). Mp 145–146 °C. <sup>1</sup>H NMR (500 MHz, CD<sub>2</sub>Cl<sub>2</sub>): δ (ppm) 7.74 (m, 2H), 7.43 (m, 3H), 7.07 (s, 1H), 6.82 (d, 1H, J=4.1 Hz), 6.15 (s, 1H), 5.90 (d, 1H, J = 4.1 Hz), 2.54 (s, 3H), 2.25 (s, 3H). <sup>13</sup>C NMR (126 MHz, CD<sub>2</sub>Cl<sub>2</sub>): δ (ppm) 159.8, 149.6, 143.5, 136.1, 136.0, 135.2, 129.7, 129.3, 127.4, 126.84, 126.83, 126.81 121.6, 120.2, 119.6, 14.7, 11.1. HRMS (APCI<sup>+</sup>) *m/z*: [M + H]<sup>+</sup> calcd. for C<sub>17</sub>H<sub>15</sub>BF<sub>2</sub>N<sub>2</sub>Se 377.0538; found 377.0536.

**Synthesis of 3-Phenylselanyl-4,4-difluoro-5,7,8-trimethyl-4-bora-3a,4a-diaza-s-indacene (2).**

The following starting material was used: **7** (40 mg, 0.15 mmol), benzeneselenol (34.9 mg, 23.7 μL, 0.22 mmol), Cs<sub>2</sub>CO<sub>3</sub> (72.8 mg, 0.22 mmol), dry acetonitrile (10 mL). Dark red solid. Yield: 38 mg (60%). Mp 151–152 °C. <sup>1</sup>H NMR (500 MHz, CD<sub>2</sub>Cl<sub>2</sub>): δ (ppm) 7.73 (m, 2H), 7.42 (m, 3H), 7.02 (d, 1H, J = 4.2 Hz), 6.17 (s, 1H), 5.94 (d, 1H, J = 4.2 Hz), 2.54 (s, 3H), 2.49 (s, 3H), 2.41 (s, 3H). <sup>13</sup>C NMR (126 MHz, CD<sub>2</sub>Cl<sub>2</sub>): δ (ppm) 158.0, 157.6, 147.5, 144.2, 139.7, 139.5, 137.7, 136.5, 133.9, 130.2, 129.7, 127.9, 125.5, 122.6, 119.7, 17.0, 16.6, 15.1. HRMS (APCI<sup>+</sup>) *m/z*: [M + H]<sup>+</sup> calcd. for C<sub>18</sub>H<sub>17</sub>BF<sub>2</sub>N<sub>2</sub>Se 391.0695; found 391.0694.

**Synthesis of 3-Phenyltellanyl-4,4-difluoro-5,7,8-trimethyl-4-bora-3a,4a-diaza-s-indacene (3).**

The synthesis was accomplished according to the method reported by Vosch and coworkers (Scheme 2).<sup>30</sup> The solution of sodium borohydride (40 mg, 1.06 mmol) in ethanol (4 mL) was slowly added to the solution of diphenyl ditelluride (91.5 mg, 0.22 mmol) in ethanol (4 mL) under nitrogen atmosphere until the solution became nearly colorless. The resulting solution was immediately transferred to the solution of the chloride **7** (40 mg, 0.15 mmol) in dry tetrahydrofuran (10 mL). The reaction mixture was stirred at room temperature under nitrogen atmosphere for 12 h. The resulting solution was extracted with dichloromethane (3×15 mL) and the organic layer was dried over MgSO<sub>4</sub>. The solvent was removed under reduced pressure, and the crude was purified by preparative TLC (silica gel GF254; *n*-hexane/EtOAc, 8 : 2, v/v). Violet solid. Yield: 45 mg (68%). Mp 131–132 °C. <sup>1</sup>H NMR (500 MHz, acetone-*d*<sub>6</sub>): δ (ppm) 8.00 (m, 2H), 7.44 (m, 3H), 7.20 (d, 1H, J = 4.0 Hz), 6.26 (s, 1H), 6.00 (d, 1H, J = 4.0 Hz), 2.57 (s, 3H), 2.51 (s, 3H), 2.44 (s, 3H). <sup>13</sup>C NMR (126 MHz, acetone-*d*<sub>6</sub>): δ (ppm) 157.7, 144.7, 141.9, 140.2, 140.1, 134.2, 132.3, 130.7, 130.2, 126.3, 124.2, 122.7, 113.65, 113.61, 113.58, 16.6, 16.3, 14.7. HRMS (APCI<sup>+</sup>) *m/z*: [M + H]<sup>+</sup> calcd. for C<sub>18</sub>H<sub>17</sub>BF<sub>2</sub>N<sub>2</sub>Te 441.0592; found 441.0591.

**Stability of the BODIPY Derivatives in the Dark.** A freshly prepared solution of the corresponding compound in spectroscopic-grade acetonitrile ( $c = 1-3 \times 10^{-5} \text{ mol dm}^{-3}$ ) in a 1 cm quartz cuvette was left in the dark at 23 °C, while UV-vis absorption spectra were periodically recorded using a diode-array spectrophotometer. The concentration changes of the compounds were calculated using the molar absorption coefficients.

**Photochemical Stability of the BODIPY Derivatives.** A freshly prepared solution of the corresponding compound in spectroscopic-grade acetonitrile ( $c = 1-3 \times 10^{-5} \text{ mol dm}^{-3}$ ) in a 1 cm quartz cuvette was irradiated with a home-made device equipped with 32 high-energy LEDs emitting at  $\lambda_{\text{em}} = 525 \pm 11 \text{ nm}$  at the distance of ~1 cm from the cuvette window. The reaction progress was monitored using a diode-array UV-vis spectrophotometer. The half-lives of the compounds were calculated from a plot of the absorbance at  $\lambda_{\text{irrad}}$  against time by fitting the data to a pseudo-first order kinetic equation.

**Determination of the Intersystem Crossing Quantum Yields.** The intersystem crossing quantum yields were calculated from the relative ratios of the areas of the absorption and ground state bleach bands in the transient spectrum. Both spectra were obtained with fresh samples under the same experimental conditions, and the measurements were repeated at least six times. The absorbance of 0.1 at the wavelength of excitation was kept to minimize the interference of the ground state absorption. The saturation conditions (quantitative excitation of molecules to its excited state) were kept for all measurements. A step-by-step procedure is described in the Supporting Information.

## Acknowledgement

This project was supported by the National Sustainability Programme of the Czech Ministry of Education, Youth and Sports (LO1214) and the RECETOX research infrastructure (LM2011028). The authors thank Jakob Wirz for fruitful discussions.

## References

1. A. C. Benniston, G. Copley, Lighting the way ahead with boron dipyrromethene (BODIPY) dyes, *Phys. Chem. Chem. Phys.*, 2009, **11**, 4124-4131.
2. M. Benstead, G. H. Mehl, R. W. Boyle, 4,4'-Difluoro-4-bora-3a,4a-diaza-*s*-indacenes (BODIPYs) as components of novel light active materials, *Tetrahedron*, 2011, **67**, 3573-3601.

3. A. Bessette, G. S. Hanan, Design, synthesis and photophysical studies of dipyrromethene-based materials: insights into their applications in organic photovoltaic devices, *Chem. Soc. Rev.*, 2014, **43**, 3342-3405.
4. N. Boens, V. Leen, W. Dehaen, Fluorescent indicators based on BODIPY, *Chem. Soc. Rev.*, 2012, **41**, 1130-1172.
5. A. Kamkaew, S. H. Lim, H. B. Lee, L. V. Kiew, L. Y. Chung, K. Burgess, BODIPY dyes in photodynamic therapy, *Chem. Soc. Rev.*, 2013, **42**, 77-88.
6. A. Loudet, K. Burgess, BODIPY dyes and their derivatives: Syntheses and spectroscopic properties, *Chem. Rev.*, 2007, **107**, 4891-4932.
7. H. Lu, J. Mack, Y. C. Yang, Z. Shen, Structural modification strategies for the rational design of red/NIR region BODIPYs, *Chem. Soc. Rev.*, 2014, **43**, 4778-4823.
8. G. Ulrich, R. Ziessel, A. Harriman, The chemistry of fluorescent bodipy dyes: Versatility unsurpassed, *Angew. Chem. Int. Ed.*, 2008, **47**, 1184-1201.
9. J. Z. Zhao, W. H. Wu, J. F. Sun, S. Guo, Triplet photosensitizers: from molecular design to applications, *Chem. Soc. Rev.*, 2013, **42**, 5323-5351.
10. T. Yogo, Y. Urano, Y. Ishitsuka, F. Maniwa, T. Nagano, Highly efficient and photostable photosensitizer based on BODIPY chromophore, *J. Am. Chem. Soc.*, 2005, **127**, 12162-12163.
11. P. Klan, J. Wirz, *Photochemistry of organic compounds: From concepts to practice*, John Wiley & Sons Ltd., Chichester, 2009.
12. K. N. Solovyov, E. A. Borisevich, Intramolecular heavy-atom effect in the photophysics of organic molecules, *Phys. Usp.*, 2005, **48**, 231-253.
13. M. Galletta, S. Campagna, M. Quesada, G. Ulrich, R. Ziessel, The elusive phosphorescence of pyrromethene-BF<sub>2</sub> dyes revealed in new multicomponent species containing Ru(II)-terpyridine subunits, *Chem. Commun.*, 2005, 4222-4224.
14. A. A. Rachford, R. Ziessel, T. Bura, P. Retailleau, F. N. Castellano, Boron Dipyrromethene (BODIPY) Phosphorescence Revealed in Ir(ppy)(2)(bpy-CC-Bodipy)<sup>+</sup>, *Inorg. Chem.*, 2010, **49**, 3730-3736.
15. S. H. Lim, C. Thivierge, P. Nowak-Sliwinska, J. Y. Han, H. van den Bergh, G. Wagnieres, K. Burgess, H. B. Lee, In vitro and in vivo photocytotoxicity of boron dipyrromethene derivatives for photodynamic therapy, *J. Med. Chem.*, 2010, **53**, 2865-2874.
16. W. H. Wu, H. M. Guo, W. T. Wu, S. M. Ji, J. Z. Zhao, Organic triplet sensitizer library derived from a single chromophore (BODIPY) with long-lived triplet excited state for triplet-triplet annihilation based upconversion, *J. Org. Chem.*, 2011, **76**, 7056-7064.
17. Y. Cakmak, S. Kolemen, S. Duman, Y. Dede, Y. Dolen, B. Kilic, Z. Kostereli, L. T. Yildirim, A. L. Dogan, D. Guc, E. U. Akkaya, Designing excited states: Theory-guided access to efficient photosensitizers for photodynamic action, *Angew. Chem. Int. Ed.*, 2011, **50**, 11937-11941.
18. S. Duman, Y. Cakmak, S. Kolemen, E. U. Akkaya, Y. Dede, Heavy atom free singlet oxygen generation: Doubly substituted configurations dominate S<sub>1</sub> states of bis-BODIPYs, *J. Org. Chem.*, 2012, **77**, 4516-4527.
19. M. Broring, R. Kruger, S. Link, C. Kleeberg, S. Kohler, X. Xie, B. Ventura, L. Flamigni, Bis(BF(2))-2,2'-bidipyrrins (BisBODIPYs): Highly fluorescent BODIPY dimers with large Stokes shifts, *Chem. Eur. J.*, 2008, **14**, 2976-2983.



20. B. Ventura, G. Marconi, M. Broring, R. Krugerb, L. Flamigni, Bis(BF<sub>2</sub>)-2,2'-bidipyrins, a class of BODIPY dyes with new spectroscopic and photophysical properties, *New J. Chem.*, 2009, **33**, 428-438.
21. K. Konig, Multiphoton microscopy in life sciences, *J. Microsc.*, 2000, **200**, 83-104.
22. A. J. Mukherjee, S. S. Zade, H. B. Singh, R. B. Sunoj, Organoselenium chemistry: Role of intramolecular interactions, *Chem. Rev.*, 2010, **110**, 4357-4416.
23. S. T. Manjare, Y. Kim, D. G. Churchill, Selenium- and tellurium-containing fluorescent molecular probes for the detection of biologically important analytes, *Acc. Chem. Res.*, 2014, **47**, 2985-2998.
24. C. W. Nogueira, G. Zeni, J. B. T. Rocha, Organoselenium and organotellurium compounds: Toxicology and pharmacology, *Chem. Rev.*, 2004, **104**, 6255-6285.
25. B. Tang, Y. L. Xing, P. Li, N. Zhang, F. B. Yu, G. W. Yang, A rhodamine-based fluorescent probe containing a Se-N bond for detecting thiols and its application in living cells, *J. Am. Chem. Soc.*, 2007, **129**, 11666-11667.
26. Z. R. Lou, P. Li, X. F. Sun, S. Q. Yang, B. S. Wang, K. L. Han, A fluorescent probe for rapid detection of thiols and imaging of thiols reducing repair and H<sub>2</sub>O<sub>2</sub> oxidative stress cycles in living cells, *Chem. Commun.*, 2013, **49**, 391-393.
27. S. J. Balkrishna, A. S. Hodage, S. Kumar, P. Panini, Sensitive and regenerable organochalcogen probes for the colorimetric detection of thiols, *RSC Adv.*, 2014, **4**, 11535-11538.
28. B. S. Wang, P. Li, F. B. Yu, J. S. Chen, Z. J. Qu, K. L. Han, A near-infrared reversible and ratiometric fluorescent probe based on Se-BODIPY for the redox cycle mediated by hypobromous acid and hydrogen sulfide in living cells, *Chem. Commun.*, 2013, **49**, 5790-5792.
29. S. T. Manjare, S. Kim, W. Do Heo, D. G. Churchill, Selective and sensitive superoxide detection with a new diselenide-based molecular probe in living breast cancer cells, *Org. Lett.*, 2014, **16**, 410-412.
30. E. Fron, E. Coutino-Gonzalez, L. Pandey, M. Sliwa, M. Van der Auweraer, F. C. De Schryver, J. Thomas, Z. Y. Dong, V. Leen, M. Smet, W. Dehaen, T. Vosch, Synthesis and photophysical characterization of chalcogen substituted BODIPY dyes, *New J. Chem.*, 2009, **33**, 1490-1496.
31. S. T. Manjare, J. Kim, Y. Lee, D. G. Churchill, Facile *meso*-BODIPY annulation and selective sensing of hypochlorite in water, *Org. Lett.*, 2014, **16**, 520-523.
32. V. Leen, E. Braeken, K. Luckermans, C. Jackers, M. Van der Auweraer, N. Boens, W. Dehaen, A versatile, modular synthesis of monofunctionalized BODIPY dyes, *Chem. Commun.*, 2009, 4515-4517.
33. V. Leen, T. Leemans, N. Boens, W. Dehaen, 2- and 3-Monohalogenated BODIPY dyes and their functionalized analogues: Synthesis and spectroscopy, *Eur. J. Org. Chem.*, 2011, **2011**, 4386-4396.
34. X. F. Zhang, X. D. Yang, Singlet oxygen generation and triplet excited-state spectra of brominated BODIPY, *J. Chem. Phys. B*, 2013, **117**, 5533-5539.
35. R. Bonneau, I. Carmichael, G. L. Hug, Molar absorption coefficients of transient species in solution, *Pure Appl. Chem.*, 1991, **63**, 290-299.
36. C. Tahtaoui, C. Thomas, F. Rohmer, P. Klotz, G. Duportail, Y. Mely, D. Bonnet, M. Hibert, Convenient method to access new 4,4-dialkoxy- and 4,4-diaryloxy-diaza-s-

- indacene dyes: Synthesis and spectroscopic evaluation, *J. Org. Chem.*, 2007, **72**, 269-272.
37. Y. H. Chen, J. Z. Zhao, L. J. Xie, H. M. Guo, Q. T. Li, Thienyl-substituted BODIPYs with strong visible light-absorption and long-lived triplet excited states as organic triplet sensitizers for triplet-triplet annihilation upconversion, *RSC Adv.*, 2012, **2**, 3942-3953.
  38. H. L. Kee, C. Kirmaier, L. H. Yu, P. Thamyongkit, W. J. Youngblood, M. E. Calder, L. Ramos, B. C. Noll, D. F. Bocian, W. R. Scheidt, R. R. Birge, J. S. Lindsey, D. Holten, Structural control of the photodynamics of boron-dipyrrin complexes, *J. Chem. Phys. B*, 2005, **109**, 20433-20443.
  39. M. J. Ortiz, A. R. Agarrabeitia, G. Duran-Sampedro, J. B. Prieto, T. A. Lopez, W. A. Massad, H. A. Montejano, N. A. Garcia, I. L. Arbeloa, Synthesis and functionalization of new polyhalogenated BODIPY dyes. Study of their photophysical properties and singlet oxygen generation, *Tetrahedron*, 2012, **68**, 1153-1162.
  40. V. Lakshmi, M. R. Rao, M. Ravikanth, Halogenated boron-dipyrrromethenes: synthesis, properties and applications, *Org. Biomol. Chem.*, 2015, **13**, 2501-2517.
  41. T. Rohand, W. W. Qin, N. Boens, W. Dehaen, Palladium-catalyzed coupling reactions for the functionalization of BODIPY dyes with fluorescence spanning the visible spectrum, *Eur. J. Org. Chem.*, 2006, 4658-4663.
  42. M. Zander, The intra-annular internal heavy-atom effect on the fluorescence and phosphorescence properties of oxygen, sulphur or selenium containing heterocyclic systems related to dibenzo[b,n]perylene, *Z. Naturforsch. A*, 1989, **44**, 1116-1118.
  43. M. Zander, G. Kirsch, On the phosphorescence of benzologues of furan, thiophene, selenophene, and tellurophene. A systematic study of the intra-annular internal heavy-atom effect, *Z. Naturforsch. A*, 1989, **44**, 205-209.
  44. Z. Shen, H. Rohr, K. Rurack, H. Uno, M. Spieles, B. Schulz, G. Reck, N. Ono, Boron-diindomethene (BDI) dyes and their tetrahydrobicyclo precursors - en route to a new class of highly emissive fluorophores for the red spectral range, *Chem. Eur. J.*, 2004, **10**, 4853-4871.
  45. S. Hattori, K. Ohkubo, Y. Urano, H. Sunahara, T. Nagano, Y. Wada, N. V. Tkachenko, H. Lemmetyinen, S. Fukuzumi, Charge separation in a nonfluorescent donor-acceptor dyad derived from boron dipyrromethene dye, leading to photocurrent generation, *J. Chem. Phys. B*, 2005, **109**, 15368-15375.
  46. L. Klicova, P. Sebej, T. Solomek, B. Hellrung, P. Slavicek, P. Klan, D. Heger, J. Wirz, Adiabatic triplet state tautomerization of *p*-hydroxyacetophenone in aqueous solution, *J. Phys. Chem. A*, 2012, **116**, 2935-2944.